Sandfill-Retaining rubble mound structures:

Evaluating the behaviour of sediments at the interface of a rubble mound with a reclamation, by means of physical modelling.

R.C. (Raoul) Tutein Nolthenius

Delft University of Technology

TU Delft Delft University of Technology

Van Oord Marine ingenuity

Challenge the future

Sandfill-Retaining rubble mound structures:

Evaluating the behaviour of sediments at the interface of a rubble mound with a reclamation, by means of physical modelling.

by

R.C. (Raoul) Tutein Nolthenius

in partial fulfilment of the requirements for the degree of

Master of Science
in Civil Engineering

at the Delft University of Technology,
to be defended publicly on Wednesday July 4, 2018 at 10:00 AM.

Student number:	4155807	
Project duration:	September 4, 2017 – July 4, 2018	
Thesis committee:	Prof. dr. ir. W. S. J. Uijtewaal,	TU Delft
	Ir. G. M. Smith,	Van Oord / TU Delft, Supervisor
	Ir. J. P. van den Bos,	TU Delft

An electronic version of this thesis is available at `http://repository.tudelft.nl/`.

TU Delft Delft University of Technology   Van Oord Marine ingenuity

Preface

This thesis concludes the research project executed to complete the MSc programme Hydraulic Engineering at DELFT UNIVERSITY OF TECHNOLOGY (TU Delft). The project took place between September 2017 and July 2018 and was executed under the supervision of both TU Delft, and VAN OORD DREDGING AND MARINE CONTRACTORS BV (Van Oord). The research focussed on a topic of which little was known in the literature currently available. When applying to this research position at Van Oord, I was well aware of the challenges ahead. I had to be open minded with respect to the research methods used, combined with a hands on and practical mentality. This brought me to the Fluid mechanics laboratory at TU Delft where I have spent most of my time building a physical scale model and researching the processes at hand. The time spent at the Fluid mechanics laboratory has been a great learning experience. To find out that the assumptions and processes I developed in theory actually work in a self-built model setup has been exciting.

I would like to thank Van Oord for the opportunity to execute the project at their office in Rotterdam, and for being able to talk with so many experts in the hydraulic engineering field. The colleagues have been very welcoming and willing to share their insights, on- and off topic.

In particular I want to thank Greg Smith (Van Oord/ TU Delft) and Jeroen van den Bos (TU Delft) for your guidance and advise, but also for stimulating me to work independently and to choose my own path during the research project. We have discussed many subjects, varying in complexity and relevance, for which I acknowledge your patience. I want to thank you for the pleasant atmosphere during our personal and team meetings. Additionally, I want to thank Wim Uijtewaal for being the chair of the committee. Not only your overall governance but especially your in depth comments during the meetings has been very helpful.

By executing this research project at both Van Oord and the Fluid mechanics laboratory at TU Delft, I have had double the amount of fun with fellow graduate students. I want to thank my laboratory friends Roland and Gustav for the endless days, evenings and weekends spent in the laboratory which would have been a lot less fun when doing it on my own. Equally, I am thankful to the Van Oord graduates for the coffee breaks, lunches, divers conversations and daily walks through the outskirts of Cappelle. Lastly, I would like to thank Eva who has been my biggest supporter over the last ten months, encouraging me to do the best I could.

R.C. (Raoul) Tutein Nolthenius
Delft, July 2018

Abstract

Currently, sand retaining rubble mound structures are often constructed with geotextiles, lining the interface between the core material and the sandfill. These geotextiles are placed to make sure the sand from the sandfill is not flushed out through the core by incoming hydraulic forces from the surrounding water. It is proposed that difficulties faced during placement, or uncertainties regarding correct installation of these geotextiles can be overcome by curtailing the geotextiles. The potential for this abbreviations is stressed by Polidoro et al. (2015) as this author concluded, that at the lower inner corner of rubble mound structures with a closed inner slope, pressures are dampened below a certain estimated critical value. However, no proof was found for the applicability of this critical value. Despite several researches predicting hydraulic loading in rubble mound breakwaters, and studies assessing the stability of sand to stone interfaces, insight in the behaviour of sediments in this particular interface configuration of a sand retaining breakwaters was lacking. Therefore, the aim of this research was to study the behaviour of sediments at the interface to a core in a sandfill. Under supervision of VAN OORD and DELFT UNIVERSITY OF TECHNOLOGY (TU Delft), a physical model is designed to study specifically this interface. The model tests took place in the Fluid mechanics laboratory at TU Delft, where a relatively small setup ($1 \cdot 0.5 \cdot 0.15 m$) was used to model on a relatively large scale ($\lambda \approx 15$). An exact scaled representation of a nominal breakwater by Polidoro et al. (2015) was used. In the model both the development of the interface during placement of the sandfill as the behaviour of the sediments when subjected to hydraulic loading is studied. The research concluded that a stable initial interface was found with a slope of approximately $35°$. In what extent the infill migrated inward through the core varied depending on the installation method. When subjected to hydraulic loading, a critical hydraulic gradient was found of $0.05 m/m$ on average and $0.04 m/m$ in the most conservative case. These results were established with a measurement accuracy of $\sim 5\%$ and the consistency over different series of tests was $\geq 80\%$. Sometimes segregation of the stones was observed. The main attribution to the deviations in the measured hydraulic gradients and sediment transport were concluded due to this variation in the positioning of the stones. It is concluded that the current existing literature is able to give reasonable initial approximations of the critical gradient in the system($5-40\%$ accurate), however, the deviation can be significant and further research by varying more geometrical parameters should conclude if the obtained approximations are constant. Concluding, the results obtained in this research suggest that the critical loading conditions for the interface stability of to a rubble mound in a sandfill are of comparable order to conventional filter criteria and are higher than the currently calculated and measured appearing gradients by for instance Vanneste and Troch (2012) and Polidoro et al. (2015). These results justify the further exploration towards the potential of the abbreviation of geotextiles at the considered interface. In order to guide further research a list of recommendations is given as well as additional model improvements.

Contents

List of Figures

List of Tables

1
Introduction

1.1. Context

All over the world people live, work and play at the intersection of land and water. Bodies of water, particularly the sea, has provided many basic resources for civilization such as food, trade opportunities and water. However, there are several challenges that limit the construction of civil structures along this intersection. The main reason for this is that the shape and stability of the land is constantly changing due to the movement and force of the water. For this reason, people have been studying and developing civil and marine constructions that can remain functional in this harsh environment. Many different structures have become widely used and accepted. For example, major coastal cities often have a form of flood protection, which protect the land from rising ocean levels, a port to enable the transport of goods and people, and land reclamations to accommodate urban expansions or industrial uses. Typical examples of these structures are the Maasvlakte 2 port in The Netherlands, the artificial island Palm Jumeriah in Dubai and the Afsluitdijk, also in The Netherlands, shown in figure 1.1.

(a) Maasvlakte 2, The Netherlands

(b) Palm Jumeirah, Dubai

(c) Afsluitdijk, The Netherlands

Figure 1.1: Various coastal structures at the border of land and water (Pictures by Van Oord).

In order to operate at this boundary, each of these structures must provide sufficient strength to withstand the forces exerted by the ocean to ensure safety for the hinterland. This is mainly because the force of the waves causes the soil in the land to slowly erode over time. For this reason, the construction and composition of these structures becomes extremely important.

A specific type of retaining structure is the sand retaining breakwater. Their primary function is to retain the sand composing the hinterland. They can be known as both sand retaining and sandfill retaining. Breakwaters are coastal structures used to decrease the incident energy of waves rising and falling, by using friction.The water passes through different layers of porous material. As the porosity of the layers decreases from the external slope to the inner core of the breakwater, increased friction slows the water (Guanche et al., 2015). Breakwaters come in different shapes and sizes, for different wave and current conditions and depending on purpose for which they are built. Breakwaters are built to enclose land as sand retaining structures or, as permeable structures to create a calm wave environments in the water body behind. In sand retaining breakwaters specifically, a retention function is combined with a protective function against the forces coming from the sea. These breakwaters are constructed as a rubble mound topped with a protective layer of larger stones or concrete elements. At the inner slope, retention measures are installed to keep the sand in, and let the water out of the structure. A typical sand retaining structure is presented in figure 1.2. The retention of sand is crucial to ensure the overall stability of the structure and the sandfill behind as, the instability of the sandfill may cause fatal damage to the works constructed on top. As a retention measure, at the sandfill-rubble mound interface, various techniques are used. For example, sometimes, geometrically closed and open filters are installed, which are basically (multiple layers of) smaller stone fractions adding resistance to the transport of sediments. While, in other instances, an impermeable clay layer is constructed or the interface is lined with geotextiles. Especially the latter is a popular tool. Geotextiles are permeable fabrics which can separate or filter soil particles while water is free to flow out of the structure when needed. They come with a variety of permeability and filter characteristics making them widely employable. A big advantage of using geotextiles is that a geotextile can be chosen based on the desired characteristic mesh width and permeability and, when correctly installed, the sand is retained by the fabric. When geometric (stone) filters are used, many different layers, or complex calculations on both the hydraulic loads and hydraulic resistance are needed.

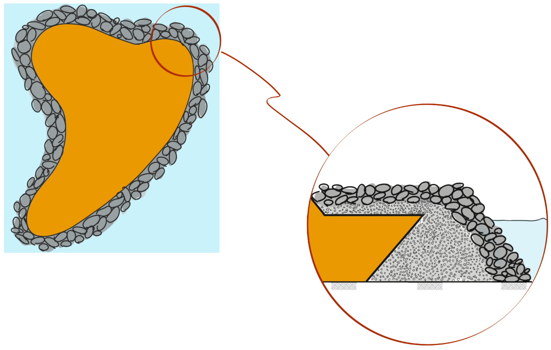

Figure 1.2: Typical sand retaining structure

Land reclamation and breakwater construction projects are mainly executed by large international marine contractors. When building such structures, one usually starts with the rubble mound core. Subsequently, a protective outer layer is constructed and geotextiles are placed on the inner slope from top to bottom. Thereafter, the inner side is filled with sand. An example of this procedure is represented in figure 1.3.

(a) Constructing the rubble mound (b) Placement of geotextiles (c) Reclamation of land

Figure 1.3: Various construction stages of a sandfill enclosed by a rubble mound breakwater (Pictures by Van Oord)

1.2. Problem definition

The installation of geotextiles can be challenging and risky under certain wave and current conditions. The geotextiles have to be brought to considerable depths, ranging $-10m$ to $-30m$. Depending on the type of geotextile, the fabrics tend to float which makes installation difficult. Furthermore, the textiles have a certain width (approx. $25m$) and are placed next to each other, were sound overlaps are essential. Because the geotextiles are placed at considerable depths sometimes divers or other inspection methods are used to ensure the correct positioning with a sufficient amount of overlap and if they have reached the predefined depth.

In general, geotextiles are applied to line the inner face of the retaining rubble mound, thus ensuring that the main sandfill cannot be washed out by waves, or tides (Polidoro et al., 2015). However, until what depth the forces coming from the sea are still large enough to endanger the stability of the sand body behind, is questioned. Therefore, when these geotextiles need to be placed, and specifically until what depth is still uncertain. Currently, to be on the safe side, the geotextiles are stretched out to the bottom of the structure. According to Polidoro et al. (2015), the key question is at which level wave-induced hydraulic gradients are insufficiently strong in the rubble mound to cause significant loss of sand from the sandfill through the rubble mound. When this level can be determined, the use of a geotextile filter from here downwards, can be limited. Shortening of the geotextiles is not yet applied in practice, as stability of the main sandfill cannot be ascertained.

Research has been carried out to study the propagation and damping of waves and wave induced pressure oscillations in the core material of rubble mound structures. Furthermore, the critical gradient for various kinds of filters in stationary and oscillatory flow have been studied (Guanche et al., 2015; Vanneste and Troch, 2012; Cantelmo et al., 2010; Muttray and Oumeraci, 2005; Van Gent, 1993; Allsop and Williams, 1991; de Graauw et al., 1984). In addition, Polidoro et al. (2015) demonstrated in a physical scale model the decrease of the hydraulic gradient in the lower inner corner of a rubble mound structure. The target area as well as the potential shorting of the geotextile is are indicated by the red square in figure 1.4. The results by Polidoro et al. (2015) justify further research into the possibilities for the abbreviation of geotextiles. This further research should focus on physical modelling of the interaction between the core material and sediments. Currently, the missing link is the correlation between the locally appearing hydraulic gradient in the lower inner corner of a sand retaining rubble mound structure and the start of loss of sediments from the sandfill.

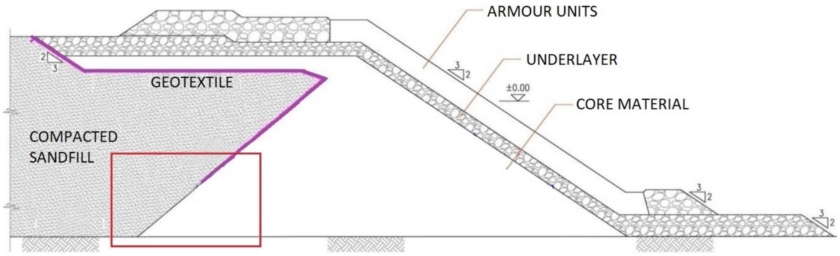

Figure 1.4: Typical cross-section of sand retaining structure and area of interest (adapted from (Polidoro et al., 2015).

1.3. Objective

In the previous section is explained what sandfill retaining structures are and how geotexiles can contribute to the stability of the sandfill behind. Although geotextiles itself are a good and practical retention measure, the installation can be challenging and risky. These challenges are potentially avoidable when more insight is obtained about the depth at which these geotextiles are needed to ensure the stability of the structure. Therefore, the objective for this thesis is to evaluate the possibilities for the abbreviation of geotextiles in sand retaining rubble mound breakwaters. In order to do so, the governing processes in the area of interest as defined in figure 1.4 are extensively researched. Hydraulic loads from the sea and landward side of the breakwater are considered and weighed against the resistance formed by the core and sandfill materials. The obtained correlation between the hydraulic gradients and the initiation of motion of sediments from the sandfill, can be used to give approximations for prototype designs and describe the potential applicability of currently available filter and stability theories for this particular situation. When sufficiently supported and calibrated to site specific characteristics, the results can allow designers to significantly shorten the depths over which geotextile filters are needed (Polidoro et al., 2015) or guarantee the stability of currently built breakwaters with questionable placement of the geotextiles.

2
Problem statement

In most sandfill retaining rubble mound designs a geotextile separates the sandfill from the rubble mound retaining the sand in the sandfill and ensuring the stability of the structure as a whole. However, the construction of this design with geotextile can be challenging. Therefore, research is needed into the added value of these geotextile separations over the full depth. It is proposed that an abbreviation of the geotextiles to reduce risk during installation is feasible without increasing the possibility of failure of the structure. A paper written by Polidoro et al. (2015) discusses the possibilities to couple the appearing hydraulic gradient to the critical hydraulic gradient of material inside a rubble mound structure to obtain a criterion for which granulates from the sand body do, or do not migrate through the core into the sea. This particular research sparked the idea to investigate the hydraulic resistance of a sandfill retained by a rubble mound structure and defines the goal of the research:

What are the possibilities for the abbreviation of geotextiles in sandfill retaining rubble mound structures without compensating on stability?

Research from e.g. (Polidoro et al., 2015; Guanche et al., 2015; Vanneste and Troch, 2012; Cantelmo et al., 2010; Muttray and Oumeraci, 2005; Burcharth et al., 1999) is mainly focussed on (empirically) approximating the course and damping of the hydraulic loading over the rubble mound. The research is often based on one data set of measurements and sometimes tested for the applicability of a second measured data set. The general applicability and predictive qualities are rather uncertain. Furthermore, literature is available on the hydraulic resistance of grains against moving at sand-rock interfaces e.g. (Wolters and Van Gent, 2012; Allsop and Williams, 1991; Adel et al., 1988; Klein Breteler, 1989; de Graauw et al., 1984; Kenny and Lau, 1985). Also this research describes mainly empirical relations with case specific boundary conditions, assumptions and simplifications. Most of these relations especially hold for parallel or perpendicular, stationary flow over a horizontal filter. Which is not the correct representation of the flow conditions and the geometry found in rubble mounds. It is therefore concluded that several methods and formulae are derived to obtain both the appearing and the critical hydraulic gradients in grains which can not be directly coupled to solve the problem at hand. The missing link is found in the (physical) interaction between hydraulic loads and hydraulic resistance of sediments in correct representation of the geometry.

Furthermore, the outline of the interface between the sand body and the rubble mound core is not evident from existing research in case a geotextile will not be in place. During placement, the sand particles might migrate through the core material to a greater or lesser extent, as presented in figure 2.1. The research by Polidoro et al. (2015) proposes that after an initial mixture of sand and core material, the interface problem can be described as an internal stability problem of the mixture with a "composite grading". The critical gradient for the case can be approximated with use of the suffusion theory by Adel et al. (1988).

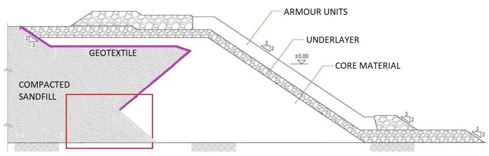

(a)

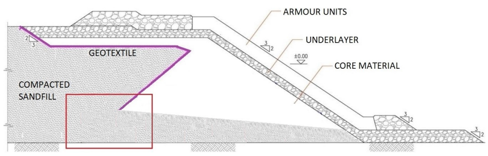

(b)

Figure 2.1: Indication of different initial migration patterns of sand during construction

In order to investigate the possibilities of applying shorter geotextiles on the inner slope of sand retaining rubble mound structures without compensating stability risks, the study was divided in two separated sections. The first section focussed on the sand particle migration from the sand body into the rubble mound core during installation and after an initial settling period. The second part was focussed on the interaction between hydraulic loading conditions and the sand-core mixture during the lifetime of the rubble mound. This second part was also used to evaluate the applicability of the currently available predictive stability criteria for this particular situation and the methods used by Polidoro et al. (2015). The use of a physical model provided insights in the processes during the initial infill and afterwards, in the behaviour of sediments at the sandfill to rubble mound interface when subjected to hydraulic loading.

$$\text{If} \quad \frac{I_{cr,appear}}{I_{cr,calc}} < X \quad \rightarrow \text{Stable} \tag{2.1}$$

A stability criterion in the form of equation 2.1 was defined in which a parameter 'X' for different combinations of methods is defined to couple appearing critical gradients in the model to the corresponding calculated critical gradients. This parameter determines the applicability of the tested stability criterion and, when constant over models with different scaling, a dimensionless scaling parameter. To guide the research, the research question and subquestions are established as follows:

Research question:

How can the behaviour of the sediments at the interface to a rubble mound in a sandfill be described, when subjected to hydraulic loading.

Subquestions

- How can the process of initial infill and the development of the interface be described?
- Can a model setup be designed which is sufficiently consistent and accurate to determine the critical gradient for this system?
- What is the critical hydraulic gradient for the sand at the interface under wave loading?
- What processes determine the appearing hydraulic gradient and govern the sediment transport rate?
- Can we define a parameter X for various filter relations?
- Is the suffusion (Allsop and Williams, 1991) appropriate to describe the behaviour of a sand-core mixture subjected to wave loading, as proposed by Polidoro et al. (2015)?

3

Approach and Methodology

3.1. Approach

In this research, various steps are taken to consider all aspects of the described problem and find an answer to the research question. First a literature review is executed to justify this research within the current insights regarding the topic. This research defines which knowledge gaps can be closed and what method is most suitable to achieve this. Furthermore, the literature review is used to make an estimation for the considered forces and resistances encountered in the sand-fill retaining structure. A physical model is designed in which these estimations provide an insight for the boundary conditions, limits and possibilities. Extra care is taken to minimize scale effects. The physical model test are divided in two phases. First, fast and simple experiments were executed to design a model setup. Afterwards, precise and accurate experiments provide useful data to be analysed and coupled to physical processes which are then used to answer the research question. Based on the available literature the obtained results are discussed and lead to conclusion regarding this research.

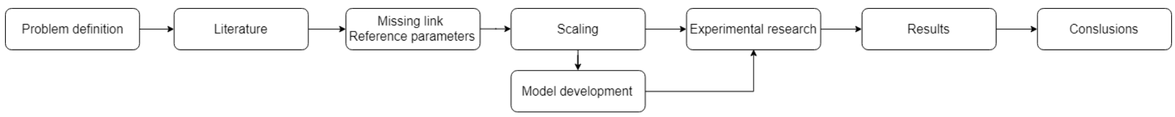

Figure 3.1: Approach of the research

Literature review

To fully understand the processes in the area of study the system has been thoroughly analysed by means of a literature review. Amongst others, general flow theory, hydraulic loads, porous flow, sediment transport processes, filter methodology and model scaling are considered. The applicable theory is used to support research strategies and explain results.

Formulation of experimental conditions

From the literature several methods are proposed to estimate parameters which intend to describe or explain certain processes. Within the research a estimation of appearing and critical forces is executed on both nominal and model scale. Various calculations originating from current research are repeated with the nominal and model characteristic values to give estimations of the expected load- and resistance parameters. These are used to build and initiate a model setup and to operate a model within logical boundary conditions.

(Model) Strategy

Various methods are considered to obtain the missing insight in the current knowledge. An analytical approach, numerical modelling and physical (scale) modelling are considered. The physical scale model appeared the best fit to the fill the knowledge gap as proposed by amongst others Polidoro et al. (2015). The design of the physical model is determined by weighing pros and cons of three different types experiments: A scaled model breakwater in a wave flume, a rock/sediment sample in a U-tank and a container in which oscillating water movement can be excited by a plunger. Pros and cons are weighed and one model setup is chosen and constructed.

3.2. Method

The chosen method is to model a sand-fill retaining breakwater and couple the hydraulic gradient to actual transport of sediment. The results are coupled to the initiation of motion of sand particles or consisting filter rules. In this research a sand-fill is placed in the model to find the load needed to transport the sediment through the core of the breakwater in terms of a hydraulic gradient. The desired scalable parameter is $X = I_{\text{critical, measured}}/I_{\text{critical, calculated}}$. The hydraulic gradient will be measured and qualitatively coupled to the occurring sediment transport. The model setup is designed for this research specifically and not used before. Therefore, first preliminary experiments were executed to outline the design and boundary conditions of the model needed for the research. The preliminary model test describe the behaviour of the setup, wall effects, the measurement equipment and suggests the order of magnitudes of forces and sediment transport. The second series of experiments are carried out with core material precisely scaled to a (common) nominal breakwater core and sediment size given by Polidoro et al. (2015). This also provides an equality in core to sediment size ratio between the nominal breakwater and the model. The designed method enables the use of relatively large stones with respect to conventional wave flume experiments at model scale. The hydraulic loads are caused by vertical oscillation of a plunger powered by a step-motor. By varying the acceleration of the motor the appearing hydraulic gradient could be controlled.

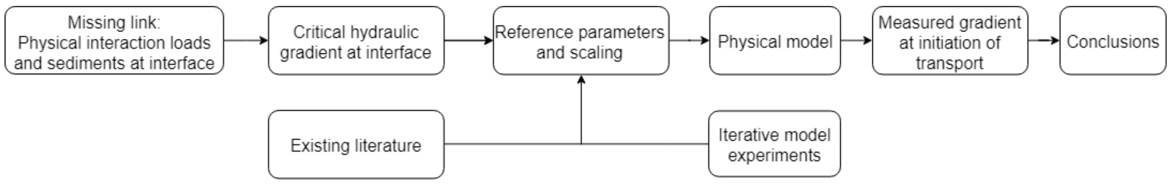

Figure 3.2: Method of the research

Preliminary experiments

In the preliminary experiments tests were executed to determine the effect of different sediment sizes, rock sizes and sediment size to rock size ratios. Furthermore, the wall-effects are analysed and examined if loose rock or glued rock models should be used. The preliminary experiments are also used for the iterative process for finding the correct measurement equipment which is, like the container, developed for this research. Lastly, the methods for wave simulation and the possibilities for sediment transport evaluation were considered. The preliminary experiments result in a set of design conditions and a set of necessary adaptations of the model setup to start with the definitive experiments.

Final experiments

The used model setup consisted of a container divided in three zones. In zone 1 a wave maker is placed which generates oscillating water movement by means of a motorised vertical plunger. In zone 2 a model breakwater core is build which is connected by an open face at the bottom to zone 3 where a sand body is installed. Two identical pressure sensors are put in the exact same places in order to obtain hydraulic gradients over the sand to rock interface, providing identical signals. By regulating the acceleration of the motor hydraulic gradients are excited ranging from 0.01-0.15. Two sets of approximately 15 experiments are carried out to couple the sediment transport to the appearing hydraulic gradient and extra experiments are executed to prove the reproducibility of the tests and to evaluate the noise signal and disturbances.

3.3. Results

The obtained measurement data is coupled to the visual inspection of flow and sediment transport. Afterwards, preliminary conclusions are stated on how the appearing hydraulic gradient is related to the observed sediment transport. Lastly, these conclusions are weighed against the available literature and inevitable imperfections of this research and recommendations for further research are given.

4
Background and Theory

In this section an overview is given on the available literature regarding the subject of this thesis. The review is divided in five sections. The first section (4.1) introduces both the processes that force the hydraulic loads acting on the structure and elaborate how these forces can be estimated. To enable the understanding how these processes influence the (internal) stability of the sandfill retaining rubble mound an overview of general flow theory is provided followed by the elaboration of porous flow in sections A.2 and 4.2 respectively. The forces and (porous) flow theory are coupled in the section 4.3 to describe the sediment transport processes and the current design methods to ensure the desired stability of the rubble mound are given in section 4.4. Lastly, in section 4.5 relevant literature is summarized regarding hydraulic scale models and the inherent scale effects apparent in models scale test.

4.1. Hydraulic loads

The considered hydraulic loads acting on the sand fill retaining rubble mounds are focussed on flows induced by (orbital) wave pressures and hydraulic head differences over the structure. Irregular (non-stationary) flows and pressures are mainly caused by wave motions, whereas the phreatic level inside a breakwater and in the potential sand fill behind is governed by amongst others wave- or wind induced set-up and tides facing the breakwater, and (excessive) precipitation or (wave-induced) pore-pressure build-up at the leeside of the breakwater. According to Lawson (1992) these loads can be separated in three hydraulic regimes:

- Impacting water flow conditions, such as wave activity;
- Gradually reversing water flow conditions, such as tidal activity;
- Unidirectional groundwater flow conditions, such as water draining out through the revetment.

Figure 4.1 gives a schematic overview the second and third flow regimes for two different designs. The designs of the two examples given in fig. 4.1a and fig. 4.1b can be combined and therefore, the flows described in fig. 4.1a can occur in fig. 4.1b and vice versa. The internal setup in a breakwater due to flow regime 1 is presented in figure fig. 4.2. This setup can lead to a waterlevel gradient over the core to sandfill interface similar as induced by tides.

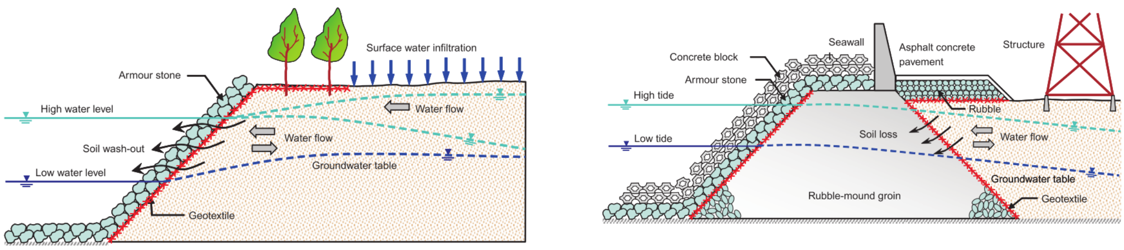

(a) Application of geotextiles in revetments, flow regime 2.

(b) Typical cross-section of rubble-mound groin, flow regime 3.

Figure 4.1: Design examples for use of geotextiles in sand retaining body's (Hsu et al., 2008)

Discussion rises when summarizing these three regimes. The first two regimes can be explained as cyclic flow which can be combined into one set of filter criteria as the water movement is both oscillatory only its frequency is different (Lawson, 1992). However, their filtration behaviours are unalike. Wave activity is much more violent, with a shorter period, than tidal activity (Hsu et al., 2008). In the reasoning of describing the first two processes as one (oscillating, with different frequencies) movement, the second regime would be a (uni)directional steady flow (e.g. drainage). This research proposes however, it can be imagined that the gradually reversing water flow conditions are of rather low time scales and are therefore more comparable with the (uni)directional flow induced by drainage and are similarly governed by hydraulic head differences. The potential for hydraulic loads induced by draw-down of drainage of storm set-up or tidally driven water levels is supported by Polidoro et al. (2015). Thus two flow regimes are considered. (1) Impacting flow conditions, such as wave activity; (2) gradually reversing or unidirectional (ground)water flow conditions such as tides and drainage.

The internal- and external flow and water levels correspond with a phase difference with respect to the free surface. The internal flow is subjected to much larger friction due to the porous breakwater core. Therefore, internal flow is dominated by friction and gravity while external flow is governed by inertia and gravity, causing a phase difference. The phreatic surface in the rubble mound is directly dependent on the internal flux and therefore will experience a similar phase difference and damping compared with the free surface, illustrated in figure 4.2 (Groot et al., 1994). The water level difference between the external- and internal water surface height during uprush and downrush is schematised in figure 4.3. The arrows indicate the resulting pressure differences along the interface between the rubble mound and the open water.

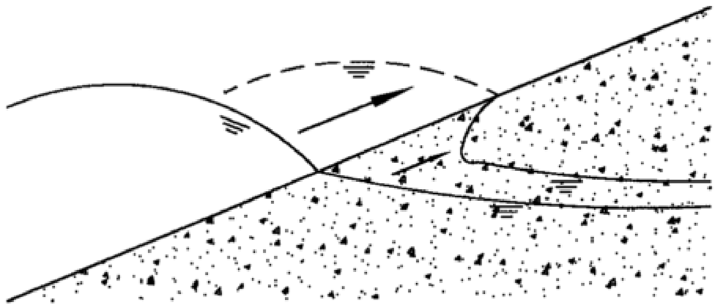

Figure 4.2: Phase difference between external and internal waterlevels (Groot et al., 1994)

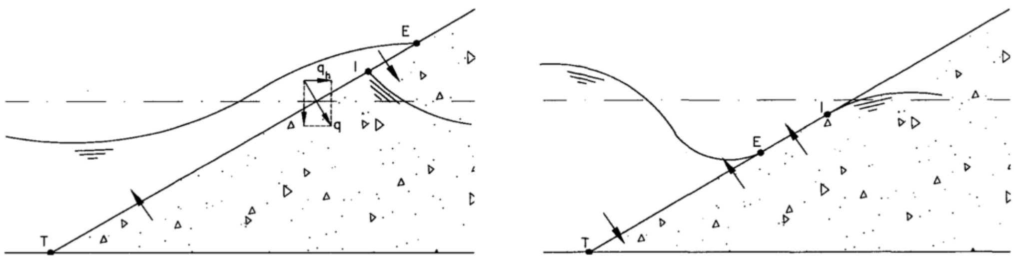

(a) At maximum run-up (b) At maximum run-down

Figure 4.3: Pore pressure course during maximum run-up and maximum run-down (Groot et al., 1994)

4.1.1. Wave loading

The loads induced by the regime of wave activity is frequently described in literature. Amongst others, Polidoro et al. (2015); Guanche et al. (2015); Vanneste and Troch (2012); Cantelmo et al. (2010); Muttray and Oumeraci (2005); Burcharth et al. (1999) provide the base of literature analysed for wave propagation and pressure distribution in rubble mound breakwaters. In Muttray and Oumeraci (2005) and Cantelmo et al. (2010) an overview is given of which some qualitative conclusions are summarized: The water surface elevation and pore pressure oscillations inside a breakwater decrease exponentially in direction of wave propagation Hall (1991); Muttray et al. (1995). Furthermore, larger wave height, wave period and structure slope cause water surface elevations, the pore pressure oscillations and the wave setup to increase. They decrease with higher permeability of the core material and with increasing thickness of the filter layer. The damping rate of pore pressure oscillations increases with wave steepness and decreases with increasing distance from the still water line. In addition, Van Gent (1993) states that for oscillatory flow the turbulent resistance is larger than under stationary flow conditions in the rubble mound.

To approach the pore pressure oscillations in rubble mound breakwaters Burcharth et al. (1999) and Troch et al. (2002) proposed an exponential damping in the form of equation 4.1. The exponential decrease has been confirmed by in field measurements (Troch et al., 1997). However, the configuration used by Burcharth et al. (1999) with an open rear face of the breakwater differs significantly with the design of a sand retaining rubble mound structure (Polidoro et al., 2015).

$$P(x) = P_0 \exp\left(-K_d \frac{2\pi}{L'} x\right) \tag{4.1}$$

P_0 = Pore pressure amplitude (x=0); $P(x)$ = Pore pressure amplitude (x);
K_d = Dimensionless damping coefficient; L' = Wave length inside the structure [m]

Muttray and Oumeraci (2005) continues that pore pressure oscillations and oscillations of the water surface (wave height) are closely linked. Biesel (1950) derived theoretically that a linear relation can be found between the wave height at a specific location and the corresponding pore pressure oscillation at a certain level below SWL (Muttray and Oumeraci, 2005). The researchers in this study evaluated and compared the wave damping process over a breakwater with linear, quadratic- and polynomial damping relations by means of comparing them to measured data from the Large Wave Flume (GWK) in Hanover. The set up from which the used data set originates(Muttray, 2000) is given in figure 4.4a and a typical representation of the measured outcomes is given in figure 4.4b. The results of the obtained descriptive theories are summarized below:

- Linear damping:
  The Forchheimer equation is used to approximate damping linearly: it gives a reasonable fit and is subjected to easy computations.
- Quadratic damping:
  The Forchheimer equation is used to approximate damping quadratically: this does not give a better fit than the linear method, and the method involves more complex computations.
- Polynomial damping:
  The Forchheimer equation is used to approximate damping by means of polynomials: this does give better results than linear approximation but not very different. However, it does represent the governing processes better. Similar to the quadratic method it involves more complex computations.

*For further explanations are found in Muttray and Oumeraci (2005).

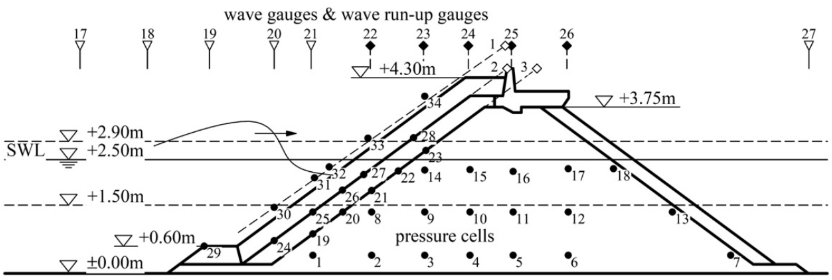

(a) Cross-section GWK breakwater model.

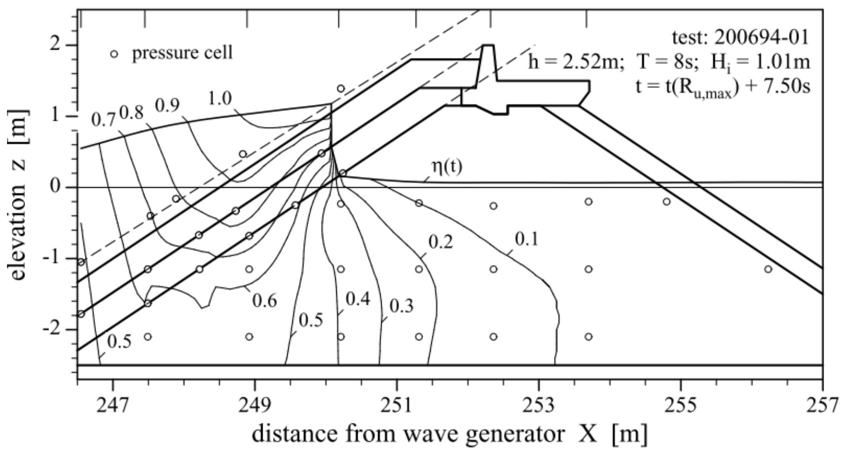

(b) Typical results of the hydraulic model tests just before max. wave run-up.

Figure 4.4: Model and results of the GWK model tests (Muttray and Oumeraci, 2005).

However, also the configuration evaluated by Muttray and Oumeraci (2005) does not account for a closed body at the lee side of the breakwater either, such as the theory proposed by Burcharth et al. (1999). The calculations approximating the pressures inside the breakwater are concluded to be more accurate (Muttray and Oumeraci, 2005). Vanneste and Troch (2012) adds that although the results proved that wave damping was described in these approaches, an empirical correction was needed to compensate for the shortcomings of the theoretical approach on which the theory is based. Furthermore, Burcharth et al. (1999)'s method is the only practical calculation method as for Muttray and Oumeraci (2005)'s method the Forchheimer coefficients should be determined experimentally (Vanneste and Troch, 2012). (The Forchheimer is further elaborated on in section 4.2.1). The fact that the configuration with a closed face was not tested (and pessimistic outcome of wave decay in these models) justified a physical model for Polidoro et al. (2015). This last author emphasizes the importance of an open rear face when modelling sand retaining structures under wave action for future research.

Case study indication of appearing gradient

Also Vanneste and Troch (2012) evaluated the (pore) pressure damping in rubble mound breakwaters. The authors developed an empirical calculation model for the spatial distribution of the wave-induced pore pressure height in the core of conventional rubble mound breakwaters. The method is based on the above discussed theoretical and experimental knowledge and calibrated by means of non-linear regression to the Large Wave Flume (GWK) model data, also used in Muttray and Oumeraci (2005). In the model a distinction is made for small to medium-sized wavelengths ($kh \geq 0.5$) and long waves($kh \leq 0.5$) and, the model has an empirical calibration for regular and irregular waves. The generality is determined by applying the calculation model to a data set from tests on a scale model in the wave flume at Ghent University (Belgium). The method provides the the spatial distribution in non-overtopping and non-breaking conditions without considering material properties related to porous flow resistance of the core, although it is stated that material properties have some influence on the porous flow resistance. Some differences occur in the obtained damping coefficients between the prototype and model data which are, by the authors, attributed to these differences in porous flow resistance. It is proposed that these parameters can be calibrated to specific core materials likewise as is done with the porous flow coefficients a, b and c in the Forchheimer equation, see section 4.2.1. According to the authors their new model predicts the pore pressure height attenuation with higher accuracy than the model by Burcharth et al. (1999), in a broad range of wave conditions.

In appendix A.1.1 the formulas and coefficients for the model of Vanneste and Troch (2012) are presented to obtain predictive outcomes for the appearing hydraulic gradients in reality. This is done for the GWK model. Also, the measured hydraulic gradients from the scale model tests by Polidoro et al. (2015) are approached with the calculation model by Vanneste and Troch (2012). Here, case 03 and case 09 are considered which are cases representing normal and storm conditions respectively. These cases are also highlighted in the paper by Polidoro et al. (2015). An area of interest is defined enclosing the lower inner corner of a breakwater. In this area, the maximum appearing hydraulic gradients for the maximum load condition by Vanneste and Troch (2012) and two load conditions by Polidoro et al. (2015) are calculated. The measured gradients from Polidoro et al. (2015) represent 98% non-exceedance values at locations given in fig. A.2. The results are given for horizontal and vertical gradients and summarized in table 4.1.

Table 4.1: Predictive outcomes of appearing gradients for model loading, calculated with Vanneste and Troch (2012).

	Vanneste GWK model	Polidoro case 03 (normal)	Polidoro case 09 (storm)
h (depth) $[m]$	2.5	12.75	12.75
$H_{inc}[m]$	0.7	3.0	5.8
kh	0.44	0.87	0.74
$I_{calc,max,hor}[m/m]$	0.02	0.016	0.032
$I_{calc,max,ver}[m/m]$	0.04	0.039	0.080

In addition, the applicability of the calculation model by Vanneste and Troch (2012) is tested on the measured results of the research by Polidoro et al. (2015). Although some simplifications needed to be made, it is suggested that there is potential for general applicability of the calculation model. The results are given in table 4.2. It can be seen that specifically at larger depths, e.g. $-z/h < -0.7$, the model is fairly accurate, at intermediate depths the model underestimates the appearing gradients. The difference might be caused by the fact that the research by Vanneste and Troch (2012) is executed with an open interface with water at the inner slope whereas the study by Polidoro et al. (2015) the inner slope is a impermeable boundary. Furthermore, from Polidoro et al. (2015) only little data is available, and interpreted from a the paper. Here gradients are given. The study by Vanneste and Troch (2012) results in pressures. A accurate evaluation of the method and prediction-capabilities can be made when both studies by Vanneste and Troch (2012) and Polidoro et al. (2015) are available with all test details and both data sets. This is however not further studied in the current research. The obtained data in the table provides some insight in the forces appearing in the lower inner conner of the breakwater which can be used as design guidelines.

Lastly, it is noted that the studies by Burcharth et al. (1999) Muttray (2000), Muttray and Oumeraci (2005) and Vanneste and Troch (2012) are all based on or validated with the datasets obtained in small and large scale model tests by Burger et al. (1988) executed in the Large Wave Flume (GWK) in Hannover or with the measurement results from the Zeebrugge breakwater (Troch et al., 1997). The resemblance in the different researches is therefore not particularly surprising and to strengthen the general applicability more (model) data sets, (potentially) available from industry projects can be used, such as the dataset by Polidoro et al. (2015).

Table 4.2: Measured appearing gradients by Polidoro et al. (2015) and calculated estimations with Vanneste and Troch (2012).

depth $[mCD]$	z/h $[-]$	x $[m]$	$I_{\text{Case 03, meas}}$ $[m/m]$	$I_{\text{Case 03,calc,max}}{}^{*}$ $[m/m]$	$I_{\text{Case 09,meas}}$ $[m/m]$	$I_{\text{Case 09,calc,max}}{}^{*}$ $[m/m]$
-4.5	-0.53	25	0.031	0.008	0.061	0.012
-5.5	-0.61	26.5	0.020	0.006	0.040	0.011
-6.5	-0.69	28	0.014	0.008	0.022	0.010
-7.5	-0.76	29.5	0.012	0.010	0.020	0.014
-8.5	-0.84	31	0.014	0.015	0.025	0.024

*The maximum gradient is taken, which was horizontal or vertical depending on z/h and x.

4.1.2. Quasi-static Hydraulic gradients

The load regime of unidirectional flow can have various causes and results in quasi hydrostatic pressures. These arise due to head differences over the structure. These head differences can have various causes. The causes have their own specific time scales which might be periodic. An example are tidal differences: In areas where a large tidal amplitude is present the water level at the ocean side of the structure may vary over $1-7m$ over a period of ± six hours. This tidal oscillation might be approached as a quasi-static water level or as a very high period wave, depending on the time scale of porous (Darcy) flow through the sand body. Furthermore, quasi-static hydraulic gradients over the structure may arise through an increased phreatic level in the sand-fill due to excessive precipitation or due to hydraulic set-up from the ocean side. In both case the time scale of the drainage of the sand body is much larger than the reduction of the water level at the ocean side of the structure.

4.1.3. Internal set-up

A frequently observed phenomenon in breakwaters which influences the pressure distribution and flow patterns is the internal set-up. The internal set-up means that the water table inside the breakwater is higher than the still water level outside. The cause of this is fairly simple: Outflow of water mainly happens in the lower part of the slope, where the water has to flow through a smaller area than during inflow. This requires a higher pressure gradient, realized by a higher water level inside (Ockeloen, 2007). This theory is supported by the pressure distribution given in figure 4.3b.

4.2. Porous flow

Prior knowledge

In this section the Reynolds-Averaged Navier-Stokes (RANS) equations (A.5) are used which are derived in appendix A.2. Furthermore, in the appendix is explained how, the RANS equations can lead to the incompressible Euler relations(4.2). The practical application of the latter is found in the fact that an (de-)acceleration of a fluid results in a pressure variation.

$$\rho\frac{D\vec{u}}{Dt} + \nabla P = 0, \qquad \frac{\rho}{Dt} = 0, \qquad \nabla \cdot \vec{u} = 0. \tag{4.2}$$

Porous flow

Flow through a granular medium like sand, gravel or stones is often described as porous flow. The porous medium is subjected to loads due to soil-on-soil (gravity) and soil-water interactions. The latter is considered by means of pressures or velocities. For example, a hydraulic head difference across an impervious structure imposed on permeable soil causes for a flow through the bearing material and possibly causes erosion and instabilities. The governing loads and failure mechanisms are elaborated in sections 4.1 and 4.3 respectively. To counteract or provide resistance to the loads and possible failures different protections can be installed to decrease the porous flow velocities inside the medium such as granular filters or geotextiles. For a complete consideration of the various processes a distinction is made between laminar and turbulent flow. Flow in fine materials like clay and sand is always laminar. This implies that pressure and velocity are related linearly. In coarse(r) media turbulent flow is usually making computations more complicated.

The ability for flow through a porous medium is often related to the porosity 'n', given by the volume of voids divided by the total volume. The volume of voids and therefore the porosity, is generally not easily determined by means of a formula combined with simple input parameters such as the characteristic particle size. The porosity of a (sample of) material depends amongst others on the gradation of particles, consolidation and clogging by suffusion* or by leaching* with other materials (Bendahmane et al., 2008) (Polidoro et al., 2015). However, porosity can be approached in various ways if a representative sample of the medium is available. It should be noted that for flow calculations the effective porosity 'n_e' should be used where the total volume of voids is replaced by the volume of voids that is interconnected and transmitting flow (Fitts, 2013). Furthermore, with processes like suffusion and leaching in mind, the porosity of a medium subjected to flow can vary in time and space. The porosities for quarry rock material as used in breakwaters, often range between $n_f = 0.3 - 0.52$ (Hannoura and McCorquodale, 1985) and Vanneste and Troch (2012) describes 0.39 and 0.4 for the GWK and UG-model tests.

* (The difference between leaching and suffusion is defined in section 4.3.2).

4.2.1. Hydraulic Resistance: Forchheimer equations

Going from the Reynolds-Averaged Navier-Stokes equation (A.5) to a practical applicable formula some simplifications are made. Within a porous medium an average flow velocity through the medium or filter is obtained. The area of actual flow is equal to the porosity. $u_{\text{filter}} = n_e \cdot u_{pore}$. Using the (average) filter velocity, the velocity differences over the pore geometry lose their physical meaning and are replaced by a coefficient multiplied with the filter velocity. Furthermore, a quadratic friction term is chosen to cover all square inertia and turbulence terms. Lastly, the viscous gradient is substituted by a linear friction term, resulting in equation 4.3 which for stationary flow is known as the classical Forchheimer-equation (Schiereck and Verhagen, 2016) or for non-stationary flow as the extended Forchheimer-equation (Van Gent, 1993) (Muttray and Oumeraci, 2005):

$$\frac{1}{\rho g}\frac{\partial p}{\partial x} = i = au_f + bu_f \mid u_f \mid + c\frac{\partial u_f}{\partial t}$$
$$a = K_a \frac{(1-n_e)^2}{n_e^3}\frac{\nu}{gd^2}\,; \quad b = K_b \kappa_0 \frac{1-n_e}{n_e^3}\frac{1}{gd} \quad \text{and} \quad c = \frac{1}{n_e g}\left(1 + K_M \frac{1-n_e}{n_e}\right) \tag{4.3}$$

Various methods have been derived to explain and estimate the K_a, K_b, κ_0 and K_M- values. A comprehensive overview of the research done on the above mentioned parameters and explanatory notes can be found in Muttray and Oumeraci (2005). However, in the current research is chosen to follow the approach by Van Gent (1993). This results in a K_a of 1000 and K_b of 1.1 when d_{n50} is used as characteristic particle size. However, some care should be taken using this theory. The non-dimensional coefficients might differ for various types of stones. It may well be possible that parameters such as grading, aspect ratio or shape must be implemented in the expressions. Additionally, van Gent states that the angle of attack between flow and particle is of possible influence on the equation. It should be understood that approaching porous flow through coarse granular material is a very complex matter, even for stationary flow and that the existing formulae are oversimplified. Especially the influence of measured porosities which are incorporated to a certain power, can cause for large errors in the final expressions (Van Gent, 1993).

Following Van Gent (1993) coefficient κ_0 is found to be unity for stationary flow whereas for oscillatory flow κ_0 is inversely proportional to the Keulegan-Carpenter number $KC(=\tilde{v}_f T/(n_e d)$, with velocity amplitude $\tilde{v}_f$ and period T). Experimentally, coefficient κ_0 is determined to be $1+7.5/KC$. However, the velocity amplitude is given as the maximum orbital velocity measured at distance d_{f50} above the filter layer and is therefore hard to approximate. K_M is a non-dimensional coefficient introduced to consider the phenomenon of "added mass". To accelerate a certain volume of water within a porous medium a larger amount momentum is needed than outside the medium, this is called "added mass". K_M will be 0.5 for potential flow around an isolated sphere and 1.0 for a cylinder. For densely packed porous medium coefficient K_M needs to be determined experimentally, as it can not be derived theoretically. However, for a rubble mound Van Gent (1993) proposed an empirical relation given in 4.4. It should be noted that with small velocity amplitudes $\tilde{v}_f$ and long periods T, the K_M value becomes negative and is physically meaningless.

$$K_M = max.\left\{0.85 - 0.015\frac{n_e g T}{\tilde{v}_f};0\right\} \tag{4.4}$$

When the filter velocity can not be determined analytically or numerically, Muttray (2000) proposes to estimate the filter velocity by means of a formula for $\bar{u}_f$ with input $H(x)$, T, k' (internal wave number), h and n (see (Muttray and Oumeraci, 2005)).

$$\bar{u}_f(x) = \kappa_v H(x) \qquad \text{With:} \qquad \kappa_v = \frac{n}{\pi}\frac{\omega}{k'h}\left[1 + \frac{2}{\pi}\left(1 - \frac{\cosh k'h}{\cosh 1.5k'h}\right)\right] \tag{4.5}$$

$$H(x) = \text{Local wave height[m]}; \qquad \omega = \text{Wave frequency[rad/s]};$$
$$k' = k\sqrt{1.4} \quad \text{(Internal wave number}[m^{-1}]\text{ (Burcharth et al., 1999))}$$

The local wave height $H(x)$ in equation 4.5 can be approached by the linear, quadratic or polynomial relations described in Muttray and Oumeraci (2005). Furthermore, a simplification of the forchheimer equation (4.3) can be considered as for typical breakwaters the quadratic term is dominating over the inertia term (Burcharth et al., 1995). In the experiments by Vanneste and Troch (2015) the theoretical contribution of the inertia term for "regular breakwaters" is < 10% in the core and < 20% in filter layers. Therefore, depending on the processes of interest, the third term at the right-hand side can be considered negligible.

4.2.2. Laminar flow

Considering flow through soil bodies with small particles such as sand, flow is generally laminar. Laminar flow is carefully evaluated in appendix A.3.1 as it is considered one of the main loading conditions defined in section 4.1. The most important results are summarised below.

Laminar flow can be described by a simplified form of the Forchheimer relation given in equation 4.6. In this case coefficient 'a' is inversely proportional to the hydraulic conductivity [K] presented in Darcy's Law (Fitts, 2013), given in equation 4.7a.

$$\frac{1}{\rho g}\frac{\partial p}{\partial x} = i = a u_f \tag{4.6}$$

Every porous medium has a characteristic value of its hydraulic conductivity and can vary in three dimensions for (non-) homogeneous and (an-) isotropic soils. In this research the hydraulic conductivity is taken as constant in all directions. With use of equation 4.7 and flow net theory the hydraulic gradients in the sand body can be determined, providing load conditions for potential internal erosion of the sandfill within accuracy of $10-20\%$ (Fitts, 2013).

$$\frac{1}{\rho g}\frac{\partial p}{\partial x} = i = \frac{dh}{dx} = -\frac{Q_x}{A}\cdot\frac{1}{K_x} \tag{4.7a}$$

$$Q_x = K\cdot\frac{dh}{dx}\cdot\frac{n_s}{n_h} \tag{4.7b}$$

When an interface is considered with two materials with different hydraulic conductivities, the flow net deflects at the interface. In ideal situations with un-stratified soil deposits general transfer conditions can be applied as described in NPTEL- Advanced Geotechnical Engineering (2014). In appendix A.3.1 an explanatory overview is given with figures. With large ratios of hydraulic conductivities of two materials at an interface, the streamlines will strongly deflect at this interface resulting in a flow nearing parallelism or perpendicularity with the interface. Ranjan and Rao (2007) quantifies this by stating that if the hydraulic conductivity of the core material is over ten times larger than the hydraulic conductivity of the sand; the core material can be assumed to be equal in conductivity or resistance as the fluid which is flowing. For this research particularly this implies, the core can be assumed to be non existent if $k_{core}/k_{sand} > 10$ and the core is assumed an discharge face or upstream face. From this theory it can be reasoned that when the core material is taken as primary material, the interface with the sand can be assumed as a closed wall. This would result in, the assumption that perpendicular flow through the interface can be assumed zero, based on hydraulic conductivity. This is however, a hypotheses.

4.3. Sandfill migration

In this chapter migration of sediments in sand retaining rubble mound structures are described. Migration is in this case the defined as the occurrence of transport of materials which can cause instability of the rubble mound initiated by hydraulic loads.

4.3.1. Threshold of motion

In general, instability of a particle is caused by an imbalance of forces. The resistance forces acting on a grain are the gravitational force due to its own weight and the friction force. The loads are induced by flow and result in a drag, shear and lift force (Schiereck and Verhagen, 2016). The forces are indicated in figure 4.5. When an imbalance is found between the load and the resistance the grain starts moving. If a grain subjected to flow is just in balance the corresponding velocity is called the critical velocity.

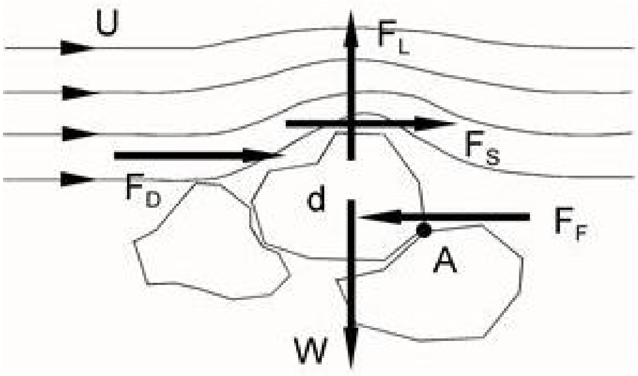

Figure 4.5: Forces on a grain in flow (Schiereck and Verhagen, 2016)

The drag, shear and lift force are given by formula 4.3.1 in which C_i are coefficients of proportionality an A_i are the exposed surface areas. All forces are proportional to the velocity squared in a place somewhere in vicinity of the grain.

$$\left.\begin{array}{rl} \text{Drag force:} & F_D = \frac{1}{2} C_D \rho_w u^2 A_D \\ \text{Shear force:} & F_S = \frac{1}{2} C_S \rho_w u^2 A_S \\ \text{Lift force:} & F_L = \frac{1}{2} C_L \rho_w u^2 A_L \end{array}\right\} F \propto \rho_w u^2 d^2$$

The stability criterion are simple as they represent an equilibrium of forces in horizontal and vertical direction, and a moment equilibrium. Formula 4.3.1 represents these relations.

$$\left.\begin{array}{ll} \sum H = 0: & F_{D,S} = f x W = F_F \\ \sum V = 0: & F_L = W \\ \sum M = 0: & F_{D,S} \cdot O(d) = W \cdot O(d) \end{array}\right\} \rho_w u_c^2 d^2 \propto (\rho_s - \rho_w) g d^3$$

The velocity used in these formulas is the critical velocity u_c since there is dealt with stability relations Schiereck and Verhagen (2016). When the critical velocity is exceeded the stability of the grain can not be assured. The threshold of motion of grains or particles can be approached with various methods. A distinction is made between forces and corresponding transport induced by parallel flow and forces and corresponding transport induced by perpendicular flow. In general, for parallel flow, the velocity difference at the interface between the free flow stream and grains of the material is considered. Two main approaches are possible: The *Izbash* approach in which the forces on the individual grain are considered. And the *Shields* approach in which the friction force caused by the water on the bed is considered (Schiereck and Verhagen, 2016). For perpendicular flow, often a hydraulic gradient over the interface needs to exceed a certain threshold to initiate the transport, sometimes referred to as the fluidisation condition. The stability approaches by *Shields* and *Izbash* are further elaborated on in appendix A.4.1.

4.3.2. Leaching and suffusion

In the proposed design of a sand retaining rubble mound breakwater Leaching and suffusion may occur if conventional filter rules- to ensure the stability of the structure- are not applied. The conventional filter rules are explained in section 4.4. In this research leaching and suffusion are defined as stated by Schürenkamp et al. (2014) and Bonelli et al. (2007). It should be noted that amongst others the work by Polidoro et al. (2015) uses other definitions. Leaching is the process where material of smaller size is carried by a fluid through the pores of the material in the adjacent layer. Suffusion is a form of internal erosion, which involves selective erosion of fine particles from the matrix of coarser particles. The fine particles are removed through the voids between the larger particles by seepage flow, leaving behind an intact soil skeleton formed by the coarser particles. The process of leaching is especially encountered in wide graded materials and only when the critical load to move the smaller particles is met (Allsop and Williams, 1991). Wide graded, or gap-graded, material is frequently used in rubble mounds because of blasting in quarries. In the considered case a sand body is retained by a rubble core. This can be interpreted as a very wide (gap-) graded material in which the small particles are most probably able to migrate through the pores of the rubble material. According to Allsop and Williams (1991) many wide graded mixtures can become unstable under both steady and non-steady flows. Furthermore, the stability of the the mixture will depend on the geometric restrictions given by the grading curve and by the hydraulic forces, generally given by the hydraulic gradient. With the geometrics in mind, the combination of sand and rubble material might be unfavourable however, the hydraulic forces may be small enough to cause stability of the structure. Likewise, the critical load inside the sand body should be met for incipient motion. Polidoro et al. (2015) uses the term suffusion for a well mixed composite grading of sand and core material. In this this manner they regard leaching of two materials as suffusion. Kovács (1981) proposed three basic conditions for suffusion by means of Hazen's uniformity coefficient, $C_u = d_{60}/d_{10}$ for well mixed materials. This is later complemented with a indication of the critical hydraulic gradient i_{cr}.

No suffusion	$C_u < 10$	$i_{cr} = 0.3 - 0.4$
Transition	$10 \leq C_u \leq 20$	$i_{cr} = 0.2$
Probable Suffusion	$20 > C_u$	$i_{cr} = 0.1$

This approach is however, highly simplistic and it can only be used as estimation. A more sophisticated approach is desirable (Allsop and Williams, 1991). Kenny and Lau (1985) described a method originally from Lubochov which uses the grading of a material as input to calculate the potential of instability of a material. This method is extended by Adel et al. (1988) by adding the critical hydraulic gradient and work by Allsop and Williams (1991) suggested a precautionary approach leading to the final method. The method calculates for every size 'D' along the grading curve the fraction 'F' under size 'D' and fraction 'H' between 'D' and '$4 \cdot D$'. At the minimum of the resulting H-F curve the potential instability is indicated. Allsop and Williams (1991) therefore proposed the relation to the critical hydraulic gradient as given in equation 4.8.

$$i_{cr} = 0.25 \cdot (H/F)_{min} \tag{4.8}$$

To use this function for leaching of a material through another material, such as sand through the rubble mound core, a composite grading should be calculated. Afterwards, the composite grading might be able to be used in suffusion theories as described above. This assumption is based on the fact that suffusion theory is developed on gap-graded materials and sand mixed with rock materials in this case is considered as a gap graded material. As an example the, composite grading and H-F "stability" curve are shown for the research by Polidoro et al. (2015) in figure 4.6. The obtained H-F minimum is at $F = 0.3$ and $H = 0.042$, which results in a critical hydraulic gradient for suffusion of $0.25 * (0.042/0.3) = 0.035[m/m]$.

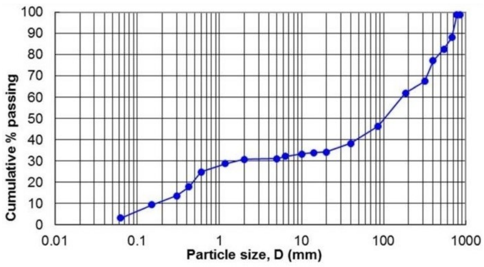

(a) Composite grading core + sand.

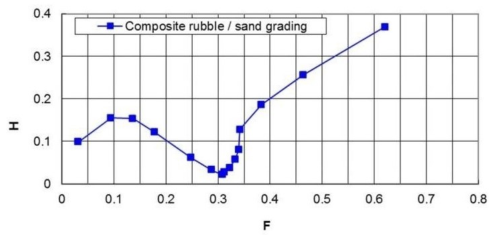

(b) H-F "stability" curve for composite grading.

Figure 4.6: Suffusion theory by Allsop and Williams (1991) for composite grading (Polidoro et al., 2015).

Care should be taken that in the recent study by Polidoro et al. (2015) it is not considered that the sand has to be brought into motion from the sand body in the first place before suffusion of the composite material takes place. Lastly, the porosity and positioning of the stones and the local gradation is of strong influence to the motion of particles from the sand body and this might influence various processes. In the experiments by Adel et al. (1988) segregation of the (wide graded) material occurred influencing the process.

4.3.3. Internal erosion

Due to hydraulic head differences over the structure porous flow may occur through the sand body behind the core. This flow can be described by means of Darcy's theory and flow-nets as explained in section 4.2.2. When the flow exceeds a critical value for transportation sediment might travel with the flow (generally) outward, causing instability of the structure. Various processes are covered by the term "internal erosion". Also suffusion as described above is a form of internal erosion. A comprehensive overview is given by Bonelli et al. (2007) and is summarised in appendix A.4.2.

4.4. Filter design

A rubble mound breakwater or sand retaining structure is subjected to various hydraulic loads as described in section 4.1. The design of the structure is optimized to protect the object behind against these forces induced by the water. Often a highly permeable outer layer is used to dissipate the energy of attacking waves. The amour layer is supported by one or multiple under layers which further decrease the hydraulic loads before reaching the core material. Considering a sand core, sand retaining structure or a foundation of soil, water induced forces might reach the sand body through the permeable rubble mound. Currently, precautionary a filter is used to prevent erosion of soil particles through the permeable structure. These filters are geometrically closed or open and of granular material, or geotextiles. The general characteristics are elaborated in the section below. A typical cross-section of a sand retaining structure is given in figure 4.7.

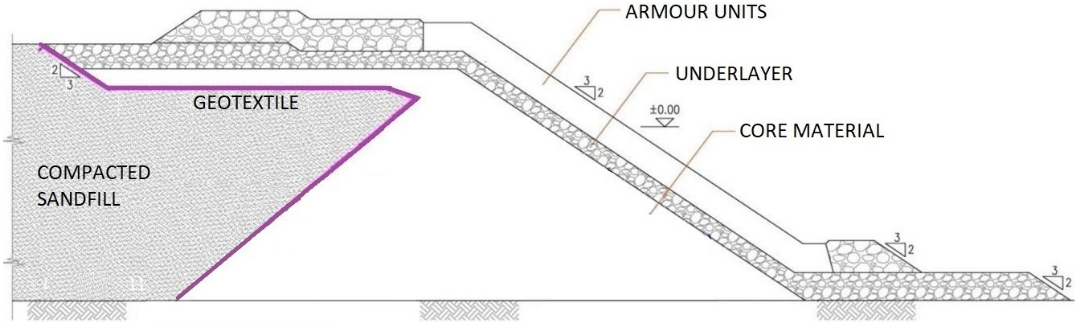

Figure 4.7: Typical cross-section of sand retaining structure (Polidoro et al., 2015)

4.4.1. Geometrically closed filters

Geometrically closed filters imply that the grains are packed in such a way that the space between the grains if much smaller than the grains themselves. For spherical grains with equal diameters this would mean that these spaces are approximately six times smaller than the grains themselves. With varying diameters of the grains the spaces between the grains are governed by the 15% smallest grains in weight, d_{15}. These spaces get clogged by the largest grains of the base layer, d_{85}, given that the base layer is internally stable. Internal stability is obtained by a sufficiently small grading of the core so that smaller grains are blocked by the larger ones. Furthermore, permeability should be guaranteed to prevent pressure build-up between the layers. Therefore, permeability of the filter layer should be larger than the permeability of the base layer. The empirical relations were initially defined by Terzaghi and are given in equation 4.9 (Schiereck and Verhagen, 2016). The relations are derived for filter types in which rock lay on top of sand on a horizontal bed for stationary uniform flow.

$$\text{Stability: } \frac{d_{15F}}{d_{85B}} < 5; \quad \text{Internal Stability: } \frac{d_{60}}{d_{10}} < 10; \quad \text{Permeability: } \frac{d_{15F}}{d_{15B}} > 5 \tag{4.9}$$

4.4.2. Geometrically open filters

On the contrary to geometrically closed filters, the grains of the different layers in geometrically open filters are able to migrate from one layer to the other. However, the design should provide that the occurring hydraulic gradient over the layers is smaller than the critical value for erosion. For perpendicular flow and parallel flow different criteria are considered. Regarding a base layer on top of the filter layer with downward flow perpendicular to the interface, gravity has an great influence on the porous flow. The finer base grains will simply erode through the filter layer. In this case the use of geometrically closed filters might be more appropriate. If the flow is upward and the filter layer is on top of the base layer the limit of erosion is governed by when the current force compensates the gravitational force (de Graauw et al., 1984). For perpendicular flow, the critical hydraulic gradient is roughly 1 from a vertical equilibrium (Schiereck and Verhagen, 2016). For perpendicular cyclic loading de Graauw et al. (1984) states that the (1st) stability relation in eq. (4.9) should no exceed 2 or 3 instead of 5 given for parallel flow.

Critical gradient as presented by de Graauw et al. (1983)
Considering parallel flow through the filter and base layer an empirical relation is derived by de Graauw et al. (1983), based solely on geometrical parameters. This theory holds for a filter placed on top of a sand bed. Combining Shields theorem (appendix A.4.1) and the Forchheimer equation (4.3) the experimental results lead to eq. (4.10) with u^*_{cr} being the critical shear velocity

$$I_{cr} = \left[\frac{0.06}{n_F^3 d_{15F}^{4/3}} + \frac{n_F^{5/3} d_{15F}^{1/3}}{1000 d_{50B}^{5/3}} \right] \cdot u_{cr}^{*2} \tag{4.10a}$$

With for sand as base material:
$$u^*_{cr} = 1.3 d_{50B}^{0.57} + 8.3 \cdot 10^{-8} d_{50B}^{-1.2} \tag{4.10b}$$

Like the Forchheimer equation, eq. (4.10) contains a term for the laminar part and the turbulent part, respectively the first and second term. Furthermore, relation 4.10 should be corrected with $\sin(\phi-\alpha)/\sin(\phi)$ for a filter on a slope (α) with ϕ being angle of repose and when combined with perpendicular flow the relation only holds when the perpendicular gradient is < 0.5 (Schiereck and Verhagen, 2016). For parallel flow under cyclic loading the critical filter velocities were found to be approximately the same, confirming that the inertia term from the Forchheimer equation is of minor importance (de Graauw et al., 1984). However, initially the hydraulic gradient increased with decreasing period whereas the material packing increased. de Graauw et al. (1984) states that apparently the cyclic flow caused hydraulic compaction leading to an increased hydraulic gradient. For perpendicular flow this is not the case. Here de Graauw et al. (1984) found that for both fine and coarse sand the critical gradient appeared to be lower for cyclic loading ($d_{50f} \leq 3to5d_{50b}$ for steady flow and $d_{50f} \leq 2to3d_{50b}$ for cyclic flow).

To obtain some insight in the order size of critical hydraulic gradients the critical gradient for the nominal (defined as: "average geometry") breakwater given in Polidoro et al. (2015) is determined. After de Graauw et al. (1983), $I_{cr} = 0.018[m/m]$. In experiments by Wolters and Van Gent (2012) the theory of de Graauw et al. (1983) is proven to be somewhat conservative and a ratio of $I_{\text{Wolters}}/I_{\text{de Graauw}} \approx 3$.

Critical gradient as presented by Klein Breteler (1989)
Klein Breteler (1989) and Klein Breteler et al. (1992) propose other formulas as a transport criterion, which estimates the critical filter velocity. In the experiments a (horizontal) steady flow through a granular filter on top of a sand bed is analysed. The beginning of transport was defined for two base particle sizes. For the smaller size, the relations are given in eq. (4.11) in which c and m are coefficients based on the characteristic grain size. The coefficients are given in appendix A.5.1 in fig. A.8. The formula for larger sediments size not presented as this is not of interest in this research. . The obtained critical filter velocities can be inserted in the Forchheimer equation resulting in an estimation of the critical filter gradient (Wolters and Van Gent, 2012). The method is verified with physical modelling with a major part on sand filter material with a steep grading curve (Wolters, 2012). Furthermore, Wolters (2012) concludes that Klein Breteler found a reduced erosion development for a sloped filter structure compared to a horizontal filter one. This seems to be caused by the combined occurrence of various loading components: currents along the interface, parallel and perpendicular gradients to the interface, gravity component along the interface and unsteady flow. The use of design guidelines for a horizontal interface are thus assumed to provide conservative outcomes when applied for a sloped structure (Wolters, 2012). Equation 4.11a is developed for steady flow, parallel to a sloped interface and eq. (4.11a) is developed for steady flow, partly parallel and partly perpendicular to a sloped interface, with $i_\perp \leq 0.5$ with α and ϕ being the slope and angle of repose respectively.

$$u_{f,cr} = \left[\frac{n_f}{c} \left[\frac{d_{f15}}{\nu_w} \right]^m \sqrt{\psi \cdot g \cdot \Delta_b \cdot d_{b50} \left(\frac{\sin(\phi - \alpha)}{\sin(\phi)} \right)} \right]^{1/(1-m)} \quad \text{for} \quad 0.1mm < d_{b50} < 1mm \tag{4.11a}$$

$$u_{f,cr} = \left[\frac{n_f}{c} \left[\frac{d_{f15}}{\nu_w} \right]^m \sqrt{\psi \cdot g \cdot \Delta_b \cdot d_{b50} \left(\frac{\sin(\phi - \alpha)}{\sin(\phi)} - \frac{i_\perp}{\Delta_b(1-n_b)} \right)} \right]^{1/(1-m)} \quad \text{for} \quad 0.1mm < d_{b50} < 1mm \tag{4.11b}$$

It is stressed that the use of the Forchheimer equation is more complex in case of wave loading as more information (velocity amplitude and wave period, or KC-number) are needed. The critical filter velocity for the nominal breakwater by Polidoro et al. (2015) $u_{cr} = 0.0111[m/s]$ for flow parallel to the horizontal bed and $u_{cr} = 0.017[m/s]$ for flow parallel to a sloped bed.
According to Wolters and Van Gent (2012) the above made calculation would result in larger values I_{cr} than the method by de Graauw et al. (1983). However, in the basic calculations in this research the opposite appears to be true. It is suggested that this difference can be attributed to the fact that in this research the core material of a breakwater is used as filter material and thus this material is rather large. This causes the laminar contribution term in the Forchheimer equation to approach zero. This term is dependent on the critical filter velocity and Forchheimer coefficient 'a'. $u_{f,cr} \sim d^{0.075}$ and $a \sim d^{-2}$ which implies using larger stones decreases the contribution of this term significantly. Furthermore, the nominal breakwater core is (very) wide graded while the theory by Klein Breteler et al. (1992) is especially verified for steep gradings.

4.4.3. Hydraulically sand-open filters

With an even larger size difference between the grains in the filter layer and the grains in the under layer, the filter layer is not considered stable. Although the loading is reduced by the filter, transport of grains of the under layer will take place during design loading. However, if the erosion is known beforehand and the necessary maintenance is accepted to repair the structure, this filter layer can turned more economic as less different filter layers are needed. Such a filter is called a hydraulically sand-open filter (Ockeloen, 2007).

4.4.4. "Unconventional" geometric filters

Although the above stated relations are considered to be the conventional (geometric) filter rules, also the suffusion theory by Kenny and Lau (1985); Allsop and Williams (1991) as discussed in section 4.3.2 is proposed as filter criterion, when applied to a mixture of sand and rocks. In compliance with conventional geometric filter rules exclusively geometric characteristics determine whether transport is possible or not. Whether or not the suffusion theory by Kenny and Lau (1985) is considered an open or closed filter rule depends on the grading of the material. The more sophisticated approach by Allsop and Williams (1991) is always an geometrically open filter rule, as a critical gradient is calculated.

4.4.5. Geotextile

Geotextiles can have many different applications throughout civil engineering, including application as a replacement for (a series of) filter layers. The synthetic sheets are placed as a particle tight boundary between a sand body or foundation and the permeable structure (e.g. rubble mound). The geotextiles have to comply with a retention, permeability and anti-clogging criteria like granular filters and meet survivability and durability requirements both during installation and operation. More information on these criteria is given in appendix A.5.2.

4.5. Models and Scaling

In the design of any model various undesirable potential influences should be considered. Firstly, scaling effects can cause inaccuracies in the results obtained by physical model test. Furthermore, during prototype (true size) experiments effects due to the limited size of the test facilities can play a role such as wall effects and the (in)ability to match design boundary conditions. Lastly, in numerical models mathematical limitations might influence test results. The scale parameter gives the length scale factor on which experiments are executed: $\lambda = L_P/L_M$ in which L_P and L_M are the characteristic length scale of the prototype and the model respectively.

4.5.1. Hydraulic scale model

Scale effects are inherent in any hydraulic model of wave structure interaction due to the inability to simultaneously obtain equality of Froude, Reynolds and Weber criteria, see eq. (4.12) (Hall, 1991). Therefore, to approach physical behaviour in scale models it is important to scale the parameters with respect to the governing forces. When gravitational forces are dominant scaling with Froude is often used whereas when viscous forces (and drag) are dominant Reynolds similarity is used. Scaling with a similarity requirement implies that the selected "number" remains of the same order magnitude in the scale model and in the prototype. The most common similarity relation are summarised below:

$$Fr = \frac{u}{\sqrt{gL}}; \quad (4.12a) \qquad Re = \frac{uL}{\nu}; \quad (4.12b) \qquad We = \frac{\rho u^2 L}{\sigma}; \quad (4.12c)$$

$$KC = \frac{\tilde{v}_f T}{L}; \quad (4.12d)$$

L = characteristic length;* u = velocity; H = wave height; L_0 = deep water wavelength; α = slope;
$\tilde{v}_f$ = velocity amplitude; ν = viscosity; σ = surface tension; T = wave oscillation period;

*Note that the characteristic length should be assessed separately for every function, object and situation

Froude (Fr)

The Froude number is a dimensionless number expressing the ratio of inertial force over gravity force, given in eq. (4.12a). The Froude number expresses amongst others the transition between subcritical($Fr < 1$) and supercritical flow($Fr > 1$). Froude similarity is especially suited for models where friction effects are negligible, provided that the filter velocity is the same (Heller, 2011). For a Froudes model law scaling also the Keulegan-Carpenter (KC) number will be identical in model en prototype scale.

Reynolds (Re)

Together with the Froude number, the Reynolds number(eq. (4.12b)) is used to explain whether flow is laminar or turbulent. The Reynolds number expresses the ratio of inertial force over viscous force. Reynolds similarity is applicable were viscous forces may be dominant e.g., laminar boundary layer problems or intake structures. For filters especially the Reynolds filter number is used (Hoffmans, 2012), given by $Re_f = (d_{f,50} \cdot \overline{u_{pore}})/\nu$. Laminar flow is found for $Re_f \leq 10$, transitional for $10 > Re_f < 1000$ and turbulent flow for $Re_f \geq 1000$.

Weber (We)

The Weber number given by equation eq. (4.12c) gives the ratio between the inertial force over surface tension force. This is particularly important for fluid interfaces such as thin film flow or bubble formation, cavitation and air-entrainment.

Keulegan-Carpenter (KC)

The Keulegan-Carpenter number gives the ratio between turbulent resistance and inertial resistance (Van Gent, 1993). Jensen et al. (2014) describes it as the ratio of the stroke of the oscillating motion to the size of the roughness. Forces on objects subjected to oscillatory flow are governed primarily by the KC-number. The resistance to flow is larger for cyclic motion than for steady flow. For KC number larger than ~ 50 the added resistance due to cyclic loading is usually negligible (Wolters, 2012). The latter author adds that at prototype scale $KC \geq 50$ thus the transport criterion for cyclic flow and stationary flow will be similar.

Re/KC

The Reynolds number expresses the importance of turbulent resistance versus laminar resistance, the Keulegan-Carpenter number expresses the importance of turbulent resistance versus inertial resistance. To obtain an expression for the magnitude of the inertial resistance relative to the laminar resistance in Van Gent (1993) a method is presented in which this relation is found by the quotient of the Reynolds- and Keulegan-Carpenter numbers: $Re/KC = L^2/(T\nu)$.

Geometry
Considering a rubble mound structure, not only the above mentioned kinematic and dynamic similarities are sometimes troublesome to reproduce (especially at the same time), ensuring geometric similarity can also be challenging. Especially in obtaining the correct permeability of the different layers on model scale for both core and base material. Considering base and filter layers, it is inconvenient to downscale granulates that are already very small on prototype scale such as sand. When for instance sand is downscaled to much clay-like granulates need to be used which have different cohesive properties. Hall (1991) stresses the importance of correct reproduced permeability of the different layers as (amongst others) this ensures correct scaling of the hydraulic gradient through different layers. Besides, downscaling of density can be challenging and the inability to scale gravity and atmospheric pressure will cause scale effects. The permeability difference between the scale model and the actual prototype will influence both the external flow (run-up and run-down elevations and velocities) and the internal flow (pore pressure, pore fluid velocity, and phreatic surface response) (Hall, 1991). According to Hall (1991) extra care should be taken when modelling the core of the rubble mound structure for above mentioned reasons. Furthermore, factors as air entrainment and two-phase flow may contribute to scale effects(Hall, 1991; Muttray and Oumeraci, 2005). In general, scale effects for a specific phenomenon increase with increasing scale parameter λ which implies λ should be small. However, the appropriate selection of λ is an economic, realizable and technical optimization and λ may intentionally be selected in a range where scale effects cannot fully be neglected (Heller, 2011).

4.5.2. Model considerations

As the research is focused on the lower inner corner of a breakwater, especially the processes in this region should be correctly reproduced. In order to do so, a strategy by Burcharth et al. (1999) is evaluated in which he proposes to retain the hydraulic gradient in the breakwater equal in the prototype and in the model at every location. Geometrical scaling of the used material might be necessary to increase the workability of the model and reduces its size. The downscaling of the chosen scalable material will cause for a general requirement for geometrical scaling of all other materials. The problem with linear geometric scaling which follows from Froude scaling is, that this may lead to much too large viscous forces corresponding with small Reynolds numbers especially in the under layers and core of small(er) scale models. Burcharth et al. (1999) suggest that not the gravity or viscosity are dominant driving mechanisms as given in Froude or Reynolds scaling, but the hydraulic gradient dominates the processes. Therefore like Hall (1991), Burcharth et al. (1999) stresses the importance of an equal hydraulic gradient in geometrically similar points, i.e. $I_P(x,z) = I_M(x,z)$. The method is however complicated, because the hydraulic gradient and (filter) velocity vary in space and time. This implies that the scaling of the core material is space and time dependent, which is obviously impossible (Burcharth et al., 1999). This theory is, however, used to correctly simulate the damping in the system over different layers. A different tactic is to try to keep the mobility of the interface equal, and impose an equal hydraulic loading. In both cases a limit arises when the sand granulates are downscaled to comply with the geometrical scaling of the core material the sand will have a decreased hydraulic conductivity and possible changing cohesiveness. Therefore, the porous flow characteristics sand are altered.

The potential scale effects due to increased viscous forces in the core material can be evaluated by means of the Reynolds number. If the Reynolds number stays above 10.000 (Dai and Kamel, 1969) the increased viscous forces are not necessarily a problem (Hall, 1991). According to the latter author, still no definitive limits for the onset of the turbulent regime in a porous medium have been established. However, the magnitude of the Reynolds number for which turbulent effects must be considered is much lower than initially found by Dai and Kamel (1969). For filter structures especially the Reynolds filter number is used by Hoffmans (2012) as described in section 4.5.1.

Lastly, Van Gent (1993) stresses the importance of certain parameters used in various researches described above, which can differ in further research. The theories, equations an process evaluations are described for a certain set of parameters such as porosity, diameter, grading, aspect ratio, shape (gross shape, roughness and surface texture) and orientation of the stones with regard to the direction of the mean flow which reduce the usability and reproducibility of a formula or theory.

4.6. Conclusion and research outline

In order to research the behaviour of the sediments at the interface to a rubble mound in a sandfill when subjected to hydraulic loading, the following conclusions were made from the literature study.

Considering loading in the research the focusses was on impacting flow conditions coming from wave activity. Although still interesting, the other loading regime(s) discussed in this literature study (being unidirectional, or gradually reversing (ground) water flow through the soil body) seems extensively researched and with the theory given in section 4.2.2, basic estimations can be found on the loading caused by this flow regime. The loading induced by wave activity is also extensively researched however, accurate predictions of the loading in the zone of interest are concluded still to be challenging. Burcharth et al. (1999) derived a practical model for pore pressure attenuation for open rear face breakwaters. Muttray and Oumeraci (2005) delivered more accurate results for the same breakwater configuration but with a more complex model (which needs some iterative calculations) and Vanneste and Troch (2012) developed an advanced calculation model, however also with many empirical coefficients and an open rear face breakwater. In the current study the applicability of these theories is questioned to the desired configuration in the zone of interest. Although not extensively evaluated, the calculation model by Vanneste and Troch (2012) does seem to make correct order size estimations of the closed rear face model tests by Polidoro et al. (2015). The results seem better at large depths ($z/h \geq -0.7$), but the current research foresees potential in matching these, and potentially other, studies. Furthermore, some datasets are available which provide order size estimations of appearing hydraulic gradients in breakwaters.

Considering the strength (resistance against movement) of the sediments at the interface to a rubble mound in a sandfill, in the desired configuration, less is known. The interaction of the core material with the sand from the sandfill is probably best described by the currently available geometrically open filter relations. The relations are however, mainly based on steady flow on a horizontal or sloped bed with a filter overlaying a sand bed and, the predictive relations are empirical. Although the general accuracy of the formula's is described positively by the authors, it does not represent the desired configuration in the zone of interest of the current research well. Also, the suffusion theory by Kenny and Lau (1985); Allsop and Williams (1991) is not yet tested for the desired configuration.

Although many different and diverse interesting research topics can follow from the above made analyses, it was concluded the most important gap of knowledge was found in the physical interaction between the hydraulic loads and resistance of sediments in correct representation of the geometry. In order to study this interaction, a physical scale model of an closed rear face breakwater with sandfill behind was proposed. The order size estimations made in the literature study showed that the appearing and critical hydraulic gradients were order size $0-0.04[m/m]$ and $0.01-0.04[m/m]$ respectively. The fact that the estimated critical and appearing gradient suggest a stable interface, demonstrates the potential for this specific research outline, as earlier proposed by Polidoro et al. (2015). The applicability of the estimation methods is still to be proven.

As described in section 4.5 many complex processes and inevitable unwanted effects are at hand when designing a hydraulic scale model. It is therefore desirable to eliminate as much complexity as possible. The desired scalable parameters are primarily:

- Hydraulic gradient
  - $[I_{calc}]$ both critical and appearing, $[I_{meas}]$ both critical and appearing, and ratio $[I_{cr,meas}/I_{cr,calc}]$, loading period $[T]$;
  - Ensuring the hydraulic gradients $I_P(x,z) = I_M(x,z)$;
- Core and sandfill characteristics
  - Porosity $[n]$, grading $[d_{10-90}]$, uniformity coefficient $[C_u]$ and (un)cohesiveness sand;
  - Filter parameter $[d_{f,15}/d_{b,85}]$;
  - Ensuring equal geometric properties of the interface in prototype and model;
- Velocity (of secondary interest)

  - Filter velocity [u_f], critical filter velocity [$u_{f,cr}$];
  - For studying possible velocity relations and scale effects;

Other important parameters which don't need, or can not be scaled are:

- Stability parameters
  - Shields parameter [Ψ], coefficients [c] and [m] (Klein Breteler et al., 1992), angle of repose [ϕ] and slope [α].
- Other parameters
  - Gravitational acceleration [g], density [ρ_w], [ρ_{stone}] and [ρ_{sand}] and kinematic viscosity [ν].

As stressed by Hall (1991); Burcharth et al. (1999) the hydraulic gradients should be equal in the prototype and the model at equal locations, $I_P(x,z) = I_M(x,z)$. The appearing hydraulic gradient is usually governed by geometric parameters (friction) and incoming wave conditions (loads). However, the literature study concludes that the pore pressure attenuation is still challenging to estimate. In this research only the appearing hydraulic gradient at initiation of transport is of interest, and not the pore pressure attenuation from wave impact towards the zone of interest. This enables to avoid complex wave scaling processes and approaching of filter velocities. The interface stability is described by means of geometric parameters resulting in a critical gradient. In theory, this gradient should be equal in prototype and model at the same locations when all geometric parameters are correctly scaled and, if the critical gradient is based solely on geometrical parameters. Also, in the current research the perpendicular gradient is assumed to be of very low influence based on the ratio of the hydraulic conductivity of the materials in the system, as discussed in section 4.2.2. In the research by Polidoro et al. (2015) dimensions are provided of a "nominal" breakwater. The author assumes these are the dimensions of how a standard or "average" breakwater looks like. Of course no such thing exists, but it was chosen to scale the geometric characteristic sizes of materials with respect to this nominal breakwater and sandfill characteristics. As scalable parameter the sediment to core size ratio $d_{f,15}/d_{b,85}$ is chosen as defined by Terzaghi. As proposed by Heller (2011) the length scale factor λ is chosen as small as possible. However, λ is limited by the minimum characteristic sand size. A workable model is designed and by choosing the correct size stones an exact scaled grading of the nominal breakwater can be obtained. By setting up a model in which only one layer of material is used, the challenges regarding the permeability scaling of different materials as discussed in the subsection geometry (section 4.5.1) are overcome.

5
Model setup

In this chapter the development of the model setup is elaborated on. The functional requirements are described and a modelling method is determined. The model is designed in an iterative process of which the main conclusions and the most essential adaptations are presented. Lastly, the final model setup is presented.

5.1. Model strategy

For the model some functional requirements were defined to enable the potential answer to the research questions. From the literature discussed in chapter 4 it is concluded that several methods and formulae are derived to obtain both the appearing and the critical hydraulic gradients in grains. The applicability of these stability relations was questioned for the specific configuration studied in the current research. Primarily, a model setup needed to be designed which was able to approach the critical hydraulic gradient for the desired configuration. In order to do so, the initial outline of the interface to the rubble mound in the sandfill must be known. Therefore, the model setup also needed to be able to approach the initial infill process. A stability criterion in the form of equation 5.1 was defined in which a parameter 'X' for different combinations of methods is defined to couple appearing critical gradients in the model to the corresponding calculated critical gradients. The value of X describes the applicability of the known stability criterion to describe the interface stability at hand. Lastly, the measured outcomes are evaluated and coupled to the test observations and available literature.

$$\text{If} \quad \frac{I_{cr,appear}}{I_{cr,calc}} < X \quad \rightarrow \text{Stable} \tag{5.1}$$

5.1.1. Functional requirements

The potential model setups were tested to a short list of functional requirements. Also, preliminary tests were executed to obtain more insight into material characteristics and physical processes. These preliminary experiments are described in section 5.1.2

Design

In the experiments the ability to carefully evaluate the sediment transport is important. Therefore, the visual inspection of sediment transport during the tests and the possibility to dissect the interface sample after the test were concluded to be important. Furthermore, it had to be possible to simulate the process of construction of the sandfill, shaping the interface.

Loading

From the literature study, order size boundary conditions were approximated. Because the hydraulic gradients don't need to be scaled, the excited hydraulic gradients in the model should include the approximated gradients. Table 5.1 summarizes these approximations. The used materials were scaled with an approach explained in section 5.3.1. The scaled geometric characteristics were inserted in the stability criteria and give order size approximations of the critical gradients in the model, showed in the last column of the table. By use of a calculation a composite grading was made from the used sand and core material. In this manner the suffusion theory as proposed by Allsop and Williams (1991) and Polidoro et al. (2015) could be tested. Also this critical gradient is presented in table 5.1 and the calculations are given in appendix B.1.1. The estimations of the appearing gradients and critical gradients lead to the conclusion that the model setup needed to be able to generate hydraulic gradients at the interface ranging between $0 - 0.15m/m$ with steps of preferably $0.01m/m$ as the differences between obtained values are very low. Also, it was already know that this was about the limit of the pressure sensors. The desired accuracy of the measured hydraulic gradient should be $\leq 0.005m/m$ to avoid rounding errors. Although the approach is somewhat rough due to missing input parameters (e.g. velocity amplitude or KC-number and specific α & β), the filter velocities corresponding to the hydraulic gradients measured in Polidoro et al. (2015) are calculated by means of the Forchheimer equation ($\alpha = 1000$, $\beta = 1.1$). These filter velocities are converted to pore velocities and provide, in combination with the Reynolds filter number whether laminar, turbulent or transitional flow occurs at prototype scale. The filter velocities range between $0.0016m/s$ and $0.008m/s$ with corresponding Reynolds filter numbers of $2453 - 3680$ thus implying turbulent conditions. For the experiments by Vanneste and Troch (2012) the specific α & β values are known and thus I_{cr}((Klein Breteler et al., 1992)) can be calculated by means of the Forchheimer equation and a rough estimation of the appearing gradient is given with the Forchheimer equation. This is calculated by means of eq. (4.5) (estimating the filter velocity) and eq. (4.3) (Forchheimer equation) with a local wave height of $H_x = 10\% * H_0$ and specific α & β given by Vanneste and Troch (2012). For Polidoro et al. (2015) this was not possible.

Table 5.1: Predictive values for boundary conditions model

Characteristics parameters used from:	Polidoro et al.	Vanneste	Model
Used calculation method:			
$I_{\text{calculated,Forchheimer}}$ (4.3 4.5)	Missing α & β	0.03	N/A
$I_{\text{calculated,Vanneste}}$	0.01-0.04	0.02-0.04	N/A
I_{measured}	0.02-0.03	missing measured data	N/A
I_{cr}, (de Graauw et al., 1984)	0.013	0.063	0.11
I_{cr}, (Klein Breteler et al., 1992)	Missing α & β	0.02	Missing α & β
I_{cr}, (Allsop and Williams, 1991)	0.04	Missing grading	0.023

Materials and dimensions
As explained in section 4.6 length scale parameter λ was desired as small as possible, limited by the minimum sediment size for which sand retains his (un) cohesive characteristics. Furthermore, in the model, a close representation of the nominal breakwater presented by Polidoro et al. (2015) was preferred. The reason is twofold: (1) It is an accurate representation of a real (existing) breakwater; (2) The results can be easily compared with the measurements executed in their research.

5.1.2. Model selection

In appendix B.1.2, three physical modelling methods are discussed which are suggested to physically approach processes as they occur in reality. The conclusions of this evaluation are presented in table 5.2.

Considering the pros and cons of the methods given in table 5.2 a model set-up is derived that is similar to method 3. With this method, it was expected that the dominant processes can be imitated while keeping the test fairly simple. First, method 1 is discarded because this method introduces complications due to the occurrence of many different processes (e.g. wave run-up, wave breaking and air entrainment) which complicate the interpretation of the obtained measurement data. As only the hydraulic gradient at the initiation of motion of sediments is of interest, the wave and pore pressure attenuation through a scaled breakwater is not of interest. Furthermore, method 2 is discarded because the oscillatory movement is excited through the core and sand body whereas, in reality, the oscillation movement is along the interface. The water does not flow through the complete sandfill. However, some considerations of method 2 are used for the design of the model set-up. Lastly, method 1 and method 2 are both discarded by the simple fact that a likewise facility was neither necessary nor available. The most important aspect of the chosen model strategy with respect to similar researches is the fact that the sand body is constructed behind the core and therefore the model is able to couple the appearing gradient to the sediment transport.

Table 5.2: Pros and cons of the considered modelling methods

	Wave Flume	U-tunnel	Container
Pros	• Good representation of physical processes; • Potentially modeling of initial interface; • Scaling of real wave conditions • Possibilities for calculated approximations of appearing gradients;	• Ability for consistent oscillatory flow; • Possibilities for different slopes due to rotation;	• Large scaling limit; • Possible flow along the interface; • Modeling of initial interface; • Possibility of process isolation
Cons	• Scaling limits on wave height and waterdepth; • Complex model and thus hard to attribute observations to correct theory;	• Only flow through the interface and not along the interface; • No modelling of initial interface;	• Unproven concept;
Remarks	Not available	Not available	Needs development

5.1.3. Initial experimental setup

Initial experiments are executed to test whether the proposed model set-up results in the intended processes, to prove is the chosen measurement equipment is appropriate and whether the proposed evaluation techniques are possible. In these experiments materials are used that were available in the Hydraulic Laboratory of DELFT UNIVERSITY OF TECHNOLOGY.

The tests are carried out on a basic level whereby oscillatory pressures were induced by manually (human powered) moving up and down a piston. The induced pressures resulted in a flow through the core accompanied by an oscillating water level. This flow was expected to cause sediment transport. No actual flow velocities where measured and only qualitative analyses were made of the occurring sediment transport. Afterwards, the proposed measurement equipment was tested. Some basic experiments are executed to check whether the equipment is suitable for research and what possible adjustments could be made. The model setup for the preliminary experiments is presented in fig. 5.1, where the red arrow presents the water movement. The experimental setup, used materials, measurement equipment and model installation are extensively elaborated on in appendix B.1.3.

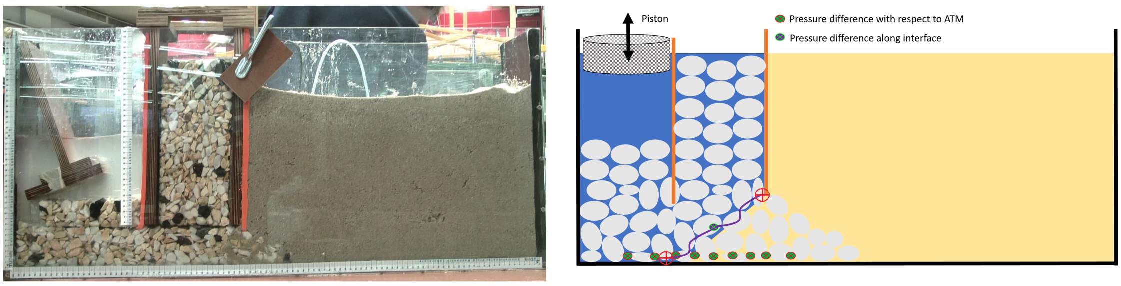

(a) Preliminary model set-up (b) Schematic overview of measurement set up

Figure 5.1: Model setup for preliminary experiments

5.2. Preliminary experiments

Various tests were executed without a predefined and detailed test sequence. However, the experiments were consistent regarding the used materials, water level variations and evaluation. The lack of a predefined test sequence was caused by the uncertainty in what to expect from the test and the ability of the model set-up to approach the actual processes. Also, after most tests limitations of the model were registered, evaluated and reduced or eliminated to improve the model. By making lots of variations and improvements during the initial test series, potential teething problems were overcome. The tests became more sophisticated over time and after some practician, all test were registered.

Amongst others, the preliminary experiments were used to test the influence of using loose rock and bonded rock, to test and design the pressure sensors, to determine the desired installation sequence, evaluate the wall effects and determine the influence of the sediment to core size ratio. Nine experiments were executed and additionally some smaller tests to obtain extra insight into the used setup. A log with an extensive description of all preliminary experiments is presented in appendix B.2.1

Per test, results are described considering the model installation, test sequence and the actual process based results, which describe the outcome of the model test. Also, the results of the non-process based tests are described. A second log provides a full overview of these results, given in appendix B.2.2. The results are summarized and evaluated in appendix B.2.3. The concluding remarks of this preliminary tests were used to improve the model set-up. Although the biggest changes are made based on these results, the testing remained an irritative process in which continuous improvements to the model are being applied. The adaptations made to arrive at the final test setup are summarized below. The changes, new equipment and resulting implications are elaborated on in section 5.3.

- The original container was used with the improvements elaborated in B.2.3, making is stronger..
- Within the model set-up only loose rock material was installed. Unfortunately, this decreased the amount of uniformity of the rock samples for different tests, however, due to the installation of the measurement equipment a rigid rock sample is not possible. Only the solid plate assuring the stability of the rocks directly under the piston remained installed.
- The used materials were chosen based on geometric scaling with respect to the characteristics used in the experiments of Polidoro et al. (2015).
- Newly designed pressure sensors measured pressure differences which can easily be related to gradients. They were installed to measure the hydraulic gradients over the sand-rock interface.
- In order to observe the sediment migration over the bottom of the container 2 CCM's were installed. Unfortunately only 2 CCM's were available at the TU DELFT laboratory and also DELTARES was not able to provide more. More information is provided in section 5.3.2.
- Cameras were put in place to record water motions and the visual sediment transport along the sides.
- The model set-up was equipped with an automated and motorised piston. This enabled for a longer duration of the experiments and made the wave oscillations more uniform and constant.
- Two lasers were installed. One laser to register the movement of the motor and one laser to register the water level oscillating above the core material in the zone of interest.

The final test setup is used to find the critical hydraulic gradient of the system. It was decided to evaluate the sediment transport processes only qualitatively, in which transport is divided into three categories: 1, no transport; 2, intermittent transport; 3, continuous transport \no stable interface. The tests were executed multiple times to check the consistency of the measurements and observations. The transport is dependent on the ratio of load over resistance in which the loads are varied by varying the excited hydraulic gradient along the interface and the resistance was intended be the same for every test and therefore geometric parameters were kept constant. Also, the oscillation amplitude and water table were taken as constants. Two pressure sensors which measured pressure differences were installed side by side to measure the gradient parallel to the interface. The obtained critical gradients could be compared with those obtained by use of theory from earlier research.

5.3. Tests with final setup

With the obtained insights from literature study and the iterative preliminary experiments, a final model setup is developed which is used to obtain the measurement data needed to answer the research questions.

All considerations for the materials and equipment used, and practical execution of the experiment are discussed in the section below. The used container is equal to the container used in the preliminary experiments with the changes and improvements elaborated on in section 5.2. A technical drawing of the definitive model set-up is given in fig. 5.2a. Also, to clarify the situation a coordinate system is given in fig. 5.2b to which is referred by means of distance from the origin in the x and the y-direction, or in height from the origin in the z-direction. In zone 1 and zone 2 core material is placed and in zone 3 the sandfill is constructed. The water level oscillation is excited in zone 1 by means of an automated piston.

In the setup the gradient is measured with pressure sensors which measure the pressure difference over two points along the interface. These are marked in fig. 5.2a by the "tube ends". The measurement computer program converts the pressure difference to the desired gradient $I_{measured}$ by dividing over the distance between the points. The oscillation of the plunger system and the oscillation of the water level were measured by use of lasers, also these are presented in fig. 5.2a. From the oscillating movement also the plunger-and water level velocity and acceleration are derived. The water level velocity is in fact assumed to be representative as an estimation of the desired filter velocity u_f further explained in section 5.3.3 and section 6.3.3. Visually and by means of camera's the sediment transport is evaluated. Furthermore, also CCMs are used, whose locations are indicated in fig. 5.2a. In table B.2 the exact location of the tube ends and CCM's is given for calculation purposes. The operation, accuracy and limitations of the measurement equipment are discussed in section 5.3.2.

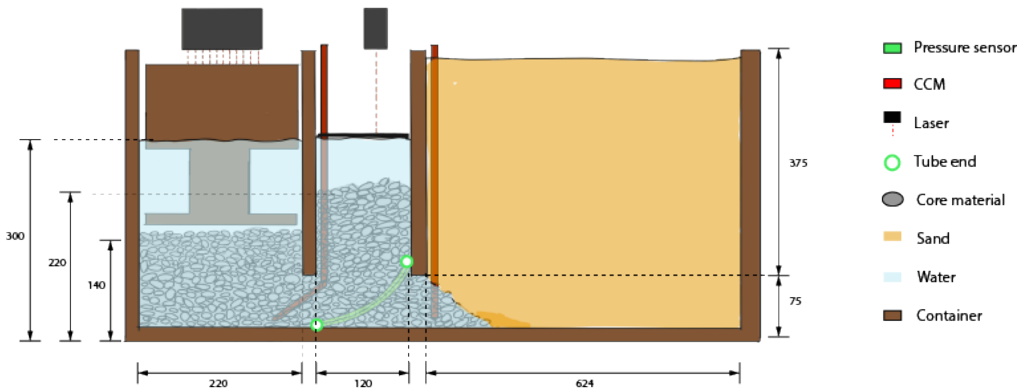

(a) Technical drawing of final model set-up

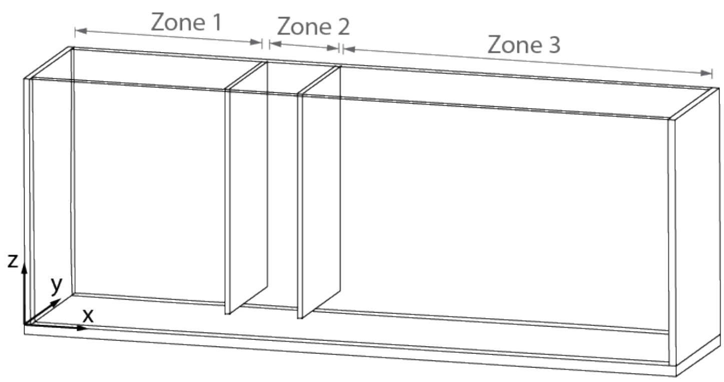

(b) Coordinate system

Figure 5.2: Final model setup

5.3.1. Model Description

Model scale

As discussed in section 4.6, length scale parameter λ was chosen as small as possible without compromising on the specific (cohesive) characteristics sand. For the model test, the smallest available sand from the distributor of the laboratory was used, called AF-100. The choice for this sand in comparison to other available sand is further elaborated on in appendix B.3.1. The AF-100 sand was the smallest sand available without significantly increased cohesive characteristics and is often used in laboratory experiments at DELFT UNIVERSITY OF TECHNOLOGY.

To determine the governing geometric scale parameter the ratio between nominal dredged sand by Polidoro et al. (2015) and the AF-100 sand was used. In which "nominal" again represents dimensions given by Polidoro et al. (2015) as a "standard" breakwater & sandfill. To define the scaling parameter λ the d_{b85} is chosen. The resulting geometric scaling parameter is defined in equation 5.2. This decision is based on the preference to keep the geometric ratio of the core material over the sand body equal to that of the nominal breakwater given by Polidoro et al. (2015). The preferred geometric constant to scale is the $d_{f,15}/d_{b,85}$ which relates to the pore size to base material size ratio of the core material over the sand body as described in section 4.4.2. In case a more conventional geometric scaling sequence was used based on d_{50} (e.g. $\lambda = d_{b,50,nominal}/d_{b,50,\mathrm{model}}$ and $d_{f,50,\mathrm{model}} = \lambda \cdot d_{f,50,\mathrm{nominal}}$), this would result in a significant change of the filter parameter $d_{f,15}/d_{b,85}$ because the grading of the nominal sand and model sand are not similar enough. Furthermore, the conventional scaling method would results in core material sizes of $\approx 15[cm]$ which does not fit the container. It is thus decided to use the scaling parameter $\lambda_{d,b,85}$ in combination with $d_{f,15}/d_{b,85}$ and thus $\lambda_{d,f,15} = \lambda_{d,b,85}$. Based on executed scaling of $\lambda_{f,15}$, the shape of the grading curve of the used model core material is made equal to the nominal breakwater. Due to practical reasons originating from sieving the scaling parameter $\lambda_{f,15} = 15.81$ instead of 15.38 . This is further elaborated on in appendix B.3.1.

$$\lambda = \lambda_{db85} = d_{b85,\mathrm{nominal}}/d_{b85,\mathrm{model}} = 15.38 \tag{5.2}$$

Geometry

The geometry of the model set-up is primarily based on two aspects: The geometric scaling parameter λ calculated in above (section 5.3.1) and the availability of materials and equipment in the laboratory at DELFT UNIVERSITY OF TECHNOLOGY. The parameter $d_{b85}/d_{f15} = 63$ is of the same magnitude to the experiments executed by Polidoro et al. (2015) and likewise parameter $C_u = d_{f60}/d_{f10} = 4.7$ is equal.

In the laboratory, no rock material was available with the specific scaled characteristics. Therefore a composite grading was build from various types of material, all sieved and weighted. In appendix B.3.1 is elaborated on the composition of the new rock material and the tests to obtain its characteristics. $14.4kg$ of rock was mixed with a resulting average density $\rho_{av} = 2650kg/m^3$ and a porosity $n_{f,model} = 0.38$. The porosity for the nominal breakwater in the study by Polidoro et al. (2015) is assumed, and does not particularly correspond with the values found for a widely graded quarry run in literature. For the nominal core $n_f = 0.3$ while in literature higher values are found. It is therefore not taken as a parameter that should be kept constant. The porosity derived for the model $n_{f,model} = 0.38$, which is fairly in line with the literature (see section 4.2 and Vanneste and Troch (2012).). The grading curve of the nominal and model sand, and of the nominal and model core are given in figure fig. 5.3.

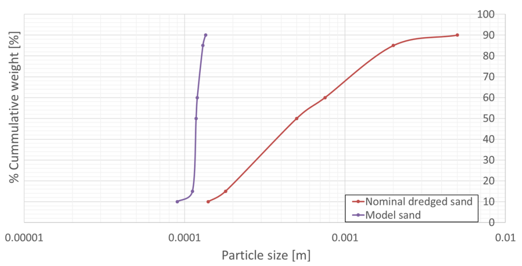

(a) Grading curve for nominal dredged- and model sand.

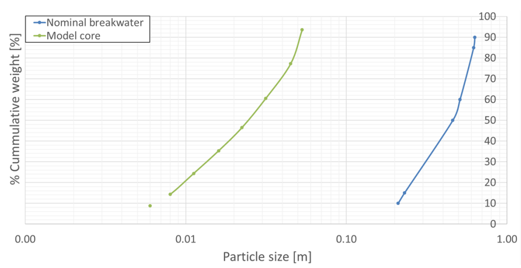

(b) Grading curve for nominal breakwater and model core.

Figure 5.3: Characteristic grain sizes nominal breakwater and model.

Scale effects

As discussed in sections 4.5.2 and 4.6 it is tried to keep the model fairly easy. The hydraulic gradients do not need to be scaled and the model itself is scaled based on the geometric scaling described in the preceding paragraph. However, some remarks are made considering scaling which are able to describe certain processes in the model or the reliability of the model outcomes. Considering design parameters with the dimension [m] the parameters are scaled to model size by use of the geometrical scaling parameter λ (e.g. grain size sand and grain size core). In conventional breakwater research load parameters need to be scaled with their respective similarity parameters, such as Froude scaling for the wave period and velocity if the inertia force over the gravitational force is retained. However, in this research these parameters are not necessarily of interest as the loading with a hydraulic gradient is not excited by scaled or currents waves. Besides, the geometric scaling by means of scaling parameter λ does not scale correctly the appearing viscous shear, as discussed in section 4.5.2. It is important, that the Reynolds filter number remains above 10, preferably above 1000. For comparison it is repeated that the Reynolds filter numbers calculated for the nominal breakwater in Polidoro et al. (2015) range between 2453 and 3680. For the model setup in the current research, the filter velocities should remain $u_f \geq 0.015 m/s$ for fully turbulent flow. The experiment was not specifically scaled to obtain Reynolds similarity and the obtained filter velocities in the experiments are afterwards tested against the limit values. Choosing the scaling parameter λ as small as possible is favourable for maintaining correct viscous forces.

Due to the small sizes of the stones and the low filter velocities during lower load conditions, scaling deficiencies occur with respect to the Reynolds filter number. The appearing filter velocities range between $0.007 m/s$ and $0.044 m/s$. After calculating the pore velocities, Reynolds filter numbers are obtained of approximately 386 to 2422, which implies transitional conditions for the lower load conditions and turbulent conditions for the higher load conditions. The limit requirement $u_f \geq 0.015 m/s$ for turbulent flow is mainly not met for gradients $I_{\text{measured}} \leq 0.02$. This transitional regime is (presumably) not encountered in reality.

Scale effects were expected due to the sizes of the model setup itself. The container is rather small and uses relatively large stones. Wall effects on the hydrodynamic conditions are normally encountered within 5-10 times the diameter of the used core material of the wall. In this case, the core material is sized $d_{50} = 0.021 m$ and thus the hydrodynamic flow processes are physically represented well, at a distance of 0.1 to 0.2m from the walls. As the container is only 0.15m deep wall effects are inherently present in the container for flow. It is however proposed that (1) not especially these flow processes are of primary interest, but the sediment transport is. And, with a $d_{50,sand}$ the wall effects are significantly smaller. (2) Furthermore, the wall effects are extensively investigated during the development of the model setup. It was concluded that the transport was constant over the full cross-section of the container (see appendix B.2.3).

Load conditions

The load conditions are based on subjecting the sandfill to core interface to the desired appearing hydraulic gradient. Two approaches were explored simultaneously. One in which the hydraulic conditions of Polidoro et al. (2015) were scaled. This resulted in scaled water levels, wave periods and wave heights but the method was concluded to be inappropriate for the considered setup and lead to unachievable hydraulic conditions (such as water levels exceeding the container limits). The second method focussed more directly on the desired physical parameter to be varied: the hydraulic gradient along the interface. From the Euler relation (eq. (A.6)) elaborated on in section 4.2 it is proposed that the acceleration of the water can induce this gradient. A test sequence is set up to determine the relation between the (de-)acceleration of the motor operating the plunger and the appearing gradient in the model, as this is the only controllable parameter in the motor setting. This relation is explained below.

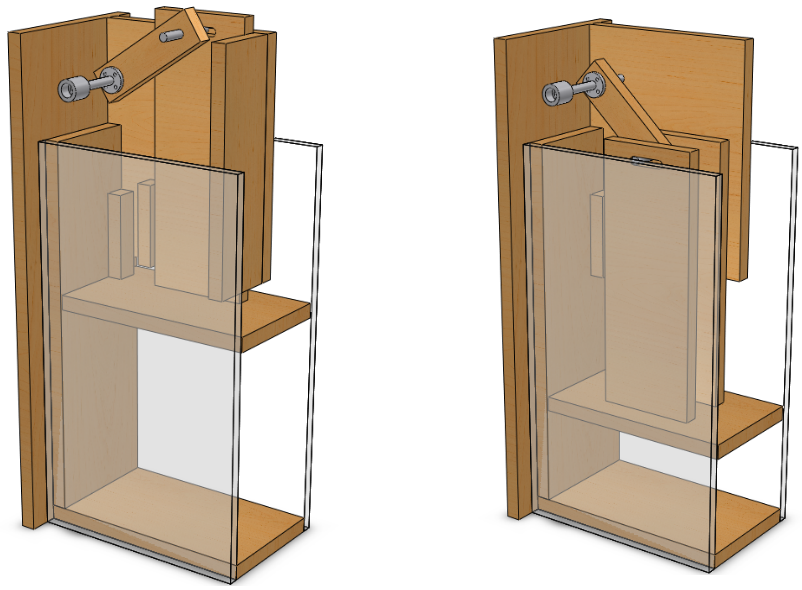

Figure 5.4: Renders made of the plunger design (van der Gaag, 2018)

A motor excites the motion of the system by transitioning a 45° rotation of the motor axis towards a vertical movement of the plunger of $6.5cm$. The rotation is alternating clockwise and anti-clockwise, resulting in an upward and downward movement of the plunger. Renders of the design are presented in fig. 5.4. The plunger is due to this rotation, limited and constant in its amplitude. The rotation velocity of the motor is set very high (20 rev/s) and the (de)-acceleration is limited. By setting the (de-) acceleration (AC), one can control the time the motor needs to make the 45° rotation and thus $6.5cm$ vertical movement of the plunger. This is in fact, the oscillation period. Although the oscillation period might be better understandable physical quantity, the acceleration is used as a control parameter to define the settings of the motor to ensure the reproducibility of the research. This is the only parameter that is set in the control program of the motor. This program accelerates the motor from point P(y= max amplitude, t=0) and knows where to stop at point P(x= - max amplitude, t=1/2· period). Given the maximum (de-) acceleration, an alternating positive and negative parabola govern the motion of the piston. The interchanging parabolas are the closest representations of a sinusoidal wave the motor could make in this research. The obtained motion, and intended pressure variations are thus oscillations but not as a sinusoidal movement. The derivative of the parabola motion is the velocity and is presented as a saw tooth.

A full model setup was installed to calibrate the motor and find the relation between the appearing hydraulic gradient and the pre-set (de-) acceleration of the motor. This resulted in a linear relation and thus, a fairly simple test program could be determined. The calibration graph is given in figure 5.5. The theoretical test program consisted of loading conditions that ranged between a hydraulic gradient of 0.01 and 0.15 in steps of 0.01. In total, the model is subjected to three series repeating 10 to 15 loading conditions with 1000 waves each. The theoretical loading program is presented in table 5.3 and the test program is discussed in the next paragraph. Lastly, a table with all executed test and characteristic file and test numbers (for evaluation of the complete data set) is presented in appendix B.3.1.

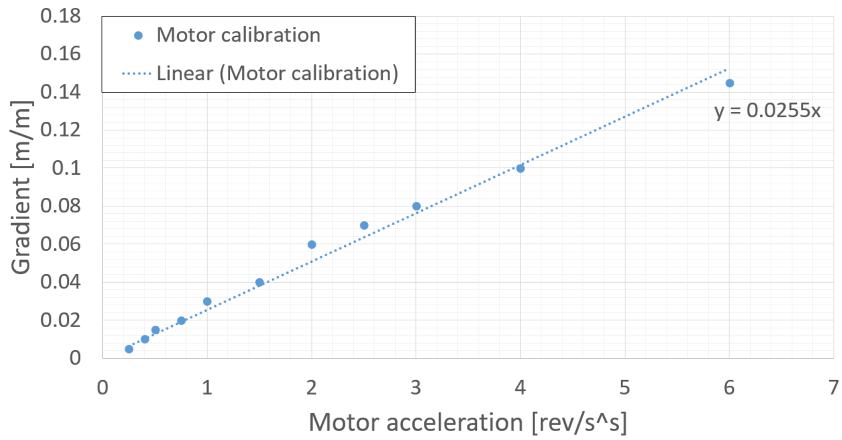

Figure 5.5: Obtained hydraulic gradients for various accelerations(AC) (or oscillation periods) of the motor

The used motor is a servo quick turner motor, which is an extremely strong motor capable of transmitting high forces on both low and high speeds. The motor is set with an velocity and (de)acceleration in revolutions/s and revolutions/s^2 respectively. A 1 : 15 transmission is installed to provide smaller movements. The velocity and acceleration are controlled very carefully as the motor is strong enough to severely damage other parts of the construction such as the wooden construction of the plunger and the transmission which translates the rotational movement of the motor to a lateral movement of the plunger. This has happened several times.

Table 5.3: Target and obtained hydraulic gradients for model tests.

Target $[m/m]$	Motor AC rev/s^2	Period $[s]$
0.01	0.4	7.72
0.02	0.8	6.46
0.031	1.2	4.13
0.036	1.4	3.87
0.041	1.6	3.65
0.046	1.8	3.46
0.051	2	3.16
0.056	2.2	3.04
0.061	2.4	2.93
0.066	2.6	2.83
0.071	2.8	2.75
0.077	3	2.58
0.082	3.2	2.51
0.087	3.4	2.45

Test program

The test program consists of 3 repetitions of a series of tests in which the hydraulic gradient was varied by means of setting the acceleration, given in table 5.3. The first series was still a bit of a trial, the second and third series resulted in a data set which provided a sound base for evaluation of the proposed research questions. After a series of tests, the transport condition became continuous, approximately four tests with higher gradients were executed and than the series was ended. The model setup and loading for the three series are discussed below, the implications of the installation and test results are elaborated on in chapter 6. The summary of all test results (including double tests) are as mentioned above, presented in appendix B.3.1. Besides these model tests, a test was executed to evaluate how the measured pressure signal was influenced by noise and what was the cause of this.

Series 1
In the first series an error occurred for which the data of the first 4 test got corrupted. These tests are only valuable to couple the acceleration of the motor to the resulting sediment transport but no valuable data regarding the hydraulic gradient could be retrieved. For the subsequent tests of this series, the problem is resolved and the hydraulic gradients are correctly measured. In this series, some tests are doubled in the total amount of waves that were excited to find out whether, after initial transport occurred, the situation would stabilise. The stones in this test were randomly placed which resulted in a somewhat less porous configuration at the front of the container than at the back. This series is discontinued at $AC = 2.35\text{rev}/s^2$ as multiple subsequent tests with continuous transport were obtained.

Series 2
In the second series no problems occurred and a full dataset was obtained with hydraulic gradients and transport conditions. The stones are again placed randomly and segregation of the larger and smaller fractions was observed, causing smaller fractions (coincidently) at the interface and larger stones around the plywood separation. This series is discontinued at $AC = 2.8\text{rev}/s^2$ as multiple subsequent tests with continuous transport were obtained.

Series 3
In the third series also no problems arose and again a full dataset was obtained with hydraulic gradients and transport conditions. In this series, some extra care was taken to ensure a well-mixed placement of the stones to decrease porosity differences. This resulted in the desired mix on the backside of the container, but at the front again segregation occurred, now with larger stones at the bottom and close to the interface, and smaller fractions close to the plywood separation. This series is discontinued at $AC = 3.4\text{rev}/s^2$ as multiple subsequent tests with continuous transport were obtained.

Signal optimization
The obtain insight into the pressure signal, the noise on this signal and possible influences which did not result from the physical processes in the model, a test was carried out. An extra pressure sensor was placed in a container filled with water, which was attached to the side of the model setup. This sensor registered the noise, resonance and other disturbances. Different loading conditions were excited and other types of disturbances such as pushing the container and shaking the table were applied.

5.3.2. Instruments and measurements
The section provides an indication of all measurement instruments needed in the research, their characteristics and specifications. Furthermore, the uses and possibly appearing implications are elaborated on and cautions are presented.

All instruments are set to obtain signals between -10 and 10 volts. Although the scaling of the individual instruments provides the range of quantity wished for in a measurement, e.g. pressure (in mm water column) or distances (in mm), all instruments are largely within range. The instruments limit frequencies are 1000Hz (pressure sensors) However, for this research a sampling interval of 0.005[s] or 200Hz is chosen. This sampling rate should be large enough to obtain all details of the pressure signals. It is noticed that when an erroneous signal is observed at one instrument this sometimes influences other instruments. During evaluation of the obtained signals, this is taken into account.

(a) Conductivity type concentration meter

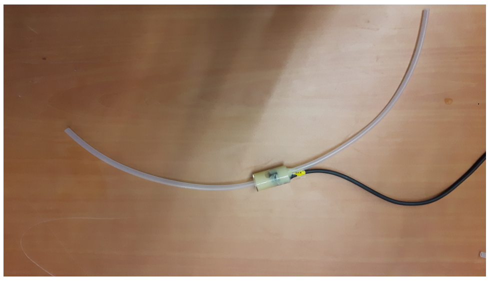

(b) Pressure sensor

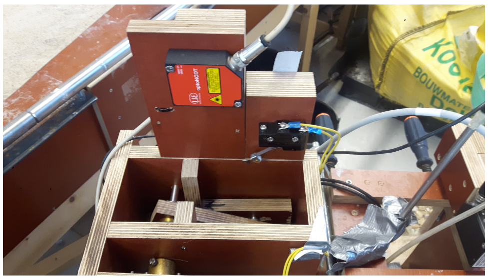

(c) Laser 1

(d) Laser 2

Figure 5.6: Overview of the different instruments used.

Conductivity type Concentration Meter

The conductivity type concentration meter (CCM) system is an instrument to measure the concentration of sand-water suspensions, see figure 5.6a. The measuring principle is based on the conductivity change of a sand-water mixture due to change of the amount of suspended sediment present in the measuring area (Delaters instrumentation, 2016). In this case, the CCM is placed at two positions in the container, varying over the distance 'x' and sampled with 200Hz. The distance 'x' varies over the different test but in most cases one CCM is placed under each plywood screen. The exact conductivity of the water-sand mixture is not measured, but the course of the signal can indicate if the amount of sediments in contact with the CCM increases or decreases. The CCM's are therefore used to register qualitatively both the propagation of the sediment front over the bottom of the container and the (potential) thickness of this propagating sand body. The CCM's are old and rarely used at DELFT UNIVERSITY OF TECHNOLOGY therefore, the CCM's are not calibrated and not used for quantitative analyses. Lastly, the reliability of the devices is uncertain, which also implies that the accuracy is questionable. Appendix B.3.2 provides the justification for the use of CCM's as described above with an explanatory result of a small test. However, also the limitations are provided.

Pressure sensors

For the final experiments new pressure sensor cases were developed because the sensors from the preliminary model tests were not watertight (as discussed in section 5.2). A picture of a new pressure sensor case is given in figure 5.6b. The used sensors are of the type Honeywell 24PC/26PC (Hon). The new pressure sensors measure the pressure difference between the two tube ends with 200Hz. Of two different sensors the ends are taped together to act matching sensors. In theory, the sensors should, after correct calibration give equal signals. This is done to easily detect malfunctioning sensors.

One set of tube ends is placed at the bottom of the container underneath the plywood screen separating zone one and zone two. The other set of tube ends is taped to the plywood screen separating zone two and zone three. In this manner, the pressure sensors provide the hydraulic gradient over the area where the interface between sand and core material is expected. The sensor's location is checked and registered at every installation to give correct gradients. Furthermore, the tube ends of the sensors which are placed at the bottom are varied over the distance after the first experiments to be in better accordance with the interface.

The pressure sensors were expected to measure both the (larger) oscillation signal of the water movement induced by the piston, and potentially turbulent fluctuations in the core material. The period of the oscillations of the piston ranges between 2.5 and 8 seconds. The Nyquist frequency of the pressure sensors is, therefore, $1/2.5 * x$ in which x ranges between 2 and 10 depending on the chosen margin. In this research $x = 10$ is chosen. Thus the Nyquist frequency is 4Hz. Because in the research only the longer oscillations are considered the turbulent fluctuation are less or non-important. The data is saved raw but afterwards subjected to a 5Hz equiripple lowpass filter (designed using the FIRPM function). In this manner the important longer period oscillations are filtered but, when necessary raw data is checked for other influences.

The pressure sensors are able to measure between 0 and $0.5psi$, corresponding with $3.45kPa$ or 0.35 meter water column and have a factory accuracy of 0.2% = $(0.7mm)$. However, the sensors are extremely sensitive. The pressure gradients are recorded between 0.01 to 0.15 in steps of 0.01, over a distance of 15-20cm. A gradient of 0.01 over 20cm implies a pressure difference of 2mm. The accuracy of the sensor is 0.7mm resulting in a 35% error for the lowest steps. This is rather large. For the second step, the error decreases to $17,5\%$ and 11% for a hydraulic gradient of 0.03. A spike or other disturbance, like a vibration of the measurement setup, has large influences on the obtained data. In section 5.3.3 is elaborated on how the characteristic frequency of the model setup is determined and how this influences the results.

The pressure sensors are calibrated by filling the tube ends with water and pulling them with known distances out of the water. The resulting pressure signal is coupled to the distance (meter water column) the tube end is out of the basin. This is done for every sensor individually as they appeared to have different calibration characteristics. This is further elaborated on in appendix B.3.2.

Lasers
Two lasers are installed to measure the movement of the piston and the water level. Both lasers have measurement frequencies of 200Hz. The lasers have a range of 6 to 36 centimetres. The first laser is installed at 7 cm above the maximum possible height of the piston. It measures the movement of the piston downward. The second laser is installed 10 centimetres above the maximum expected water level. A floater made of duct tape is placed on the water. The laser measures the distance to the floater and by this, registers the oscillation of the water level. The lasers are calibrated by moving a target away from the laser with over a know distance. The rate of change of the signal is then coupled to the distance. The initial values of the lasers are set in correspondence with the rulers which are placed on the container. The accuracy of the lasers is 4 decimals or 0.001 mm. However, the ductape float sometimes gets washed over with water resulting in some deviation of the accuracy due to reflections. The wished accuracy of the lasers is 1mm, which is proven with visual observations. The location of the laser is given in fig. 5.2a and photographs are provided in fig. 5.6c and fig. 5.6d.

Camera's
Two cameras are used. One static video camera is installed to record the larger processes in and around the container. It registers when people are walking by, if the model setup is touched, when additional experiments are executed, like adding dye and whether or not breaching subsidence of the sand body occurs. All these processes can influence the measurement data and processes and are easily missed by the researcher. A second (photo) camera is used to make pictures of start and end conditions to make visual evaluations of the sediment transport. Furthermore, processes are recorded in close up to register processes of sediment transport and the movement of the fluid. This is done by adding purple dye and observing how it moves. Examples are again provided in appendix B.3.2.

5.3.3. Pressures, Forces and Flow

Pressures
The used pressure sensors are very sensitive. This causes the sensors not to measure the pressure (differences) exclusively, it registers resonance of the model setup, vibrations of the ground or table on which the container is placed and vibrations of cables and connections of the electric circuit that connects the sensors to the computer. From the preliminary experiments, it was learned that the pressure sensors are sometimes subjected to zero drift. The newly fabricated sensors with improved cases have shown to be of higher quality and less prone to this zero drift. However, two out of five sensors did encounter zero drift. The upside is that the other three function with very little or without zero drift. Temperature variation of the water in the container does not seem to influence the pressure sensors. Besides, the measurements take approximately between 1 hour and 2.5 hours and are executed during the day. The biggest temperature differences take

longer periods and vary most over day and night. The CCMs are more prone to this problem as these measure the hydraulic conductivity.

In section 5.3.4 the resonance of the model setup is evaluated and is explained how a clean pressure signal is obtained from the raw data. Various tests are executed to obtain the resonance frequencies of the container, to evaluate external effects and define the possible measures to extract these frequencies from the measured pressure signals. It is concluded that the higher frequencies or 'noise' that is seen in the signal is caused by the resonance of the model set-up. The forces caused by the tilting of the plunger, which is explained in the next paragraph, largely contributes to this. Also, by calibrating the step-motors internal settings, which is not executed in this research, the inaccuracies can be decreased.

Forces
The CCM's and pressure sensors were taped to the container or plywood screens. Afterwards the container was filled with the core material. With this, the sensors and CCM were assumed to be embedded in the rock layer and very stable. The evaluation of the signals obtained did not show any strange frequencies which were resulting from moving instruments by the force of the water. Although not an instrument, the motor did show some force induced inaccuracies. The piston was moved downwards by the motor pushing the water from zone 1 towards zone 2. Also, water moved along both sides of the piston upward in zone 1. Right before the end of the downward stroke, the piston tilted causing the flow of water to go upward at one side only. This also caused a shock wave. The tilting is caused by the transition from kinematic to dynamic resistance of the plunger against the container walls and is called stick-slip. At the moment of tilting of the piston, disturbances are observed in the signals of the pressure sensors and the water level. The laser that recorded the movement of the piston did not record any disturbances. It was therefore concluded that this "shock" is only felt in the water but is not influencing the motor itself.

The Container itself is very thin an relatively high and heavy. This causes the container to be rather unstable. Furthermore, the table on which the container is placed is not very heavy and also rather unstable. This causes that the resistance against vibrations of the total setup is low and small vibrations can easily disturb measured signals.

Flow velocity
The pore velocities are not measured in the research, however, purple dye is injected via a long tube into the area of interest. With this method, the flow of the water can be visually evaluated qualitatively. It is checked if the fluid moves fast or slow and whether the purple dye reaches the interface. Furthermore, the water level movement in zone 2 is measured. The velocity of the water level is derived from this which equals the vertical filter velocity (u_f) in the top of zone 2. The average pore velocity is obtained by dividing the filter velocity with the porosity ($\overline{u_{pore}} = u_f/n$). Inserting the pore velocity into the Reynolds filter number lead to an indication whether flow was laminar, turbulent or transitional between both.

Damage determination
The sediment transport is determined qualitatively. This implies that only whether or not sediment is transported or not is of interest. However, much more notes are taken during the experiments. Over the distance 'x' both at the front and the back of the container the start and end values of furthest point of sediment are registered and the development of the thickness. Furthermore, notes are taken on which kind of transport is seen, being suspended or bedload transport. Lastly, the characteristic erosion patterns like breaching are registered.

5.3.4. Data handling
The obtained 200Hz data signal gave lots of noise. With the use of the extra experiments carried out to find out the causes of this noise, a cause-based filter was designed. An example of the raw obtained data for the plunger movement, the water level movement and the hydraulic gradient is given in figure 5.7.

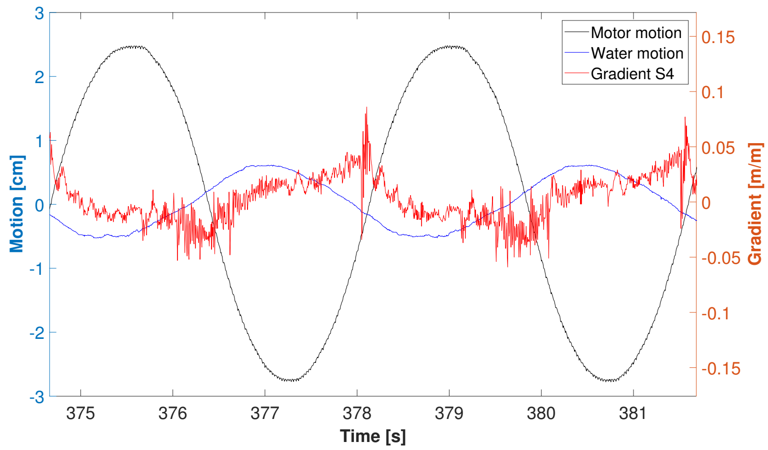

Figure 5.7: 200Hz signal obtained for plunger motion, water motion and hydraulic gradient

To obtain the specifications of the filter, the signal with noise was evaluated by means of a frequency analysis. The frequency analysis determines which frequencies are part of the desired signal and which signals are part of the noise. Extra information of the noise frequencies was obtained by the extra pressure sensor placed in a container attached to the side of the model setup. By comparing the two signals with visual observations made during the tests, the filter properties were designed. Specifically, a 5Hz equiripple lowpass filter (designed using the FIRPM function) is used. The full frequency analysis is elaborated on step-by-step in appendix B.3.3 and an example of the filtered signals is given in fig. 5.8.

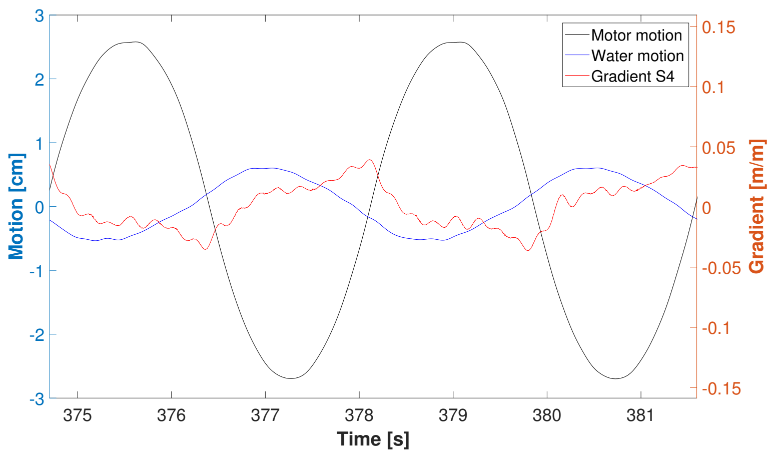

Figure 5.8: Filtered signal obtained for plunger motion, water motion and hydraulic gradient

6
Results

First, the obtained results on the research of the development and dimensions of the initial infill and interface are discussed. These results are used to answer the first research question. Furthermore, the obtained information on the interface provides the initial conditions of the second stage of the research, finding the hydraulic gradient for which sand from the sandfill migrates through the core material.

6.1. Initial interface

During the setup of every experiment an initial slope is formed. During the preliminary experiments tests were executed especially to evaluate this process. However, as for installation of a regular test series such a slope is formed, later these slopes were evaluated.

6.1.1. Shape and dimensions

The variation of sediment to core size ratio resulted in differences in the initial slope. In the preliminary experiments, narrow graded and smaller core material was used than in the final experiments. Furthermore, the sand particle size was much larger. This resulted in less sediment transport through the core and a different size and shape of the slope. This is presented in figure 6.1. Reductive, the sand particles did not fit as easy through the core pores as in the definitive experiments.

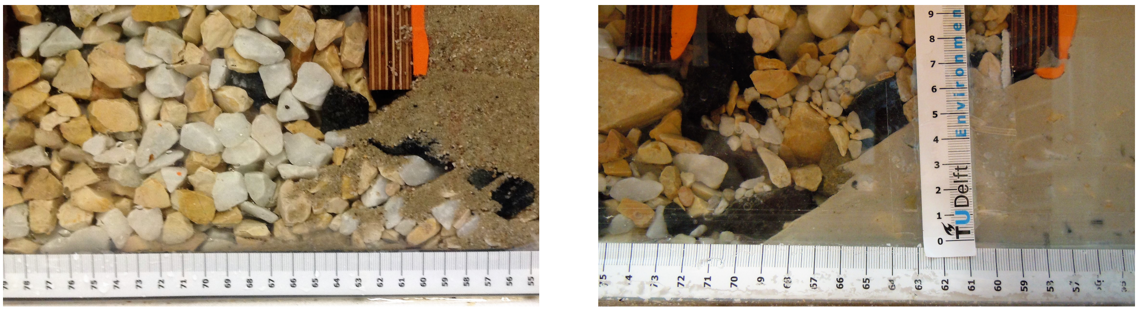

(a) Initial slope development $d_{15,f}/d_{85,b} = 8.6$.

(b) Initial slope development $d_{15,f}/d_{85,b} = 63.2$.

Figure 6.1: Initial slope development for different sand to core size ratios.

Various types of installations techniques were tried in order to find dominant influences on the development of the observed initial slope. First, the sand body was constructed dry whereafter water was added at the other side of the container or; first the container was filled with a layer of water after which the sand body was constructed. The results for both test were visually the same for constant sediment size to core size ratios. In the tests where the container was first partially filled with water, the added sediments got suspended after they came in contact with water. Due to gravity the particles sunk to the bottom. Meanwhile a gradient of the water level was observed over the container as the water level rose where the sand is added. This gradient would in reality not occur or only in a weaker form, as (1) a geotextile separation is permeable and the plywood screen is not and, (2) the water body in which the sand is deposited is larger and often connected with the open ocean. However, the appearing flow caused by the water level gradient is an important factor as in reality the dredged sludge is discharged through pipes resulting in flow of sediments. Besides, the adding of sand to the setup initiated waves. The combination of the waves and the water level gradient caused an (oscillating) flow towards and through the core. The (sinking) suspended sediments were taken in this flow and formed a slope in the core material. The described process took several seconds. Because the water level was initially higher than the sand body the sediments internal stability was low and the sediments were easily displaced. Furthermore, the angle of repose for fully saturated sand is lower than for dry sand, causing the sand to flow out through the opening underneath the plywood screens that separates zone 2 and zone 3. The latter reason is why for the tests in which the sand body was constructed first, the same pattern was observed. In this case, the sand body was placed on top of the rocky slope separating zone 2 and zone 3. Afterwards, water was added in zone 1 and zone 2. When the sand body came in contact with water, the interparticle shear strength reduced and the sediments flowed through the core. As the water was in motion the suspended sediments flowed from zone 3 towards zone 2.

The similarities in the results between the two methods are presented in figure 6.2. Figures 6.2a and 6.2b represent wet installation and 6.2c and 6.2d pictures after dry installation. The four cases are similar in shape and no very obvious or specific differences for wet and dry installation were found.

The slope dimensions obtained do vary for the four presented initial slopes. The largest deviations are seen in the movement of the triangle inwards through the core and whether or not upward transport has occurred. The angles of the initial slopes do not vary significantly. For both the wet installed sand bodies, the resulting slope has an angle of 34° and the dry installed sand bodies results in slope angles of 35° and 36°. This corresponds to characteristic values of dry sand (35°). Saturated sand may have an angle of repose ranging from 15° – 30°. The core material, however, is likely to have provided extra stability to the sand body and therefore, the extra strength to retain an angle of 35°. The movement of the sediments inward varied over the four tests causing the interface lengths to range $95mm$, $135mm$, $98mm$ and $73mm$ for figures 6.2a, 6.2b, 6.2c and 6.2d respectively. Again, the differences can not undisputedly be explained by the difference in wet and dry installation.

(a) Initial slope development wet installation of sand.

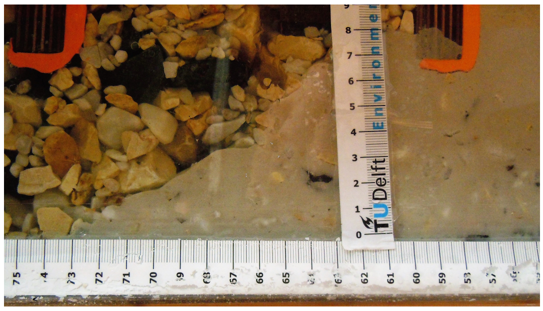

(b) Initial slope development wet installation of sand 2.

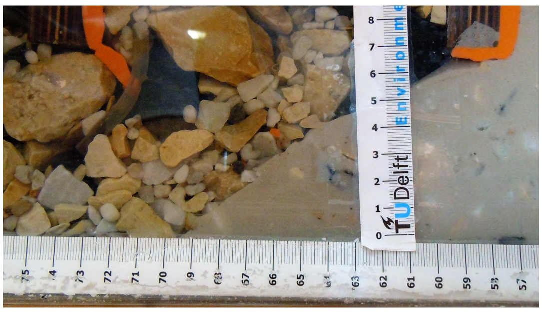

(c) Initial slope development dry installation of sand.

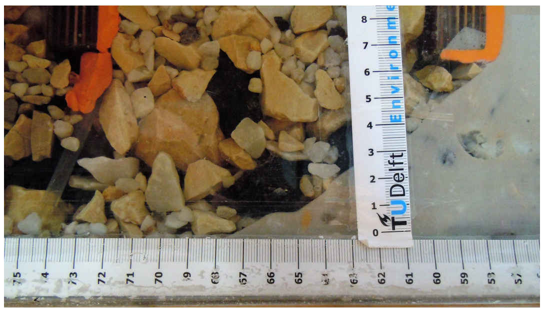

(d) Initial slope development dry installation sand 2.

Figure 6.2: Initial slope development when installed with or without water.

6.1.2. Processes

Although the results above do not provide a clear outcome of the differences in development or eventual dimensions of the initial slope, some remarks were made during the installations regarding processes influencing the outcome. The dry installation was a far more constant process than the wet installation. The sand was initially static, stable and available, and the water was added through the rocks in zone 1 or zone 2. The filling with water was turbulent but relatively constant and the process of the sediments moving through the core seems comparable for different tests. The most important parameter appeared to be the water level which governed at what height sediment particles became unstable and thus, how many at once. A fast-rising water level excited more transport than a slow-rising water level.

The wet installation procedure had much more variables and therefore, the processes that governed the development of the infill changed over the different tests. The variables were: Cohesion of the sand, how densely sand has been packed, pouring height, pouring velocity, amount of sand added at once and water level. For all parameters a positive relation holds, thus higher cohesion of the sand caused more transport, and even so higher pouring velocities increased propagation speeds of sediments etc. Furthermore, greater cohesion, pouring height and pouring velocity all caused increased wave action, which in her place caused oscillating motions that increased the sediment transport. When a larger amount of sand was added at once or with a higher velocity, the water level difference over the plywood screen between zone 2 and zone 3 became larger. This caused higher velocities of the flow into the core, which enhanced the sediment transport and the inwards movement of particles. Especially when the cross-sectional flow area reduced due to the closure of the gap, the flow- and transport velocities increased. After the water level differences were reduced to zero and the waves were dampened, the situation became stable.

6.2. Physical model

In section 5.3.1 is elaborated on the ability of the motor to excite oscillating motion and the inability to approach exact sinusoidal movement. This implies the piston and water level movements can be described by (interchanging parabolic) waves with a period and an amplitude. The velocities can be described as a saw-tooth motion with a period and a amplitude and if the system were frictionless, the appearing gradient should in theory be interchanging positive and negative constants. Due to friction in the system, and due to the operation of the motor, a period and an amplitude were observed. The three signals are given in fig. 6.3. The fourth figure (fig. 6.3d) presents the signal obtained by the Conductivity type Concentration Meters (CCM) which for all tests did not behave as during the preliminary experiments and the data is not considered any further.

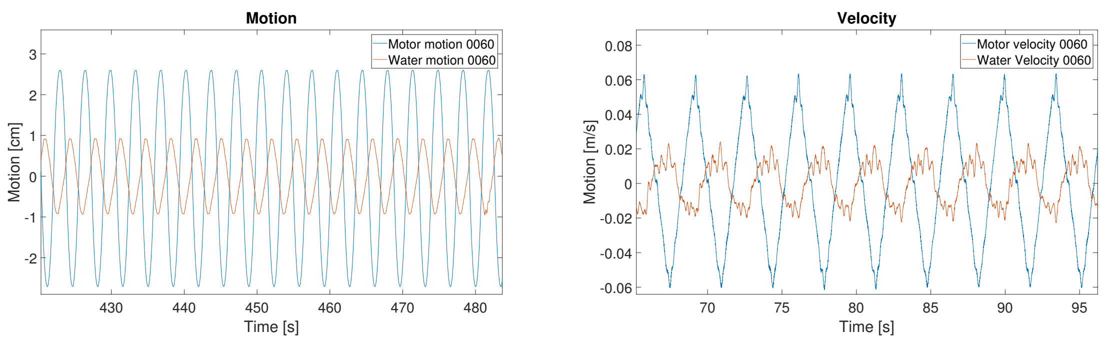

(a) Motion motor and Waterlevel

(b) Velocity motor and waterlevel

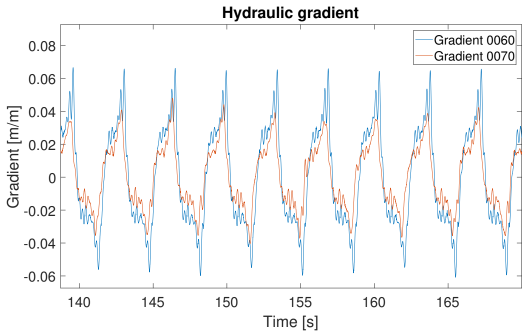

(c) Gradient for two tests with equal motor settings

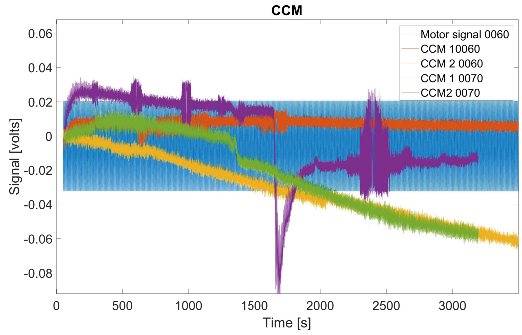

(d) CCM for two tests with equal motor settings

Figure 6.3: Various obtained signals

In appendix C.1.1 an overview of graphs is provided presenting the signals of tests with equal motor settings for the same parameter, and of higher and lower frequencies to show that the shape of the signal is fairly constant over all executed tests. The wiggles and disturbances in the signals are observed for both lower and higher loading proving the measurements to be consistent. Also the relation between the operation of the motor and the appearing loading conditions is quantified. The outcomes are further discussed in section 6.3.2. For every test, every parameter has a characteristic value. This value is the mean amplitude of the oscillating signal. For example, when stated that a motor acceleration of *'x'* rev/s^2 resulted in a gradient of *'y'* m/m, an oscillation pressure signal with a mean amplitude *'y'* m/m was observed. The extraction of the characteristic parameters such as the piston-, wave- and gradient-, period and amplitude is elaborated on in appendix C.1.2. All mean values were obtained in combination with standard deviations. These standard deviations were used to validate the reliability of the averaging process. Furthermore, each test was categorised in the domain which fitted the transport regime the most. These transport regimes were categorised as (1) No transport; (2) Intermittent transport and (3) Continuous transport. The obtained characteristic values and the sediment transport regime for every test is given in table 6.1.

Table 6.1: Obtained characteristic values and transport regimes.

			Repetition 1			Repetition 2			Repetition 3		
Target	Motor AC	Period	Gradient	Transp. regime	Velocity	Gradient	Transp. regime	Velocity	Gradient	Transp. regime	Velocity
$[m/m]$	[rev/s^2]	$[s]$	$[m/m]$	$[-]$	$[m/s]$	$[m/m]$	$[-]$	$[m/s]$	$[m/m]$	$[-]$	$[m/s]$
0.01	0.4	7.72	corrupt*	1		0.016	1	0.0074	0.007	1	0.007
0.02	0.8	6.46	corrupt*	1		0.023	1	0.0107	0.014	1	0.0091
0.031	1.2	4.13	corrupt*	1		0.043	1	0.0156	0.025	1	0.0111
0.036	1.4	3.87				0.045	1	0.0151	0.029	1	0.0118
0.041	1.6	3.65	0.051	2	0.0127	0.053	1	0.0186	0.033	1	0.014
0.046	1.8	3.46				0.062	2	0.0192	0.038	1	0.0141
0.051	2	3.16	0.068	3	0.0149	0.081	3	0.0234	0.044	2	0.0157
0.056	2.2	3.04				0.086	3	0.0241	0.051	3	0.016
0.061	2.4	2.93	0.113	3	0.022	0.092	3	0.023	0.058	3	0.017
0.066	2.6	2.83				0.105	3	0.0236	0.061	3	0.0183
0.071	2.8	2.75				0.11	3	0.0274	0.067	3	0.0183
0.077	3	2.58							0.077	3	0.0197
0.082	3.2	2.51							0.084	3	0.0229
0.087	3.4	2.45							0.09	3	0.0233

*corrupt, means that the measurement file got corrupted and data obtained was not valuable.

The standard deviation of the extracted mean amplitudes of the signals, justified the use of a test averaged amplitude as characteristic values. The extraction of the characteristic amplitude per tests sometimes encountered some spreading over the 1000 executed piston oscillations. For every test and for every parameter, the standard deviation was extracted corresponding to the extracted parameter, given in table 6.2. This provided the obtained accuracy of this method per parameter. Furthermore, the expected accuracy of the final answer was evaluated. The desired accuracy was set at a critical hydraulic gradient of 2 decimals. This implies that for every test the characteristic amplitude multiplied by the corresponding standard deviation should not have exceeded $0.005 m/m$. This was observed only one time, for Series 1, the first time $AC = 2.35$ was tested. All 25 other test from which data is extracted complied with the accuracy requirement.

Table 6.2: Standard deviations of extracted characteristic amplitudes per parameter.

	Average Std. [%]	Maximum Std. [%]	Minimum Std. [%]
Plunger oscillation	0.27	2.07	0.04
Water level oscillation	3.57	12.87	0.28
Gradient	6.17	15.91	1.42
Water level velocity	3.82	7.64	1.74

6.3. Critical hydraulic gradient

The critical gradient for sediment transport from the sand body through the core was not obtained easily. The measurement setup was especially designed for this research and needed to be calibrated and validated. Furthermore, whether or not processes were reflected in a correct way regarding reality was questioned. First, the possibility to govern the hydraulic gradient was tested. This was done by means of varying the acceleration of the motor. As the acceleration of the motor is one of the only parameters that can be controlled in this research, and is not dependent on other parameters, the acceleration of the motor was compared to the appearing sediment transport. Afterwards, these results were coupled. A direct comparison between the appearing hydraulic gradient was made with the appearing transport. These results provide the information needed to answer the research questions and validate the two earlier obtained relations (acceleration vs. gradient and acceleration vs. transport). Furthermore, the results were weighted against other parameters like porosity and positioning, to discuss the influence of various boundary conditions to the appearing gradients and transport. Lastly, the obtained results are explained with theory from earlier chapters, supported by the data.

In appendix C.2 the three relations are discussed contributing to the overall understanding of the functioning of the model set up and the processes occurring in the container. These relations are: the relation between the acceleration of the motor and the measured hydraulic gradient; the relation between the acceleration of the water level and the measured hydraulic gradient; the relation between both accelerations and the observed sediment transport. The relations are extensively elaborated on and supported by graphs and calculations. The main conclusion are summarised below:

Acceleration motor and hydraulic gradient

- Variability occurred between the measured gradients for tests with equal motor settings. The standard deviation is on average 20%. The larger deviations are found for the extreme values of loading conditions (both small and large)
- Two sets of series gave very similar results, comparing the obtained relations within the respective sets reduced the standard deviation to 5% and 13% and their respective linear regressions were almost perfectly aligned.
- Within one test series, the relation between the acceleration of the motor and the appearing gradient is consistent with its linear regression resulting in standard deviations ranging 5% to 10%.

Acceleration water level and hydraulic gradient

- An evaluation of all measured water level accelerations with their respective gradients gave a fairly scatter result, mainly due to measurements from Series 1.
- The relation between the water level acceleration and the measured gradient evaluated per series is linear with low ($\leq 5\%$) standard deviations and for Series 2 and Series 3 the linear coefficients are almost equal.

Acceleration and sediment transport

- The relation between the acceleration of the motor and sediment transport gave different transport regimes for equal motor settings for 20 out of 30 points. For the water level acceleration this is 12 out of 31. The relation between the motor acceleration and the appearing transport is therefore not very accurate and not consistent over the different series.

General

- The amount of conflicting data points is considered as a "reproducibility" score, providing whether the same input in the relation gives the same output for every series.

- The obtained relation between the water level acceleration and the hydraulic gradient & sediment transport is concluded to be more accurate and more consistent than between the motor evaluation and hydraulic gradient & sediment transport. The transmission of energy from the motor towards the water, inducing the hydraulic gradient is thus not optimal and differs between the different series.

6.3.1. Hydraulic gradient and sediment transport

The sediment transport qualitatively evaluated by in the domains: no transport, intermittent transport and continuous transport. With 'no transport' literally no particle movements were observed. 'Intermittent transport' means that only little transport was observed or transport was not constant over every wave oscillation. It was sometimes noticed that randomly, wave oscillations do or do not caused transport. For 'continuous' transport it was evident that continuous transport occurred for every wave oscillation in the test. Each test was categorised in the domain which fitted the transport regime the most. The obtained characteristic hydraulic gradients for each test are plotted against these sediment transport regimes. The results are given in figure 6.4.

A 'no transport' regime is seen for hydraulic gradients of $I < 0.043 m/m$. Depending on the tests, the amount of observed transport varies for $0.043 m/m \leq I < 0.063 m/m$. For all measurement series continuous sediment transport is observed for hydraulic gradients $I \geq 0.081 m/m$. The amount of conflicting data points (intermediate zone) is 10 out of 33, which is the lowest ratio and thus highest reproducibility score. This implies that comparing the measured appearing gradient with the observed sediment transport leads to the most uniform results of the three test series. However, also here one data point (gradient) can be found for which three transport regimes were observed at $I \approx 0.049 m/m$

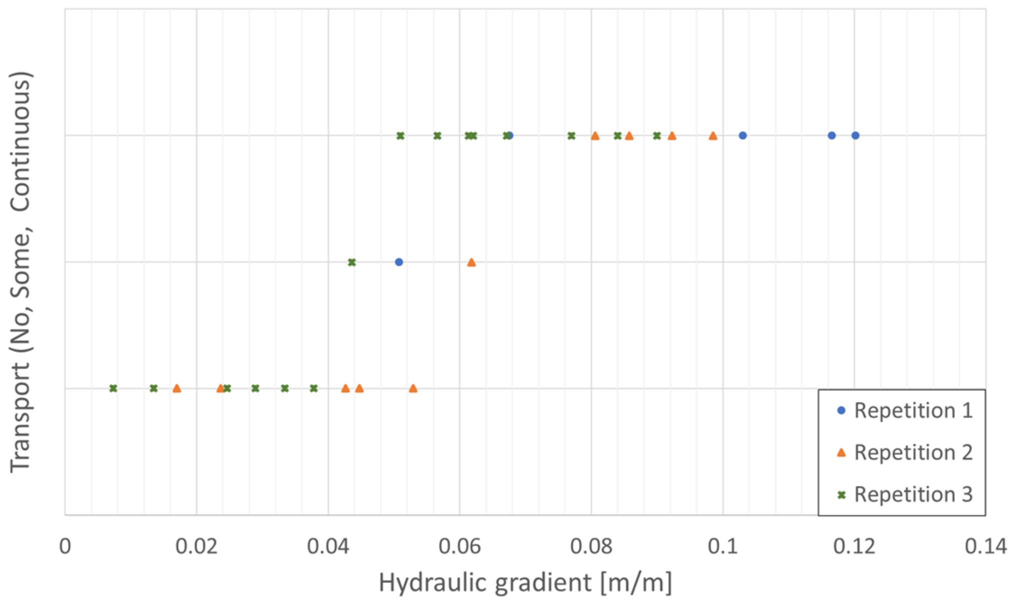

Figure 6.4: Sediment transport regimes for appearing hydraulic gradient.

Taking a closer look on the intermediate zone with conflicting results, the relation between the gradient and transport regimes appears to be similar for the different series. The series have their own 'shift' of which the third series has the most left shifted results and the second series the most right shifted results. The shape of the graph and the amount of measurement point before and after the transition in transport regime are approximately the same. The average hydraulic gradient of the second and third series for which 'no transport' changes to 'intermittent transport' is 0.046m/m with a standard deviation of 23%. The average hydraulic gradient for which all series change from 'intermittent transport' to 'continuous transport' is 0.0523m/m with a standard deviation of 17%. The transition to continuous transport is complete, on average at 0.067m/m with a standard deviation of 23%, this is summarized in table 6.3.

Table 6.3: Hydraulic gradients for transition in sediment transport regime.

Transition	**Mean** $[m/m]$	**St.Dev.** [%]	Series 1 $[m/m]$	Series 2 $[m/m]$	Series 3 $[m/m]$
Initiation of motion	**0.046**	**23**		0.053	0.038
Initiation of continuous motion	**0.052**	**17**	0.051	0.062	0.044
Continuous motion	**0.067**	**23**	0.068	0.081	0.051

For some tests, the transport regime "intermittent transport" was observed. The interchanging stable and unstable situations sparked the curiosity whether a longer duration would cause stabilisation. For two of such tests, the test was immediately repeated with another 1000 waves, total 2000. However, for these tests the sediment transport regime remained constant and no stabilisation occurred. For one test with "continuous transport" the duration was also doubled, this ended with the same result: no change in sediment transport regime.

6.3.2. Hydraulic gradient, sediment transport, porosity and slope

Besides notion on the quantity of the appearing sediment transport (as categorised in the previous section) the observations registered during the tests (see appendix C.2.4), provided more insights. One of the outcomes was the often encountered difference between the sediment transport at the front and at the back of the container. The flow conditions were assumed to be fairly uniform over the cross-section of the container implying that the load conditions would be are similar. This was confirmed during high load conditions in which suspended sediment was turbulently moved back and forward with, at first sight similar stream patterns indicated with dye. However, during these test and especially with tests with lower load conditions differences in sediment transport occured between the front and back of the container. Also, appearing hydraulic gradients did not necessarily result in identical sediment transport regimes for all tests. A possible cause for these inconsistent relations between measured data and observed sediment transport, and the varying sediment transport over the cross-section was found in the resistance against sediment transport.

As discussed in section 4.3, the potential for sediment transport is highly depended on both the acting load on the particles and their resistance. The porosity, stone positioning and pore size key parameters. For the three executed tests, especially the positioning of the stones have proven to vary over the experiments. The used rock is very wide graded enabling a large variety of positions for the rocks and pore size in between. The rocks can be well mixed or sorted, and when sorted, increasing or decreasing in size, in all directions over the container. Although usually wide graded materials have low(er) porosities, above mentioned sorting or 'segregation' of fractions can also cause high(er) porosities than expected. The encountered segregation is not new and was also encountered by Adel et al. (1988) during their research into wide-and gap graded materials.

In the current research, it was it was observed that the finest fractions of stones fall through the pores of the bigger stones during installation, making their way to the bottom of the container and towards where later the sand-core interface would form. The consequence is two fold: (1)A layer of very fine rock on the bottom and, in and on the sand-core interface seemed to function as a geometric filter; (2) The flow resistance through these fine fractions is larger, for which preferential short-circuit flow appears through the bigger pores in the larger core material. This was also observed when injecting dye into the system via a tube. For similar loading situations the dye tended to move more in the direction (horizontally or vertically) were larger stones and (thus) pores were positioned. In fig. 6.5 two figures are presented illustrating this difference for two test with equal loading ($AC = 2.4\text{rev}/s^2$ and $T = 2.93s$).

The filter parameter for the smallest core fractions $d_{f,15,\text{smallest fraction}}/d_{b,85} \approx 15$. This implies that the filter

(a) Separation causing flow away from the interface.

(b) Separation causing flow along the interface.

Figure 6.5: Dye experiments showing the flow difference caused by positioning of stones.

is geometrically open and thus sediment was able to migrate through the pores of the finest fraction of core material. However, the thickness of this fraction of core material and its positioning still determined the resistance to the flow and the whether or not the excited load were big enough to initiate motion. In figure 6.6, examples were given of situations where porosity and positioning (might have) caused differences in sediment transport. Figures 6.6a and 6.6b show the initial situation of Series 1. In this section, for all hydraulic gradients more transport was apparent at the back of the container than at the front, probably caused by the higher porosity (less filter-like layer) at the back. In figures 6.6c and 6.6d the situation of series two is displayed where short-circuit flow was observed during the tests due to a higher porosity close by the plywood screen. In the third series it was tried to counteract both processes. At both sides a uniform rock core was formed. However at the front, more than intended, the flow along the interface was stimulated as the flow path along the interface was much more open. This is presented in figures 6.6d and 6.6e. Although not very clear in the picture, it is observed that at the back bigger pores were present more towards the middle of the core material. The sediment propagated from top to bottom until point (X=37cm, Y=2.8cm), just underneath stone 'A' where the sediments moved inward and disappeared for visual evaluation.

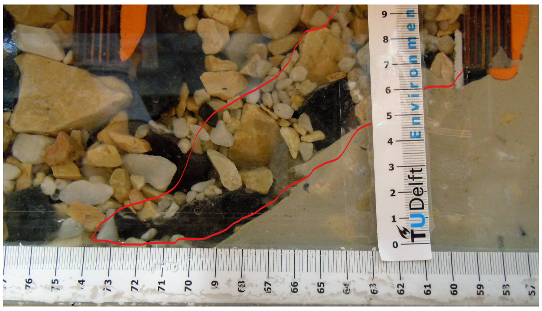

(a) Lower porosity at the front (from Series 1).

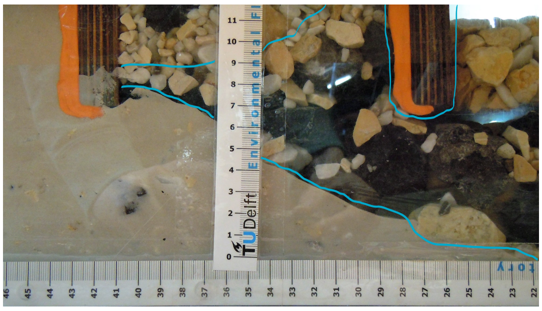

(b) Higher porosity at the back (from Series 1).

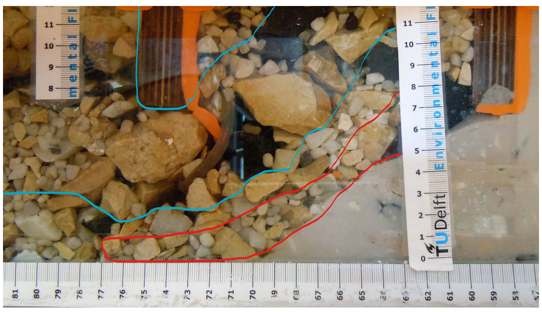

(c) Porosity causing short circuit flow (from Series 2).

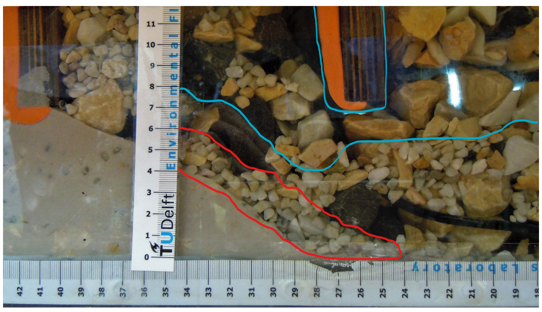

(d) Porosity causing short circuit flow (from Series 2).

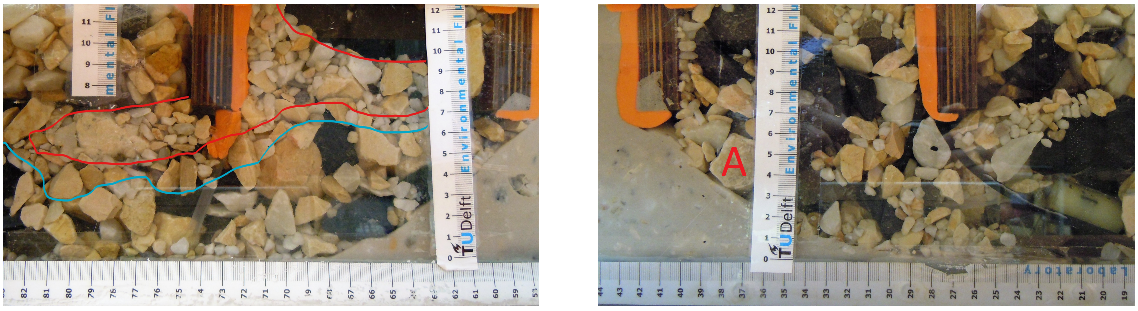

(e) Porosity causing 'long circuit flow' (from Series 3).

(f) Uniform porosity at the back (from Series 3).

Figure 6.6: Variations observed in porosity and positioning influencing transport*
*Red zones have lower porosities and cause higher resistance for flow than blue zones.

When linking the obtained hydraulic gradient, the observed transport and the porosity and positioning of the stones some interesting relations are proposed. From Series 1 only measurement data is available for tests in which already transport was seen. Therefore, this series is only to a certain extend compared with the other series. In section 6.3.1 (table 6.3) it is concluded that in Series 3 the lowest gradient was measured for transition in sediment transport regime. Supported by the processes described above, this can be explained by the "long-circuit flow" forced by the positioning and porosity of the layers, indicated by the blue zone in figure 6.6f. In the second series, the gradient for which the transition of sediment transport regime occurs was the highest. As indicated by the red zones in figures 6.6c and 6.6d, the filter function of the specific layer on the interface was large and thus short circuit flow along the plywood screen was forced. The exact gradients for which sediment transport started, going from no transport to intermittent transport is unknown for the first series. However, the transition from intermittent transport to continuous transport was observed at a lower gradient then in Series 2 and at a higher gradient than in Series 3. As the dominant transport was observed at the backside of the container, figure 6.6b is used to explain that the porous and open positioning caused earlier for transport than in Series 2 but caused later for transport than in the situation of Series 3. This was probably forced by 'long-circuit flow' with even higher sediment transport rates.

Besides, it is proposed that the form of the interface is a parameter which influences the appearing sediment transport. This is caused by the higher flow velocities that appear along the plywood screen. The closer the interface is to this path flow, the more sediment is transported. In some experiments a elongated tongue formed under the plywood screen. In these experiments the sediment transport tended to increase rapidly after the tongue was formed. Pictures of this tongue are given in appendix C.2.1.

6.3.3. Critical filter velocity

The Forchheimer equation can be used to describe the relation between the filter velocity and the appearing gradient when one of both is know in combination with coefficients α and β. Where in this study the critical gradients was measured, other studies speak of the critical filter velocity as a loading criteria for transport. Because zone 2, were the water level was oscillating, was filled over the full cross-section with core material, but not filled up towards where the velocity was measured, the measured velocity was in fact the filter velocity, denoted by u_f. In appendix C.2.2 an evaluation of the obtained filter velocities is made of which the most important aspects are summarised below:

- The filter velocities could only be obtained very roughly and provide a first approximation of the filter velocities in the model, but it is not a sound estimate of the filer velocities appearing along the interface. The filter velocities in the model are by means of a calculation estimated to range between $0.007 m/s$ and $0.044 m/s$.
- As discussed in section 5.3.1 corresponding Reynolds filternumbers range between 386 to 2422 implying that the viscous shear is incorrectly scaled and the flow regime is partly laminar. This is supported by the evaluation of the Forchheimer coefficients executed in this section. These were approximated by coupling the measured appearing gradient to the measured filter velocities. An increase of the influence of the laminar term was observed when comparing the Forchheimer coefficients to those found by calculating the coefficients for the dimensions of the nominal breakwater by Polidoro et al. (2015).

- For the three transport regimes the mean critical filter velocity were obtained from the different series. These are presented in table 6.4 with their corresponding standard deviations.
- To find the relation between the measured hydraulic gradient and the measured filter velocities, the Forchheimer equation is fitted to the data and the Forchheimer coefficients are calculated. The results are presented in fig. C.11 and the obtained coefficients are $a = 1.16$, $b = 109.24$, $\alpha = 719.08$ and $\beta = 1.21$, The critical filter velocities were approached from the measured critical gradient with use of the Forchheimer coefficients to obtain the deviation of the regression and the measured data. These results are shown in the third column of table 6.4, showing very high resemblance with the measured vertical critical filter velocities.

Table 6.4: Vertical filter velocity amplitudes for transition in sediment transport regime.

Transition	**Mean** $[m/s]$	**St.Dev.** [%]	Calc (Forchheimer) $[m/s]$	Series 1 $[m/s]$	Series 2 $[m/s]$	Series 3 $[m/s]$
Initiation of motion			0.015		0.019	0.014
Initiation of continuous motion	**0.016**	**20.1**	0.016	0.013	0.019	0.016
Continuous motion	**0.018**	**25.3**	0.019	0.015	0.023	0.016

6.4. Filter relations

In this section is elaborated on the applicability of conventional filter theories for the target area investigated in this research. If relevant, the parameter X for the existing filter formula is determined. For this evaluation the gradients are rounded to the pre-set accuracy of 2 decimals.

$$\text{If} \quad \frac{I_{\text{critical,appearing}}}{I_{\text{critical,calculated}}} < X \quad \rightarrow \text{Stable} \tag{6.1}$$

The relations between the appearing sediment transport and the calculated critical gradients or velocities are described below. In appendix C.2.3 the stability relation $I_{\text{appearing}}/I_{\text{critical,calculated}}$ is plotted against the sediment transport regimes defined in section 6.3.1 for the different measurement series. This graphical representation provides insight in the spreading of the transport regime over the ratio $I_{\text{appearing}}/I_{\text{critical,calculated}}$.

6.4.1. Stability criteria

Critical gradient as presented by de Graauw et al. (1983)

The relation by de Graauw et al. (1983) is based on geometric parameters only and therefore constant for all executed tests in this research. The critical gradient obtained with this method is $I_{\text{cr,calc}} = 0.11 m/m$. For the current research the lowest and average appearing gradients at initiation of transport are $I_{\text{cr,appear}} = 0.04 m/m$ and $I_{\text{cr,appear}} = 0.05 m/m$ respectively. The result is a parameter $X = I_{\text{cr,appear}}/I_{\text{cr,calc}} = 0.36 - 0.45$. This results is remarkable as Wolters (2012) found that the relation by the de Graauw et al. (1983) was conservative. In their research a similar parameter was found describing a critical gradient of ~ 3 times larger than calculated via de Graauw et al. (1983). However, the value of the obtained critical gradient via de Graauw et al. (1983) for this research is a factor 10 larger than for the reference researches by Polidoro et al. (2015) and Vanneste and Troch (2012). This does not necessarily mean that the formula by the de Graauw et al. (1983) is not applicable but it deserves attention. It is seen that when sand is made smaller and smaller without changing other parameters, a very high critical gradient results from the calculation, which is not necessarily logical.

Critical gradient as presented by Wolters (2012)

The method proposed by Klein Breteler (1989) made use of a critical filter velocity. As this research did not measure filter velocities accurately, the critical filter velocity by Klein Breteler (1989) is inserted in the Forchheimer equation as proposed in Wolters (2012). The critical filter velocity by Klein Breteler (1989) is uniform for the experiments executed in this research: $u_{cr} = 0.0136 m/s$, which results in $I_{\text{cr,calc}} = 0.04 m/m$. This approach leads to a parameter $X = I_{\text{cr,appear}}/I_{\text{cr,calc}} = 1.0 - 1.25$.

Although the approximated filter velocities have some uncertainties, the critical filter velocities are related to those approximated via Klein Breteler (1989). $X_{\text{u,filter}} = 1.17 - 1.30$ vertically, (thus from the vertical oscillation of the water level), and $X_{\text{u,filter}} = 1.88 - 2.12$ in the horizontal direction (calculated over the horizontal cross-section underneath the plywood screen). A second approach is used by calculating the critical filter velocities from the measured critical gradient by means of the Forchheimer equation (eq. (4.3)) $X_{\text{u,filter,Forch}} = 1.10 - 1.40$ with coefficients a= 1.62, b=99.8.

Suffusion as presented by Polidoro et al. (2015)
In the research by Polidoro et al. (2015) it was assumed that the suffusion theory by Allsop and Williams (1991) could be used to approximate the critical hydraulic gradient for a sand- core material mixture. The resulting critical gradient for the current research using this method was $I_{cr} = 0.023$. The desired parameter X in this theory values $X = I_{\text{cr,appear}}/I_{\text{cr,calc}} = 1.74 - 2.17$ depending on the lowest or average value of the test series. The obtained scalable resistance parameters X describing the relation between the currently available predictive literature and the results of this research are summarised in table 6.5. Furthermore, the parameter X for the applicability of the Forchheimer equation (eq. (4.3)) is given, which is elaborated on in section 6.4.2.

Table 6.5: Parameter X for various evaluated relations

Ratio	Used method	X
$I_{\text{cr,appear}}/I_{\text{cr,calc}}$	de Graauw et al. (1983)	0.36-0.45
$u_{\text{f,cr,appear}}/u_{\text{f,cr,calc}}$	Klein Breteler (1989)	1.17-1.30
$I_{\text{cr,appear}}/I_{\text{cr,calc}}$	Allsop and Williams (1991)	1.74-2.17

6.4.2. Case study hydraulic load versus measured resistance

The critical hydraulic gradients found in this research range between 0.04 and 0.05 for initiation of motion and continuous transport respectively, when taken the conservative values. By means of the approximations made by Vanneste and Troch (2012) and the measurement executed by Polidoro et al. (2015) the relative depth at which these gradients appear are estimated.

Considering the calculation model by Vanneste and Troch (2012) the lower inner corner is evaluated for $z/h \leq -0.46$, in the zone of interest as defined in section 4.1.1. In this complete zone, the maximum calculated gradient is $0.037 m/m$, which is lower than the obtained critical gradients in the current research. This implies that under the wave loading conditions by Vanneste and Troch (2012), calculated with their method, the interface is proposed to be stable.

For the nine loading conditions used by Polidoro et al. (2015) the gradients observed in the zone of interest for the current research all remained under an appearing gradient of $I_{\text{appear}} = 0.03$ which implies the critical loading condition is not met. The measured gradients $I\text{APPEAR} \geq 0.04$ are found only for the storm load condition (condition 9) at depths $z0mCD$ to $-5.5mCD$ and thus $z/h \geq -0.43$. This implies that for the loading conditions by Polidoro et al. (2015) and the critical gradient obtained in the current research, sediments would be stable in the lower inner corner of the breakwater.

7 Conclusion

In this chapter the conclusions of this research are elaborated on and the research questions described in the problem statement are answered. The main objective of the research was to study the behaviour of the sediments at the interface to a rubble mound in a sandfill, when subjected to hydraulic loading. Subsequently, the potential for the shortening of geotextiles used in sandfill retaining rubble mound structures is discussed. By means of answering the subquestions, conclusions are drawn leading to the main conclusion and contribution of this thesis to the currently available literature on this topic. In chapter 8 the recommendations for further research are elaborated on to help and guide potential future research.

In order to study the physical interaction between the sediments of a sandfill at the interface to a rubble mound when subjected to hydraulic loading, a physical scale model was developed. This model was designed to study both the development of the interface between the sandfill and the rubble mound during construction (with a shortened geotextile) and the response of this interface to hydraulic loading.

Development of initial interface

The processes during the initial infill and the development of the interface were studied for wet and dry installation. The resulting interface dimensions do not seem to differ much. However, the observed processes during installation do. It is therefore concluded that using this model, a consistent installation technique is important. In practice, land reclamation tends to be a rough process where the sand is deposited by dump trucks or dredged sludge is discharged through pipes at high velocities. The observed processes during wet installation, such as the turbulent spreading of sediments subjected to flow driven by the water level gradient and waves, are expected to represent the reality well. Furthermore, with wet installation on average further penetration of the sediments into the core and slightly more gentle slopes were observed. This resulted in a higher total amount of transported sediments. The angle of the slope was approximately constant over all tests and can be roughly estimated at 35°. Considering the model setup, the packing density and cohesion of the sand, the pouring height, pouring velocity and amount of sand added at once are preferred to be controlled as they all have a positive correlation with the amount of sediment transported into the core. Besides, the sediment to core size ratio is an important parameter influencing filling of the core pores. In the research, sediment ratios of $d_{15,f}/d_{85,b} = 8.6$ and $d_{15,f}/d_{85,b} = 63.2$ were tested and only in the latter case fully filled core pores were observed.The geometric ratio of $d_{15,f}/d_{85,b} = 63.2$ is realistic on prototype scale and thus results obtained in this setup are assumed normative. When a geotextile in a sandfill retaining structure is shortened, migration of sediment through the core can be expected to be similar to the wet installation in this setup (as presented in figure 6.1b). Furthermore, the results of the experiments show that the installation of conventional open filter with according filter rules provides resistance against the initial transport during installation. After the waves and flow by discharged dredge sludge are dissolved, a stable sand body is formed. In practice, an estimation of the core pore size, the shortening depth of the geotextile and the interface slope of $\approx 35°$ can lead to an approximation of the amount of sediments lost due to the initial infill per meter.

Consistency and accuracy of the model setup

Besides the modelling of the interface development, the test setup was used to evaluate the processes occurring at the interface when subjected to hydraulic loading. It was therefore important to gain insight in the consistency, accuracy and reproducibility of the model tests. The results obtained in the experiments support the feasibility of the model setup. The iterative process of designing the model has lead to a model setup in which successfully comparable loading conditions were obtained for equal system settings. This was concluded from the deviations between the measured data and their respective linear regression. For the water level velocity and water level acceleration the standard deviations range between $\sigma = 4\%$ and $\sigma = 13\%$ (n=3) and for the hydraulic gradient deviations between $\sigma = 5\%$ and $\sigma = 9\%$ (n=3) were found. Also when comparing the full dataset promising results were obtained. For the water level velocity and the hydraulic gradient standard deviations of $\sigma \approx 20\%$ were found for identical motor settings over the tests. The water level amplitude and water level acceleration were observed with higher deviations of $\sigma \approx 30\%$ for the different series. Although the latter spreading seems rather large, the reason for the deviations were easily traced and were attributed to the transmission between the motor operation and the plunger, and how forces were transmitted from the plunger to the water. The predefined accuracy of the measured hydraulic gradient, set to be conclusive at two decimals, was achieved as for all tests the absolute standard deviation remained lower than $0.005 m/m$.

The transition of sediment transport regime was observed at equal or neighbouring acceleration steps of the motor. When comparing the transition of sediment transport regime based on the measured gradient the spreading between the series was less and a mean value with ($\sigma \sim 20\%$) was found.

Concluding, a model set up was designed which delivered fairly accurate and consistent measurements over three series of tests. With the lessons learnt from the current research, after a series of improvements, the model setup is presumed to be very suitable for researching the hydraulic gradient for initiation of sediment transport in sand-core material mixtures. The use of the pressure sensors has proven to be fairly accurate and with multiple sensor couples in place a realistic course of the pressure through the core material could be obtained. Especially the enlargement of the amount of test series would contribute to the validity and reproducibility of the model, although with the current test series the general outcome is already carefully positive.

Critical hydraulic gradient

It is concluded that the appearing hydraulic gradients in the tests were measured accurately. The hydraulic gradients obtained in combination with the dominant transport regime gave a concise overview of the initiation of transport. On average, no transport was observed for gradients below $0.046 m/m$, for gradients above $0.052 m/m$ also continuous transport was seen and, for a gradient above $0.07 m/m$ only continuous transport was observed with standard deviations of respectively $\sigma = 23\%$, $\sigma = 17\%$ and $\sigma = 23\%$ (n=3). The former two limit gradients both round to $0.05 m/m$ resulting in only 1 initiation of transport criterion. The standard deviations are considered fairly large and can be attributed to the differences in porosity and positioning as described in the previous section. When using these conclusions in an practical application it is recommended to use conservative values. The lowest hydraulic gradient found for the initiation of transport and for continuous transport were both $0.04 m/m$ rounded. Both for tests where some transport and where continuous transport occurred, extended tests did not lead to change in sediment transport regime or stabilisation. It is thus suggested in all cases the transport regime remained constant.

Indicative values of the (critical) filter velocities are proposed. Although these estimates are rough, they provide basic approximations for comparison. The filter velocities are the test averaged velocity amplitudes measured directly from the oscillating water level. The measured critical filter velocities correspond well with velocities obtained from the Forchheimer equation inserting critical hydraulic gradients. However, as critical stability parameter it is recommended to use the critical gradient determined in this research over the critical filter velocity as this was measured more accurately. The vertical average filter velocities for the start of continuous and solely continuous transport and are $0.016 m/s$ and $0.018 m/s$ with fairly large standard deviations 20% and 25%. As the deviations are considerable, in practice, if any, more the conservative values $0.013 m/s$ and $0.015 m/s$ should be used for the two highest transport regimes.

It is suggested that the porosity, positioning and size of the pores have a large influence on the measured appearing gradient and sediment transport processes in the container, and thus on the variation in the obtained measurement data. This is based on the visual evaluation of the installed stones, were segregation was observed, coupled with the obtained test results. Most inconsistencies mentioned above can be explained by the variability in the placement and pore size of the core material. Short circuit flow, caused by small rocks on the bottom and larger rocks close to the plywood screen, tends to decrease the amount of observed sediment transport. The other way around, large stones at the bottom and smaller fractions close to the plywood screens (1) tend to make the streamlines more horizontal and (2) increase the sediment transport. This finding is supported by the measured hydraulic gradients. In series with a less open core structure the hydraulic gradients were lower at equal motor acceleration settings and, lower sediment transport regimes were observed. The cause of the variance in positioning, and thus in porosity and pore size, over the tests and also over the cross-section of the container, was found in the segregation of the material during placement. This problem has been earlier encountered by Adel et al. (1988) and has proven very difficult to control.

Stability relations

A parameter X was defined to compare the results obtained from the current research to predictive stability criteria from earlier research. Furthermore, they provide the base for additional, future research in which more parameters can be varied. In section 6.4 it is discussed that some stability criteria are dependent on geometrical input parameters only. The geometric characteristics of the core material and sand were not varied. In terms of statistics, this means that the obtained X-parameter was "one draw of a population" which means that, when different sediment to core size ratios are tested, X could be different. By varying this ratio, it can be decided if parameter X is constant, or what its deviation is and thus if it is generally applicable. It was observed that obtained values X in the current research generally ranged around roughly 1.2 with a spreading of ~ 40%. The current known filter relations therefore seem to approximate the critical limits of the interface stability rather well, and except for de Graauw et al. (1983), always under predicting the critical gradient which provides conservative approximations. Although the filter velocities were measured roughly, the best representation was given by Klein Breteler (1989) when approximating critical filter velocities. The relations by de Graauw et al. (1983) and Allsop and Williams (1991) seem less applicable for the estimation of the critical gradient for the configuration tested in this research. However, the critical gradient by de Graauw et al. (1983) calculated with the input parameters for the current research was a factor 10 higher than the critical gradients calculated for reference research (both model and prototype scale) and did not match the measured critical gradient. From a case study the suffusion theory by Allsop and Williams (1991) appeared to be highly dependent on the accuracy of the composite grading curve because the transition of the largest sand particles to the smallest core particles determines were the H-F curve minimum is. The composite grading was in this research roughly estimated because the sieve curves are combined by means of a calculation and not sieved as a whole.

Whether or not the suffusion theory by Allsop and Williams (1991) is appropriate to describe the behaviour of a sand-core mixture subjected to wave loading, could be questioned based on the obtained results as discussed in the paragraph above. However, some extra remarks are made stressing the potential for this theory. The current research was executed with a gap-graded material of which the distribution of the particles ranging between the largest sand particles (200um) and smallest gravel particles (1-6mm) was very uncertain. As explained in sections 5.1.1 and 6.4 this contributed to the uncertainty of the composite grading curve, on which the calculated critical gradient is highly dependent. Extra calculations and explanations were given which provided that the critical gradient obtained with the suffusion theory for the current research was better estimated at $I_{cr} = 0.04 - 0.05$ resulting in an X-parameter of $X = 1.0 - 1.25$. This implies that the suffusion theory has potential for describing the situation described in this research in an equal matter as for instance the theory by Klein Breteler (1989).

This research is concluded by stressing the potential for the shortening of geotextiles at the interface to a rubble mound in a sandfill. In the scale model a critical hydraulic gradient of $I \geq 0.04m/m$ was found for the initiation of transport for the most conservative case when the geotextile was shortened 25%. For continuous transport, higher gradients were found. The case study suggests that the critical gradient obtained is larger than the appearing gradients in the lower inner corner of a breakwater as determined physically or analytically by Polidoro et al. (2015) and Vanneste and Troch (2012) respectively. This implies that potentially, the geotextiles can be shortened without compensating on stability. The current available literature studied in this research provides initial approximations of the critical gradient that could represent the configuration at hand. This should, however, be further tested for more different sediment to core size ratios and on larger scale. Furthermore, curiosity was sparked toward the suffusion theory by Allsop and Williams (1991), as this theory seems to describe the stability of the configuration as well.

8

Discussion and recommendations

In order to define how the current research has contributed to the knowledge known from literature, the results are discussed. Some assumptions and simplifications made, contribute to the uncertainty of the model and the conclusions based on the model tests. Especially for relating the conclusions to full scale configurations, some thoughts are shared. Again, the topics are split in the development of a physical model setup and exploring the critical hydraulic gradient for the interface to a rubble mound in a sandfill.

8.1. Physical model

The developed physical model setup was concluded to be fairly accurate, and to a certain extent considered to generate reproducible results. The largest deviations between results of different test could be attributed to the positioning of the used materials and equipment. However, also some model deficiencies are encountered.

The development of the initial interface was concluded to be rather independent on the used installation technique and resulted in a infiltration of the placed sand into the core of the rubble mound. The initial infill formed a 35° slope which had migrated into the core in a more or lesser extend during installation. Unfortunately, during the installation process no accurate measurements were executed and thus the appearing forces causing the development are unknown. Furthermore, during installation no forces were exerted (e.g. wave oscillations), which could appear in reality. On the other hand, the use of an impermeable plywood screen instead of a geotextile gives more conservative results as no a water level gradient occurred which increased the inwards transport. When a geotextile was installed it is suggested to be less as the water can flow through the textile. However, it is still suggested that the lack of exerted forces during installation could cause further infiltration of sand into the core, even with a geotextile in place. Besides, during the installation in reality dredged sludge is used and with higher water depth over shorting depth ratios which increase the suspended sediment load in the water. Based on visual observations in the model also this could increase the infiltration of sediments into the core. Considering all aspects the model installation gives a good first approximation the processes at hand but cannot be scaled and evaluated for full scale purposes directly. The obtained slope is considered to hold for full scale application, however, it is recommended to test the development at larger scale. The biggest problem with this would be the evaluation of the inward transport. Either, a large see-through wall is needed, or perhaps more advanced measurement equipment is can be obtained for larger scale research. A downside of a larger scale experiment with see through wall, is that on large scale wall effects tend to increase. Secondary improvements can be obtained by researching the effects of compaction, which extensively applied in reality and was only minor applied in the current research.

After the development of the interface proved to be constant, the interface stability was studied when subjected to hydraulic loading. The observed and measured processes were rather constant over tests with equal loading settings. However, better results were obtained combining the flow parameters with the observations (thus flow velocity or hydraulic gradient vs. sediment transport). This implies that an improvement can be found in ensuring equal flow parameters for equal loading settings of the motor. In order to do so, the operation of the motor and plunger system should be improved. An advancement in this system ensures a targeted control of the model setup and enables to force a hydraulic gradient as loading condition by simply setting the motor computer. This can be easily improved in second version of the model setup. Furthermore, constant porosity and positioning of stones in the model should be assured. To the contrary, the porosity and positioning of stones may differ largely in various real cases. This implies that in future research, the test series should be extended with tests in which the variation of the positioning of stones is controlled. The above conclusion is based on the observations made on the positioning of stones and sediment transport, the measured hydraulic gradients, and the observed flow patterns combined with theoretical knowledge. However, the detailed flow processes in this research were hard to analyse. Although the experiments with dye provided some kind of estimation, the presumed short- and long circuit flow were qualitatively and roughly indicated. To obtain constant positioning of stones, glued models could be made similar to those made in this research. This would be beneficial for the continuity of all flow related (or porosity) related processes. The transport was proven to be fairly constant without significant difference between the sediment transport along the side or in the middle, the implies that loose rock is not necessarily needed for evaluation. However, a way should be found to ensure the wall effects are minimized. Furthermore, the interface did not form at the same position at every test. The sensors were assumed to measure the hydraulic gradient along the interface, but the distance to the interface varied. Also, only one gradient over the $17cm$ interface is measured. Although this complied in order size with appropriate earlier research, the amount of sensors should be increased to gain more insight in the gradients varying both horizontally and vertically around the interface. By making use of a grid with multiple pressure meters and/ or flow meters a more detailed overview of the distribution of pressures and velocities could be obtained. The drawback of the insufficient amount of measurement is observed over the whole research. Although the data obtained in the three series has some strong resemblance, the amount of generated data with this model is rather low to make conclusive remarks. Moreover, in the first series a part of the measurements got corrupted. With standard deviations for some parameters ranging 20% to 30% between measurement series, the error rate is also significant. As mentioned these deviations were mainly attributed to the variability of the positioning of stones, however, also the floater used to measure the water level oscillation (and thus velocity and acceleration) sometimes encountered friction with the walls or got partly submerged, resulting in measurement errors. It is thus recommended to implement a series of improvements in the model setup after which the interface stability of sand-core material mixtures studied. With this improvements, the complete scaling should be enlarged (including container size) as currently Reynolds filter numbers were observed implying that an transitional flow regime occurred between laminar and turbulent flow for the lower range of loading conditions. This should be prevented in future research.

8.2. Critical hydraulic gradient

The various relations between the motor acceleration, (measured) flow parameters, hydraulic gradient and sediment transport regimes have proven consistent and fairly accurate relations. Also the values obtained form the measurement signals were in most cases conclusive. However, especially for the measured pressure signal some remarks should be considered. The characteristic values were obtained from the filtered signal. Although most spikes were proven to be filtered out, the maximum amplitude might still be somewhat influenced by the noise signal. Moreover, the disturbance caused by the tilting of the plunger remained partly in the signal after filtering. If the tilting also resulted in a peak/through in the appearing hydraulic gradient, or only in the signal, is unknown. Due to the 1000-wave averaging process also some measurement errors were included, potentially resulting in small deviations between the physically appearing value and the values used in the analyses. It is therefore that the obtained gradients might be not as accurate as presented by the analyses in the report. After the model is improved with amongst others signal-noise mitigation measures such as an improved motor operation system and an overall increased stability of the setup, better and more accurate results can be obtained.

The hydraulic gradients were desired to be measured along the interface, however, as already indicated the distance between the measured 'line' and the interface varies. The gradient at the interface itself therefore might differ from the measured gradients and lower the accuracy of the obtained critical gradient. Furthermore, the sediment transport regimes only gave qualitative results and the classification is made by visual evaluation. Although some criteria for each regime were listed, the outcome of this process is based purely on the consistency of the researcher's judgement.

The hydraulic gradient is obtained by varying the acceleration of the motor. As explained, by this the loading frequency (or period) is different for tests of unequal loading. The influence of the loading frequency on the sediment transport is not considered. The occurrence of a transition of sediment transport regime is attributed to a higher hydraulic gradient. However, from literature by amongst other de Graauw et al. (1984)

(discussed earlier in section 4.4.2) it is know that the frequency does effect this processes. Depending on whether parallel flow or perpendicular flow to the interface is dominant, this could lead to higher or lower values of the critical hydraulic gradient. Also, cyclic flow parallel to the interface was observed to lead to compaction. After compaction, the critical gradient was no longer dependent on the period. Additional test should provide insight in the influence of the frequency and by not doing tests subsequently or doing more series repetions on the same setup the influence of compaction can be studied. This is further elaborated on in section 8.3.

The obtained filter velocities are used to gain some insight in the order size of the filter velocities in the model. However, the flow patterns through the core material form presumably, a complex system for which the filter velocities under the plywood screen and over the interface can only be roughly approach. The determined filter velocities do give good results when combined with the regression analyses of the Forchheimer coefficients. Remarkably, the obtained critical filter velocities calculated with the Forchheimer equation from the critical hydraulic gradients are within 5% of the measured values. However, in general the relation between the measured filter velocity and the measured appearing gradient with use of the regression- Forchheimer relation is 75 – 99% accurate. Furthermore, the Forchheimer coefficients 'a' and 'b' were considered constants in all calculations while in this and the preceding chapter is stressed that the positioning and segregation of stones largely contributed to the (local and averaged) porosity. This implies that the porosity had to be determined test specifically and corresponding Forchheimer coefficients determined. The obtained critical filter velocities differ within a factor 1.2-1.4 from critical filter velocities approximated with conventional filter relations implying the stability criterion for the specific configuration in this research is of the same order size as for conventional filter relations. However, also in these calculations a constant porosity over all test series was assumed which in fact were series specific.

Although the currently available literature was not developed specifically applicable to the interface stability studied in this research, the order size outcomes were similar. This could imply that: (1) the stability criterion for the configuration at hand might be comparable to earlier studied filter configurations; (2) the currently available literature might be applicable to give a rough first approximation of the critical loading conditions. It is, however, important to understand that the obtained X-parameters were statistically "one sample of a population" and variations in geometric characteristics of the used materials need to be made in order to find out whether the X-parameters are actually constant and thus, generally applicable.

8.3. Recommendations

The results obtained in this research suggest that the critical loading conditions for the interface stability to a rubble mound in a sandfill are of comparable order to conventional filter criteria. Furthermore, the results justify the further exploration towards the potential of the abbreviation of geotextiles at the considered interface. From the literature study it was already concluded that this topic can be approached by looking at the interaction between the loading to and resistance of the interface. This research contributed to the better understanding of the resistance against loading of the sediments at the interface. Although already interesting results were obtained, further research can be provide more accurate and reliable results, potentially generated with an improved version of the model setup used in this research. Recommendations for the improved setup and test program are given below. Nevertheless, it is recommended to focus further research into the approximation of the hydraulic loads in the zone of interest. The calculation model by Vanneste and Troch (2012) and/or Burcharth et al. (1999) could, for example, be more extensively tested against the data set obtained by Polidoro et al. (2015) and potentially other available data sets. Now only the results from the papers were compared where a full calculation towards all measured pressures in the research by Polidoro et al. (2015) could prove the applicability of the calculation model by Vanneste and Troch (2012). This is especially interesting as this calculation model was developed with an open rear face breakwater whereas Polidoro et al. (2015) has modelled a closed rear face breakwater. Also, the applicability and/or further development of numerical models is of interest. The potential outcomes of such a research could provide more insight on the wave attenuation and prediction of pressures in the core material, which is could be beneficial more general than only for the target area of this research. Self-evident, a full scale model of a rubble mound with a sandfill behind would be the best method to obtain the necessary insight to determine the pore pressure attenuation in such a structure and simultaneously determine the possibilities for the abbreviation of geotextiles. However, at this stage the investment towards this research is not recommended as more knowledge could be obtained from the above mentioned further research.

Improvements of the model setup

- Install a grid of pressure sensors over the full area of interest in order to obtain accurate 2D- gradients in and around the interface.
- Use a bigger, especially wider, container to enable an (even) smaller length scale parameter λ, ensuring Reynolds filter numbers to go up.
- Signal noise mitigation measures in order to obtain more accurate measurement signals: Better calibration of the internal transmission of the motor; more advanced programming for the operation of the motor; a more rigid setup + table and ensuring overall stability; an improved design for the plunger with smooth operation: decrease to use of wood in vital parts.
- The construction of a sloped separation between the core and the sand body, preferably of geotextile will improve the approach of reality.
- Use a more wide graded sand to have a better representation of a reclamation and simultaneously enabling a better evaluation of the suffusion theory.
- Improve the method for measuring filter velocities for verification purposes, preferably at various locations.

Guidance for further research

The differences between $d_{85}/d_{15} = 8.6$ and $d_{85}/d_{15} = 63.2$ sediment to core size ratios suggest opportunities in using a geometrically open filter on top of the core material at the open interface where the geotextile is shortened. This is something that can be easily tested with the model setup used in this research. Also, a more extensive evaluation of different geometric relations could be interesting to find an optimum for the resistance against the initial infill, and the sediment transport induced by hydraulic loading. In any case, more test series should be executed in order to obtain conclusive results.

In the current research little parameters are varied. Interesting would be:

- Core size to sediment size ratio, different sizes of core material for instance up to a d_{50} of $10cm$ which is the d_{50} obtained when scaling based on d_{50} instead of the filter parameter $d_{f,15}/d_{b,85}$. Enabled by making use of a larger container.
- Core grading and sediment grading. Especially a wider graded sediment which resembles "dredged" sand as for instance proposed by Polidoro et al. (2015). When making use of scaling for model tests, also the scaled sand should be wide graded.
- Shorting length and shorting length/depth ratio. In the current research the geotextile was shortened over a length which resembles 25% of the water depth. Both the effects of the absolute shortening length and shorting length/depth ratio should be tested. Based on the obtained results especially larger shortening seems interesting as this was proposed possible. However, also smaller shortening is of interest to acquire prove for the stability of such a measure. Thus, for instance ranging between 15% and 45%.
- Variation in application of loading conditions: is the transport criterion independent of earlier exerted gradients and does compaction due to cyclic loading occur and influence the results.
- Evaluate the influence of the loading frequency on the system. By developing a new/other test program it could be tried to generate equal gradients with different oscillation frequencies by setting larger and smaller oscillation amplitudes. In this manner the influence of the frequency can be isolated. Also, equal frequencies with varying gradients could exclude the influence of the frequency.

Nomenclature

Abbreviations

Symbol	Description	Unit
Fr	Froude number	-
KC	Keulegan-Carpenter number	-
mCD	Meters below Chart Datum	-
Re	Reynolds number	-
We	Weber number	-

Symbols

Symbol	Description	Unit
A	Surface Area	m^2
a	Forchheimer friction coefficient	s/m
AC	Acceleration of the motor	rev/s^s
b	Forchheimer friction coefficient	s^2/m^2
c	Forchheimer friction coefficient	s^2/m
C_u	Hazen's uniformity coefficient	-
d_x	Characteristic grainsize filter for which x% of mass is smaller than this size	m
g	Gravitational acceleration = 9.81	m/s^2
H	Wave height	m
h	Depth	m
I	Hydraulic gradient	m/m
K	Hydraulic conductivity	m/s
k	Wave number	m^{-1}
k'	Internal wave number (inside a structure)	m^{-1}
K_a	Dimensionless (Forchheimer) coefficient	-
K_b	Dimensionless (Forchheimer) coefficient	-
K_d	Dimensionless damping coefficient	-
K_m	Dimensionless added mass coefficient	-
L	Characteristic length (assessed separately for every function, object and situation)	m
L'	Internal wave length (inside a structure)	m

L_0	Deep water wave length	m
n	Porosity	-
$P(x)$	Pressure amplitude at (x)	m
T	Wave oscillation period	s
u	Velocity	m/s
u^*_{cr}	Critical shear velocity	m/s
$u_{f,cr}$	Critical filter velocity	m/s
α	Bed slope	$^\circ$
Δ_b	Relative density base material	m/s
κ_0	Dimensionless resistance coefficient for oscillatory flow	-
κ_v	Velocity coefficient	s^{-1}
$\nabla \cdot \overrightarrow{u}$	Divergence velocity vector	-
∇P	Gradient of pressure field	-
ν_w	Kinematic viscosity water $= 1 \cdot 10^{-6}$	m^2/s
ω	Angular wave frequency $2\pi/T$	rad/s
ϕ	Angle of repose	$^\circ$
Ψ	Shields stability parameter	-
ρ_s	Density sand	kg/m^3
ρ_s	Density stone	kg/m^3
ρ_w	Density water	kg/m^3
σ	Surface tension	N/m
$\overline{u_{pore}}$	Pore averaged filter velocity	m/s
$\overline{u}_f$	Depth averaged, time averaged velocity	m/s
$\tilde{v}_f$	Velocity amplitude	m/s

General Subscripts

Symbol	**Description**	**Unit**
t	Time	-
u	Velocity	-
0	Location subscript at (x=0)	-
$\parallel$	Parallel	-
$\perp$	Perpendicular	-
appear	Appearing	-
av	Average	-
b	Base	-

cr	Critical	-
f	Filter	-
hor	Horizontal	–
inc	Incoming	–
M	Model	-
max	Maximal	–
meas	Measured	-
min	Minimal	–
P	Prototype	-
ver	Vertical	–

Bibliography

Adel, H. d., Bakker, K., and Breteler, M. K. (1988). Internal stability of minestone. In *Proceedings of international symposium of modelling soil–water-structure interaction. Balkema, Rotterdam*, pages 225–231.

Alfonsi, G. (2009). Reynolds-Averaged Navier–Stokes Equations for Turbulence Modeling. *Applied Mechanics Reviews*, 62(4).

Allsop, W. and Williams, A. F. (1991). Hydro-geotechnical performance of rubble mound breakwaters. Technical Report SR183, HR Wallinford.

Bendahmane, F., Marot, D., and Alexis, A. (2008). Experimental Parametric Study of Suffusion and Backward Erosion. *Journal of Geotechnical and Geoenvironmental Engineering*, 134(1):57–67.

Biesel, F. (1950). Equations de l'ecoulement non lent en milieu permeable. *La Houille Blanche*, (2):157–160.

Bonelli, S., Marot, D., Ternat, F., and Benahmed, N. (2007). Assessment of the risk of internal erosion of water retaining structures: dams, dykes and levees.

Burcharth, H., Liu, Z., and Troch, P. (1999). Scaling of Core Material in Rubble Mound Breakwater Model Tests. *Copedec V*, (April):1519–1528.

Burcharth, H. F., Frigaard, P., Uzcanga, J., Berenguer, J. M., Madrigal, B. G., and Villanueva, J. (1995). Design of the ciervana breakwater: Bilbao. In *Conference on Coastal Structure and Breakwater*.

Burger, W., Oumeraci, H., and Partenscky, H. (1988). Ceohydraulic investigations of rubble mound breakwaters. *Coastal Engineering Proceedings*, 1(21).

Cantelmo, C., Allsop, W., and Dunn, S. (2010). Wave pressures in and under rubble mound breakwaters. In *Proceedings of the Fifth International Conference on Scour and Erosion, 2010*, number October.

Cantelmo, C., Dunn, S., Cuomo, G., and Allsop, W. (2011). Hydro-Geotechnical stability of rubble mound breakwaters under wave action. In *Proceedings of the 6th International Conference on Coastal Structures*. World Scientific Publishing Company Pte Ltd.

de Graauw, A. F., van der Meulen, T., and van der Does, M. R. (1983). *Design criteria for granular filters*. Delft Hydraulics Laboratory.

de Graauw, A. F., van der Meulen, T., and van der Does, M. R. (1984). Granular filters: design criteria. *Journal of Waterway, Port, Coastal and Ocean Engineering*, 110(1):80–96.

Delaters instrumentation (2016). Instrument, conductivity type concentration meter v1.1.

Fitts, C. R. (2013). *Groundwater Science*. Elsevier Inc., second edition.

Groot, M. B. D., Yamazaki, H., and Kheyruri, Z. (1994). Pore pressures in rubble mound breakwaters. *Coastal Engineering*, pages 1727–1738.

Guanche, R., Iturrioz, A., and Losada, I. J. (2015). Hybrid modeling of pore pressure damping in rubble mound breakwaters. *Coastal Engineering*, 99:82–95.

Hall, K. R. (1991). Trends in Phreatic Surface Motion In Rubble Mound Breakwaters. *Journal of Waterway, Port, Coastal, and Ocean Engineering*, 117(2):179–187.

Hannoura, A. a. and McCorquodale, J. a. (1985). Rubble Mounds: Hydraulic Conductivity Equation. *Journal of Waterway, Port, Coastal, and Ocean Engineering*, 111(5):783–799.

Heller, V. (2011). Scale effects in physical hydraulic engineering models. *Journal of Hydraulic Research*, 49(3):293–306.

Hoffmans, G. J. (2012). *The influence of turbulence on soil erosion*, volume 10. Eburon Uitgeverij BV.

Hsu, C.-Y., Ho, C.-C., and Chen, R.-H. (2008). The effect of fine soil content on the filtration characteristics of geotextile under cyclic flows. *Geosynthetics International*, 15(2):95–106.

Hunter, J. K. (2006). An introduction to the incompressible euler equations. *Notes, Univ. of California, Davis*, 1.

Jensen, B., Christensen, E. D., and Mutlu Sumer, B. (2014). Pressure-induced forces and shear stresses on rubble mound breakwater armour layers in regular waves. *Coastal Engineering*, 91:60–75.

Kajishima, T. and Taira, K. (1997). *Computational Fluid Dynamics, Incompressible Turbulent Flows.* Number March. Springer International Publishing.

Kennedy, M. W., Zhang, K., Bakken, J. A., and Aune, R. E. Determination and verification of the forchheimer coefficients for ceramic foam filters using comsol cfd modeling.

Kenny, T. and Lau, D. (1985). Internal stability of granular soils. *Canadian Geotechnical Journal*, 21:634–643.

Klein Breteler, M. (1989). Sand transport in granular filters, horizontal and steady flow. *Report H869, Deltares, Delft.*

Klein Breteler, M., Den Adel, H., and Koenders, M. (1992). Taludbekledingen van gezette steen. ontwerpregels voor het filter. *WL rapport H195 deel 21 voor Rijkswaterstaat, DWW (TAW).*

Kovács, G. (1981). *Developments in water science—seepage hydraulics, Chap 3.2.* Elsevier, Amsterdam.

Lawson, C. R. (1992). Geotextile revetment filters. *Geotextiles and Geomembranes*, 11(4-6):431–448.

MC, M. C. (2017). Multifunction usb data acquisition device.

Muttray, M. (2000). Wellenbewegung an und in einem geschütteten wellenbrecher-laborexperimente im grossmassstab und theoretische untersuchungen.

Muttray, M., Oumeraci, H., Zimmerman, C., and Partenscky, H. (1995). Wave induced flow in a rubble mound breakwater. In *Proc. of the International Conference on Coastal and Port Engineering in Developing Countries (COPEDEC)*, pages 1219–1231.

Muttray, M. O. and Oumeraci, H. (2005). Theoretical and experimental study on wave damping inside a rubble mound breakwater. *Coastal Engineering*, 52(8):709–725.

NPTEL- Advanced Geotechnical Engineering (2014). Lecture notes Permeability and Seepage-4, Module 2, lecture 8.

Ockeloen, W. J. (2007). Open filters in breakwaters with a sand core. Master's thesis, Delft Univeristy of Technology, Delft.

Perzlmaier, S. (2005). Hydraulic criteria for internal erosion in cohesionless soil. In *Internal Erosion of Dams and their Foundations: Selected and Reviewed Papers from the Workshop on Internal Erosion and Piping of Dams and their Foundations, Aussois, France, 25- 27 April 2005*, number April, pages 25–27, Munich, Germany. Technical University of Muncih.

Polidoro, A., Allsop, W., and Pullen, T. (2015). Exploring the Need for Geotextile Filters for Rubble Bunds Retaining Sand-Fill Islands. In Wallendorf, L. and Cox, D. T., editors, *Coastal Structures and Solutions to Coastal Disasters 2015*, pages 763–773. the American Society of Civil Engineers, Boston, Massachusetts.

Ranjan, G. and Rao, A. (2007). *Basic and Applied Soil Mechanics.* New Age International (P) Limited.

Schiereck, G. and Verhagen, H. (2016). *Introduction to Bed, bank and shoreline protection.* Delft Academic Press, Delft, second edition.

Schürenkamp, D., Oumeraci, H., Kayser, J., and Karl, F. (2014). Numerical and Laboratory Experiments on Stability of Granular Filters in Marine Environment. *Coastal Engineering Proceedings*, 1(34):17.

Smith, G. M. and Hall, K. R. (1990). Oscillatory flow investigations in porous media. In *Coastal Engineering 1990*, pages 2616–2629.

TenCate geosynthetics (2018). Properties of woven geotextiles.

Troch, P., De Rouck, J., and Burcharth, H. F. (2002). Experimental study and numerical modelling of wave induced pore pressure attenuation inside a rubble mound breakwater. In *Coastal Engineering 2002: Solving Coastal Conundrums*, pages 1607–1619. World Scientific.

Troch, P., De Somer, M., De Rouck, J., Van Damme, L., Vermeir, D., Martens, J.-P., and Van Hove, C. (1997). Full scale measurements of wave attenuation inside a rubble mound breakwater. In *Coastal Engineering 1996*, pages 1916–1929.

Van Gent, M. R. A. (1993). Stationary and oscillatory flow through coarse porous media. Technical report, Delft University of Technology, Delft.

Vanneste, D. and Troch, P. (2012). An improved calculation model for the wave-induced pore pressure distribution in a rubble-mound breakwater core. *Coastal Engineering*, 66:8–23.

Vanneste, D. and Troch, P. (2015). 2d numerical simulation of large-scale physical model tests of wave interaction with a rubble-mound breakwater. *Coastal Engineering*, 103:22–41.

Vargas Luna, A. (2016). *Role of vegetation on river bank accretion*. PhD thesis.

Vargas Luna, A., Collot, L., Crosato, A., and Uijttewaal, W. (2015). Laboratory investigation on the hydrodynamic characterization of artificial grass. *E-proceedings of the 36th IAHRWorld Congress 28 June-3 July, 2015, The Hague, the Netherlands*, pages 728–834.

Wolters, G. (2012). Interface stability of granular filter structures. *Delft: Deltares*.

Wolters, G. and Van Gent, M. R. A. (2012). Granular open filters on a horizontal bed under wave and current loading. *Proceedings of the Coastal Engineering Conference*, 161(1993):1–10.

A

Background and Theory

A.1. Hydraulic loads

A.1.1 Wave loading

Case study indication of appearing gradient

The empirical calculation model by Vanneste and Troch (2012) is summarized below. The paper gives the needed coefficients for different depths by the ratio of depth over total depth (z/h). To make a complete evaluation, wherever needed a linear interpolation is executed and coefficients for every depth to total depth ratio are obtained. The resulting coefficients for regular waves are presented in table A.3 at the end of this section. The used geometric and material properties of the GWK and UG breakwater model are given in figure A.3. With the calculation model, first the expected appearing hydraulic gradients are calculated in the zone of interest. Afterwards, the expected appearing hydraulic gradients for the physical model tests by Polidoro et al. (2015) are calculated and compared with the measured hydraulic gradients from that research. The zone of interest is defined as proposed by Polidoro et al. (2015). The author desired to explore the possibility to curtail the downward extent of the geotextile at levels between $z/h = -1$ and $z/h = -0.55$ and pressure sensors are installed in the experiments between $z/h = -0.86$ and $z/h = -0.53$. The zone of interest is bounded horizontally by where the still water level and inner core slope intersect, calculated by: horizontal boundary = $\tan\alpha_{\text{innerslope}} * h$. The area of interest is presented in figure A.1, the blue lines indicate where the measurement equipment of Polidoro et al. (2015) was installed.

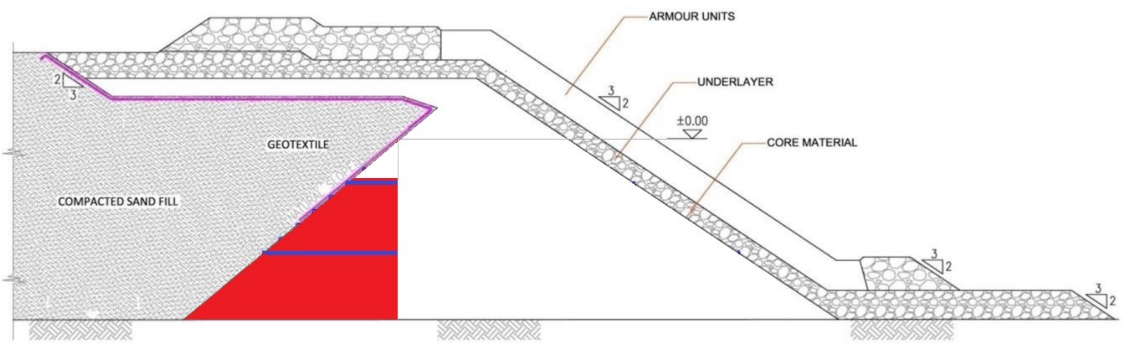

Figure A.1: Area of interest for evaluation of hydraulic gradients.

First the appearing hydraulic gradients in the model of Vanneste and Troch (2012) are calculated in the zone of interest. For regular waves a calculation is made with a water depth of $2.5m$, an incoming wave-height (H_0) of $0.7m$ and wavelenght (kh) of $0.44m$. This is the maximum load condition in this research. The maximum obtained hydraulic gradients are in horizontal and vertical direction, respectively $0.02[m/m]$ and $0.04[m/m]$. For the maximum (storm) loading conditions used in the research by Polidoro et al. (2015), in the above defined area of interest, the maximum hydraulic gradients are $0.032[m/m]$ horizontally and $0.08[m/m]$ vertically. For "regular" loading conditions the maximum horizontal and vertical hydraulic gradients are $0.016[m/m]$ and $0.039[m/m]$ respectively. Table A.1 summarises the obtained predictive values and loading conditions.

Table A.1: Predictive outcomes of appearing gradients for model loading, calculated with Vanneste and Troch (2012).

	Vanneste case 1	Polidoro case 03	Polidoro case 09
h (depth) $[m]$	2.5	12.75	12.75
$H_{inc}[m]$	0.7	3.0	5.8
kh	0.44	0.87	0.74
$I_{calc,max,hor}[m/m]$	0.02	0.016	0.032
$I_{calc,max,ver}[m/m]$	0.04	0.039	0.080

Besides the above given predictions of maximum gradients in the zone of interest, the calculation method by Vanneste and Troch (2012) is used to calculate the exact appearing gradients at locations where Polidoro et al. (2015) executed measurements. These locations and results are given in fig. A.2. For the calculation, the maximum calculated gradient is taken, which is the horizontal or vertical gradient depending on the location and loading condition. The locations and hydraulic gradients are presented in table A.2. From these results it can clearly be seen that for the two cases the calculation model by Vanneste and Troch (2012) under predicts the gradients at intermediate depths and gives fairly accurate results at depths larger than $z/h < -0.7$. It is also observed that the measured gradients dampen less at higher depths and the calculated gradients are higher at larger depths. However, the initial pore pressure is higher closer to the surface. This corresponds with the theory that the damping rate of pore pressure oscillations decreases with increasing distance from the still water line as described in section 4.1.1.

Table A.2: Measured appearing gradients by Polidoro et al. (2015) and calculated approximations with Vanneste and Troch (2012).

depth $[mCD]$	z/h $[-]$	x $[m]$	Case 03_{meas} $[m/m]$	Case $03_{\text{calc,max}}$ $[m/m]$	Case 09_{meas} $[m/m]$	Case $09_{\text{calc,max}}$ $[m/m]$
-4.5	-0.53	25	0.031	0.008	0.061	0.012
-5.5	-0.61	26.5	0.020	0.006	0.040	0.011
-6.5	-0.69	28	0.014	0.008	0.022	0.010
-7.5	-0.76	29.5	0.012	0.010	0.020	0.014
-8.5	-0.84	31	0.014	0.015	0.025	0.024

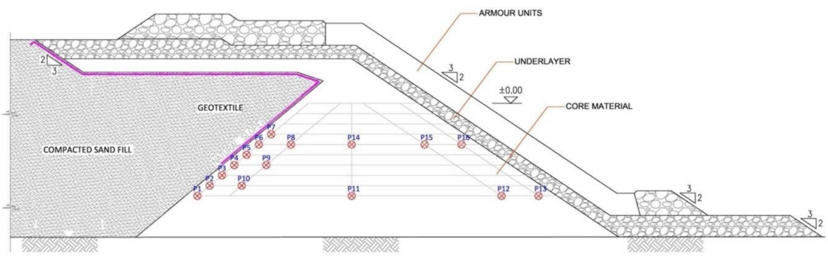

(a) Locations of pressure sensors in research by Polidoro et al. (2015).

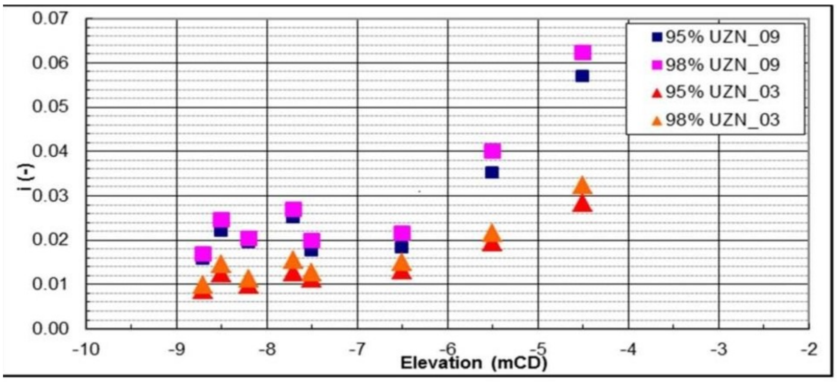

(b) Hydraulic gradients $I_{98\%}$ against tranducer pair elevation Polidoro et al. (2015).

Figure A.2: Information on Polidoro et al. (2015)

Remarks on used evaluation method

To apply this theory some simplifications are made. For both Vanneste and Troch (2012) and Polidoro et al. (2015) the total width of the (base of the) used breakwater is unknown in the current research. Therefore, the exact location of the inner slope is questionable, and thus also the location of the interface from the core to a potential sandfill. The width is approximated by breakwater height/tan($slope$) $*$ 2, implying the breakwater core is built as a isosceles triangle. Furthermore, the measured gradients by Polidoro et al. (2015) are obtained in a 1:32 scale model while the used boundary conditions for the model are given on prototype scale only. The calculations made with the Vanneste and Troch (2012) model are thus made on prototype scale and are only valid to approximate the scale model values by Polidoro et al. (2015) if the latter authors succeeded in obtaining a model in which scale effects are absolutely minimal. This is often a troublesome task. The obtained results of the comparison however, suggest that a study into the applicability of the calculation model by Vanneste and Troch (2012) to the full data set by Polidoro et al. (2015) might provide an extra validation of the calculation model. An accurate evaluation can be made when both the studies by Vanneste and Troch (2012) and Polidoro et al. (2015) are made available with all test details and both data sets.

Table A.3: Emperical coefficients for pore pressure attenuation (Vanneste and Troch, 2012)

	c1,i(z)			c2,i(z) $kh>0.5$		c2,i(z) $kh<0.5$		c3,i(z)		K(z)	
z/h[−]	c1,1	c1,2	c1,3	c2,1	c2,2	c2,1	c2,2	c3,1	c3,2	kh>0.5	kh<0.5
-1	0.74	1.07	0.00	0.42	1.70	0.31	1.17	1.64	0.11	-0.06	-0.08
-0.85	0.74	1.07	0.28	0.59	1.56	0.36	1.08	1.68	0.11	0.07	-0.02
-0.68	0.84	1.07	0.60	0.78	1.40	0.42	0.98	1.72	0.11	0.22	0.04
-0.54	0.92	0.98	0.96	0.94	1.27	0.47	0.90	1.76	0.10	0.34	0.10
-0.5	0.94	0.95	1.07	0.99	1.23	0.48	0.88	1.77	0.10	0.37	0.11
-0.42	0.99	0.90	1.28	0.90	1.08	0.66	0.89	1.97	0.09	0.45	0.20
-0.25	1.09	1.02	1.72	0.70	0.77	1.05	0.92	2.40	0.08	0.63	0.40
-0.22	1.08	1.04	1.72	0.66	0.71	1.12	0.92	2.47	0.08	0.66	0.43
-0.09	1.02	1.13	1.72	0.51	0.47	1.42	0.94	2.80	0.07	1.00	1.00
-0.08	1.02	1.14	1.72	0.50	0.45	1.44	0.94	2.82	0.07	1.01	1.02
-0.0001	0.99	1.20	1.72	0.40	0.30	1.62	0.95	2.47	0.08	1.14	1.20

	GWK-model			UG-model		
	Armor	Filter	Core	Armor	Filter	Core
Type	Accropode (40 kg)	Quarry rock (50/150 mm)	Quarry rock (22/56 mm)	HARO/antifer/gravel (35/50 mm)	Gravel (25–40 mm)	Crushed rock (5/25 mm)
Layer thickness [m]	0.40	0.40	N/A	0.115/0.102/0.115	0.07	N/A
d_{50} [m]	0.297	0.104	0.036	0.070/0.060/0.043	0.033	0.0138
d_{85}/d_{15} [−]	N/A	1.58	1.74	N/A/N/A/1.18	1.37	1.84
l/d	N/A	2.6	2.0	N/A/N/A/not specified	Not specified	2.3
Porosity n [−]	0.510	0.394	0.388	Not specified	Not specified	0.407
a [s/m]	0.001	0.03	0.89	Not specified	0.68 (*)(**)	3.36(**)
b [s^2/m^2]	2.0	14.9	22.9	Not specified	59.0 (*)(**)	224.2(**)
c [s^2/m]	0.30	0.43	0.26	Not specified	Not specified	Not specified

(*) based on a hypothetical value of $n = 0.4$.
(**) derived from stationary flow test.

Figure A.3: Geometric and material properties of the GWK and UG breakwater model (Vanneste and Troch, 2012).

A.2. General flow theory

This section provides a general overview of flow theories required to fully understand processes and computations made throughout the research. The theory elaborated on below will eventually lead to the description of the governing processes in the sand retaining rubble mound. Starting point are the principles of conservation of momentum and mass. Figure A.4 provides a visual representation of these principles for a given volume.

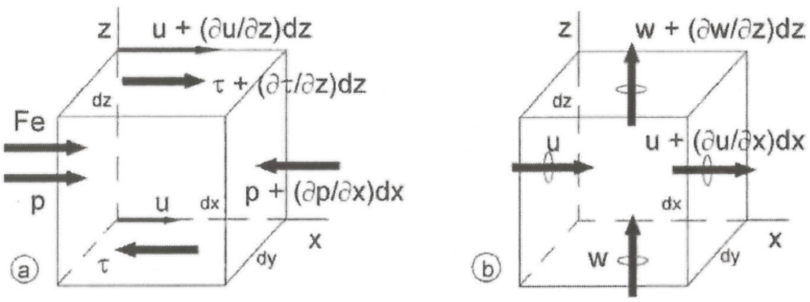

Figure A.4: Forces and flow with regard to dxdydz (Schiereck and Verhagen, 2016)

.

The momentum equation (conservation of momentum, figure A.4a) for two-dimensional flow is given for a resulting flow in x-direction in equation A.1.

$$F_x = -\frac{\partial p}{\partial x} dx(dydz) + \frac{\partial \tau}{\partial x} dz(dxdy) + F_{external}(x) \tag{A.1}$$

Assuming a Newtonian fluid in which μ is the dynamic viscosity implies: $\tau = \mu \cdot \frac{\partial u}{\partial z}$ and therefore, $\frac{\partial \tau}{\partial z} = \mu \cdot (\frac{\partial^2 u}{\partial z^2})$. Furthermore, external forces in x-direction are neglected. Applying some mathematical computations this leads to the (simplified) *Navier-Stokes equation* (in x-direction) valid for both laminar and turbulent flow (A.2). Similarly, this can be derived for flow in the z-direction, given in equation A.3.

$$\rho \left(\underbrace{\frac{\partial u}{\partial t}}_{\text{Local inertia}} + \underbrace{u\frac{\partial u}{\partial x} + w\frac{\partial u}{\partial z}}_{\text{Convective inertia}} \right) = \underbrace{-\frac{\partial p}{\partial x}}_{\text{Pressure gradient}} + \underbrace{\mu\frac{\partial^2 u}{\partial z^2}}_{\text{Viscous shear}} \tag{A.2}$$

$$\rho \left(\frac{\partial w}{\partial t} + u\frac{\partial w}{\partial x} + w\frac{\partial w}{\partial z} \right) = -\frac{\partial p}{\partial z} + \mu\frac{\partial^2 w}{\partial x^2} \tag{A.3}$$

The continuity equation (A.4a) gives the relation for conservation of mass(figure A.4b) in an infinitely small element without a free surface, which for an again Newtonian fluid can be simplified to equation A.4b, essentially expressing the conservation of volume.

$$\frac{\partial \rho}{\partial t} = -\left[\frac{\partial}{\partial x}\rho v_x + \frac{\partial}{\partial y}\rho v_y + \frac{\partial}{\partial z}\rho v_z\right] \tag{A.4a}$$

$$0 = \left[\frac{\partial}{\partial x} v_x + \frac{\partial}{\partial y} v_y + \frac{\partial}{\partial z} v_z\right] = \nabla \mathbf{V} \tag{A.4b}$$

For turbulent flow the flow velocity and pressure can be split up in an mean value and corresponding turbulent fluctuation, also called Reynolds decomposition. The horizontal and vertical velocities can be approximated by $u = \bar{u} + u'$ and $w = \bar{w} + w'$ respectively. Velocities and pressures averaged over the turbulence period can be used to work with average values. Averaged linear terms such as $\overline{\frac{\partial u}{\partial t}}$ become $\frac{\partial \bar{u}}{\partial t}$, and likewise do w and p. For quadratic terms the Reynolds decomposition and averaging results in multi-component terms, for example: $\overline{u^2} = \bar{u}^2 + \overline{u'^2}$. Equivalently, $u \cdot w = (\bar{u} + u') \cdot (\bar{w} + w') = \bar{u}\bar{w} + u'\bar{w} + w'\bar{u} + u'w'$ therefore, $\overline{uw} = \bar{u}\bar{w} + \overline{u'w'}$. Integrating Reynolds averaging into equation A.2 and adding the continuity relation (A.4b) results in the Reynolds-Averaged Navier-Stokes (RANS) equations (A.5). For full derivations and explanation appropriate literature should be consulted, e.g. Alfonsi (2009), Kajishima and Taira (1997), Schiereck and Verhagen (2016) or others.

$$\rho\left(\underbrace{\frac{\partial \bar{u}}{\partial x} + \bar{u}\frac{\partial \bar{u}}{\partial x} + \bar{w}\frac{\partial \bar{u}}{\partial z}}_{\text{Inertia}}\right) = -\underbrace{\frac{\partial \bar{p}}{\partial x}}_{\text{Pressure gradient}} + \underbrace{\mu\frac{\partial^2 \bar{u}}{\partial z^2}}_{\text{Viscous shear}} - \rho\left(\underbrace{\frac{\partial \overline{u'^2}}{\partial x} + \frac{\partial \overline{u'w'}}{\partial z}}_{\text{Reynolds-stresses}}\right) \tag{A.5}$$

From the work by Hunter (2006) is learned that using the conservation of volume equation (A.4b), the conservation of momentum equations (A.1) and (A.2) can be rewritten and combined. Generalizing this statement for non-uniform fluids confirms that the incompressibility condition of conservation of volume under the flow ($\nabla \cdot \overrightarrow{u} = 0$) is equivalent to the condition that the density of a material particle does not change in time ($D\rho/Dt = 0$). This eventually results in the incompressible Euler Equations for ($\rho, \overrightarrow{u}, p$) written as equation A.6. The practical application is found in the fact that an (de-)acceleration of a fluid results in a pressure variation.

$$\rho\frac{D\overrightarrow{u}}{Dt} + \nabla p = 0, \qquad \frac{\rho}{Dt} = 0, \qquad \nabla \cdot \overrightarrow{u} = 0. \tag{A.6}$$

A.3. Porous flow

A.3.1 Laminar flow

Laminar flow can be described by a simplified form of the Forchheimer relation given in equation A.7. In this case coefficient 'a' is inversely proportional to the hydraulic conductivity [K] presented in Darcy's Law (Fitts, 2013), given in equation A.8a. Every porous medium has a characteristic value of its hydraulic conductivity which should be tested separately and can vary in three dimensions for (non-) homoeneous and (an-) isotropic soils.

$$\frac{1}{\rho g}\frac{\partial p}{\partial x} = i = a u_f \tag{A.7}$$

In this case coefficient 'a' is inversely proportional to the hydraulic conductivity [K] presented in Darcy's Law (Fitts, 2013), given in equation A.8a. Every porous medium has a characteristic value of its hydraulic conductivity which should be tested separately and can vary in three dimensions for (non-) homoeneous and (an-) isotropic soils. In this research the hydraulic conductivity is taken as constant in all directions.
More generic estimations of K-values are presented in figure A.5a. Darcy's Law works in three dimensions for (non-)homogeneous and (an-)isotropic soils. However, in this research a constant hydraulic conductivity for the soil body is assumed. In homogeneous soils hydraulic gradients within the soil body can be determined by means of a flow net. A flow net is a scaled drawing of the structure including hydrostatic pressures which can be assessed analogously. In the drawing flow lines and equipotential lines indicate the behaviour of flow through the soil. An example is given in figure A.5b in which the more or less vertical aligned lines

represent lines op equal hydraulic potential and the horizontally aligned lines give flow lines where between each two adjacent lines form a stream tube and in every stream tube the discharge is equal. The discharge through the soil body can be determined by means of equation A.8b in which n_s is the number of stream tubes and n_h is the number of head drops. According to Fitts (2013) a fairly crude flow net will give estimates of n_s/n_h of within $10-20\%$ and the uncertainty obtained by n_s/n_h from the flow net is usually smaller than the uncertainty in the hydraulic conductivity of the soil. Therefore this method is assumed very helpful for initial estimations of the hydraulic gradients in the soil body.

$$\frac{1}{\rho g}\frac{\partial p}{\partial x} = i = \frac{dh}{dx} = -\frac{Q_x}{A}\cdot\frac{1}{K_x} \tag{A.8a}$$

$$Q_x = K\cdot\frac{dh}{dx}\cdot\frac{n_s}{n_h} \tag{A.8b}$$

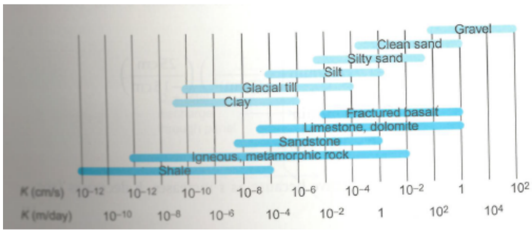

(a) Hydraulic conductivity for various soil types according to Fitts (2013)

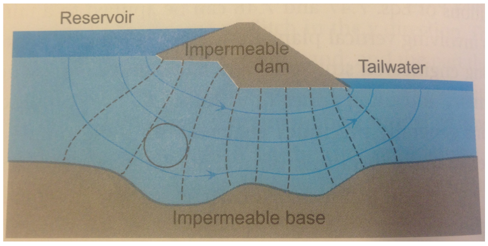

(b) Example of a flow net Fitts (2013)

When an interface is considered with two soils with different hydraulic conductivities the flow net deflects at the interface. In ideal situations with un-stratified soil deposits general transfer conditions can be applied as described in NPTEL- Advanced Geotechnical Engineering (2014). An explanatory overview is given in figure A.6. From this figure some simple calculations lead to the relations given by equation A.9. With large ratios of hydraulic conductivities the deflection will be fairly large resulting in a flow nearing parallelism or perpendicularity with the interface and the ratio of length- to- width of the flow net squares will be very large (corresponding with low average flow velocities) or very small (corresponding with very high flow velocities) with respect to the soil chosen as k_1. Ranjan and Rao (2007) quantifies this by stating that if the hydraulic conductivity of the core material is over ten times larger than the hydraulic conductivity of the sand; considering flows based on hydraulic conductivity or resistance, the core material can be assumed to be equal in conductivity or resistance as the fluid which is flowing. This is particularly interesting because in this research a situation is considered where the hydraulic conductivity of the core material is (much) larger than that of sand. In other words, the core can be assumed to be non existent if $k_{core}/k_{sand} > 10$ and the core is assumed an discharge face or upstream face. From this theory it can be reasoned that when the core material is taken as primary material, the interface with the sand can be assumed as a closed wall. This would result in, the assumption that perpendicular flow based on hydraulic conductivity can be assumed zero. This is however, a hypotheses.

$$tan\alpha_1 = \frac{b_1}{l_1} \quad \text{and} \quad tan\alpha_2 = \frac{b_2}{l_2} \tag{A.9a}$$

$$\frac{k_1}{k_2} = \frac{tan\theta_1}{tan\theta_2} = \frac{tan\alpha_2}{tan\alpha_1} \tag{A.9b}$$

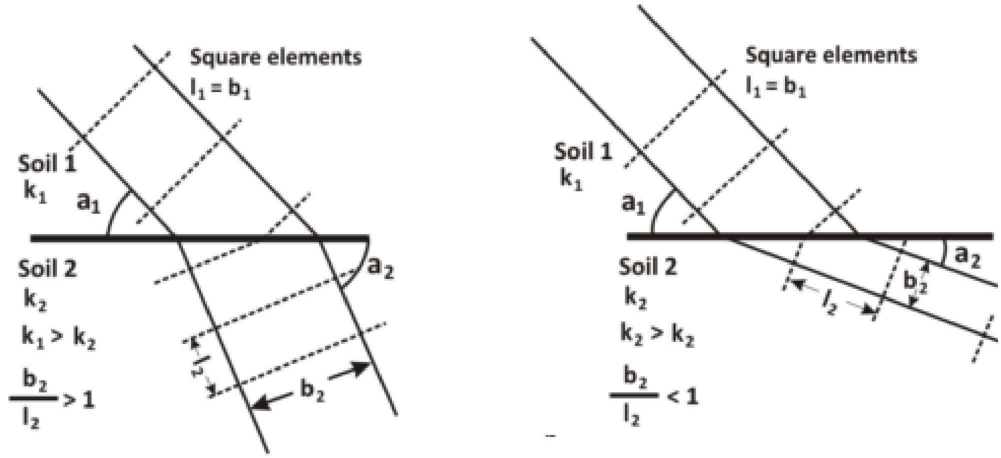

(a) $k_1 \leq k_2$ (b) $k_1 > k_2$

Figure A.6: Deflection of flow net in non-homogeneous soils. (NPTEL- Advanced Geotechnical Engineering, 2014)

A.4. Sandfill migration

A.4.1 Stability against parallel flow

For permanent uniform flow, a well known formula for the critical flow velocity is the one that is adapted of Shields given by relation A.10. This formula is the basis for many stability relations in flow situations Schiereck and Verhagen (2016). A stability parameter ψ_c is used which can have different values for different transport regimes. The stability parameters are $\psi_c = 0.03$ for occasional movement at some locations and $\psi_c = 0.055$ indicates continuous movement at all locations. Considering a breakwater care should be taken using shields relation as uniform flow may not be assumed.

$$d_{n,50} = \frac{{K_v}^2 \cdot \bar{u_c}^2}{K_s \cdot \psi_c \cdot \Delta \cdot C^2} \quad or \quad \bar{u_c} = \sqrt{\frac{d_{n,50} \cdot K_s \cdot \psi_c \cdot \Delta \cdot C^2}{{K_v}^2}} \tag{A.10}$$

With: K_s = slope correction factor; K_v = load increase factor

ψ_c = threshold of motion; C = Chézy coefficient $= 18 \cdot log(12 \cdot \frac{R}{k_r})$.

For cases were uniform flow may not be assumed, an Izbash approach might give better results. Although the approach seems fairly simple, it is unclear were the velocity should be measured and or numerically approached. The Izbash approach for the critical velocity is given in equation A.11.

$$u_c = 1.2\sqrt{2 * \Delta g d} \qquad \text{or} \qquad \frac{u_c}{\sqrt{\Delta g d}} = 1.7 \qquad or \qquad \Delta d = 0.7\frac{u_c^2}{2g}. \tag{A.11}$$

A.4.2 Internal erosion

Due to hydraulic head differences over the structure porous flow may occur through the sand body behind the core. This flow can be described by means of Darcy's theory and flow-nets as explained in section 4.2.2. When the flow exceeds a critical value for transportation sediment might travel with the flow (generally) outward, causing instability of the structure. Various processes are covered by the term "internal erosion". Also suffusion as described above is a form of internal erosion. A comprehensive overview is given by Bonelli et al. (2007) and is summarised below.

Internal erosion

Internal erosion is the process when soil particles from the soil body, are carried downstream by seepage flow. Internal erosion can be initiated by concentrated leakage, backward erosion, suffusion or soil contact erosion.

Backward erosion
Backward erosion involves the detachment of soils particles when the seepage exits to a free unfiltered surface.

Piping
Piping is the mode of failure of internal erosion which forms due to backward erosion or concentrated leakage erosion in a highly permeable zone and results in the formation of a continuous tunnel called a 'pipe' between the upstream and the downstream side of the embankment.

Heave, blow out or liquefaction
Heave occurs in cohesionless soils when seepage pore pressures are such that the effective stress becomes zero (pore pressure equals total stress). Heave may often be followed by backward erosion if the seepage gradient remains high at the surface. It is known that internal erosion and suffusion may initiate at gradients lower than the resulting zero effective stress. This can be explained by assessing the process on a micro scale where the hydraulic load on single particles in cross flow exceeds their drag force (Perzlmaier, 2005).

In Cantelmo et al. (2011), measurements of wave induced pore pressure inside the porous medium have been used as input to assess liquefaction risk of the breakwater foundation. The research shows that loose sands show deformation considerably greater than dense sands, and that such difference becomes more significant as the storm duration increases. Furthermore, storm duration causes excess pore pressure to build up and the soil strength to reduce with subsequent greater deformation of the structure. Also the wave height influences this process. When wave heights doubled, both the dense and loose sand beds exhibit a displacement up to times greater than for the initial case (Cantelmo et al., 2011).

As described in section 4.2.2 about laminar flow in soil body, the hydraulic conductivity of a sand body and the breakwater core material can differ a magnitude which lets the core material behave like an open face or upstream face. When subjected to a high hydraulic head difference over the interface sand to rock interface, especially heave, backward erosion and internal erosion can cause failure. An overview of critical flow velocities for internal erosion are given in figure A.7.

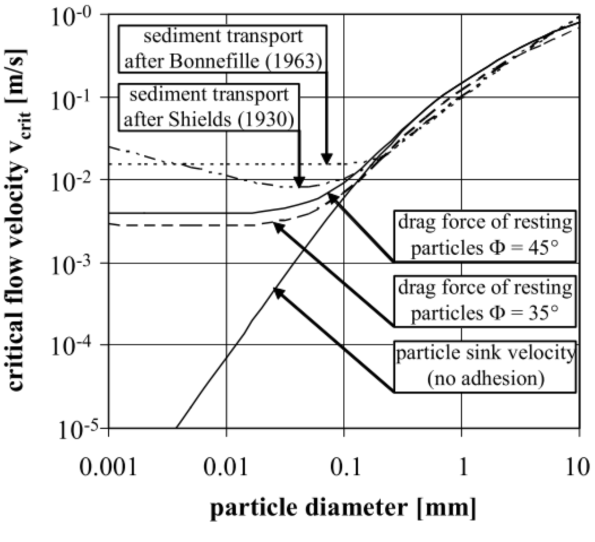

Figure A.7: Critical flow velocity V_{crit} versus particle diameter according to different theories after Muckenthaler(1989) (Perzlmaier, 2005)

A.5. Filter design

A.5.1 Geometrically open filters

Critical gradient as presented by Klein Breteler (1989)

. In section 4.4.2 is elaborated on the formula for the critical hydraulic gradient by Klein Breteler (1989). The necessary coefficients c and m are given in figure A.8 for various characteristic grain sizes.

Table 1. Parameters according to Klein Breteler *et al* (1992)

D_{b50} (mm)	c (-)	m (-)
0,1	1,18	0,25
0,15	0,78	0,20
0,2	0,71	0,18
0,3	0,56	0,15
0,4	0,45	0,11
0,5	0,35	0,07
0,6	0,29	0,04
0,7	0,22	0
0,8	0,22	0
1,0	0,22	0

Figure A.8: Coefficients c and m (Klein Breteler, 1989)

A.5.2 Geotextile

For stationary flow the stability criteria $O_{90} < 2 \cdot d_{90B}$ and for oscillatory flow the openings should be 2 to 4 times as small. The permeability is of geotextiles can be approached in Darcy-type relations (see section 4.2.2) but is given by the physical quantity “permittivity", defined in equation A.5. The downside of Darcy’s-Law is the assumption of laminar flow whereas flow through geotextiles is often in a semi-turbulent regime. Therefore, the permeability is often expressed as the volume flow rate at a specific head. However, these quantities can not be directly related to soil permeabilities (Lawson, 1992). Some indicational values for various types of geotextiles are given in table A.4.

$$P = \frac{u_f}{\Delta h} = \frac{k}{e} \tag{A.12}$$

Δh = head difference; k = normal permeability coefficient; e = thickness of the geotextiles.

Table A.4: Sandtightness O_{90} and permittivity P for various geotextiles.

Type	O_{90}(mm)	P(1/s)
Non-woven (Schiereck and Verhagen, 2016)	0.002-0.2	0.01-2
Woven (TenCate geosynthetics, 2018)	0.18-0.6	0.007-0.35

B

Model setup

B.1. Model strategy

B.1.1. Functional requirements

Besides the critical gradients by de Graauw et al. (1984) and Klein Breteler et al. (1992) also the suffusion theory by Kenny and Lau (1985); Allsop and Williams (1991) is tested. As explained in section 4.3.2 a composite grading needs to be developed for the sand core mixture and afterwards the critical gradient for internal instability is calculated. The composite grading and H-F curve are given in fig. B.1. The H-F curve show a minimum at $F = 0.027$ and $H = 0.294$. With the formula $I_{cr} = 0.25 * (H/F)_{\min}$ this results in a critical hydraulic gradient of $I_{cr} = 0.023$. It is noticed that the composite grading is strongly gap graded. This is different than the grading obtained from Polidoro et al. (2015). This is caused by the fact that dredged sand for reclamations is very wide graded and the sand can range between $180um$ and $5mm$ of which the latter is in fact gravel. This makes the curve less gap graded. A small calculation experiment is executed for which the model half of the sand was replaced with larger sand. This resulted in a critical $I_{cr} = 0.05m/m$. For comparison the same curves for Polidoro et al. (2015) are shown as well.

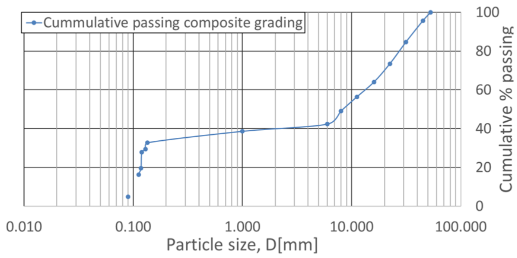

(a) Composite grading core + sand.

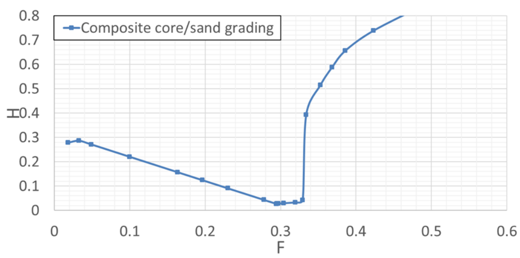

(b) H-F "stability" curve for composite grading.

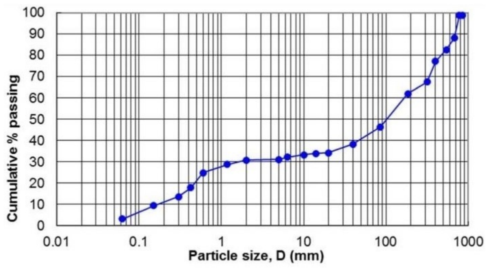

(c) Composite grading core + sand.

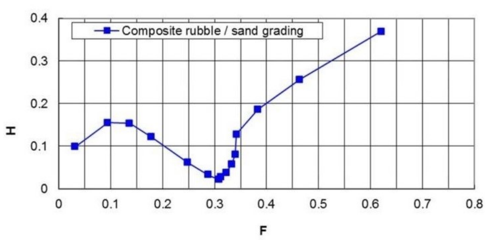

(d) H-F "stability" curve for composite grading.

Figure B.1: Suffusion theory by Allsop and Williams (1991) for composite grading model and Polidoro et al. (2015).

B.1.2. Model selection

Method 1

First a conventional wave flume is considered. A big advantage of using the wave flume is the physical representation of the model. The model includes many different processes that occur in reality such as wave breaking, internal setup and wave attenuation over different layers. In the other two methods explained below the water pressure induced movement of sand granulates through the core is simulated in a rather theoretical and elementary manner. It might turn out that the simplified models do not represent the occurring processes from prototypes well. Therefore, this proposed model set-up is an experiment which approaches the physical behaviour and appearance of the actual design. An example is given in figure B.2. Advantages are that processes have might to be analysed analytically to a lesser extend beforehand to obtain input loads in the schematic model. The disadvantage is that the amount of different processes influencing the movement increases like wave impact, wave run up and wave over topping which also increase the overall model complexity. It will make the analysis and interpretation of results more difficult. Furthermore, scaling effect become increasingly difficult with complexer models, in this case: including air entrainment and surf-similarity.

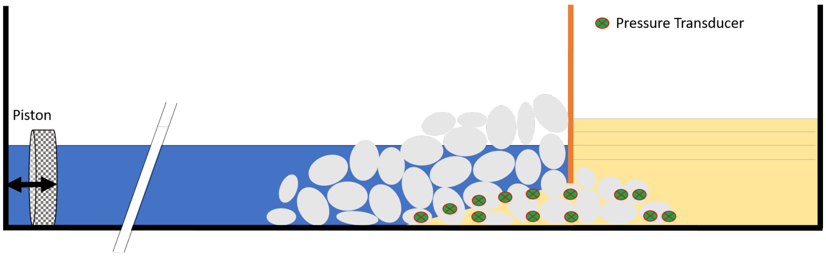

(a) Model set-up for method 3, version container

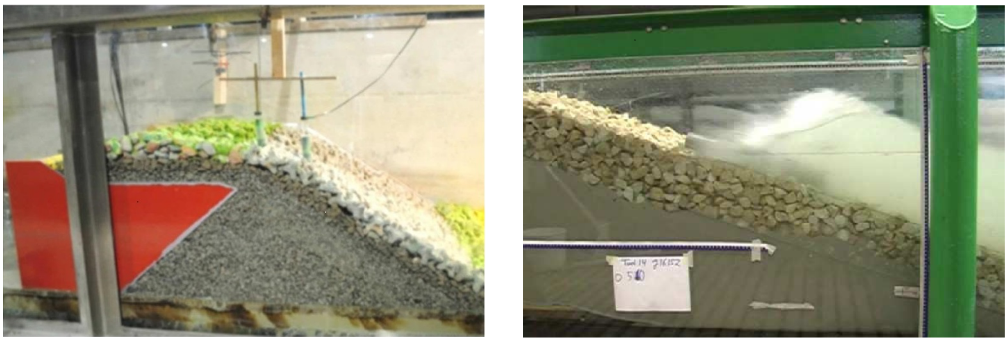

(b) Model set-up for method 3, version flume Polidoro et al. (2015) and (Ockeleon, 2007)

Figure B.2: Method 3 type experiments

Method 2

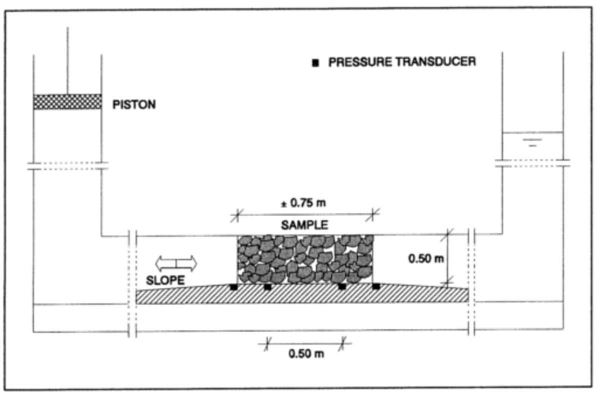

Figure B.3: Oscillating water tunnel at Delft Hydraulics Van Gent (1993).

A second model set-up is up for discussion to obtain the test results which might answer the research questions. This experiment is based on the model setups used by Smith and Hall (1990) and a different but similar model set up used by Van Gent (1993) from which he approximated the coefficients of the extended Forchheimer equation (section 4.2.1). A indicational sketch of the experiment is given in fig. B.3. The actual model set-up is somewhat more complex, for the similar set-up used by Smith and Hall (1990) a top down cross-section and photo are provided in fig. B.4.

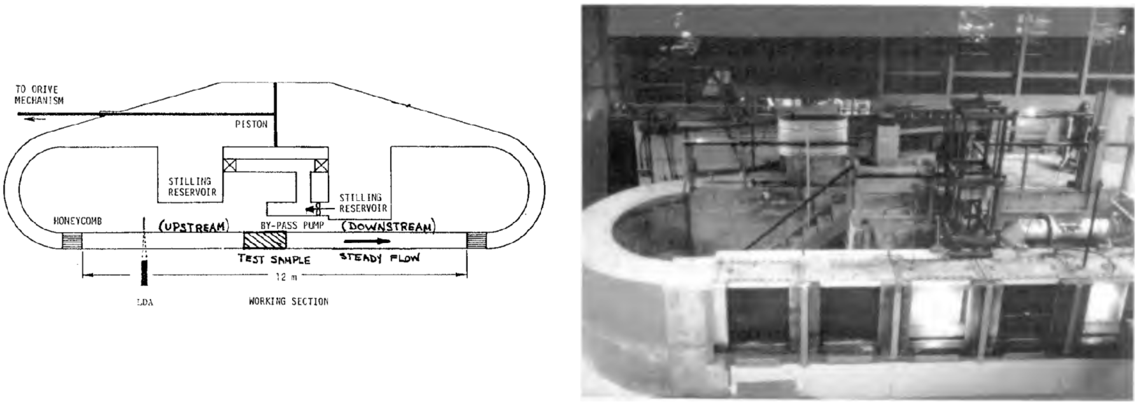

(a) Top view (b) Photo

Figure B.4: Oscillating water tunnel at Queens university, Canada used by Smith and Hall (1990)

The adapted experiment uses the strategy by Smith and Hall (1990) to use a U-tube tunnel. A sand body will be constructed on the opposite side of the rock sample with respect to the piston. An oscillatory flow can be induced by Smith and Hall (1990)'s method. A variation on this model set-up is given below in figure B.5. Similar to the method explained in section B.1.2 this model set-up uses vertically aligned pipes to induce (large) pressures both hydrostatic and oscillatory. The piston is used to simulate wave induced pressure by periodic movement or replicate a head difference with the high elevation at the seaside of the structure when installed stationary with a certain penetration depth into the column. A reversed head difference can be induced by adding water or a second piston at the lee side of the structure. Two version are considered: One with a sloping sand-core interface as generally will be the case in real life design (figure B.5a), and the second with a vertical interface with the possibility of pivoting the complete test set-up for a various interface possibilities (figure B.5b). A disadvantage for this approach is the fact that the water is pushed through the interface where in reality the flow is (possibly) mainly along the interface.

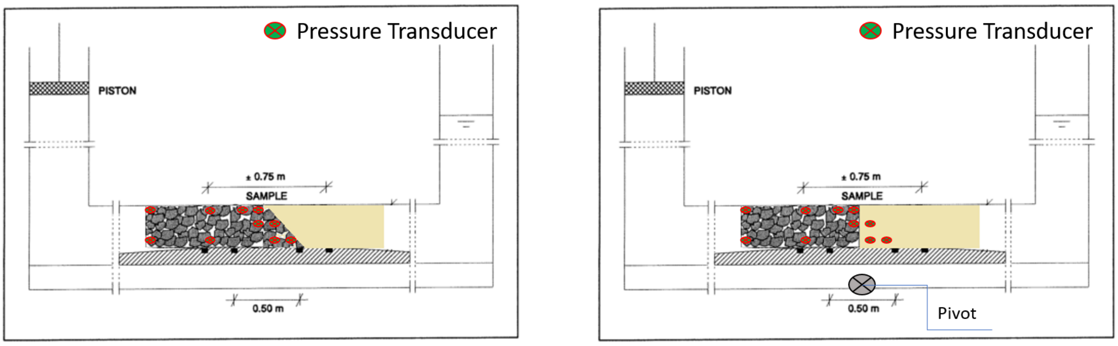

(a) (b)

Figure B.5: Design drafts of adapted test from Smith and Hall (1990) and Van Gent (1993)

Method 3

Method 3 enables to simulate installation of a sand-fill by means of a physical scale test. This is hereafter described as: "*Stage 1 modelling*". Also, this model provides the dimensions to design a test in which the geometrical (scaled) properties of the model are very similar to a prototype scale. Within a transparent container with the approximate size of $1 * 0.5m^2$ surface and $1.0m$ height, a sand tight geotextile barrier is placed in the middle, with an opening at $0.25m$ from the bottom. At one side the container will be filled with core material and subsequently filled with water. At the ‘empty’ side of the container sand is poured in to simulate a reclamation process. The development of the sand-core interface and porous flow will be evaluated. The experiment is set-up for both a vertical and a sloping face of the core material. A raw sketch is given in figure B.6a and B.6c.

New experiments should be executed to model hydraulic loads on the structure. The results from the initial *stage 1* test might indicate the location of the interface. Depending on the interface the next model test is designed. For the situation where the initial infill is small, the interface is expected to resemble the interaction of a sand body and a open filter in an upside down configuration. A key difference between a regular open filter and the one considered in an inverted position is that besides flow induced loads also gravity can cause sediment transport through the core. Various tests with hydrostatic pressure differences, wave induced pressures or combinations of both can result in obtaining measured hydraulic gradients corresponding with sediment transport.

The results from the *stage 1* test might also indicate a situation where the sand filled the outer corner of the core and an interface is formed with an inward facing slope. In this case the interface is more like a normal (but possibly unsuccessful) open filter from which sand can erode through the pores of the core if the hydraulic resistance criterion is met. Like the experiment mentioned in the paragraph above: various tests with different loading conditions can result in obtaining measured hydraulic gradients corresponding with sediment transport.

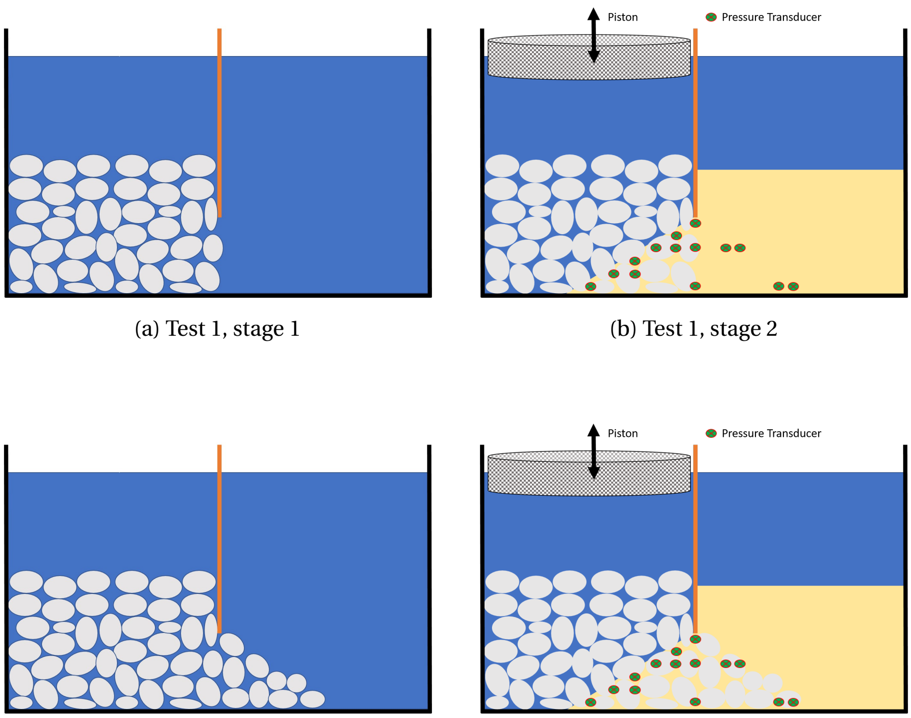

(a) Test 1, stage 1 (b) Test 1, stage 2

(c) Test 2, stage 1 (d) Test 2, stage 2

Figure B.6: Design drafts of initial infill tests

B.1.3. Experimental setup

The measurement set-up is designed as presented in figure B.7a. A wooden container of shuttering plywood with see-through perspex sides is used. The container is $1m$ wide, $0.45m$ high and $0.15m$ deep. The sizes of the container are determined by the fact that this container was available in the lab. The implications caused by the dimensions of the container with respect to scaling, wall-effects and other model influences will be evaluated in section 5.3.1. The container is separated into three zones. The first zone, left, is used to induced the water movement by moving a piston up and down manually. In the second zone, middle, the water movement through a breakwater core is simulated. The third zone mimics a sand body. The different zones are separated by shuttering plywood screens with a 0.075m gap between the bottom of the container and the plywood screens. This causes the water to flow up and down and along the bottom in zone 2. The separation between zone 2 and 3 is also made of shuttering plywood. To physically approach the prototype situation a geotextile could be installed at this separation. However, as the plywood will cause for a higher hydraulic gradient over the interface between the core and the sand body, the approach with the use of plywood is therefore conservative. The use of plywood is easier and less fragile executing the experiments and therefore no geotextiles are used. The 0.075m gap in a 0.3m water depth mimics an possible abbreviation of a geotextile of 25%. First, in zone 2 a rigid glued rock body is placed as representation of the core, see figure B.7b. A rigid body is considered so the porosity and stone-configurations are constant over all experiments. Furthermore, in zone 1 the loose rock is placed, initially designed this way to save time and a uniform rock body over several tests was assumed not of primary interest in this area. In a second series of experiments, in zone 2 loose rock was placed at the bottom of the container with a smaller rigid glued rock body on top. With this method is was possible to evaluate the sediment transport through the loose rock but still have a semi-uniform rock body over several tests for evaluation of the water flow. Also, in zone 1 a flat piece of glued rock was place on top of the loose rock to counteract the getting into suspension of the rock material when the piston is moved.

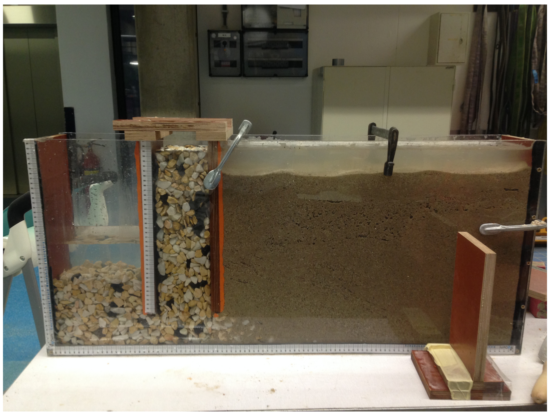

(a) Model set-up

(b) in-side view during the demount of the setup.

Figure B.7: Experimental setup for preliminary experiments

Materials

The used sand has a d_{50} equal to $1 \cdot 10^{-4} m$ and the corresponding grain size distribution is given in figure B.10a. This sand was chosen for the preliminary experiments because it has the same characteristics as prototype sand (e.g. hydraulic conductivity) and was available in the Laboratory.

The sediment used in the initial experiments is extensively described in research by Vargas Luna et al. (2015). An empirical expression for the Chézy coefficient for this sediment is proposed and given by equation B.1. The equation is valid for the considered sediment under Reynolds numbers, Re, between $2.4 \cdot 10^3$ and $2.11 \cdot 10^5$ and energy gradients, i_b, between 0.0005 and 0.002(m/m).

$$C_b = 1.313 Re^{0.2097} i_b^{-0.2243} \tag{B.1}$$

Various rock materials where available at the lab. The materials were visually inspected and judged on their roughness, brittleness, cleanness, uniformity, shape and size. For all materials the grading was unknown and therefore very small fractions were of approximately 50 stones where taken to give an idea of the grading. Three examples of materials are given B.8 examples are given of the rocks sieved and evaluated for the experiments.


(a) Smooth pebbles


(b) Mixed blasted rock


(c) Chalk-sand stone

Figure B.8: Various judged rocks

For the preliminary experiments the mixed blasted rock rock was chosen to be most comparable to the prototype core material. Over 8000 stones of this material were sieved manually and an adequate grading curve was produced. Results of the sieving process are given in table B.1 and photos of the process are given in figure B.9.

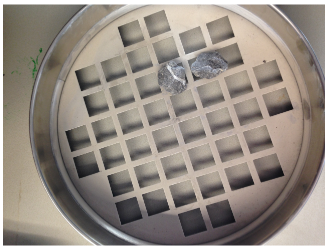
(a) Sample of 31.5mm


(b) Sample of 22.4mm


(c) Sample of 16mm


(d) Sample of 11.2mm


(e) Sample of 8mm


(f) Overview of stones by sieves size

Figure B.9: Sieving process

The rock material used for the initial experiments is of two types: In the first experiment with only one rigid glued rock body, rocks are used from the sieve with stones ranging 11.2 – 16 cm. These are assumed to be spread uniformly. The grading width d_{85}/d_{15} is 1.26 and d_{60}/d_{10} is 1.22. In the second series of experiments with loose rocks and the smaller rigid glued body the full grading of the material is used with a grain size distribution as shown in figure B.10b. This rock has a grading width d_{85}/d_{15} of 1.52 and d_{60}/d_{10} of 1.23 which is very narrow. To represent a quarry run core grading and obtain similar conditions, this rock should be wider graded with a $d_{60}/d_{10} \geq 2.5$ or in reference to the experiments of Polidoro et al. (2015) $d_{60}/d_{10} \approx 4.5$. To consider the core and sand material as a non-closed filter $d_{15F}/d_{85B} \geq 5$ must be true. In this case the ratio has a value of 8.6 and complies to the non-closed filter criterion, although not with a very large margin. In the experiments of Polidoro et al. (2015)the ratio d_{15F}/d_{85B} was approximately 65. The gradation curve of the full rock grading is given in B.10b.

Sieve size [mm]	Number of rocks [-]	Mass [kg]	Cumulative Mass [kg]	Cumulative Mass [%]
0	634	0.067	0.07	0
8	1271	1.83	1.90	0.31
11.2	3741	15.32	17.21	8.97
16	261	3.01	20.22	81.44
22.4	23	0.73	20.95	95.67
31.5	2	0.18	21.13	99.14
45	0	0	21.13	100

Table B.1: Results sieving rock material

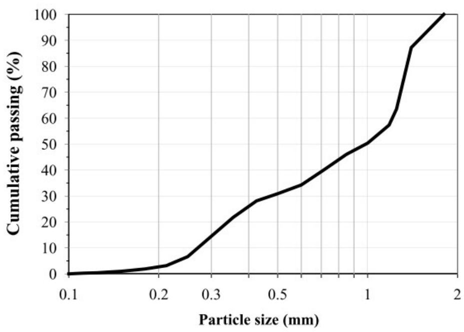

(a) Grain size distribution sand (Vargas Luna, 2016).

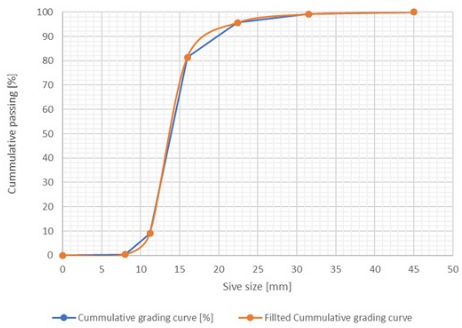

(b) Grain size distribution core material

Figure B.10: Grading of used materials in preliminary experiments

The glued rock models are made by a mix of the rock-core material with polypox glue and a polypox harder in a bucket. After the rocks and glue are thoroughly mixed they can be poured in a plywood cast. The mix has to dry for about 24 hours. Due to a mistake in the lab the first sample failed to harden. The cause of the failure was unknown which caused a delay in the first experiment due to primarily waiting until the glued rock model became hard, and afterwards finding the cause for the failure. It turned out that a mistake was made in the combination of polypox and harder, one can notice the shiny soft glue especially at the bottom of the sample in figure B.11a. Afterwards three new rock models where made. First, one with the dimensions $40*15*13$ cm to fit as one full column. During tests with this model it appeared that a hybrid design with both loose rocks and a solid column was preferred. Therefore a new column with dimensions $30*15*13$ cm is fabricated. Furthermore a thinner plate with dimensions $5*15*20$ cm is made to place on the loose rocks in the zone (1) where waves are generated. Pictures are given in figure B.11.

(a) Failed glued rock model.

(b) Correct glued rock model

(c) Smaller glued rock model

Figure B.11: Manufacture of glued rock models

Measurement equipment

Measurement equipment is installed to determine the hydraulic gradients corresponding with the observed sediment transport. Furthermore, the visual evaluation of sediment migration through the core material can be supported by measured data. Both processes are proposed to be measured with pressure sensors. These pressure sensors determine the pressure difference between their two outlets. The outlets can be connected to tubes to measure pressure differences between exact defined places. The first application of the sensor is to measure the hydraulic gradient occurring in the rock sample, given by the purple sensor in figures B.12a and B.12b. The second application of the pressure sensors is somewhat easier. The sensor is not used to determine the pressures or pressure differences but indicates where the sand has moved. When the sand migrates and overlays the sensor, the signal will go flat and this indicates the transport of sand over time and space. These are indicated by the green/red sensors in figures B.12a and B.12b. All pressure sensors are covered with very fine mesh to avoid sand particles migrating in the open end of the pressure sensor. This will cause immediate failure of the sensor. The mesh is secured with a tie rap.

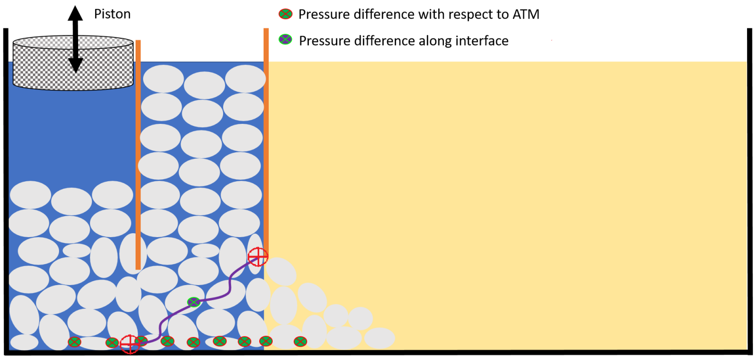

(a) Initial situation at start test.

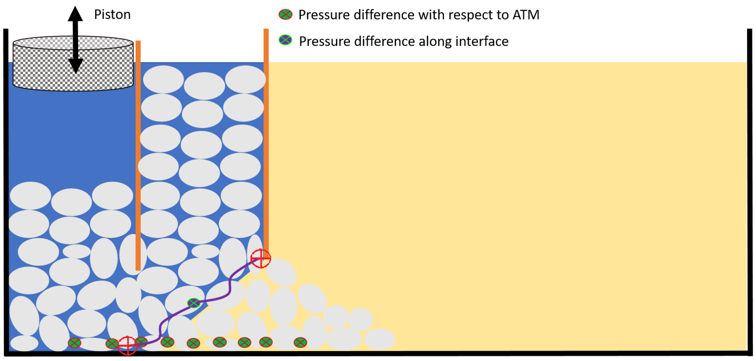

(b) Expected migration of sand over time

Figure B.12: Expected course of experiments with measurement equipment in place

The pressure sensors are connected to signal amplifiers which can handle ranges of 0 – 35 cm water column. These amplifiers are connected to a USB data acquisition (DAQ) device ((MC, 2017)). This device converts the analogue signal to a digital signal and transfers this to the computer. The software program called DASYLAB (*Full name: Data Acquisition System Laboratory*) is installed to govern the acquisition, real-time analysis and control of the data. Every sensor has its own signal amplifier and cables which are connected in completely equal manner every test. This makes sure that if a sensor, amplifier or set of cables causes noise signals, it can be traced easily. Pictures of the pressure sensor, amplifier and DAQ device are given in figures B.13a, B.13b and B.13c respectively.

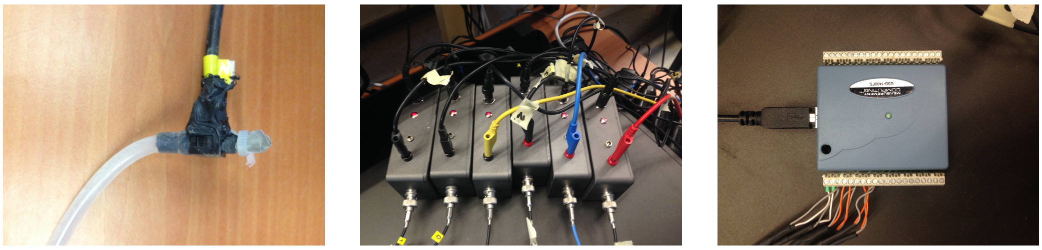

(a) Pressure sensor (b) Signal amplifier (c) DAQ device

Figure B.13: Measurement equipment

In this stage of the research water elevations were observed visually. The waves were generated by hand and real-time corrected if wave heights were visually not consistent. This was done by pushing the piston harder or less hard. In the secondary set of tests the waves are generated with an automated piston and then waves are assumed to be more consistent. In this case the excitation of the piston is registered. Furthermore, for the secondary a wave gauge or water elevation gauge is installed to obtain the a series of wave heights observed in zone 2 were water is pushed through the core. The wave gauge is also connected to an amplifier and DAQ device so the data can be registered and ordered by DASYLAB.

Model installation

For every model test the model set-up has to be rebuild and every part had to be placed in the container. The installation process is given in figure B.14 on page 88. The container is first cleaned (with window cleaner) and dried to ensure the best sight for visual observations. The pressure sensors are placed on the bottom of the container and to best practice kept at position with their open ends facing the sand body (towards zone 3). This is a delicate process which takes time and adjustment. Often a nut is used to keep the sensor in place (figure B.14a). In the second series of experiments this nut was taped to the bottom to ensure the location of the sensors to be constant. Afterwards, the first layer of rock is placed at the bottom of the container with a thickness of $7.5cm$ in zone 1 and till $10cm$ in zone 2 (figure B.14b). A temporary closure underneath the screen between zone 2 and zone 3 keeps the stones in place. The rigid glued rock body is placed and the plywood screens are installed. This is quite difficult as the screens have to be pushed into $2.5cm$ of loose rock in zone 2 by wiggling while the rock body is on top. Furthermore, the total of screen and rock body need to end up in the appropriate place. Where the plywood screens and perspex wall touch, watertightness is ensured by ('childrens') coloured modelling clay, as shown in figure B.14c. Afterwards, loose rock is added to obtain a total height of $10cm$. The temporary closure is removed and in zone 3 the toe is constructed by pushing stones against the stones from zone 2 and against the underside of the plywood screen. Potential holes need to be filled. A little sand barrier is constructed in front of the toe to ensure that the stones stay in place when adding the water, shown in figure B.14d. The water is added in zone three. This is important because filling via zone 1 and zone 2 has showed to displace the stones into zone 3. The water is added to about 10 – 15 cm height depending on whether wet or dry(er) sand is used, see figure B.14e. The sand is added until a height of $5-10cm$ below the edges of the container, also depending on the wetness of the sand, as given by figure B.14f. A dry top layer is ensured. During the filling, the container gets pressured by the sand and water which causes the perspex walls to bend out. Therefore, during filling bar clamps are installed which remain on the container for the full duration of the test. It is possible that a to small amount of water is present in zone 1 to generate wave pressures after installing. In this case water is added via zone 1. A plunger is used to generate waves. The plunger consist of three pieces of plywood screwed together. The plunger is moved up and down manually by the researcher. Halfway the tests a small bar clamp was attached to the plunger to make the plunger more easy to hold and therefore extending the possible duration of the tests without getting cramp and making the induced wave pressures more consistent, given in figures B.14g and B.14h.

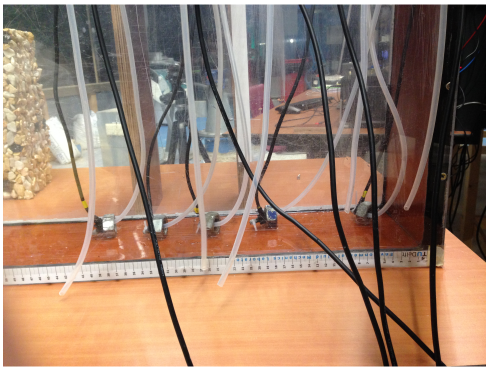

(a) Container with pressure sensors*.

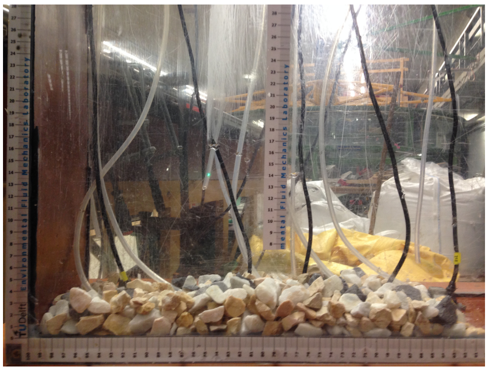

(b) Pressure sensors underneath first rock layer

(c) Installation of modelling clay

(d) Contruction with sand-toe

(e) Small amount of water is added

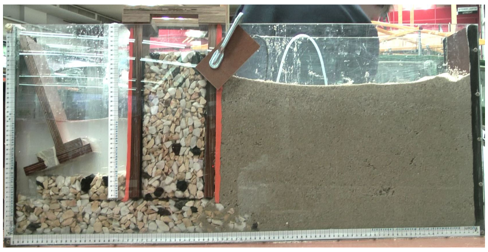

(f) Container is filled with sand

(g) Plunger

(h) Plunger with bar clamp

Figure B.14: Installation of model set-up
*Photo taken from backside of container.

B.2. Preliminary experiments

B.2.1. Test sequence

Various test are executed without a certain test sequence. However, the experiments are consistent regarding the used materials, excited water level variations and evaluation. The lack in a predefined test sequence is

caused by the uncertainty in what to expect from the test and the ability of the model set-up to approach the actual processes. Also, after most tests disabilities of the model were registered, evaluated and reduced or eliminated to improve the model. By making lots of variations and improvements during the initial test series, potential teething problems are overcome. Furthermore, the preparation and use of the model set-up needed to be explored and learned as mistakes were easily made. The test were becoming more serious over time and after some practising all test were registered. The observations are elaborated on below.
In the first two tests the main objective was to find the influences of using loose and bonded rock in the model setup. Afterwards, in tests three and four the pressure sensors were tested and calibrated. Furthermore, the reaction of the pressure sensors when encountering contact with sand was tested and the potential damping of the signal was evaluated. Test five was the first test in a full setup with several pressure sensors. This was repeated in test six with only one pressure sensor. Because only minor sediment transport occurred also a test was carried out without rocks, but with the plywood screens in tests seven and eight. Lastly, experiment nine was installed with sand in combination with a rock berm. A full description of the specifications of every experiment, including pictures of the setup is given in appendix B.2.1.

Besides the experiments described above and in appendix B.2.1, additional measurements were carried out. These experiments were less process based and often executed to test how measurement equipment functioned. For instance, the equipment was placed in the container with only water or in a full model set-up without generating any changes for longer periods of time. In such a manner two $1.5 hour$ measurements, a $17 hour$ and $70 hour$ measurement are recorded. During these tests the researcher was not present at the container, and therefore no visual observations were made. Furthermore, four short period measurements were recorded of approximately half an hour. During these periods the researcher was present at the model set-up.

Test 0001, Loose rock
Because the glued rock model was still under construction a first test was executed in the container with loose rock only. The biggest flaw of this method is the inconsistency of the rock (both placement and porosity) when various test should be carried out. During this test no measurement equipment was installed as it was not available jet. The plywood screen was used however, initially without modelling clay its need was still unknown. Some waves were made with a small plunger.

Test 0002, Glued rock model
The main improvements in TEST 0002 are: A glued rock model, increase of amount of bar clamps, ensured water tightness by modelling clay and the effort made to evaluate sediment transport. The rigid glued rock model with sizes $45 * 15 * 12$ cm was used and the still water level was approximately 23 cm. Lastly, the plungers surface area was increased enable bigger variations of the water level. Two tests were carried out: TEST 0002A without a loose rock fore slope and TEST 0002B with a loose rock fore slope.

Test 0003, Pressure sensors
In TEST 0003, the pressure sensors are tested. First one, and later more. The pressure sensors were placed in the container and water was added. Underwater, all pressure sensors were injected with water by means of a needle to make sure no air bubbles remained entrained in the fluid in the sensor. Afterwards, a calibration sequence is started, divided in four tests. In TEST 0003A the first pressure sensor was calibrated by moving the sensor from top to bottom in steps of 5 cm with a 30 second pause every step. The output file gave a volts over time diagram and could be calculated to a volt over depth diagram. This test was repeated (TEST 0003B) and executed with a second sensor (TEST 0003C). These both tests were executed by a period of rest at the bottom first (e.g. 10 minutes), and afterwards calibrating bottom to top. The last test in this sequence, TEST 0003D, four pressure sensors were placed in the container and (after initial rest) waves were made with the plunger.

Test 0004, Pressure sensors and sand
In TEST 0004 the reaction of the pressure sensors to sand was tested. To recap: it was assumed that when a pressure sensor was blocked by sand particles or covered under lots of sand particles, the sensor would stop working. This would imply that the sand migrated from the sand body to the place of the pressure sensor. To test this, four pressure sensors were placed in the container. From one side sand was added in different steps until three out of four sensors were covered. In between the steps waves were generated to observe the

reaction of the pressure sensors. The set-up is given in figure B.15 on page 90. After the first series of waves the measurement equipment was left in place for 15 – 20 minutes to check if the sensors were influenced by the tests. A stable and flat signal was expected and hoped for. Afterwards, without changing anything a second series of waves was forced.

(a) Container pressure sensors

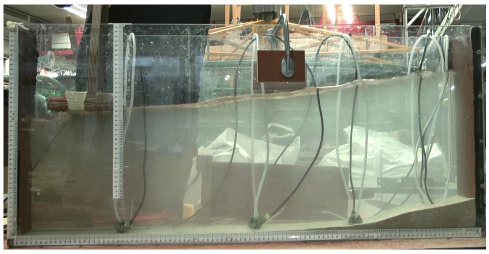

(b) Filling sand 1

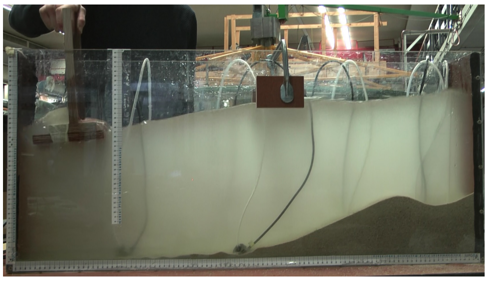

(c) Filling sand 2a

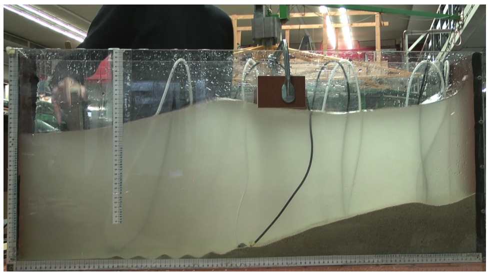

(d) Filling sand 2b

Figure B.15: Test 0004, pressure sensors and sand

Test 0005, Full set up
In TEST 0005 the full experimental set up as described in section B.1.3 is used. Tests TEST 0005 and TEST 0006 were executed rather fast as some results had to be obtained before a meeting. Also by this cause, in TEST 0005 the use of modelling clay was forgotten.

Test 0006, Full set up with one sensor in sand body
In TEST 0006 the experimental set up as described in section B.1.3 is used without the installation of pressure sensors. Only one pressure sensor is installed at about 5 cm into the sand body to detect is pressure differences could be observed. The set-up is given in figure B.25a on page 99, were the sensor is somewhat further right than the cables are.

Test 0007, Set up with sand and one sensor in sand body
After the six tests described above the question rose whether sand was able to move underneath the plywood screen. Until now only tests with rocks were executed however, the transport was low enough to justify a test without rocks. In TEST 0007 rock is placed in zone 1 were the water level oscillations are excited. Zone 2 was left empty, zone 3 was filled with sand and one pressure sensor was installed in the sand body. Unfortunately the modelling clay to ensure water tightness was forgotten. A picture of the model set-up is given in figure B.26a.

Test 0008, set-up with sand only
After the problems encountered in TEST 0007 the experiment is repeated in TEST 0008. No rocks are used and only in zone 3 sand is placed. Initially a small plywood screen kept the sand from flowing into zone 2 and 1 during installation and modelling clay was in place to ensure water tightness. To have more space for the evaluation of the sediment transport, zone 3 was made smaller. A picture of the model installation is given in figure B.16a. Two series of waves are executed after which the sand body was restored with extra sand. Two more series of waves were simulated.

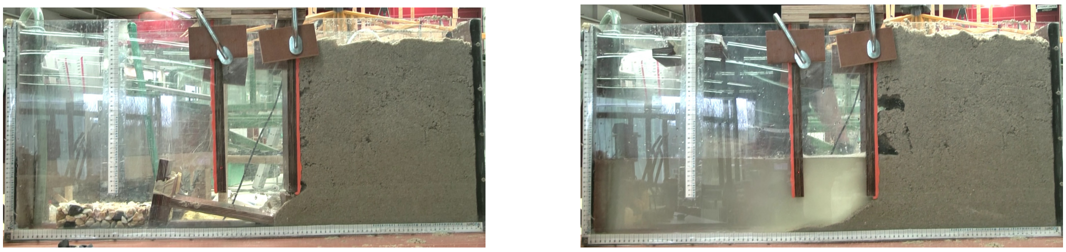

(a) Model set-up. (b) Initial displacement of sand.

Figure B.16: Test 0008, installation with sand only.

Test 0009, set-up with smaller compartment zone 3

TEST 0009 is divided in two tests: TEST 0009A and TEST 0009B. In both tests zone 3 and the sand body are made smaller because the thought rose that the hydraulic conductivity, and therefore the size of the sand body, were of smaller influence than initially thought. TEST 0009A is executed with sand only and in TEST 0009B a rock berm is added, see figures B.17a and B.17b. The experiment is intended to be able to make bigger waves.

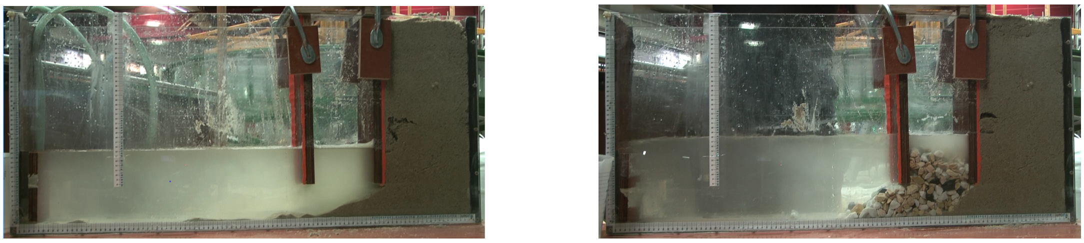

(a) Model set-up with sand only (b) Model set-up with sand and rock berm

Figure B.17: Test 0009, smaller size of zone 3.

Additional non-process based experiments

Besides the experiments described in section 5.2 additional measurements were carried out. These experiments were less process based and often executed to test how measurement equipment functioned. For instance, the equipment was placed in the container with only water or in a full model set-up without generating any changes for longer periods of time. In such a manner two $1.5 hour$ measurements, a $17 hour$ and $70 hour$ measurement are recorded. During these tests the researcher was not present at the container, and therefore no visual observations were made. Furthermore, four short period measurements were recorded of approximately half an hour. During these periods the researcher was present at the model set-up.

B.2.2. Results

Test 0001, Loose rock

Main conclusions with respect to installation TEST 0001:

- Stones need to be thoroughly washed (figure B.18a).
- Bar clamps are needed to prevent bending of the side walls of the container(figure B.18b).
- Modelling clay should be applied before water is added.
- Enough space should be available to walk around and camera's should be placed.

Main conclusions with respect to actual TEST 0001:

- During installation sand migrates immediately through the rubble foreslope.
- During installation sand migrates to a certain extend through the rubble core.

- After an initial amount of filling, further filling itself does not cause any transport.
- Little sand migration is observed during tests however, stones get suspended in zone 1.

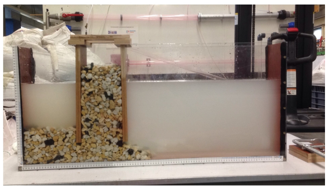

(a) un-thoroughly washed stones cause long settlement times.

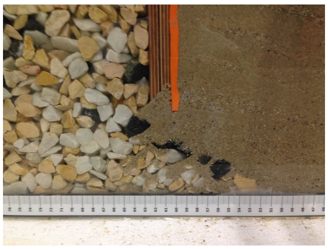

(b) Sand migration from above seal, therefore bar clamps needed.

(c) Migration through foreslope

Figure B.18: Results test 0001

Test 0002, Glued rock model
Main conclusions with respect to installation TEST 0002:

- Installation of glued rock model with plywood screens was relatively easy.
- Care should be taken constructing the interface between the glued rock model and loose rock to minimize holes.
- Visual evaluation of sediment transport through the glued rock model is difficult. Flushing, sieving and weighing is considered very inaccurate.

Main conclusions with respect to actual TEST 0002:

- The larger plunger causes more suspension of rocks.
- The glued rock model without foreslope causes large sediment transport along the wall, see figure B.19a.
- Sediment transport through the core with the glued rock model with foreslope behaves similarly to TEST 0001 with loose rock only, considering wall flow (see figure B.19b).
- The differences in wall-effects without and with foreslope are also observed at the bottom of the container, presented in figures B.19c and figure B.19d respectively.

(a) Test 0002a without foreslope, wall transport.

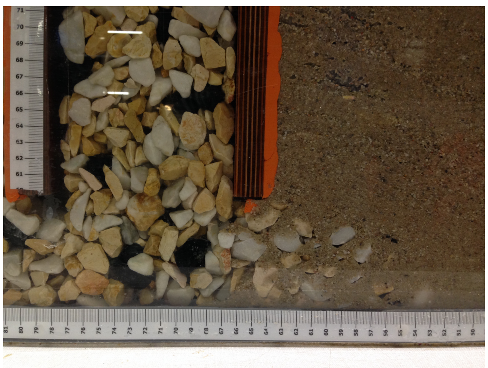

(b) Test 0002b with foreslope, wall transport.

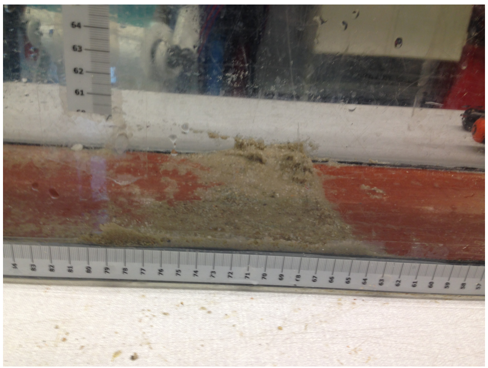

(c) Test 0002a without foreslope, bottom transport.

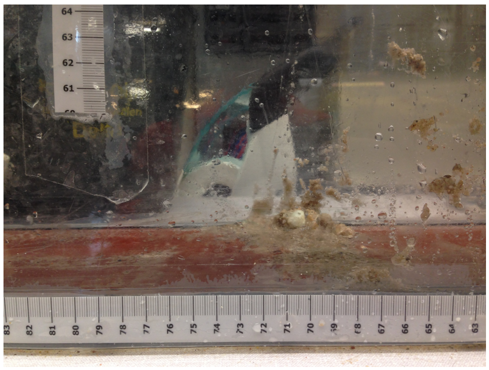

(d) Test 0002b with foreslope, bottom transport.

Figure B.19: Wall-effects with and without foreslope

Test 0003, Pressure sensors
Main conclusions with respect to installation TEST 0003:

- Pressure sensors should first 'rest' inside the water (e.g. 10 minutes) before use.
- Calibration from bottom to top is preferred, as decreasing pressure is less prone errors than increasing pressures.
- The pressure sensors should be kept in place by for instance nuts.

Main conclusions with respect to actual TEST 0003:

- TEST 0003A Showed that after the pressure sensors are placed in the water some time is needed for the pressure sensors to get adjusted to the water and temperature. The signal during the calibration runs with an upward trend, see figure B.20a.
- Pressure sensors are assumed to be calibrated and uniform with an averaged ratio of $\Delta signal/\Delta h = 0.132 v/cm$, as shown in figure B.20.
- There is no direct relation between volt and water level for a sensor. Every test a start signal and corresponding water height should be recorded.
- From figure B.20b it seems the pressure sensors react well to waves, they keep up with the wave frequency. However, the cause for difference in amplitude between the three sensors is unknown. Taking into account that that the signal of sensor L2 has a large disturbance at $t = 150$ this measurement is considered erroneous.
- The (better) wave signals L1 and L3 in figure B.20b have smaller and larger amplitudes. The larger mean-amplitudes are $0.24v$ and $0.41v$ respectively. These signals are converted to pressures leading to pressure oscillations with an amplitude of 1.8 and 3.1 centimetre water column.

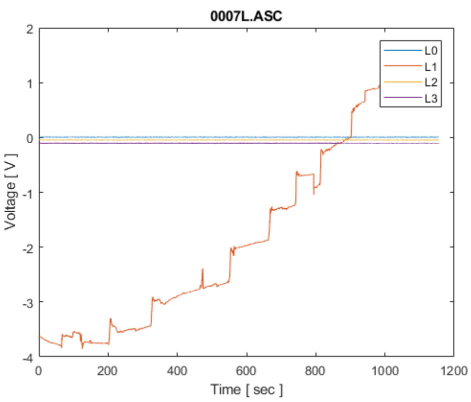

(a) Test 0003a, Calibration

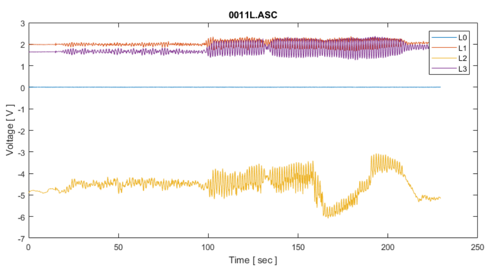

(b) Test 0003d: reaction to waves, raw signal

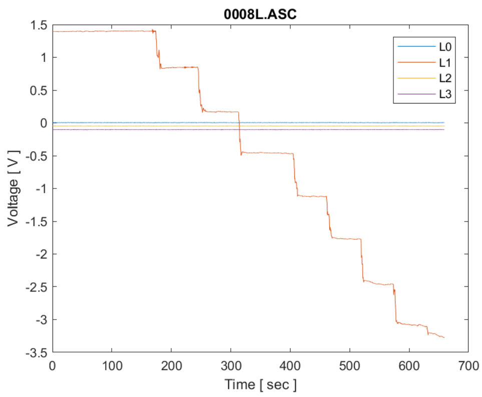

(c) Test 0003b, calibration

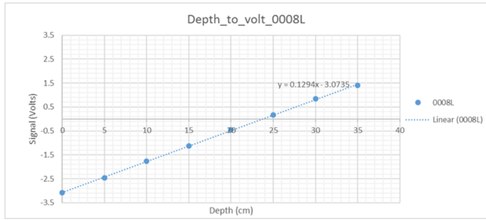

(d) Test 0003b, calibration curve

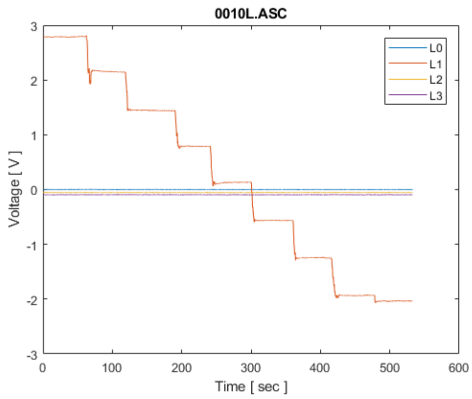

(e) Test 0003c, calibration

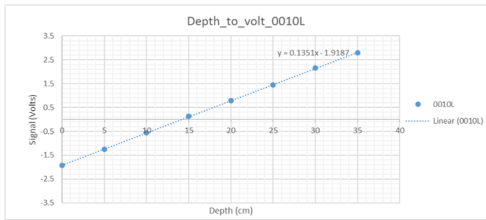

(f) Test 0003c, calibration curve

Figure B.20: Test 0003 Calibration of pressure sensors

Test 0004, Pressure sensors under sand

Main conclusions with respect to installation TEST 0004:

- Uncovered sensors tend to move with the waves. When placed under rocks this should not be an issue.

Main conclusions with respect to actual TEST 0004:

- When the sensors are covered with sand this can be clearly noticed in the signal, given by the arrows in figure B.21a.
- The varying pressure under a wave is noticed by the pressure sensor when the sensor is covered with sand. This is, in hindsight quite logical. The sensor was assumed to go break down or go flat after getting covered with sediment. However, the sensor still works. The pressure variations in the water are passed via the water in the saturated sand to the pressure sensors, therefore the waves signal is registered.
- Although not very clearly, it seems like the wave signal is somewhat dampened by the sand, given that signal L5 in figures B.21a and B.21c has smaller amplitudes than signal L1, L3 and L4. The sensors L1, L3, L4 and L5 were at the (viewers) right side of the container were waves were higher due to the run up on the sand slope. Sensor L2 is at the left side of the container were smaller waves were observed. This is noticed in the figure as well.
- Unfortunately, the results of the "still water test" show that the sensors are not very stable, see figure B.21b. Eventually they came to a more or less stable situation.

- In the second series of waves the sensors seem to work properly (again). Furthermore, the signal of the thick covered sensor (L5) has lower amplitudes than the less covered sensors implicating that the sand dampens the pressure oscillations, see figure B.21c.
- The thickness of the sand cover needed to dampen the signal from the sensor is very large, larger than the expected cover thickness caused by sand migration in the full experimental set-up. In addition, it is noticed that also sensor L3 was under a relative thick layer of sand and the signal is not significantly dampened.
- The observed pressure oscillations of the second series of waves (given in figure B.21c) is evaluated because this test gave the most clean signal. The mean pressure amplitudes are $L1 = 0.23v$, $L2 = 0.16v$, $L3 = 0.25v$, $L4 = 0.33v$ and $L5 = 0.16v$ resulting in Pressure oscillations with an amplitude of $L1 = 1.77$, $L2 = 1.24$, $L3 = 1.93$, $L4 = 2.56$ and $L5 = 1.22$ centimetre water column.

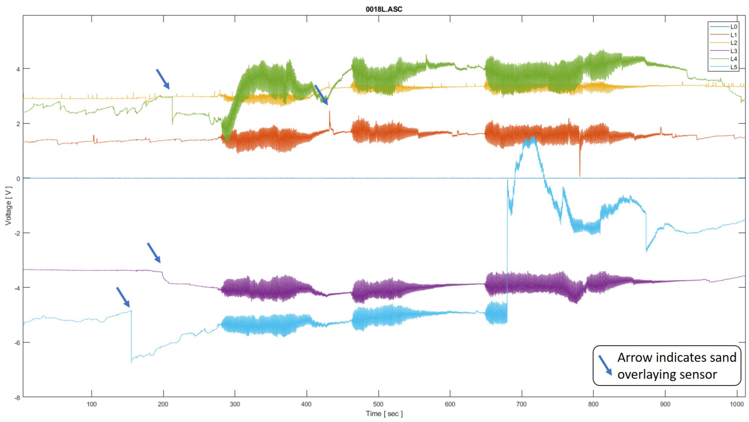

(a) Test 0004, obtained signal during installation and waves

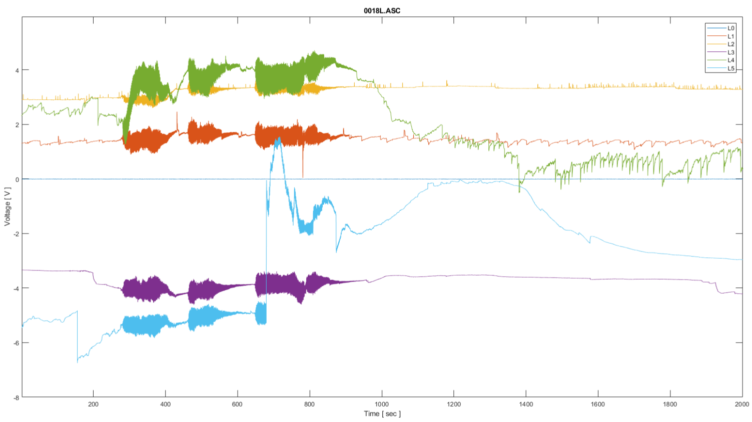

(b) Test 0004, obtained signal after waves

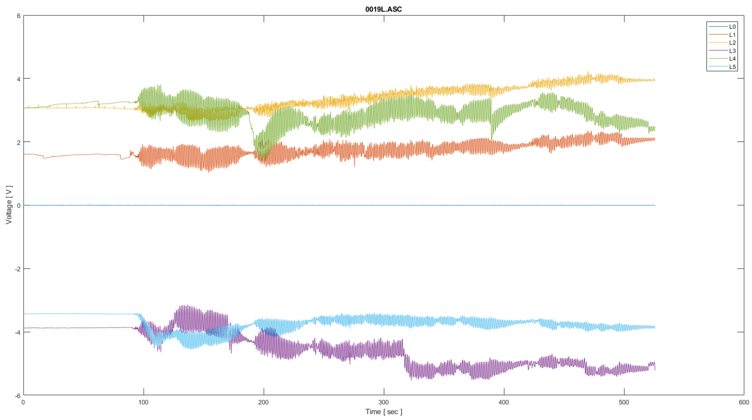

(c) Test 0004, second series of waves

Figure B.21: Test 0004, pressure sensors, sand and wave interactions.

Test 0005, Full set up
Main conclusions with respect to installation TEST 0005:

- The forgotten modelling clay caused some additional sediment transport along the sides of the plywood screens. The influenced the sediment transport observations made at the side of the container. For the evaluation of the middle part this (obviously) had no effect. Furthermore, the evaluation of the video footage made it possible to roughly estimate what transport would have been with modeling clay as the origin of the transport sediment can be observed.
- To much water was added initially which had to be scooped out before the test. This made the sand body fully saturated up to the surface.
- The use of the plunger was complicated due to all cable which came out of the container along side.
- The pressure sensors reacted as expected to the installation (adding water and sand) without disturbances, see figure B.22a.

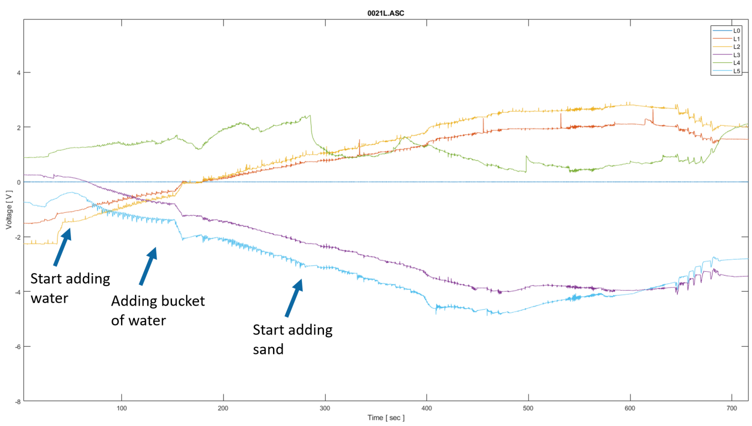

(a) Measurements during installation.

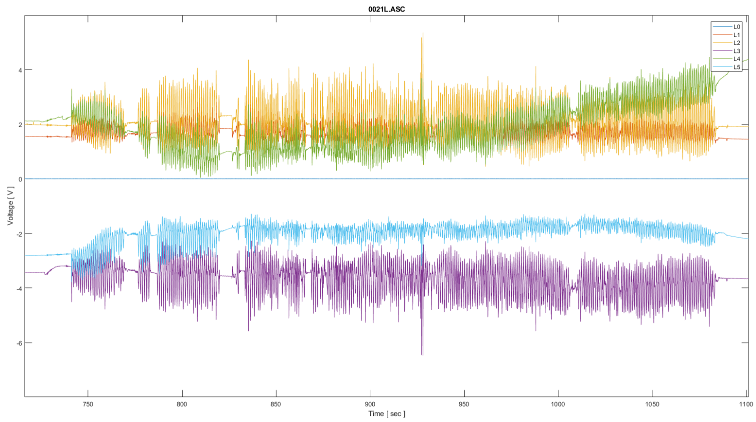

(b) Measurement during wave simulation.

Figure B.22: t0005, obtained measurement results.

Main conclusions with respect to actual TEST 0005:

- Sediment transport seemed minor but subsidence was noticed in the sand body. However, a considerable amount of sand was transported between the perspex and plywood screens.
- Due to test time-length limitations it could not be stated that a stable interface formed however, it seemed like there was initial displacement of sand from the sand body to the core, and afterwards only sediment transport up and down the interface slope.
- All sensors measure pressure oscillations, even those which were at the front of the toe, completely embedded in the sand body. However, this sensor (L5) has the lowest amplitude, see figure B.22b.
- The signal of the sensors does not change clearly during the test. The test was however very short.
- Considering sediment transport the results seem uniform over the cross-section, therefore wall flow is not necessarily devaluing the test, see figures B.24a and B.24b.
- Figures B.24b and B.24c show that the quantification of the sediment transport is rather difficult. The problems lies within (1) setting boundaries from where to where sediment transport should be assessed and (2) if the sediment found between the rocks is transported during the experiment or during the decommissioning of the model set-up.
- Figures B.24d shows the locations of the first two pressure sensors with respect to the toe of the model set-up. The first sensor highlighted with the yellow circle, is positioned at the front of the toe inside the sand body and was fully surrounded with sand. This sensor shows a signal with a low amplitude compared with the other sensors. The second sensor in the red circle is covered with rocks were sand has migrated by suffusion. Figure B.24d shows that this sensor is in contact with sand however, figure B.22b shows that the signal (L4) does not have a significantly dampened signal compared to the other sensors.
- The results of TEST0005 give potential for an evaluation method for sediment transport by "deposited sediment bottom length". However, careful decommissioning of the model set-up is essential and the method is prone to inaccuracies.
- The amplitudes of the wave simulation is evaluated between $t = 877s$ and $t = 924s$. During this period the wave signal is observed to be more or less uniform compared to the rest of the signal. The mean-amplitudes of the signals L1 to L5 are respectively 3.78, 8.77, 6.96, 5.12 and 2.50 centimetre water column. Signal L5 has a very low amplitude compared to the others, this is in correspondence with the fact that sensor L5 was placed at the interface of the toe and the sand body. The amplitude of signal L4 is also somewhat lower than L3 which could indicate that the pressures decrease towards the sand body where pores are getting filled with sand. The highest amplitude is found directly underneath the plywood screen separating zone 1 and zone 2. Furthermore, the measured pressures correspond with

the maximum wave amplitudes of about $5-7cm$ observed on the video recordings. In figure B.23 the mean-amplitudes are graphically given with respect to their distance x.

- The maximum pressure difference between a peak and a through of the signal L2 within the evaluated time frame is $3.3280v$, measured in zone 2. This corresponds with $25.22cm$ water column. If the water level difference is assumed uniform over zone 2 a total volume of $length * width * \Delta h * n(porosity) = 0.15 * 0.13 * 0.2522 * 0.4 = 0.00019672m^3$ is displaced in 0.45s resulting in a time and pore averaged velocity of $0.56m/s$. This is considered a very high velocity which raises questions. A similar calculation is carried out to approximate the maximum time averaged pore averaged velocity at various distances over x. With velocity $\approx 2 \cdot$ mean amplitude $\cdot$ number of waves/duration. For signals L1, L2, L3, L4 and L5 this results in $0.15m/s$, $0.35m/s$, $0.27m/s$, $0.21m/s$, $0.1m/s$ respectively. The results are again considered to be relatively high. The pressures and velocities are plotted in figure B.23 over distance x. In the same figure, the results of the video analyses are given in terms of water level amplitudes and corresponding velocities (calculated in the same manner as given above). These results are significantly lower. As the pressure sensors should maximally measure the water level in the video with an "visual observation margin" of $10-20\%$ the pressure sensors are decided to be too inaccurate to measure absolute pressures.

- If, very roughly, the velocities are inversely proportional with their cross-sectional area, the velocity underneath the plywood screens is $0.13/0.075 \approx 1.75$ times as large as the vertical velocity calculated in zone 2. This results in $0.60m/s$ and $0.24m/s$ for the measured signal and video analyses respectively.

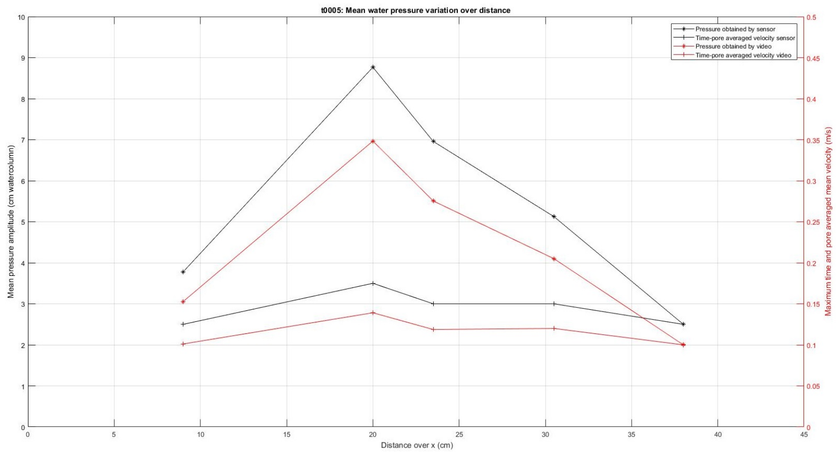

Figure B.23: Mean-amplitudes over distance

(a) Sediment transport evaluated over the cross-section.

(b) Sediment transport evaluation in decommissioned model set-up.

(c) Sediment transport evaluation in decommissioned model set-up.

(d) Position of pressure sensors and amount of sedimentation.

Figure B.24: Test 0005, observed visual results.

Test 0006, Set up with one sensor in sand body
Main conclusions with respect to installation TEST 0006:

- There were no real remarks on the installation other than that the modelling clay did not stay put on the plywood screens. This was noticed in other tests as well.

Main conclusions with respect to actual TEST 0006:

- The signal of the sensor in the sand body remained flat throughout the test. No water pressure variations were observed, see signal L5 in figure B.25b.

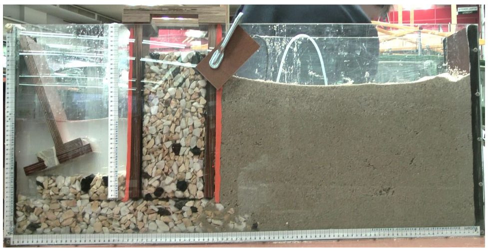

(a) Location of pressure sensor

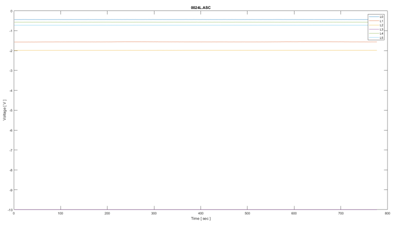

(b) Measurement during wave simulation.

Figure B.25: Test 0006, testing pressure sensor in sand body

Test 0007, Set up with one sensor in sand body
Main conclusions with respect to installation TEST 0007:

- Forgotten modelling clay and bar clamps caused considerable initial sediment transport.

Main conclusions with respect to actual TEST 0007:

- After the initial transport, little transport is observed. However, due tot the installation errors no clear results can be obtained. The video footage is valuable as comparison to other tests.
- From the signal of the pressure sensor shown in figure B.26b, it can be concluded that pressure oscillations are felt within the sand body. From the figure (B.26a) this seems logical because a more open sand structure is formed than in the other experiments. However, the signal is large disturbed with large variations and the signal runs with a downward trend.
- Signal L3 corresponds with a pressure variation of approximately 0.3 centimetre water column which was measured inside the sand body at approximately 15cm from the sand body.

(a) Overview of the model set-up

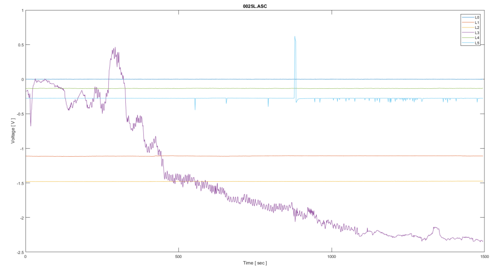

(b) Measurement during wave simulation.

Figure B.26: Test 0007, testing sediment transport without rocks

Test 0008, set-up with sand only
Main conclusions with respect to installation TEST 0008:

- It appeared to be difficult to keep the sand in place when water was added. It fluidized the sand from the bottom causing it to spread out, also when a plywood closure screen was used. Figure B.16b gives the results immediately after removing the closure screen.

Main conclusions with respect to actual TEST 0008:

- Sediment transport can be considered large, mainly observed by the subsidence of the sand body (figures B.27a and B.27b).
- With both smaller and bigger waves the sand is transported from the body towards zone 2 and zone 1 of the container. However, this simulation is far from the initial design of the model set-up, see figures B.27c and B.27c).

Test 0009, set-up with smaller compartment zone 3
Main conclusions with respect to installation TEST 0009:

- It appeared in the experiment that making waves was harder with this tested model set-up. The waves are less like pressured water level variations and more like propagating waves. Therefore, the water level oscillation in the second zone (between the plywood screens) is much smaller.

Main conclusions with respect to actual TEST 0009:

- In the sand only experiment the waves with the more propagating character were able to move somewhat under the plywood screens and sediment transport occurred. In the video footage turbulent eddies are observed. The result is given in figures B.28a and B.28b.
- The propagating character of the waves causing a low water level variation cause the sediment to stay put. Very little transport is observed. Even when the layer of stones was halved the sediments did not move. Analysing the video footage the experiment the situation seemed like a classical -open filter on a rock berm- situation where the flow- and impact forces were to cause sediment transport. The small water level variation is indicated in figure B.28c.

(a) Transport after first set of waves.

(b) Subsidence of the sand body.

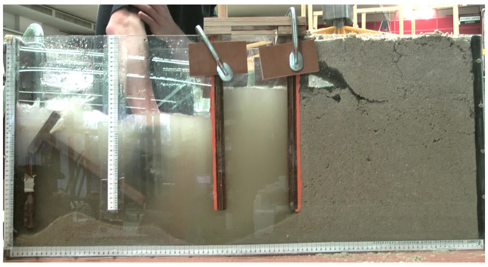

(c) Restored model set up, and increased transport.

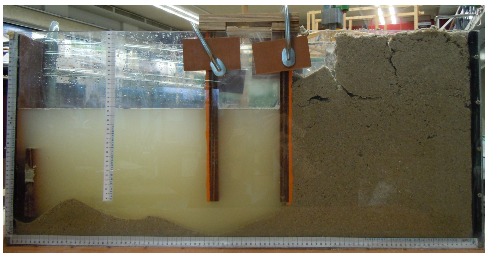

(d) Final result, sediment transport and subsidence.

Figure B.27: Test 0008, observed visual results.

(a) Water level oscillations in zone 2 are observed.

(b) Sediment transport is observed.

(c) Small water level oscillations are observed.

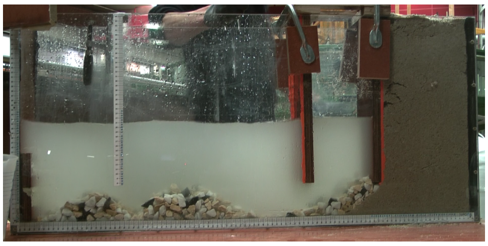

(d) With little rocks no sediment transport is observed.

Figure B.28: Test 0009, observed visual results.

Results non-process based experiments

In general, the non-process based measurements tend to devaluate the results elaborated on above. These test all give scattered or running signals. Considering the running signals, the direction of the trend (upward or downward) is not important as this is only a pre-defined setting of the signal amplifier. However, the fact that it is running causes uncertainties: If the signal does not stay flat for the duration of the measurement while nothing changes (e.g. amount of water/sand in the container, temperature, or salinity), the sensors might be broken or not functioning properly. The results obtained with these sensors in other test might be false as well. This results in the warning not to blindly trust the measurement equipment and the potential need for improvement. The results of the long duration measurements are given in figure B.29. In figure B.29a signal L3 shows a sharp increase and gentle decrease. This can be explained by the fact that it might be subjected by a disturbance which slowly restores ending with the original signal. However, signal L2 is clearly scattered and at $t \approx 2400$ the sensor gives the $10V$ signal. This can not be explained and means the sensor is broken or has bad connection. In figure B.29b only signal L1 is measured inside the container. The signal is clearly running but the cause is unknown. It could be the slow temperature drop in the night however, the running signal of $1.5V$ corresponds with $\approx 1.5/0.132 = 11.36cm$ water column, being a bit much for $1-3°C$ variation. In figure B.29c The signals are not necessarily running. With some wishful thinking one could project a day-and-night cycle over signal L2. This is however not clear from the other signals. The overall disturbances and scattering of the signal show in all three signals. What might have caused them is unknown. In figure B.29d signal L4 gives a very scattered signal, signals L0, L3 and L5 seem to keep relatively quite. Especially the small variations of about $0.25V$ to $0.5V$ in signals L1 and L2 are considered strange as they don't peak but have very low periods. It seems like short-circuit however, then it should peak to $(-)10V$.

Furthermore, they seem rather regular.

During the short duration test similar results are obtained. The measured data is projected in figure B.30. Most striking are the results of the measurements projected in figures B.30c and B.30d were the subtle, small and regular variations are seen in signal L2. During the test given in figure B.30d some waves are made at $t \approx 700$. This is clearly seen in the signal.

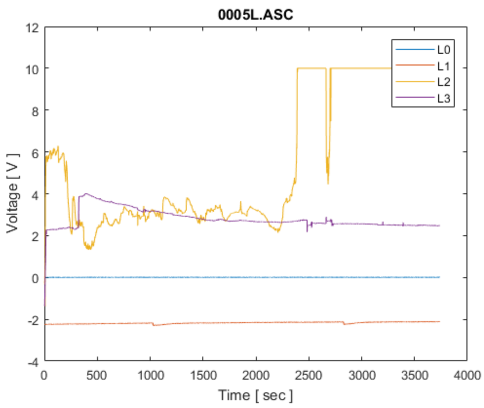

(a) Just after test 0003C (fig: B.20e) during lunch, L0 is P_{atm}.

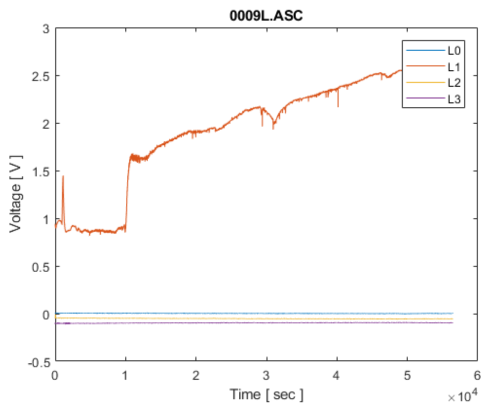

(b) During the night after figure B.29a, L0 is P_{atm}, only L1 in water.

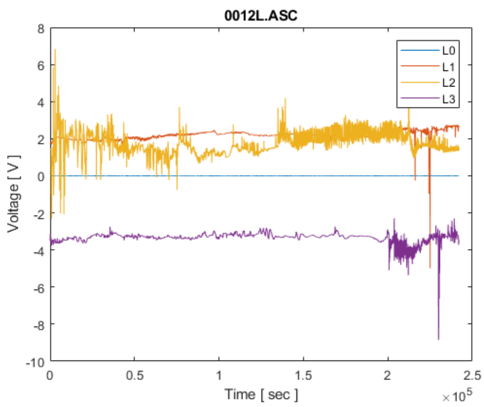

(c) The weekend after figure B.29b, L0 is P_{atm}.

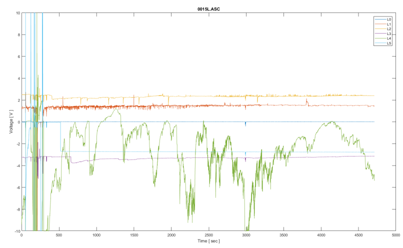

(d) During lunch the day after figure B.29c, L0 is P_{atm}.

Figure B.29: Longer duration measurements.

To resolve the problems with the sensors various methods are tried. The sensors are, while already underwater, injected with water by use of a needle to overcome the potential problem of air bubbles that are stuck in the opening. Furthermore, after tests in which sensors failed the sensors were dried and water tightness was improved by adding a new layer of caulk. Also, sensors were kept long periods of time in the water to get 'acclimatised' and potential initialisation problems would resolve. Although results got better, (e.g. the results presented in appendix B.2.2), the measurement equipment and method are not bullet proof. Therefore care is taken judging the obtained measurement signals and the use of the sensors is thoroughly evaluated.

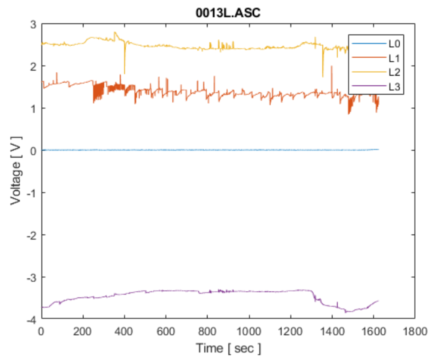

(a) Morning test while asking for advice results fig B.29c, L0 is P_{atm}.

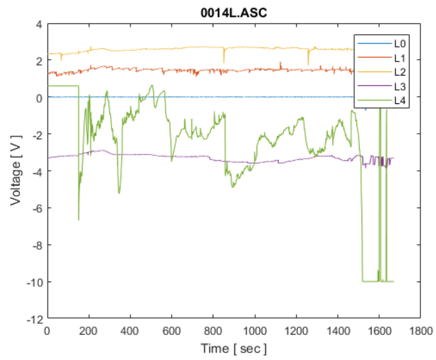

(b) Adding extra sensors with respect to fig B.30a, L0 is P_{atm}.

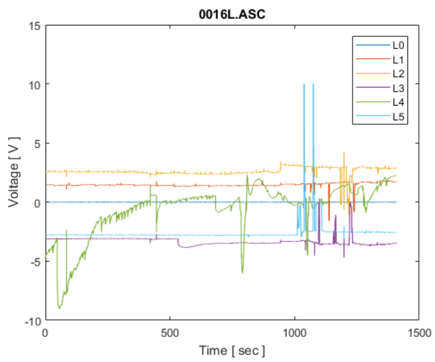

(c) Afternoon test after fig B.29d, L0 is P_{atm}.

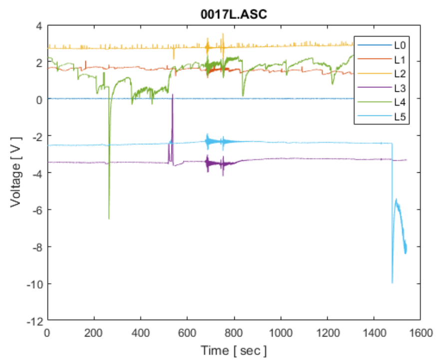

(d) Afternoon test after fig B.29d, L0 is P_{atm}.

Figure B.30: Short duration measurements, all executed in still water.

B.2.3. Conclusion and adaptation

Per test results are described considering the model installation and test sequence and the actual process based results, which describe the outcome of the model test. Also the results of the non-process based tests are described. From these results some conclusions can be drawn. These conclusions lead to an improved model set-up. Although the biggest changes are made based on these results, the testing remained an irritative process in which continuous improvements to the model are be applied.

Used materials and model set-up

In addition to the enhancement of measurement techniques and evaluation methods, first some simple improvements were proposed to the model set-up. The plungers surface area needed to be increased to approximately the surface area of zone 1 (with $\approx 1mm$ spare on all sides). Furthermore, a steel angle and more bar clamps prevent the container from bending out to much when subjected to large (water/sand) pressures. Also, more measurement tapes are glued on the container at various strategic places for easier evaluation of video images. Likewise, better camera's and/or with higher resolutions ensure an upgrade in these analyses. Lastly, the chosen size of sand and rocks (including their particular grading) should be matched to design conditions, in stead of the now chosen -randomly available- sand and stones in the lab.

Sediment transport and wall-effects

During the initial test some disturbances caused by model inefficiencies were observed. Without a foreslope, it prevailed that both at the interface between the rigid rock sample and the bottom and between the rigid rock sample and the perspex sides sediment was transported. Deeper in the rock sample the amount of transported sediment was less and therefore the visual sediment transport along the wall should is this case not be taken as representative for the sediment transport over a full cross-section. By the use of a foreslope these wall effects can be decreased. The observed wall-transport is significantly less and more uniform over the cross-section, see figure B.19. Similar differences were found evaluating the sediment transport on the bottom. Furthermore, the tests without foreslope are not necessarily a good presentation of the processes at prototype scale. Therefore it is concluded that solely tests with a foreslope should be executed. Still, wall effects remain an important aspect to be assessed. The loose rock against perspex wall might seem to sufficiently block the sediment however, it could also cause preferential pathways for water flushing sediments. In this case the visual observations from the side will give an under estimation of the sedimentation compared to the full cross-section where without a foreslope and overestimation was observed.

Besides, it is concluded that the total amount of displaced sediment was rather low. This can be caused by the short durations of the tests or by the fact that the load/resistance ratio was not sufficiently large to transport the sediments. The ratio that defines the openness of the filter in the preliminary experiments is $8.6[-]$. Although this value is larger than the criterion for open filters ($d_{15F}/d_{85B} \geq 5$) it is not as high as for instance the very open conditions in the experiment of Polidoro et al. (2015) ($d_{15F}/d_{85B} = 65$). Besides, a relatively small grading of the core material was used. Both a wider grading and the use of a smaller sand can result in an increase of sediment transport while keeping the remaining parameters the same. The increase in the amount of total transport was presumed needed because when we encounter a high ratio of the differences over the total, it results in statistically large errors. Therefore it is wished for to enlarge the total amount of displaced sediments.

Visual evaluation of sediment transport

As discussed in section B.2.3 some wall effects occurred which complicated the visual evaluation of sediment transport through the core material by observing the sand through the perspex walls. Furthermore, the use of a rigid rock sample in zone 2 caused difficulties evaluating if and how much sediment was transported through the rock material, and until what height and width. Therefore, the proposed model set-up in which the bottom part of zone 1 and zone 2 are filled with of loose rock and the upper (largest) part is a rigid body is preferred. This design causes semi-uniform conditions over different tests. After the rigid rock sample is removed the stones can be taken out one by one to evaluate the transported sediment. However, the quantification of the amount of sediment transport proved to be very difficult. The mixture of sand, rocks and water is not easily separated and residue from the large sand body will always pollute the area up for evaluation. Besides, a big challenge remains to integrate measurement equipment in a bonded rock model in a further stage of the research. In this case a design with solely loose rock is proposed.

Flow induced forces

The forces acting on the stones in zone 1 induced by the wave piston were of a high level resulting unwanted in suspended rock material. The suspension is in accordance with the pore velocity evaluation from TEST0005. However, the exact obtained quantitative signals (values) are most probably incorrect. To counteract the suspended rocks, a combination of loose material at the bottom with a rigid rock sample on top is used. The loose rock reduces wall-transport effects and the rigid body avoids material coming into suspension. A fully rigid rock sample in zone 1 is not considered to be an option because it reduces the possibilities for observing the transported sediment through the core material as discussed in section B.2.3.

Pressure sensors

The preliminary tests were executed to determine whether pressure sensors can be used to define various processes. The preliminary tests TEST0004 and TEST0007 showed that the sensors could not be used to indicate the propagation of the sediment over the floor of the container. The differences in measured pressures by sensors covered with sand or not, were not sufficient to make clear observations. Considering the recording of pressure oscillations the sensors prove to be very vulnerable and sensitive. Most (long term) measurements failed due to the inability to make the sensors water tight, or due to activities in the laboratory that influenced the signal from the sensors. Eventually the signals obtained by the sensors got better and some nice pressure oscillation- signals were recorded. Unfortunately many sensors broke down or signals kept to running over time. Furthermore, the obtained pressure signals did not correspond quantitatively with the video analyses. For these three mentioned reasons it is decided that the sensors in this form are not suited for the research. New pressure sensors in a different set-up (e.g. other method for making watertight and installing) were thought to be useful but large improvements were made. For the analyses of the propagation of sand over the floor of the container another technique is thought of using Conductivity type Concentration Meters or CCM. This is further elaborated in section 5.3.2.

B.3. Tests with final setup

The location of the pressure sensors, and CCMs are given in table B.2 for every test. Location 1 describes the location for 1 tube and location 2 for the other tube end. Pythagoras describes the distance over which the gradient is measured at the interface.

Table B.2: Location of Tube ends of pressure sensors and CCMs with respect to coordinate system.

	Repetition 1		Repetition 1		Repetition 1				
	Pres. Sensors	CCM 1	CCM 2	Pres. Sensors	CCM 1	CCM 2	Pres. Sensors	CCM 1	CCM 2
X location 1	27	24	43	24.8	23.5	42.5	24	22	42.5
Y location 1	0	0.5	0.5	0	0.5	0.5	0	0.5	0.5
X location 2	41	-	-	40.5	-	-	40.5	-	-
Y location 2	8.5	-	-	8.5	-	-	8.5	-	-
Distance	16.4	-	-	17.9	-	-	18.6	-	-

B.3.1. Model description

Model scale

The possible sand types were NAME_UNKNOWN (specifications in (Vargas Luna, 2016)), M32 and AF100 sand. The gradings of the various sands are compared to the grading considered "nominal" by Polidoro et al. (2015). In fig. B.31 the sieve curves for the different types of sand are given. It is noticed that the sieve curve for dredged sand is much wider than the laboratory sands. The is caused by the fact that dredged sand often contains some gravel, depending on where the dredging takes place. Due to time constrains, the different sands are not mixed to obtain an exact scaled representation of the sieve curve by Polidoro et al. (2015). The to obtain the smallest possible length scale factor λ the smallest available sediment size is taken. $\lambda_{db85} = d_{b85,\text{nominal}}/d_{b85,\text{model}}$ resulting in a value of $\lambda = 15.38$.

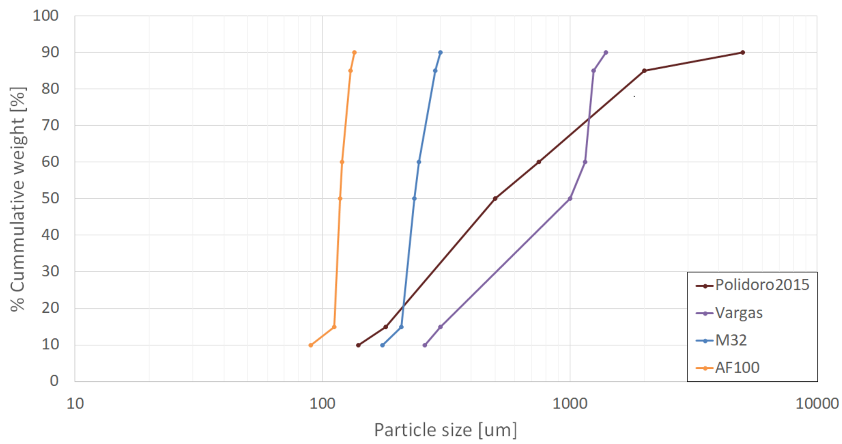

Figure B.31: Sieves curves for sand Polidoro et al. (2015), Vargas Luna et al. (2015), M32 and AF-100.

After the sand is picked the core material is scaled. This is done with respect to the nominal core proposed by Polidoro et al. (2015) as this is suggested to resemble a real breakwater. The preferred geometric constant to scale is the $d_{f,15}/d_{b,85}$ which relates to the filter function of the core material over the sand body as described in section 4.4.2. When a more conventional geometric scaling sequence was used (e.g. $\lambda = d_{b,50,nominal}/d_{b,50,\text{model}}$ and $d_{f,50,\text{model}} = \lambda \cdot d_{f,50,\text{nominal}}$), this would result in a significant change of the filter parameter $d_{f,15}/d_{b,85}$ because the grading of the nominal sand and model sand are not similar enough. The sieve curve sizes for the core material by Polidoro et al. (2015), the scaled core and the used model core are given in table B.3 including stability parameter C_u and sediment to core size ratio $d_{f,15}/d_{b,85}$. Also, the core when scaled based on the d_{50} is presented. It is observed that (1) the sediment to core size increases significantly and (2) the largest stones to use are $\approx 15[cm]$ which does not fit the container. Due to practical reasons originating from sieving and the model core sizes composition, $\lambda_{df15} = 15.81$, which is assumed acceptable to consistent with the scaling of sand. The grading curve for the nominal core, the scaled core and the used model core are presented in fig. B.32.

Table B.3: Core material scaling

Size	Core Polidoro [m]	Core on scale [m]	Model core [m]	Scaled on d_{50} [m]
d_{10}	0.21	0.007	0.007	0.024
d_{15}	0.23	0.008	0.008	0.030
d_{50}	0.46	0.025	0.025	0.09
d_{60}	0.51	0.031	0.031	0.11
d_{85}	0.62	0.052	0.051	0.19
d_{90}	0.63	0.053	0.055	0.19
C_u	4.7	4.7	4.7	4.7
$d_{f,15}/d_{b,85}$	65	65	63	236

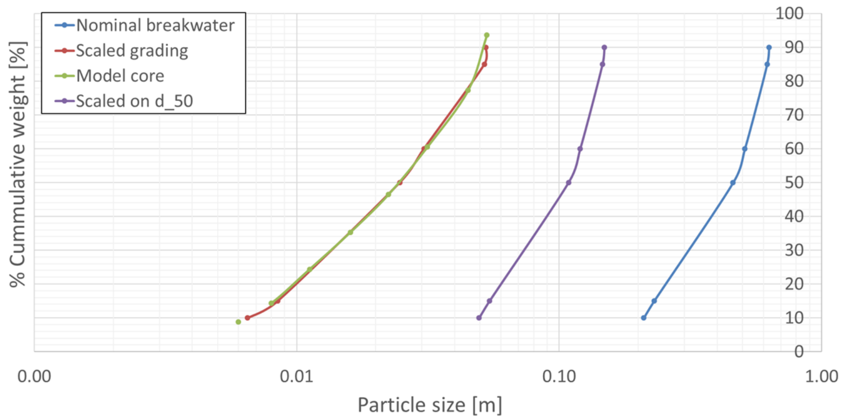

Figure B.32: Sieves curves for core material Polidoro et al. (2015), scaled core, model core and d_{50}-scaled core.

Geometry, Grading core material

In order to obtain the correct grading as determined in the section 5.3.1 two types of three types of rocks are used. "Yellow sun black mix" $8-16mm$, "Ardenner split grijs" $35-63mm$ and "Limburgs extra wit grind" $2-5mm$. The given sizes are only indication and give according to the sieve-test executed in the lab an 80% accuracy of the sizes of rocks. e.g. in every bigbag of stones 20% of the rocks in smaller or larger than the indicated size. The different stones are sieved as presented in section B.1.3. The sieve results are gathered in a spreadsheet and the target grading is approached by varying the amount (and weight) of stones from each sieve. The result of this process is shown in tables B.4 and B.5 and figure B.33.

Table B.4: Theoretical analyses of ideally scaled grading

Sievesize [mm]	Mass[kg]	Cum. Mass [kg]	% Weight under sieve
58	0	0	100
53	0.92	0.92	93.57
45	2.33	3.25	77.31
31.5	2.39	5.64	60.58
22.4	2.01	7.65	46.53
16	1.61	9.27	35.28
11.2	1.56	10.82	24.38
8	1.44	12.27	14.31
6	0.79	13.06	8.76
0	1.25	14.31	0

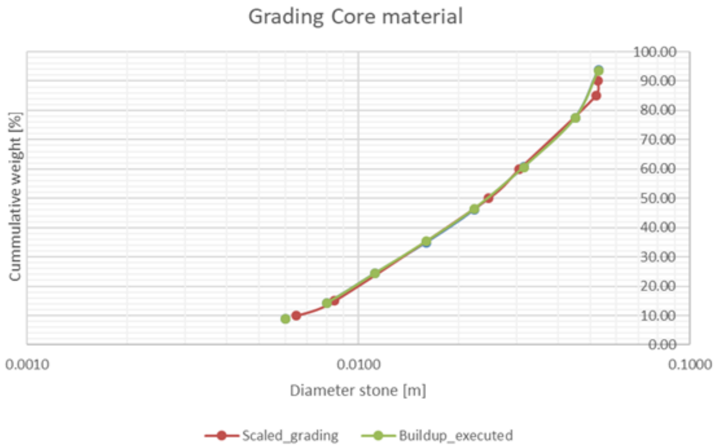

Figure B.33: Theoretical analyses of ideally scaled grading

Table B.5: Results of ideally scaled grading

	Size [m]	Wanted [m]	Delta_d [%]
d_{10}	0.0066	0.0065	-2.03
d_{15}	0.0082	0.0085	2.72
d_{50}	0.0246	0.0247	0.21
d_{60}	0.0311	0.0306	-1.89
d_{85}	0.0512	0.0520	1.53
d_{90}	0.0552	0.0527	-4.92
CU	4.7	4.7	0.14
d_{f15}/d_{b85}	63.2	65.0	2.72
d_{f15}/d_{b15}	73.4	75.4	2.72

To obtain the porosity of the material porosity test and calculated. A container was filled with the newly obtained combined rock grading. Afterwards the container was filled with water until the rocks were submerged. The amount of added water was noted and describes the so called "Volume of voids" or V_{voids}. The height of the water was marked and the container emptied. After, the container was filled with only water until the marked height. This amount of water is described as the "Total Volume" or V_{total}. From the these volumes the "volume of rock" (V_{rock}) and porosity ($n_f = V_{voids}/V_{total}$) can be calculated. As a control measure the density of the rock is calculated as follows: $\rho_{rock} = Mass/V_{rock}$. The mass of the sample does not change so the outcome of the calculation is used to say something about the accuracy of the test. The test of calculating the porosity is executed ten times. The results are gathered in table B.6.

Table B.6: Determination of porosity

Test number	Vvoids	Vtotal	Vrock	Mstones	Density	Porosity
1	0.0037	0.0092	0.0055	14.4	2618	0.402
2	0.0033	0.0087	0.0054	14.4	2667	0.379
3	0.003	0.0084	0.0054	14.4	2667	0.357
4	0.0032	0.0086	0.0054	14.4	2692	0.374
5	0.0031	0.0085	0.0054	14.4	2667	0.365
6	0.0034	0.0089	0.0055	14.4	2618	0.382
7	0.0034	0.0089	0.0055	14.4	2618	0.382
8	0.0031	0.0086	0.0055	14.4	2618	0.360
9	0.0036	0.0089	0.0053	14.4	2717	0.404
10	0.0032	0.0087	0.0055	14.4	2618	0.368
Average	0.0033	0.008735	**0.0054**	14.4	**2650**	**0.377**

Load conditions

The test program consists of 3 series of tests in which the hydraulic gradient is varied by means of setting the acceleration. In the first series an error occurred for which the data of the first 4 test got corrupted. These tests are only valuable to couple the acceleration of the motor to the resulting sediment transport but no valuable data regarding the hydraulic gradient could be retrieved. For the subsequent tests of this series the problem is resolved and the hydraulic gradients are correctly measured. The test program is given in table B.7.

Table B.7: Test program

(a) Series 1

Test	AC	Gradient
040	0.4	corrupted
041	0.8	corrupted
042	1.2	corrupted
043	1.6	corrupted
050	1.6	0.051
051	1.95	0.068
052	2.35	0.103
053	2.35	0.120
054	2.35	0.116

(b) Series 2

Test	AC	Gradient
55	0.40	0.016
56	0.80	0.023
57	1.20	0.043
58	1.40	0.045
59	1.60	0.053
60	1.80	0.062
61	2.00	0.081
62	2.20	0.086
63	2.40	0.092
64	2.6	0.100
64_2	2.80	0.110

(c) Series 3

Test	AC	Gradient
65	0.40	0.007
66	0.80	0.014
67	1.20	0.025
68	1.40	0.029
69	1.60	0.033
70	1.80	0.038
71	2.00	0.044
72	2.20	0.051
73	2.40	0.058
74	2.6	0.061
75	2.60	0.062
76	2.80	0.067
77	3.00	0.077
78	3.20	0.084
79	3.40	0.090

B.3.2. Instruments and measurements

Conductivity type Concentration Meter

In fig. B.34 for one of the model development test, the curve of the pressure sensors (S4 and S5) and the CCM meters (CCM1 and CCM2) are shown. The signal of CCM1 is of interest here, it is observed that the CCM registeres the oscillating signal by the waves, which implies the CCM registers an oscillating conductivity of the water and thus variation in the sediment concentration. The trend of the signal is going up and increasingly damping the oscillation. The oscillation itself is explained by the build up and breaking of arches in the grain structure. After a while, the sediment layer encloses the CCM and the oscillating signal decreases. In this manner the CCM is used to track the sediment propagation at the container floor. It is concluded that the propagation in this manner can be roughly evaluated. However, no quantitative analyses can be made.

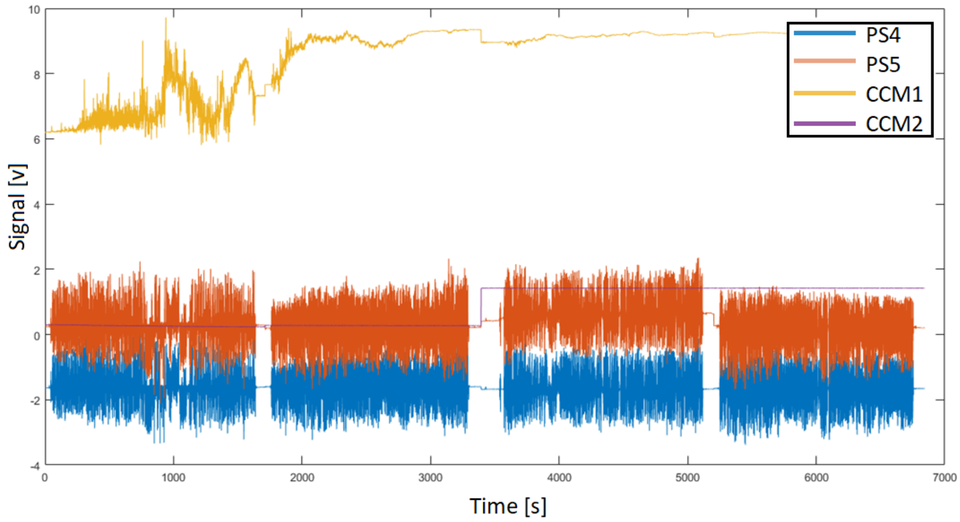

Figure B.34: Damping of CCM signal as the sensor gets enclosed by sand.

Pressure sensors

The pressure sensors had to be calibrated. It is expected that the individual sensors have similar calibration graphs however, small differences occur. Therefore, every individual sensor is calibrated. The sensors provide a signal in Volts for a given pressure, which has a linear relation with the pressure in meter water column. The relation $a \cdot x + b$ or in this case specifically signal in Volts = $a \cdot$ Signal in meter water column + b. The 'b' term is dependent on various initial conditions and might vary every test. Therefore, this value is not very important. At the start of every test b is adapted in a manner that the tests starts with a gradient of 0. After the test the b value is measured again to checked whether the signal ran or not. The linear relation is shown in figure B.35.

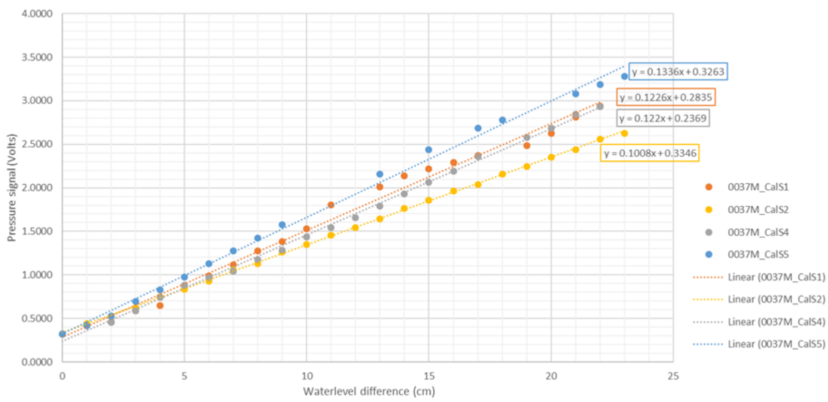

Figure B.35: Calibration graphs for first calibration test.

The sensors are calibrated by marking the tubes every cm and filling the tubes with water. The sensors and tubes are submerged in the container filled with water. The marked tube ends are pulled out of the water vertically stopping 30 seconds at every marked position. Because the tube sticks out of the water in the container, and is filled with water itself, the sensor measures the difference between the two water levels. The markings on the tube provide the height of this waterlevel difference. The sensors are calibrated two to three times. The average linear relation is taken resulting in the characteristics provided in table B.8.

Table B.8: Results of Pressure sensor calibration

Test	S1	S2	S3	S4	S5
1	0.1226	0.1008		0.122	0.1336
2		0.1045			
3		0.1047		0.1328	0.1443
Average	**0.1226**	**0.1033**		**0.1274**	**0.13895**
Std [%]		2.13		6.0	5.45

Camera's

In the fig. B.36 Four subsequent snapshots from a experiment with dye are presented. This experiments were executed to get insight in the flow patterns. These flow patterns are also registered in the log book describing all test results (appendix C.2.4). In every test such an experiment is executed, in many test this evaluation is carried out twice or three times. In the first picture the blob of dye is seen, the second and third picture show the propagation of flow and the fourth picture shows the diffused dye in the core material.

(a) t=1, Dye inserted via tube

(b) t=2, Dye indicates right flow

(c) t=3, Dye filtrated towards interface

(d) t=4, Dye has diffused through model

Figure B.36: Results of flow evaluation using dye

B.3.3. Data handling

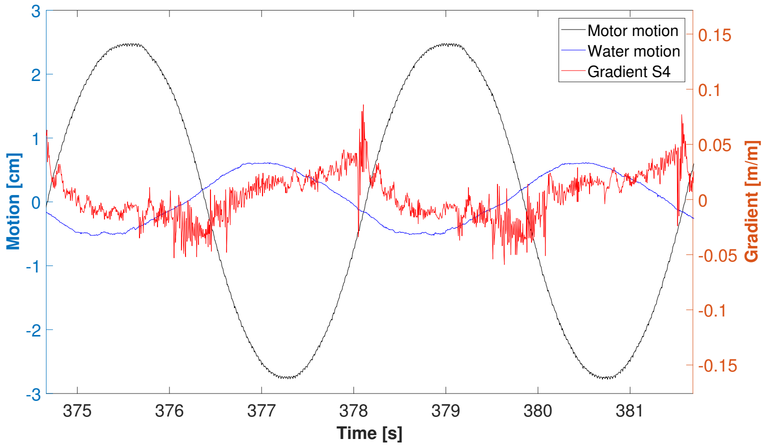

Figure B.37: 200Hz signal obtained for plunger motion, watermotion and hydraulic gradient

To obtain the specifications of the filter, the signal with noise is evaluated by means of a frequency analysis. It determines which frequencies are part of the desired signal and which signals are part of the noise. Extra information of the noise frequencies was obtained by the extra pressure sensor placed in a container attached to the side of the model setup. By comparing the two signals with visual observations made during the tests the filter properties were designed. An example of the hydraulic gradient measured inside the setup and the noise signal are presented in figure B.38. It is clear that at the point that the highest gradient occurs, also a noise signal is measured both in the model and in the extra sensor. This signal is observed to coincide with the tilting movement of the plunger, somewhat after the middle of the downward movement of the motor (also apparent in figure B.37). Going upward at the same position the tilting is also observed. In this picture, it is also noticed that for the model signal, the decreasing gradient oscillates with a frequency of approximately 7Hz after the disturbance at the peak is observed. Evaluating the signal for various tests this secondary oscillation can clearly be attributed to the stick-slip as discussed in the previous section

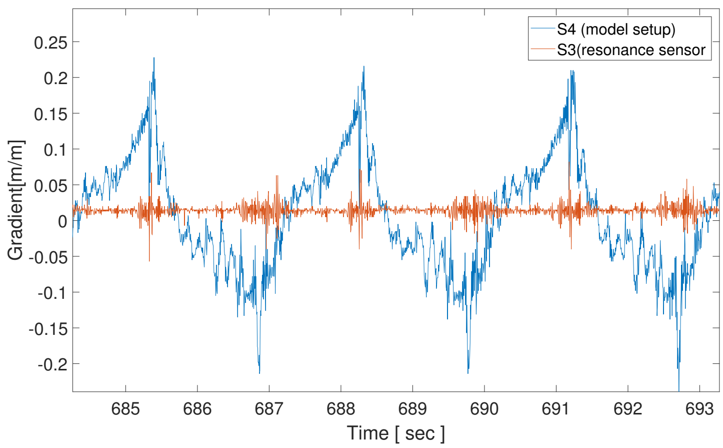

Figure B.38: 200Hz signals obtained in the model setup and in the resonance container.

A frequency spectrum analysis is executed to extract the exact frequencies measured by the sensors, as shown in figures B.39a and B.39b. In the model signal, the highest peak and thus most of the energy is observed at $\approx 0.27Hz$ which is the frequency of the motor. Higher order harmonics are observed at $\approx 0.54Hz$, $\approx 0.81Hz$, $\approx 1.35Hz$ etc. In figure B.39b the frequency spectrum of the resonance sensor is presented, it is observed that mainly energy is found at higher frequencies, $20Hz - 100Hz$. The analyses is extended with an PWELCH spectral density estimate for multiple motor setting ($AC = 0.8; 1.4; 1.6; 2.0;$ and 2.4 rev/s^2). Here the energy maxima in the frequency spectrum follow each other up as the motor frequency increases. The higher order harmonics occur in succession in the same manner. Figure B.39c presents this with the primary signals between 0.2Hz and 0.39Hz and a higher order harmonics between 0.6Hz and 1.1Hz. Furthermore, a high concentration of energy is found at 7Hz, which was the frequency disturbance caused by the tilting of the motor. When evaluating the peaks around 7Hz the similarity with the higher order harmonics cannot be found. In figure B.39d the same PWELCH analysis is shown for the resonance signal, also here the energy is found at high frequencies. Based on these results it is decided that a 5Hz filter is suitable to obtain the desired signal, cleared from noise. Specifically, a 5Hz equiripple lowpass filter (designed using the FIRPM function) is used. The results of the filtered signal are plotted in log-log scale over the spectral density graphs and prove the functionality of the filter in figure B.39e. Lastly, figure B.39f gives the filtered signal for the five different motor settings, with its spectral density as it is used for the evaluation of the experiments.

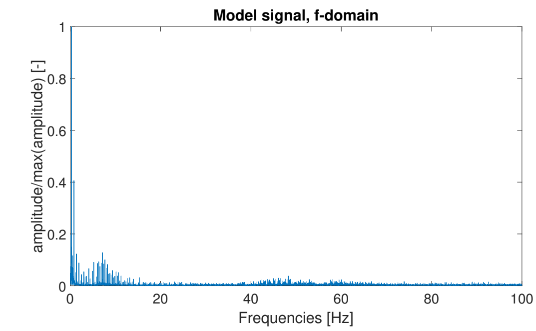

(a) Frequency spectrum model setup

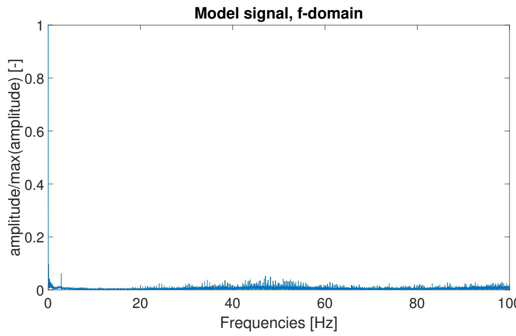

(b) Frequency spectrum resonance sensor

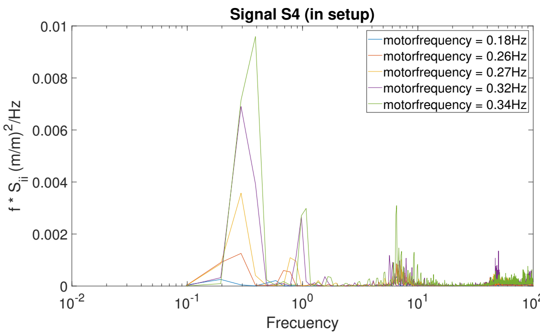

(c) Spectral density of model for five motor settings

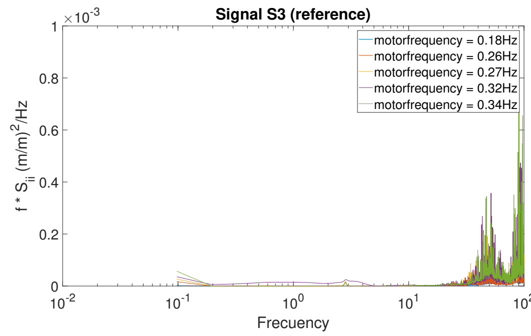

(d) Spectral density of resonance for five motor settings

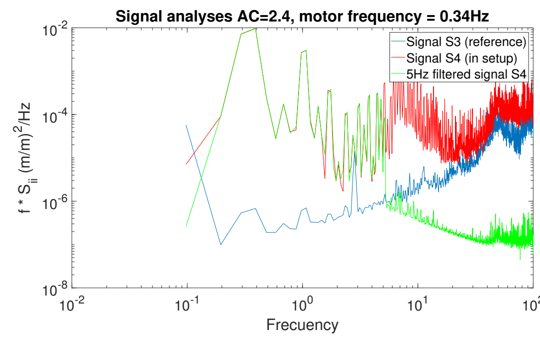

(e) Spectral density model, resonance and filtered sensors.

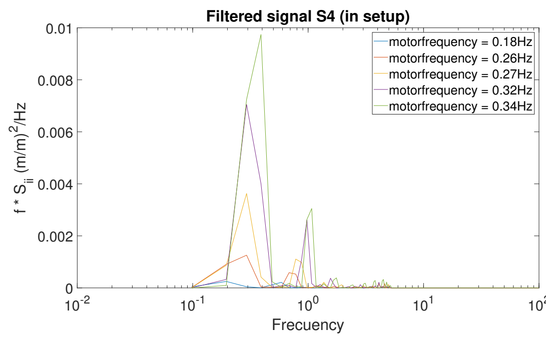

(f) Spectral density of the filtered signal

Figure B.39: Frequency spectrum analyses

C
Results

C.1. Physical model

C.1.1 Signal evaluation

In fig. C.1 for four different motor accelerations the plunger movement is showed as measured by the laser. The legend also provides the corresponding period. The same overview with graphs is made for the water level oscillations, presented in fig. C.2. Furthermore, the shape of the gradient signals is presented in fig. C.3. In fig. C.4 the obtained signals for two test with the same pre-set motor setting are presented for the plunger movement, water level oscillation and the hydraulic gradient. At the end of this section the overall consistency of the executed test is quantified. It gives the relation between the water level output conditions (motion, velocity, acceleration) for equal settings of the motor.

From the figures some conclusions are drawn. From figures C.1, C.2 and C.3, it is observed that the shape of the signals is similar when the loading conditions are varied. This results is obtained for the motor motion, water level motion and hydrualic gradient. The same details in the signals are found. Especially in the signal of the hydraulic gradient the 7Hz oscillations caused by the tilting and transitioning kinematic/dynamic resistance (explained in section 5.3.3) are clearly observed. Although in the signal of the water level motion the same characteristics are observed, such as the little dent in the through, the small peak in the peak of the graphs and the backwards skewness, the shape changes somewhat with the loading conditions. However, it is still considered to be very consistent. From figure C.4 the conclusion is drawn that also for different test with the same loading conditions the obtained signals are very similar. The motor motion is exactly the same (proving nothing more than the consistency of the motor operation), the water level motion again shows the same characteristics such as the little dent in the through and gradient also has the same characteristic shape. This all contributes to the consistency of the measurements, providing that the characteristic shape of a measurement does not depend on the test setup and if (minor) differences are observed, the can be contributed to the loading and thus probably to the physical processes in the measurement setup.

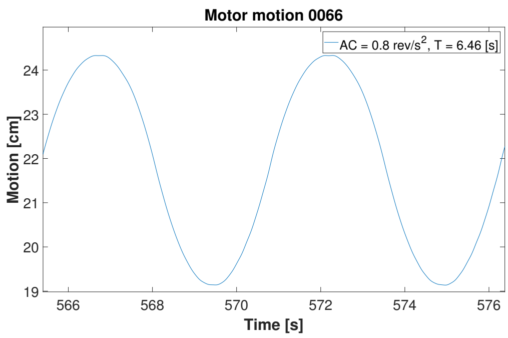

(a) $AC = 0.8\text{rev}/s^2$ and T = 6.46 s

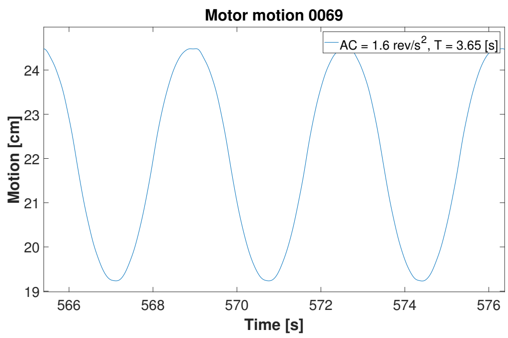

(b) $AC = 1.6\text{rev}/s^2$ and T = 3.65 s

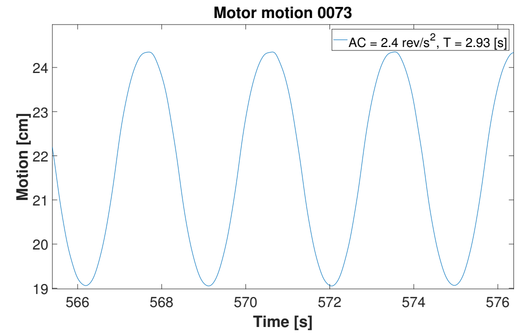

(c) $AC = 2.4\text{rev}/s^2$ and T = 2.93 s

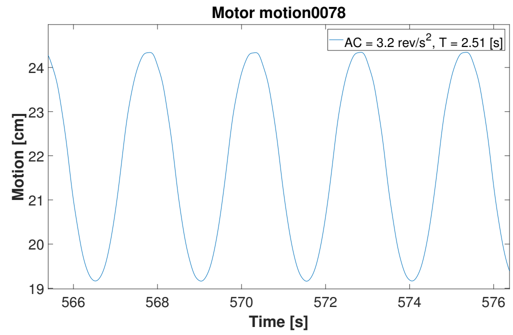

(d) $AC = 3.2\text{rev}/s^2$ and T = 2.51 s

Figure C.1: Obtained signals of the plunger oscillation for different pre-set accelerations of the motor

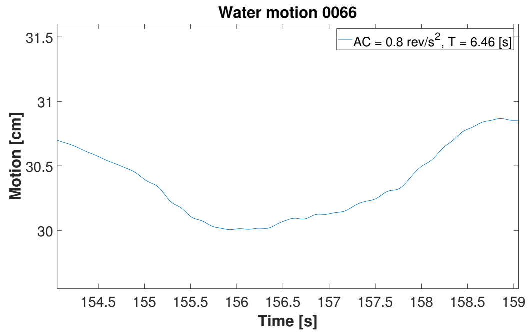

(a) $AC = 0.8\text{rev}/s^2$ and T = 6.46 s

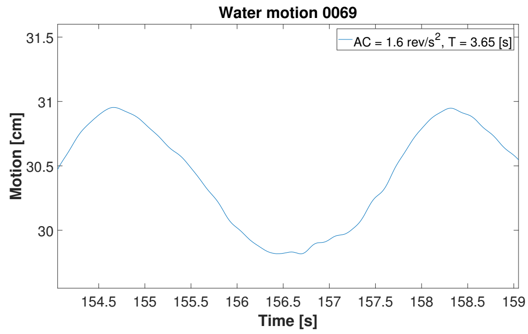

(b) $AC = 1.6\text{rev}/s^2$ and T = 3.65 s

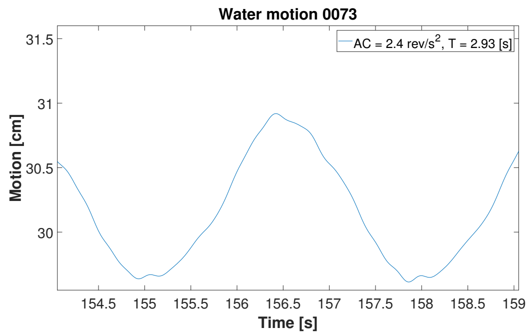

(c) $AC = 2.4\text{rev}/s^2$ and T = 2.93 s

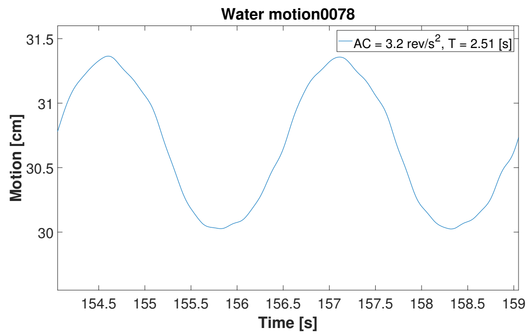

(d) $AC = 3.2\text{rev}/s^2$ and T = 2.51 s

Figure C.2: Obtained signals of the water level oscillation for different pre-set accelerations of the motor

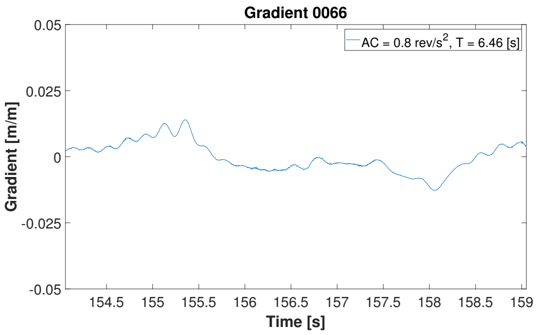

(a) $AC = 0.8\text{rev}/s^2$ and T = 6.46 s

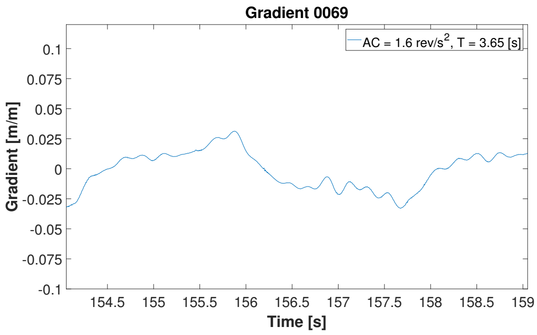

(b) $AC = 1.6\text{rev}/s^2$ and T = 3.65 s

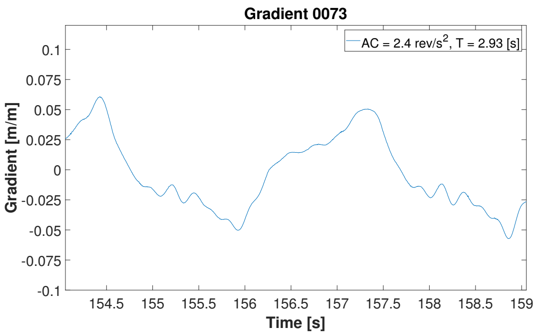

(c) $AC = 2.4\text{rev}/s^2$ and T = 2.93 s

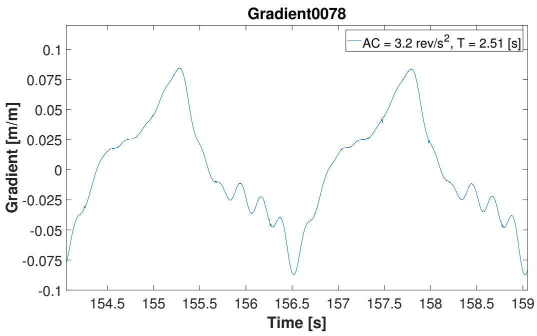

(d) $AC = 3.2\text{rev}/s^2$ and T = 2.51 s

Figure C.3: Obtained signals of the gradient oscillation for different pre-set accelerations of the motor

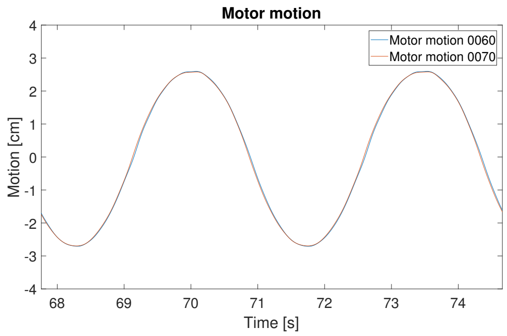

(a) Motor motion

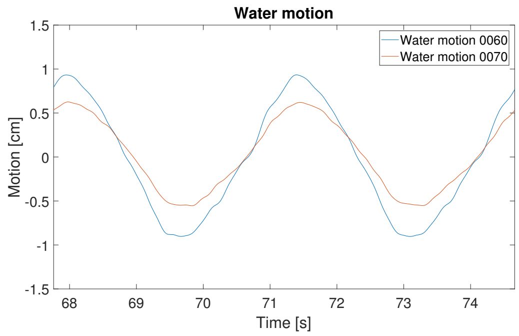

(b) Water level motion

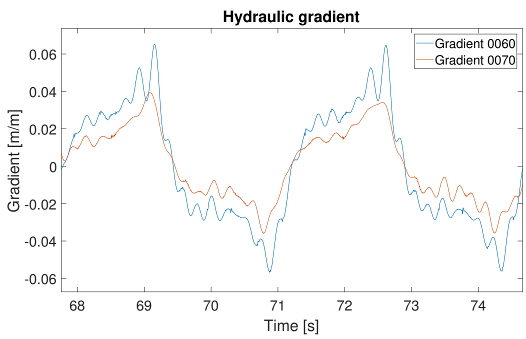

(c) Gradient

Figure C.4: Obtained signals for different tests with for $AC = 1.8\text{rev}/s^2$ and T = 3.46 s

Water level oscillations

In the report and appendixes many relations between input and output parameters of the model are described (e.a. motor settings vs. appearing gradients, motor settings vs. sediment transport, appearing gradients vs. sediment transport etc.). Also, the relation between the water level output conditions (motion, velocity, acceleration) for equal settings of the motor is evaluated. These evaluations are not particularly intended to obtain insights on the processes that govern the sediment transport or, hydraulic gradients, or the relation between them, but the research is also intended to develop and validate a method to evaluate these relations. Therefore, for the three series the resulting water levels, water level velocities and water level accelerations are evaluated for equal setting of the motor. This results are needed to discuss the consistency and accuracy of the model setup. The results are graphically projected in figure C.5. The standard deviation for the various outputs range between 5% and 40% with an average of 25%. To get more insight in the variation of the standard deviation per parameter (e.g. water level, water level velocity or water level acceleration), the results are split and summarised in table C.1.

Table C.1: Standard deviations for equal motor settings in [%] for different parameters.

	Max [%]	Min [%]	Mean [%]	STD [%pp.]
Waterlevel	37.38	18.19	28.31	6.02
Vel waterlevel	28.28	3.93	19.31	7.24
AC waterlevel	39.32	14.14	28.99	7.66

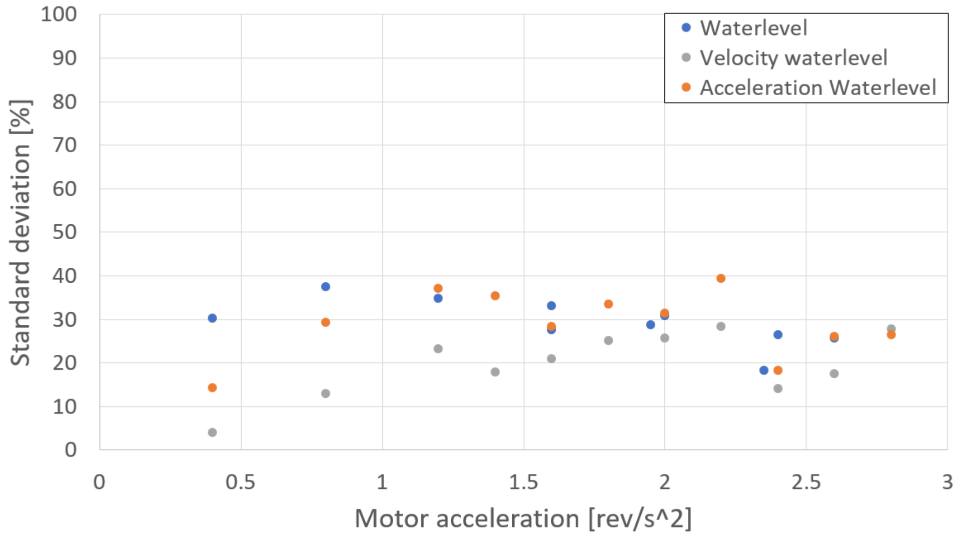

Figure C.5: Standard deviations for equal motor settings in [%] for different parameters

C.1.2 Parameter extraction

The characteristic values were extracted from the measurement data per parameter per test. After the filtering process described in section 5.3.4 a matlab code extracted the peaks and troughs of the signal with their value and time characteristics. From this, the average peak and through value and the average oscillation period were defined. The process was executed for the plunger motion, the water level oscillation and the hydraulic gradient. Furthermore, the velocity was evaluated, by using the GRADIENT function in MATLAB the derivative of the water level oscillation was taken which resulted in water level velocity graphs. Also here, the peaks and troughs were extracted providing the mean amplitude and period for the signal. In the described sequence, besides the amplitude, also the standard deviation was calculated. The mean amplitude was determined over 1000 waves and some spreading of the amplitude was observed. The deviation gave an approximation of the reliability of the obtained characteristic value. Unsurprisingly, the motion of the piston has very low deviations ranging 0.04% and 2.1% with an average of 0.3%. The standard deviations of the obtained water level signal are between 0.3% and 12.9% with an average of 3.6%. For the water level velocity the obtained characteristic values have an accuracy of 3.8% average, with a minimum and maximum of 1.7% and 7.6% respectively. For the hydraulic gradient a standard deviation of 6.2% average, ranging between 1.4% and 16.0%

was found. This is summarised in table C.2.

Furthermore, the expected accuracy of the final could be evaluated. It was desired to obtain a critical hydraulic gradient with an accuracy of 2 decimals. This implies that for every test the characteristic amplitude multiplied by the corresponding standard deviation should not exceed $0.005[m/m]$. This was observed only one time, for Series 1, the first time $AC = 2.35$ is tested. All 25 other tests from which data was extracted comply with the accuracy requirement.

Lastly, the acceleration of the water level was extracted. This was done by assuming a constant acceleration. This assumption is based on the fact that the loading was excited by constant acceleration of the motor. However, probably the acceleration of the water level was not constant due to resistance and inertia in the system. The acceleration was determined by means of $S = 0.5 * a * T^2$ in which S is the distance the water level travels during one oscillation, an T is the oscillation period. In the research it was not chosen to take the second derivative of the water level oscillation (which would in theory also result in the acceleration) because the disturbances in the signal were then amplified so much the outcomes were not reliable.

Table C.2: Standard deviations of extracted characteristic amplitude per parameter.

	Average Std. [%]	Maximum Std. [%]	Minimum Std. [%]
Plunger oscillation	0.27	2.07	0.04
Water level oscillation	3.57	12.87	0.28
Gradient	6.17	15.91	1.42
Water level velocity	3.82	7.64	1.74

C.2. Critical Gradient

In this section the evaluation of the measurement data is discussed an various relations are tested to obtain insight in the operation and functioning of the model setup. Also, the measurement results are discussed and the accuracy is elaborated on. In tables C.6, C.7, C.8 on page 127 and onwards, all characteristic values and parameters of each test are presented. In section C.2.4 all comments made on sediment transport and flow characteristics are summarised for the executed tests. These comments are used for the evaluation of the sediment transport in section C.2.

Acceleration motor and hydraulic gradient

As discussed in section 5.3.1, prior to the definitive experiments a series of test was executed to obtain the relation between the hydraulic gradient and the acceleration of the motor. This relation was used to define the settings for the tests. Three series of test were executed afterwards for which the relation between the hydraulic gradient and the acceleration of the motor could be (re-)evaluated. The first series of tests contains results for $AC_{motor} > 1.6$ rev/s^2 only, as the data for (earlier) tests with lower accelerations got corrupted. The results of the calibration test and definitive tests are plotted in figure C.6.

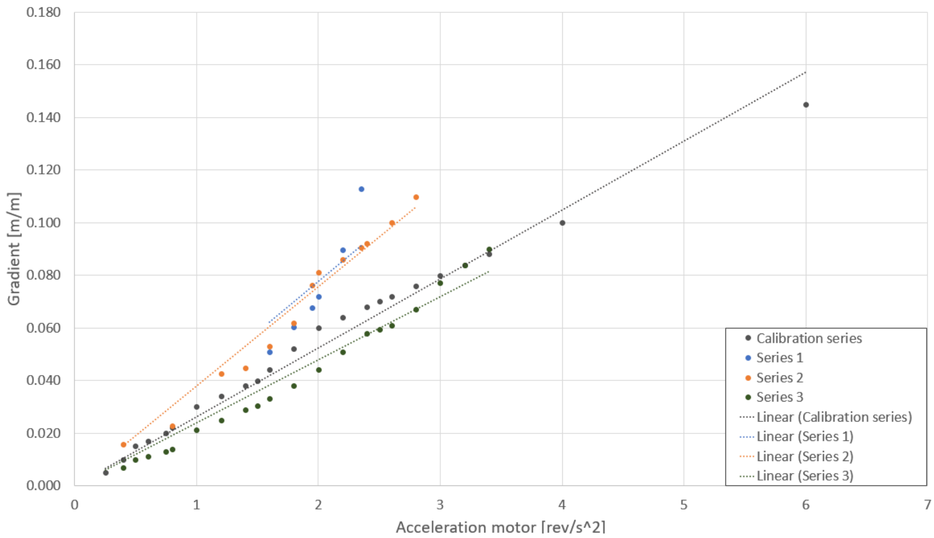

Figure C.6: Appearing hydraulic gradients for changing motor acceleration.

From the figure it is clear that the obtained hydraulic gradients are not equal for every test with the same acceleration of the motor. It is noticed that the first two series of experiments have similar order results, and the results of the third series resembles the values obtained in the calibration series. The gradients in the first two series were significantly higher. The results are firstly compared as a whole. In order to make a complete evaluation, were needed, missing data was interpolated. As the relation between the acceleration and the gradient is especially uncertain for higher values extrapolation was not used.

For motor accelerations of 0.4; 0.8; 1.4; 1.6; 1.8; 2.0 and 2.4rev/ s^2 the acceleration to gradient relation was evaluated as at least 3 tests or more incorporated these measurement points. Table C.3 provides the obtained results. The differences are described by means of the standard deviation which is ≈ 20%. From the points given in the table, supported by the results of all executed tests, the standard deviation was larger for the extreme values of the test series. The tests with 0.4rev/ s^2 has the largest variability with a standard deviation of over 40%. The best relation was found for an acceleration of 1.6 rev/ s^2 with a standard deviation of just under 20%.

Table C.3: Average gradients [m/m] and deviation for given motor acceleration.

AC motor [rev/ s^2]	CAL	Series 1	Series 2	Series 3	Mean	STD %
0.400	0.010		0.016	0.007	0.011	40.17
0.800	0.022		0.023	0.014	0.020	24.70
1.400	0.038		0.045	0.029	0.037	21.27
1.600	0.044	0.051	0.053	0.033	0.045	19.93
1.800	0.052	0.060	0.062	0.038	0.053	20.69
2.000	0.060	0.072	0.081	0.051	0.066	19.99
2.400	0.068	0.121	0.092	0.061	0.074	22.07

To gain some extra insights the two more similar pairs of relations were evaluated. The first two test series are shown in figure C.7a. The linear regression of both lines over the mutual interval is clearly visible and is almost identical. The appearing gradients for equal motor acceleration result in standard deviations ranging 1.8 – 15%, average 5%, which confirms their alikeness. The third series and calibration series also show comparability presented in figure C.7b. Their standard deviations are between 0 – 31%, average 18%. The higher deviations are again found especially for the lower accelerations of $AC \leq 1.2$ rev/ s^2. Considering accelerations from 1.2rev/ s^2 to 3.4rev/ s^2 the standard deviation decreases to 13% .

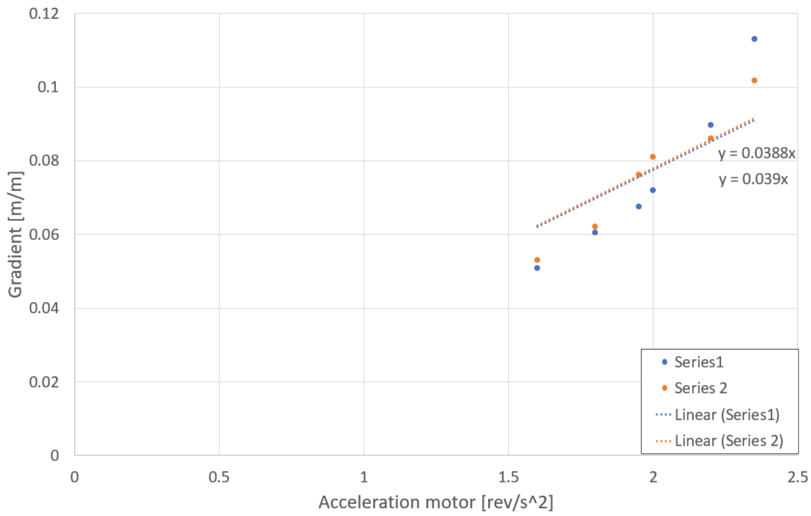

(a) Series 1 and Series 2.

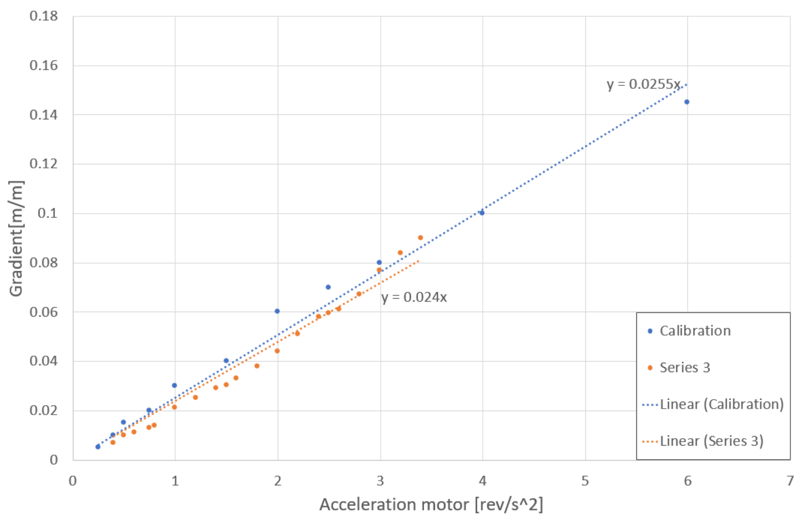

(b) Series 3 and calibration series

Figure C.7: Obtained gradients for motor accelerations for pairs of series.

The test results were also compared to their respective linear regression to determine the accuracy of the fit. For the first two series the deviation from their linear regression seems considerably in the graph, although the linear regressions of both series were almost identical. The average standard deviations for Series 1 and Series 2 from their respective linear regressions are respectively 9,3% and 5.4%. For Series 3 and the calibration series the average deviation from their linear regressions are 5.7% and 8.7%. Therefore, the obtained gradients within one test for a given acceleration are considered well correlated.

Acceleration water level and hydraulic gradient

The relation between the acceleration of the motor and the appearing gradient was assumed to be accurate because the acceleration of the motor was the only controllable parameter of the system. However, how the plunger reacts to the excited acceleration and if the water displacement and acceleration are constant over every excitation was questioned based on the measurement data. Therefore, the acceleration of the water level was also coupled to the appearing gradient. As proposed by the Euler Relation (eq. (A.6)), this correlation should without resistance, also be linear.

In figure C.8a the acceleration of the measured waterlevel in zone 2 is plotted against the measured hydraulic gradient. The relation seems to be linear but has a fair amount of spreading. The dots of equal colour give an equal setting of motor acceleration. In figure C.8b the data is split into the measurement series. The first series appears to be somewhat corrupted and the data is very scattered. In series two and series three the acceleration of the water has a linear relation with the obtained gradient. The measured accelerations and gradients could not be linked directly thus the linear regressions were used to compare. From the figure it is observed that the linear regressions of Series 2 and Series 3 are very similar. The standard deviation between the two is 4.2%.

This result is fairly better than the relation obtained in the previous section where equal motor accelerations gave a spreading of the appearing hydraulic gradient of ≈ 20% over the different tests.

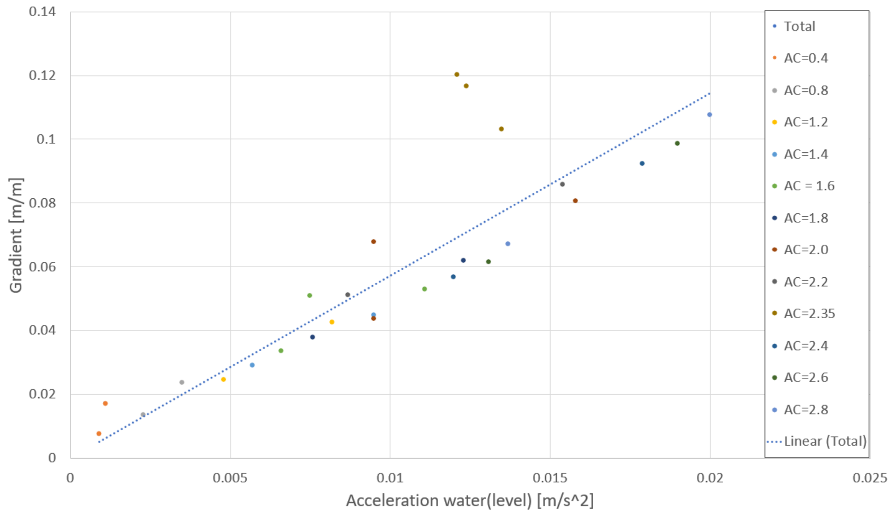

(a) Relation over total data

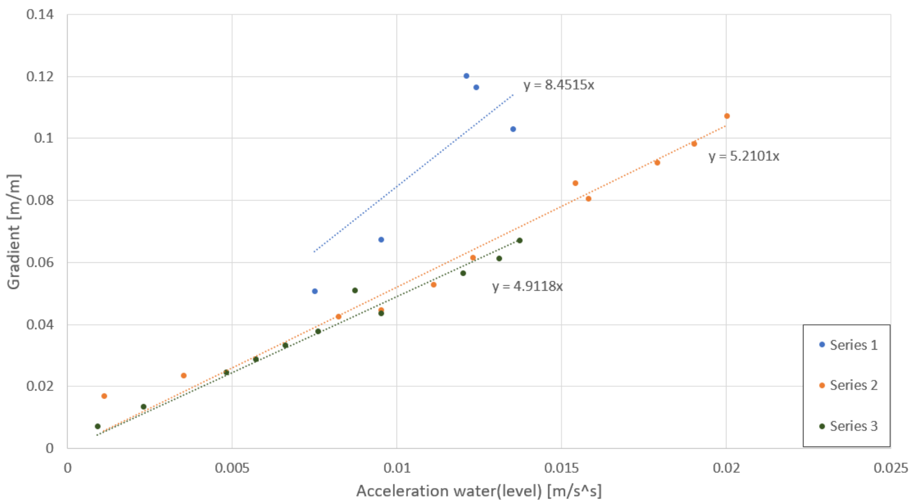

(b) Relation given for measurement series.

Figure C.8: Obtained gradients for water accelerations.

Acceleration and sediment transport

In appendix C.2.4 a full overview is provided of all observations made regarding sediment transport and flow characteristics during the experiments. The appearing sediment transport is coupled to both the appearing acceleration of the waterlevel and the pre-set acceleration of the motor. This provides insight in the reproducibility of the experiment and the initiation of motion of the sediments. The transport is qualitatively evaluated by in the domains: no transport, some transport and continuous transport. With 'no transport' literally no particle movements are observed. 'Some transport' means that only little transport is observed or transport is not constant over every wave oscillation. It is sometimes noticed that randomly, wave oscillations do or do not cause transport. For 'continuous' transport it is evident that continuous transport occurs for every wave oscillation in the test. Each test is categorised in the domain which fitted the transport regime the most and afterwards plotted against the motor acceleration and water level acceleration respectively. The results are given in figure C.9.

Motor acceleration

For pre-set motor characteristics the graphs show a 'no transport' regime under $AC < 1.2$ rev/s^2. An intermediate regime where depending on the test, no- some- or continuous transport is seen up to $AC = 2.2$ and from $AC \geq 2.35$ rev/s^2 continuous transport is seen for all tests. The obtained data in the intermediate regime is conflicting and provides different transport regimes for same order motor acceleration. The amount of conflicting data points in this evaluation technique is 20 from a total of 36 points.

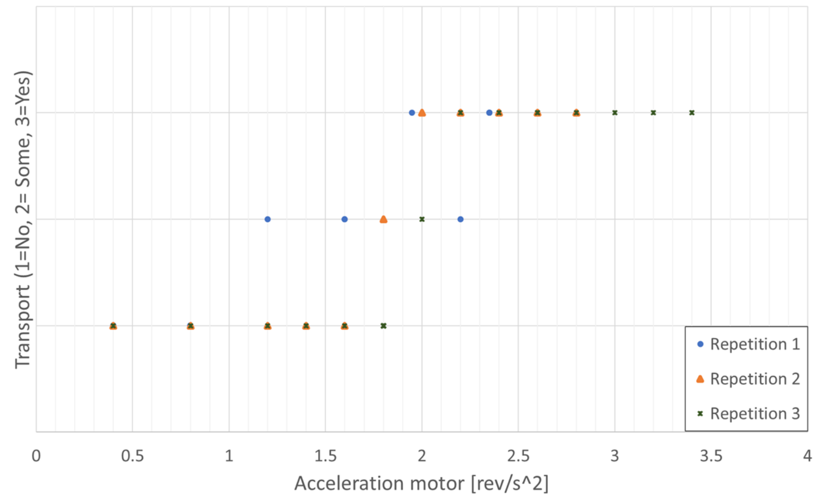

(a) For motor acceleration

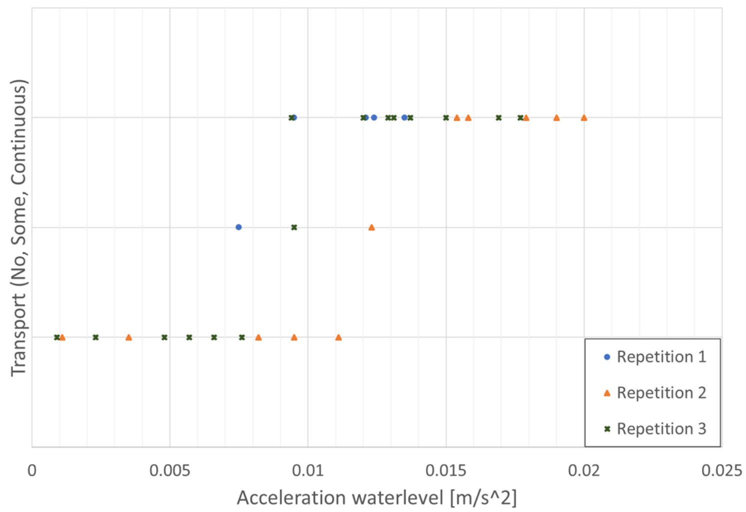

(b) For waterlevel acceleration

Figure C.9: Observed sediment transport in three domains for acceleration of motor and water.

Waterlevel acceleration

The same evaluation for the acceleration of the waterlevel (ACW) results in a 'no transport' regime for $ACW < 0.0076 m/s^2$, an intermediate regime up to $ACW = 0.0124 m/s^2$ and for $ACW > 0.013 m/s^2$ continuous transport is observed. Striking is that linking the results, the amount of points where an equal order acceleration results in a different transport regime is lower: only 12 from 31 points give conflicting outcomes and thus a higher reproducibility score is obtained.

In the same way as in section C.2, the connection between two types of accelerations related to one physical quantity has the best results for the measured waterlevel acceleration. The obtained relation between the pre-set acceleration and the sediment transport has a fairly large spreading. Besides it is observed that for one data point (waterlevel acceleration) a spreading over three transport regimes is observed, which is at $ACW \approx 0.095 m/S^2$.

C.2.1 Hydraulic gradient, sediment transport, porosity and slope

Figure fig. C.10 the propagation of the slope over three tests is shown. The three test are all amply within the continuous transport regime. It is observed the total propagation of the slope over a test increases. It is proposed that this is caused by the higher flow velocities that appear along the plywood screen. The closer the interface is to this path flow, the more sediment is transported. In the experiments a elongated tongue formed under the plywood screen. The picture show that the sediment transport tended to increase rapidly after the tongue was formed.

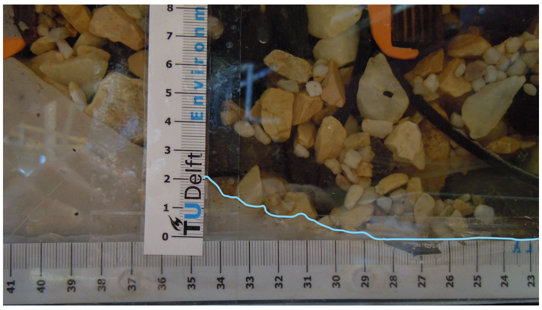

(a) Before test 0075, ($AC = 2.6 \text{rev}/s^2$ and $T = 2.83s$)

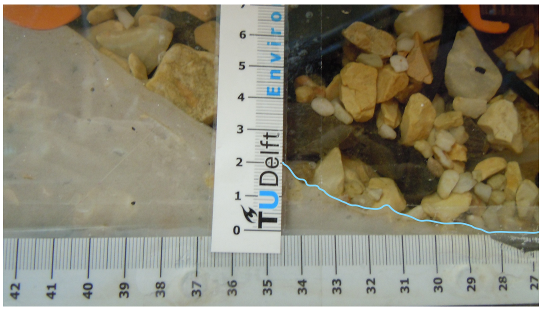

(b) After test 0075, ($AC = 2.6 \text{rev}/s^2$ and $T = 2.83s$

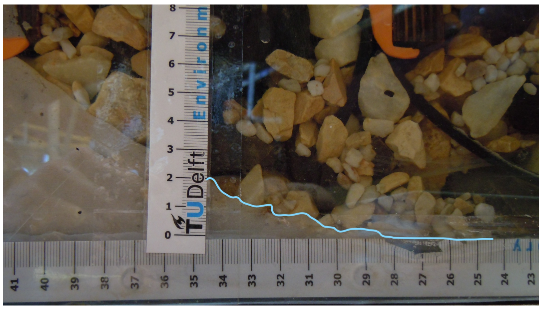

(c) Before test 0076, ($AC = 2.8 \text{rev}/s^2$ and $T = 2.75s$

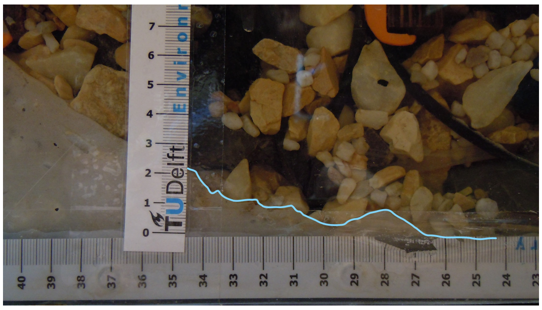

(d) After test 0076, ($AC = 2.8 \text{rev}/s^2$ and $T = 2.75s$

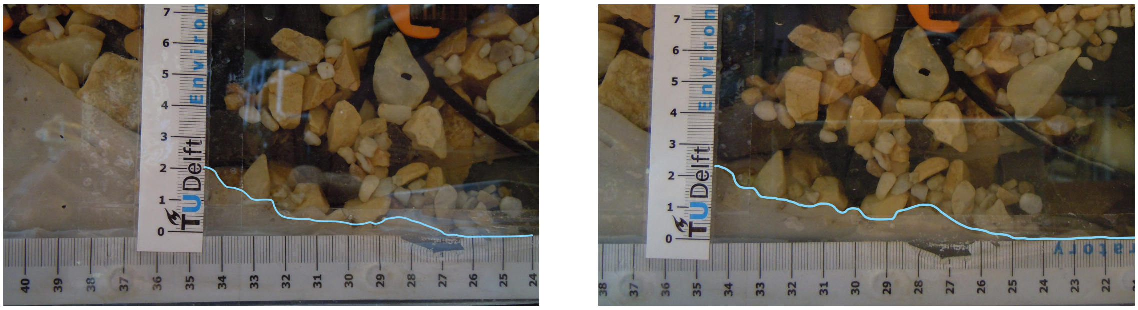

(e) Before test 0077, ($AC = 3.0\text{rev}/s^2$ and $T = 2.58s$

(f) After test 0077, ($AC = 3.0\text{rev}/s^2$ and $T = 2.58s$

Figure C.10: Propagation of tongue, with increasing speed when approaching plywood screen.

C.2.2 Filter velocity

For the experiments the test averaged filter velocity amplitudes calculated. This approaches the vertical filter velocity in zone 2 if this were uniform flow over the vertical cross-section. To obtain the test averaged filter velocity amplitude, horizontally, under the plywood screens the vertical filter velocities are multiplied with the vertical cross-section of zone 2 and divided by the cross-sectional area underneath the plywood screen, this is a factor of 1.6. The resulting filter velocity amplitudes range between $0.007m/s$ and $0.027m/s$ over the vertical and between $0.011m/s$ and $0.044m/s$ horizontally underneath the plywood screen. The filter velocity amplitudes are plotted against the hydraulic gradient in table C.5. The obtained filter velocities used as a very rough estimation of the appearing filter velocities. The filter velocity decreases through the core material due to friction and. It could be argued that the filter velocity along the interface is the average of the horizontal and vertical velocities as the streamlines at the place of the interface already diverge into the wider cross-sectional area were the water is forced vertically. However, the vertical and horizontal approximations are already very rough and an extra calculation based on this guess will not provide more certainty on the appearing filter velocity. The filter velocities are thus assumed to range between $0.007m/s$ and $0.044m/s$.

It is proposed that the relation between the water level velocity or the filter velocity and the hydraulic gradient is quadratic. This is derived from the two (basic) relations between the motor acceleration, the distance and the velocity. Distance S is constant as it is the amplitude of the plunger. When writing both equations in terms of time t, a relation can be obtained between the velocity and the acceleration. This relation is quadratic. As the hydraulic gradient is linear with the acceleration, the hydraulic gradient is also quadratic with the velocity. Obviously, the Forchheimer equation also proposes a quadratic relation between the gradient and the filter velocity. This extra analysis was executed because for this particular data, a linear regression would fit as well/better.

$$\left.\begin{aligned} S &= 0.5 \cdot a \cdot t^2 \\ V &= S/t; \end{aligned}\right\} \qquad 0.5 \cdot a = v^2/S; \tag{C.1}$$

By plotting the hydraulic gradient against the filter velocities, the Forchheimer equation is evaluated. In fig. C.11 the equations are given for the quadratic approximations of the data. The two relations for Series 3 give negative Forchheimer coefficients 'a' which have no physical meaning. After additional research this problem was subscripted to an internal problem in MS EXCEL (Kennedy et al.). By Kennedy et al. a method was proposed in which the gradient was divided by the filter velocity and afterwards an linear regression was performed. This again resulted in negative coefficients. Therefore, MATLAB was used to give a quadratic regression resulting thing in the Forchheimer coefficients presented in table C.4. However, whether this program is able to do this correct is questioned due to the errors made by MS EXCEL. Although the obtained filter velocities are assumed to be very rough, it is seen that coefficient 'a' is larger and α is smaller than often observed (e.g. $\alpha = 1001$ in Van Gent (1993). This is supported by the Forchheimer coefficients 'a' and 'b' found by Vanneste and Troch (2012) that also show a larger influence of the laminar term. A regression analyses made for the total data set of repetition 2 and repetition 3 leads to coefficients a= 1.16, b=109.24, $\alpha = 719.08$ and $\beta = 1.21$ for the vertical filter velocity. When the Forchheimer relation is used with these coefficients and the measured vertical filter velocities are inserted a reasonable accurate estimate of the measured gradients arises. When the critical gradients are inserted, the resulting critical filter velocities are between $0-5\%$ accurate. This is shown in fig. C.11.

Table C.4: Obtained Forchheimer coefficients from vertical and horizontal filter velocities.

	a	b
	s/m	s^2/m^2
Reptition2$_{ver}$	1.215	104
Reptition2$_{hor}$	0.733	41.33
Repetition3$_{ver}$	0.396	181.71
Repetition3$_{hor}$	0.299	68.87
Model $_{regression}$	1.16	109.24
GWK breakwater (Vanneste and Troch, 2012)	0.89	22.9

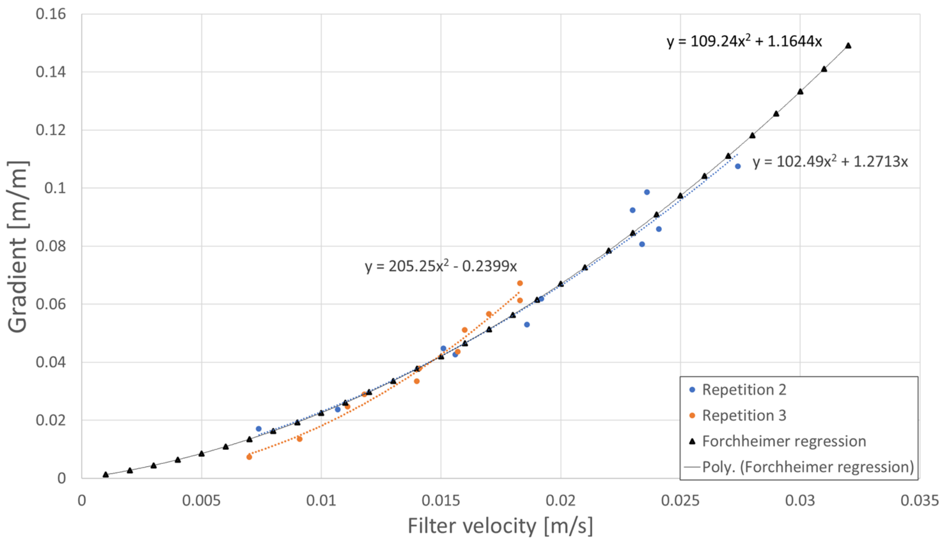

Figure C.11: Vertical filter velocities and Forchheimer regression (with a= 1.16, b=109.24, α = 719.08 and β = 1.21)

For the three transport regimes defined in section 6.3.1 and the three test series, the critical filter velocity amplitudes for which a change in transport regime occurred, are given in table C.5. Also the mean velocity amplitudes for a transition, and their corresponding standard deviations are given. The first measurement series has significantly lower values for the filter velocity to appear to be critic. As the initiation of motion phase was not registered in this series this data point is left out, which was causing a false average critical filter velocity. The average critical velocity is therefore also left out for the first phase.

Furthermore, the critical filter velocities are approached by means of the measured critical gradient and the calculated Forchheimer coefficients (a= 1.62, b=99.8). This lead to the critical filter velocities given in the last column of table C.5.

Table C.5: Vertical filter velocity amplitudes for transition in sediment transport regime.

Transition	**Mean**	**St.Dev.**	Series 1	Series 2	Series 3	Calc (Forchheimer)
	$[m/s]$	[%]	$[m/s]$	$[m/s]$	$[m/s]$	$[m/s]$
Initiation of motion				0.019	0.014	0.015
Initiation of continuous motion	**0.016**	**20.1**	0.013	0.019	0.016	0.016
Continuous motion	**0.018**	**25.3**	0.015	0.023	0.016	0.019

C.2.3 Filter relations

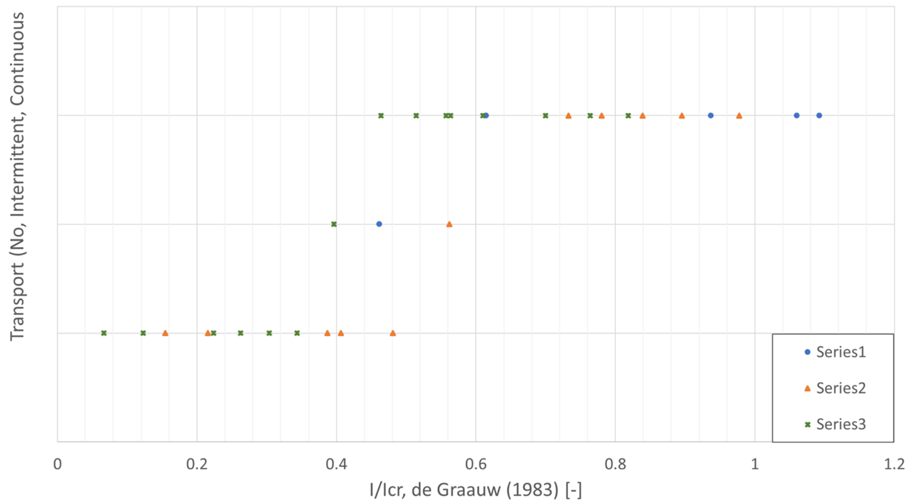

(a) I/I_{cr} de Graauw et al. (1983) vs. transport regime

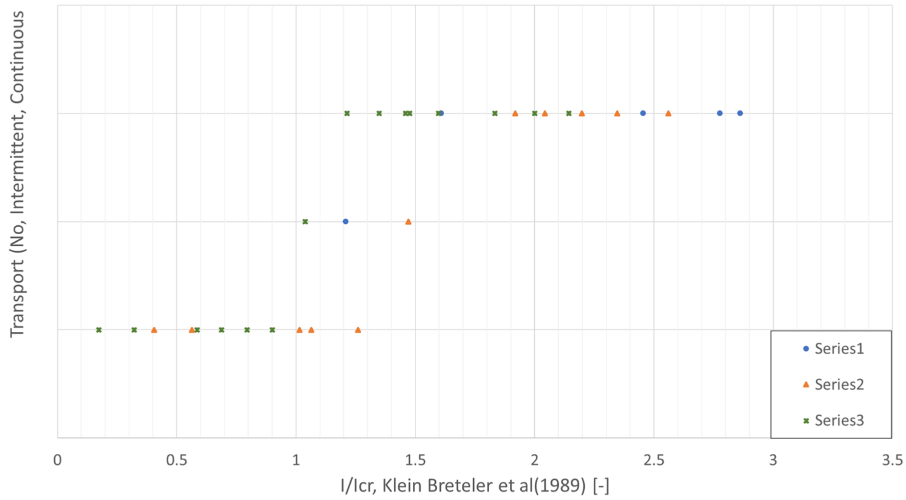

(b) I/I_{cr} Klein Breteler (1989) vs. transport regime

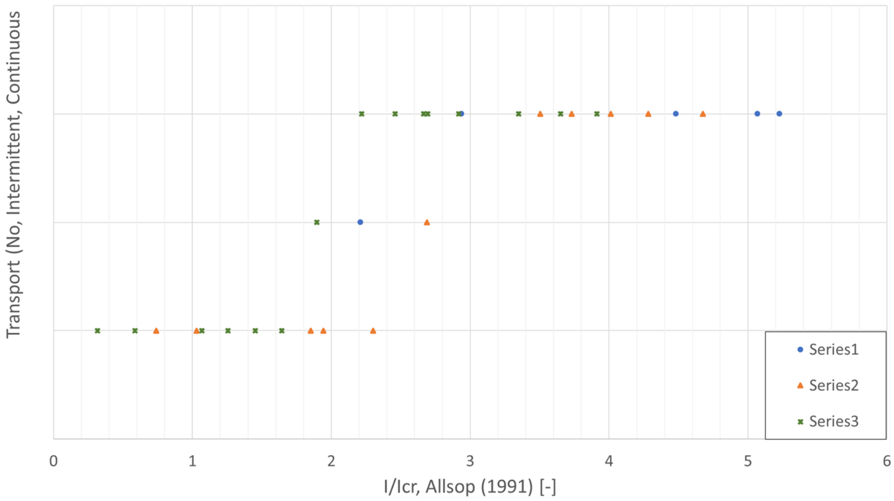

(c) I/I_{cr} Allsop and Williams (1991) vs. transport regime

Figure C.12: Transport regimes for $I_{\text{appearing}}/I_{\text{critical,calculated}}$ for different stability criteria

Table C.6: Series 1

Test-number	AC	Period	Duration	Amplitude plunger	Wav-height plunger	Period Water	Amplitude Water	Wave-height Water	Period S4	Amplitude S4	Positive gradi-ent	Negative gradi-ent	Standard dev pos [%]	Standard dev neg [%]	Comment
50	1.6	3.6422	3642	2.648	5.30	3.6423	6.317	12.63	3.6423	0.0509	0.0605	-0.0412			
51	1.95	3.2993	3299	2.6576	5.32	3.2993	6.456	12.91	3.2992	0.0676	0.0636	-0.0716			
52	2.35	2.92	2920	2.65	5.30	2.92	7.30	14.60	2.92	0.103	0.09	-0.12			
53	2.35	2.92	2920	2.65	5.30	2.92	6.70	13.40	2.92	0.120	0.12	-0.12			
54	2.35	2.92	2920	2.65	5.30	2.92	6.70	13.40	2.92	0.116	0.12	-0.11			

Table C.7: Series 2

Test-number	AC	Period	Duration	Amplitude plunger	Wav-height plunger	Period Water	Amplitude Water	Wave-height Water	Period S4	Amplitude S4	Positive gradi-ent	Negative gradi-ent	Standard dev pos [%]	Standard dev neg [%]	Comment
55	0.40	7.72	7720	2.64	5.28	7.72	4.24	8.48	7.72	0.016	0.024	-0.007			
56	0.80	5.47	5470	2.65	5.30	5.47	6.89	13.78	5.46	0.023	0.024	-0.021			
57	1.20	4.13	4134	2.64	5.29	4.14	9.00	17.99	4.13	0.043	0.053	-0.025			large difference between up and down gradient
58	1.40	3.87	3868	2.64	5.29	3.87	8.95	17.90	3.87	0.045	0.0548	-0.0349			large difference between up and down gradient
59	1.60	3.65	3646	2.64	5.28	3.65	9.29	18.59	3.65	0.053	0.0584	-0.0474			
60	1.80	3.46	3460	2.64	5.29	3.46	9.26	18.52	3.46	0.062	0.0682	-0.0554			
61	2.00	3.16	3159	2.64	5.29	3.16	9.90	19.79	3.16	0.081	0.08	-0.08			
62	2.20	3.04	3035	2.64	5.29	3.04	9.78	19.56	3.04	0.086	0.08	-0.09			
63	2.40	2.93	2925	2.64	5.28	2.93	9.58	19.17	2.93	0.092	0.09	-0.09			
64	2.6	2.83	2830							0.100					
64_2	2.80	2.75	2750							0.110					

Table C.8: Series 3

Test-number	AC	Period	Duration	Amplitude plunger	Wav-height plunger	Period Water	Amplitude Water	Wave-height Water	Period S4	Amplitude S4	Positive gradi-ent	Negative gradi-ent	Standard dev pos [%]	Standard dev neg [%]	Comment
65	0.40	7.73	7726	2.64	5.28	7.73	3.36	6.72	7.73	0.007	0.011	-0.004	0.09	-0.20	
66	0.80	5.46	5457	2.64	5.28	5.46	4.38	8.75	5.47	0.014	0.017	-0.011	0.08	-0.06	
67	1.20	4.13	4134	2.64	5.28	4.13	5.17	10.35	4.13	0.025	0.026	-0.024	0.08	-0.09	
68	1.40	3.87	3866	2.64	5.28	3.87	5.44	10.88	3.87	0.029	0.032	-0.025	0.08	-0.04	
69	1.60	3.65	3647	2.64	5.27	3.65	5.66	11.33	3.65	0.033	0.036	-0.031	0.06	-0.03	
70	1.80	3.46	3459	2.63	5.25	3.46	5.75	11.50	3.46	0.038	0.016	-0.060	0.29	-0.03	
71	2.00	3.16	3158	2.63	5.27	3.16	6.02	12.04	3.16	0.044	0.049	-0.038	0.73	-0.05	
72	2.20	3.04	3035	2.65	5.29	3.03	6.35	12.69	3.04	0.051	0.055	-0.047	0.08	-0.12	
73	2.40	2.93	2925	2.64	5.29	2.92	6.48	12.95	2.93	0.058	0.058	-0.055	0.08	-0.07	
74	2.6	2.83	2826	2.65	5.29	2.83	6.60	13.21	2.83	0.061	0.064	-0.059	0.07	-0.03	
75	2.60	2.83	2825	2.64	5.29	2.83	6.53	13.05	2.83	0.062	0.064	-0.060	0.03	-0.02	
76	2.80	2.74	2737	2.63	5.27	2.74	6.51	13.02	2.74	0.067	0.068	-0.066	0.03	-0.02	
77	3.00	2.58	2582	2.63	5.25	2.58	6.48	12.97	2.58	0.077	0.081	-0.074	0.04	-0.07	
78	3.20	2.51	2511	2.62	5.23	2.51	6.78	13.55	2.51	0.084	0.086	-0.083	0.02	-0.04	
79	3.40	2.45	2448	2.62	5.24	2.45	6.79	13.57	2.45	0.090	0.089	-0.090	0.04	-0.01	

C.2.4 Log book of test results

In the table below, C.9 all comments made on sediment transport and flow characteristics are summarised for the executed tests. These comments are used for the evaluation of the sediment transport in section C.2.

Table C.9: Comments regarding sediment transport

Cal	0.4			0.01					
1	0.4		[-]	[-]	First Test, Pressures set zero in scaling file	Pink fluid does not reach bottom			At The end of test: 1mm max displacement of interface at the bottom
2	0.4	55	0.0011	0.017	Full set up of experiment, transport starts at front 69,8. At back: 28.2 plus some sediments already at the bottom	No transport seen, Pink fluid does not touch bottom and just minorly moves back and forward. The rocks seem very porous in the backside close to the plywood and less porous at the interface. This might cause preferential path flow/short circuit flow	No transport seen		
3	0.4	65	0.0009	0.0073	New sequence with more porous interface. Sediment start at front at:67,7 and at back at: 28,0 with elongated tongue of approximately 3-5mm thick	No transport			Sediment start at front at:67,7 and at back at: 28,0 with elongated tongue of approximately 3-5mm thick. No transport observed
Cal	0.8			0.022					
1	0.8	41	[-]	[-]	First Test, Pressures set zero in scaling file	pink fluid nearly touches bottom	pink fluid nearly touches bottom		Sand appear to have moved max 1mm

Table C.9: Comments regarding sediment transport

Series	AC	test	Accelera-tion water	Gradient	Start	comment1	comment2	comment3	End
2	0.8	56	0.0035	0.0237	Full set up of experiment, transport starts at front 69,8. At back: 28.2 plus some sediments already at the bottom	No transport seen, Pink fluid does not touch bottom and just minorly moves back and forward. The rocks seem very porous in the backside close to the plywood and less porous at the interface. This might cause preferential path flow/short circuit flow	No transport seen		end transport: 69,8 and 28.2
3	0.8	66	0.0023	0.0135	New sequence with more porous interface. Sediment start at front at:67,7 and at back at: 28,0 with elongated tongue of approximately 3-5mm thick	No tranport observed			Sediment start at front at:67,7 and at back at: 28,0 with elongated tongue of approximately 3-5mm thick
Cal	1.2			0.034					
1	1.2	42	[-]	[-]	First Test, Pressures set zero in scaling file	pink fluid nearly touches bottom	Backside of the container is more porous. This causes more visual sediment transport	Streams seems to touch bottom better, however. No pink fluid to confirm	

Table C.9: Comments regarding sediment transport

Series	AC	test	Acceleration water	Gradient	Start	comment1	comment2	comment3	End
2	1.2	57	0.0082	0.0426	Full set up of experiment,transport starts at front 69,8. At back: 28.2 plus some sediments already at the bottom	No transport seen, Pink fluid does not touch bottom and just minorly moves back and forward. The rocks seem very porous in the backside close to the plywood and less porous at the interface. This might cause preferential path flow/short circuit flow	No transport seen		end transport: 69,8 and 28.2. ONLY 500 WAVES EXCITED
3	1.2	67	0.0048	0.0246	New sequence with more porous interface. Sediment start at front at:67,7 and at back at: 28,0 with elongated tongue of approximately 3-5mm thick	no transport to be seen. pink fluid moves only very little			No transport observed. Sediment start at front at:67,7 and at back at: 28,0 with elongated tongue of approximately 3-5mm thick
Cal	1.4			0.038					
1	1.4								
2	1.4	58	0.0095	0.0447	Full set up of experiment. transport starts at front 69,8. At back: 28.2.	No transport seen. The rocks seem very porous in the backside close to the plywood and less porous at the interface. This might cause preferential path flow/short circuit flow			end transport: 69,8 and 28.2. No transport observed during test

Table C.9: Comments regarding sediment transport

Series	AC	test	Acceleration water	Gradient	Start	comment1	comment2	comment3	End
3	1.4	68	0.0057	0.0289	New sequence with more porous interface. Sediment start at front at:67,7 and at back at: 28,0 with elongated tongue of approximately 3-5mm thick	no sediment is transported	It seems like the water movement is very slow according to the purple fluid. It does not mover very tuburlently		Sediment start at front at:67,7 and at back at: 28,0 with elongated tongue of approximately 3-5mm thick
Cal	1.6			0.044					
1	1.6	43	[-]	[-]	First Test, Pressures set zero in scaling file	backside is more porous and more transport appears. Bedload and also some suspended transport. "small clouds".	backside still some clouds. However the sediment does not seem to travel very far.	at front very little particles moving. Stabalised? back: particles still moving. Sediment bed seems to get somewhat higher.	Talud from 69.3 to 70.6 at front. And enlargement of 5mm width. at back from 22.2 to 21.8. the increase is about 5-7mm and clearly sand is originating from the top of the interface slope (5mm erosion).
1	1.6	50	0.0075	0.0508	First Test, Pressures set zero in scaling file. However, very difficult to see with the 200HZ oscillations	At front very little particles moving. Stabalised? backside is more porous and more transport appears. Bedload and also some suspended transport. "small clouds".	Pink fluid nearly reaches the interface	at front no transport, at the back 1-2 mm max horizontal. 1 mm vertical (20.3-20.1)	transport to 19.9

Table C.9: Comments regarding sediment transport

Series	AC	test	Acceleration water	Gradient	Start	comment1	comment2	comment3	End
2	1.6	59	0.0111	0.0529	Full set up of experiment, transport starts at front 69,8. At back: 28.2.	no transport is observed. Pink fluid does reach the interface but not turbulently.			Endtransport: 69,8 and 28,2
3	1.6	69	0.0066	0.0334	New sequence with more porous interface. Sediment start at front at:67,7 and at back at: 28,0 with elongated tongue of approximately 3-5mm thick	No sediment transport is seen. Pink fluid moves very slowly.			Sediment start at front at:67,7 and at back at: 28,0 with elongated tongue of approximately 3-5mm thick. No transport observed
Cal	1.8			0.052					
1	1.8			0.060443					
2	1.8	60	0.0123	0.0618	Full set up of experiment, transport starts at front 69,8. At back: 28.2.	At the front some movement of sand (10-20 particles per stroke) and at the back nothing. Back is also less porous. Pink fluid seems to move less turbulently than in previous experiments with comparable gradients. The strok seems to be dampend by the filter	Seems like there is very little transport. None at the back and very little at the front. Approx. 10 particles per stroke.		Endtransport: 69,8 and 28,2

Table C.9: Comments regarding sediment transport

Series	AC	test	Acceleration water	Gradient	Start	comment1	comment2	comment3	End
3	1.8	70	0.0076	0.0378	New sequence with more porous interface. Sediment start at front at:67,7 and at back at: 28,0 with elongated tongue of approximately 3-5mm thick	We do see flow but we dont see transport. Pink fluid not turbulent at all			
Cal	2			0.06					
1	1.95	51	0.0095	0.0676	First Test, Pressures set zero in scaling file.	Many transport, 100particles/cm. Especially at the back also higher up the slope+ bressen. At front slope some transport. More than test 0050M but much less than at the back	At front litte transport. Furthest point:72mm. 19,7max point. erosion at 26cm around the stones.		furthest point front72,7 . furthest point back 19,7
2	2	61	0.0158	0.0806	Full set up of experiment, transport starts at front 69,8. At back: 28.2.	Front small cloud of transport at several places. Small amounts of bressen. At the back much less transport. Pink fluid does reach the interface	Sediment transport seems to be decreased.	Sediment front at 70,1. Sediment back at 28.0. Sediment transport observed. No clouds but some bedload. Lower places along the interface more than upper sections of the slope.	End transport. Front:70,2, back:28,0

Table C.9: Comments regarding sediment transport

Series	AC	test	Acceleration water	Gradient	Start	comment1	comment2	comment3	End
3	2	71	0.0095	0.0436	New sequence with more porous interface. Sediment start at front at:67,7 and at back at: 28,0 with elongated tongue of approximately 3-5mm thick	we do see flow but we dont see transport	At some moments we see some grains move back and forewards. Pink fluid does not go anywhere		Sediment start at front at:67,7 and at back at: 28,0 with elongated tongue of approximately 3-5mm thick
Cal	2.2			0.064					
1	2.2			0.08973					
2	2.2	62	0.0154	0.0858	Full set up of experiment. Front:70,2, back:28,0	At front and back both somewhat more transport than in the previous test. However mainly bedload and not really clouds	Front: Sediment against wall is stuck, but deeper in the model a channel is eroded. Small bed load transport. Front: 70,2 , Back: 27,9 and small transport is observed . Pink fluid nicely along interface. Streamlines seem to be more straigth than before.		end transport at: front 70,2 and back at 27,9. Foto analyses should provide the answer for if a thicker layer has evolved.

Table C.9: Comments regarding sediment transport

Series	AC	test	Accelera-tion water	Gradient	Start	comment1	comment2	comment3	End
3	2.2	72	0.0094	0.051	New sequence with more porous inter-face. Sediment start at front at:67,7 and at back at: 28,0 with elongated tongue of approximately 3-5mm thick	at front some trans-port but very little at back Continious bedload transport and some bressing of steep slopes	At front no trans-poprt. At back smaller but still continious transport especially on the upper (steeper) slope. Not bressing but rolling of parti-cles. pink fluid not very turbulently		Sediment start at front at:67,7 (nothing really happend) and at back at: 28,0 with elongated tongue of approximately 3-7mm thick. Some erosion holes appeared at the top of the slope and accretion of 1-2mm over the lower slope.
Cal	2.4			0.068					
1	2.35	52	0.0135	0.1031	Pressures set zero in scaling file.	In the front: sus-pended sediment. Especially clouds of dust. In downrush, the sediments is bedload transported along the slope down-ward. In uprush the sediment is mostly stirred up but not moving up much. In The Back: somewhat less transport. More bedload like. Mainly downward (like at the front). Clouds are less but it seems to be a bit less porous too.	transport front to 77,2. Transport back to 20,4. experiment with purple fluid failed. 2nd time better but also failed. Purle fluid is thought to reach interface	transport at frond to 80 with tongue. At the back the transport is not in x but is in-screasing with about 1cm from start	End value sand front: 79,5 with tongue . Start value sand back: 20,6 with 0.5mm height

Table C.9: Comments regarding sediment transport

Series	AC	test	Acceleration water	Gradient	Start	comment1	comment2	comment3	End
1	2.35	53	0.0121	0.1202	Start value sand front: 79,5 with tongue . Start value sand back: 20,6 with 0.5mm height	Pink fluid does not seem to touch the interface. However, tube is not very far into the rock mixture	Sediment transport to 80.5 and increasing fast. Tongue is increasing. At the back less transport. Tongue somewhat thicker but not further.	At the front a 2cm thick tong form until 82.2. At the back it appears from photo comparison that very little sediment is transported	End transport at front at 84,5. and at back at 20,5
1	2.35	54	0.0124	0.1166	Begin transport at front at 84,5. and at back at 20,5				End transport front at 86.0. A 2cm thick tongue has formed throught the core. The slope at the interface looks less steep (evaluate via pictures). At the back the transport is untill in a very thin layer until 18-18.5mm with 0.5mm thick. Might be thicker inside the porous rock.

Table C.9: Comments regarding sediment transport

Series	AC	test	Acceleration water	Gradient	Start	comment1	comment2	comment3	End
2	2.4	63	0.0179	0.0923	Full set up of experiment. Start at front 70,2 and back at 27,9.	At front some sediment transport. Channel is being deepend (see results 0062). At the back some sediment is seen. However, not many. Both cases only bedload transport.	Pink fluid reaches the interface. Preferential pathflow is seems to be apparent along the plywood screens. Tongue at back does not show variability. At the front the tongue does not elongate bot increases somewhat in thickness in the lower part of the slope.		Sediment transport at front till 70.2 (thus zero) but an increase of the tongue of about 5mm. At the back this is not seen. At the back till 27.9
3	2.4	73	0.012	0.0566	New sequence with more porous interface. Sediment start at front at:67,7 and at back at: 28,0 with elongated tongue of approximately 3-5mm thick	at front still no transport to be seen. At the back increased transport velocity. The sediment is transported inward of the model and thus tongue seems not to elongate	sediment transport at both side. More transport somewhat deeper in the model. At the back more than in the front	Fluid is somewhat more turbulent and flows nicely along the interface	Sediment transported at front and back. At front max 1mm accretion and some sediment transported alongshore (thus inside the model). End point: at the front 67,8 (1mm further) and 1mm thicker. At the back not further (28,0) but 1-3 mm thicker over the lower slope
Cal	2.6			0.072					
1	2.6								

Table C.9: Comments regarding sediment transport

Series	AC	test	Accelera-tion water	Gradient	Start	comment1	comment2	comment3	End
2	2.6	64	0.019	0.0985	Full set up of experiment. Sediment transport at front till 70.2 but an the is quite thick tongue of about 5mm with respect to previous tests. At the back 27.9	Transport, gradient = 0.1			No end evaluation carried out
3	2.6	74	0.0131	0.0613	New sequence with more porous interface. Start at 67,8 at the front and 28,0 at the back. "new layer" of 1-3mm thick at the back and 0.5-1mm at the front	At the front transport with every stroke. At the back also transport but not very different than previous (0073) test	pink fluid moves up and down semi turbulently. At front still some small sediment transport is seen. At the back in the alongshore direction some transport but crossshore seems stabalised(??)		In the earlier accreded zones dunes are formed from the wave pattern. At the toe at the front a small hill formed. At the back the 1-3mm accretion is now gone but not very clear where it went. At front till 68,1 and the thickness of the tongue increased. at back till ~28. the tongue is of different shape and where accretion or erosion appear should follow from photo analyses.
Cal	2.8			0.076					
1	2.8								
2	2.8	64_2	0.02	0.1075	No begin evaluation carried out	Turbulent transport, gradient =0.11.			No end evaluation carried out

Table C.9: Comments regarding sediment transport

Series	AC	test	Acceleration water	Gradient	Start	comment1	comment2	comment3	End
3	2.8	76	0.0137	0.0671	New sequence with more porous interface. Sediment until at front: 68,2 and up to 4mm thick. At the back still to 28,0 and the tongue 5-7mm thick.	Sediment transport is observered. Somethat stronger than in test 0075	from several places along the plywood interface between sand and rocks, sediments are lost. The slope at the front become higher and the slope at the back moved from 28,0 to 26,0	stones seem to get loose from the sand at the plywood interface and slopes get increasingly thicker towards the bottom. They get increasingly thinner towards the top of the slope.	end transport at 68,2 with 10-15mm thick tongue. At back transport till 26,0 with 5mm tongue. Both side upper eroded en lower accreded.
3	2.6	75	0.0129	0.062	New sequence with more porous interface. In the earlier accreded zones dunes are formed from the wave pattern. At the toe at the front a small hill formed. front till 68,1 . at back till ~28. the tongue is of different shape than before 0074	Continued of experiment 0074	Transport at the back seems stabilised crossshore but sediments keep going alongshore back and foreward. In the front transport in both sides. Only bedload, no clouds etc.	Transport at the back also crossshore transport and sediments keep going alongshore back and foreward. In the front transport in both sides. Only bedload, no clouds etc.	Sediment until at front: 68,2 and up to 4mm thick. At the back still to 28,0 but the tongue inscreased from 3mm to 5-7mm thick.
3	3	77	0.015	0.077	New sequence with more porous interface. Sediment until at front: 68,2 and up to 4mm thick. At the back still to 28,0 tongue 5-7mm thick.	small clouds seen between 31 and 33 at the back side. Some more turbulent transport. At the front equal transport to measurement 0076	A hole appeared between 57 and 60 at the front. It seems like the sediments are transported inwards. The slope gets thinner but not really longer. Tongue somewhat thicker but not much	At the back the slope also becomes much thinner. At the upper slope between 40 and 37 a hole appears like at the front.	sediment at the back is equal to last test and stops at 26. slope became mucht thinner. At the front until 68,2 with a somewhat thicker tongue at the very end but overall thinner slope.

Table C.9: Comments regarding sediment transport

Series	AC	test	Acceleration water	Gradient	Start	comment1	comment2	comment3	End
3	3.2	78	0.0169	0.084	New sequence with more porous interface. sediment at the back stops at 26. slope is relatively thin. At the front until 68,2 with a somewhat thicker tongue at the very end but overall thin slope.	At the front some transport but not very clear. At the back turbulent clouds, this is also caused by the semi rippeld bed which acts like a ramp for the sediment particles	Sand dunes arise along the back side upto 23. Continious process seems excited. Interesting would be to see what happens longer period. Probably setup dependend. At the front litte transport is seen	pink fluid moves fast up and down along the interface. However, the fluid fastly dissolves and becomes a stable purple stain	Sediment transported to 69 with 1 mm thick. From 68 the sand is 10mm thick tongue. Transport to 25 of 5mm thick and a hill at 23.
3	3.4	79	0.0177	0.09	New sequence with more porous interface. Sediment transported to 69 with 1 mm thick. From 68 the sand is 10mm thick tongue. Transport to 25 of 5mm thick and a hill at 23.	Transport very turbulent at the back. In the front not much transport is observed.			At the front 69,3. at the back hills are connected between 22-26 of 1mm. Furthermore, between 24-26 its 5mm.